Low endurance fatigue of cast irons and cast steels

by

Cestmir Radon

Thesis submitted for the Degree of Ph.D. in the Faculty of Engineering of the University of London and for the Diploma of Imperial College

Mechanical Engineering Department

Imperial College

March 1966

ABSTRACT

The object of the present investigation was to show the influences of strain range, ambient temperature, strain concentration (notch) and hold times at maximum and minimum strains on the low-endurance (50-10,000 cycles) fatigue behaviour of a selection of cast irons and cast steels which were considered suitable as diesel-engine combustion-chamber materials.

Two vertical hydraulic tension-compression ($\pm$ 15 tons) fatigue machines suitable for operation at low frequency and at high temperature were designed. Instrumentation was developed to record automatically hysteresis loops and to control load cycling or strain cycling. Reversed strain-cycling tests were carried out on plain and notched specimens at room temperature and at $450^{\circ}C$. Comparative load-cycling tests on plain specimens at room temperature were performed to show the differences between the two types of cycling. Calibration tests for conversion of total diametral to total axial strain range at room temperature were developed. Stabilised cyclic stress-strain curves were derived and total energies to fracture investigated.

Cyclic thermal stresses produced in combustion-chamber components by starting and stopping or running a diesel engine on part-load may lead to fatigue failures.

There is evidence that the resistance materials offer to cycles of mechanical strain, total and plastic, has an important bearing on their thermal fatigue strength.

The present results suggest that cast steels and nodular cast irons will have better thermal fatigue properties than flake graphite cast irons.

However the superiority of the cast steels and nodular cast irons is not so marked when a strain concentration is present.

When thermal conductivity and coefficient of expansion are also taken into account in relation to complex thermal fatigue, the cast steels are still indicated as the best materials but there is less distinction between the nodular and flake irons.

ACKNOWLEDGEMENTS

The author takes pleasure in recording his indebtedness to Professor Hugh Ford, D.Sc. (Eng.), Ph.D., F.C.G.I., Wh.Sch., M.Inst.C.E., M.I.Mech.E., F.I.M., for his valued advice and encouragement throughout the work. He also wishes to thank Messrs. D.J.Burns, B.Sc. (Eng.), Ph.D. and P.P.Benham, D.Sc.(Eng.), Ph.D. for their help and advice during the numerous discussions in the course of the programme.

The author is also indebted to the British Ship Research Association who provided financial support for the research programme and to the British Cast Iron Research Association for their kind assistance in several aspects of the work. Also much appreciated was the helpful cooperation of the workshop staff of the Mechanical Engineering Dept, Imperial College of Science and Technology.

CONTENTS

NOMENCLATURE

a = crack length
E = modulus of elasticity
f = frequency of cycling
K = thermal conductivity
also stress intensity factor
K_f = effective fatigue strength reduction factor
K_p = plastic stress concentration factor
N = cycles to failure
r = radius of plastic zone
T = temperature ^{o}Centigrade
T_m = temperature of the melting point
t = duration of test

α = exponent in Coffin-Manson relation (1)
also coefficient of linear expansion
α' = exponent in Sachs equation (111), close to 2
ϵ = strain
ϵ_m = mean strain
ϵ_e = elastic strain
ϵ_f = fracture ductility
ϵ_f' = apparent fracture ductility
ϵ_{fr} = remaining fracture ductility, Sachs, Eqn.(6)
ϵ_p = plastic strain
ν = Poisson ratio
σ = stress
σ_m = mean stress
σ_y = yield stress
Δ = range

1. INTRODUCTION AND TEST PROGRAMME

1.1.1 Combustion-Chamber Cracks in Compression-Ignition Engines

Cast irons and cast steels are widely used in the production of combustion-chamber components. They deserve particular attention because of their specific properties and behaviour under the strenuous conditions of repeated applications of high thermal and mechanical loading.

Since the earliest days of large diesel engines cracks have been found in those parts exposed to the combustion process. In some cases these cracks have appeared very early in the engine's expected life and often major failure has followed rapidly the appearance of cracking. Such failures are an extremely serious matter for both the engine manufacturer and the user. They are particularly serious and costly when very large marine engines are involved because of the difficulties of repair at sea and the possible consequences of loss of motive power at sea.

In the design of compression-ignition engines the primary emphasis is placed on maximising the power/weight ratio. Various expedients are used to accomplish the desired improvement, namely supercharging, raising compression ratios and increasing engine speeds. However, all such devices inevitably lead to increased operating temperatures, particularly in the combustion chamber, and thus there has been a tendency for thermal stress failures to rise with the increase of engine ratings resulting from technical development.

The most important parts of a normal combustion chamber are the piston, the cylinder head, the exhaust valve, the liner and the injector nozzle. Each of these parts is affected by increased temperature and by temperature fluctuation. A piston running hot may cause seizure of the top rings or may crack and break. Excessive cylinder head temperature can distort the head and break the gas seal or cause thermal cracking on the inner surface. Valve temperature is particularly important when residual fuels are being burnt and is to some extent dependent on the head temperature. High nozzle temperature is important when burning heavy fuels, but too high a temperature will impair the needle seat life. The liner temperature can play an important part in determining piston temperature.

Cracks are often found across the valve bridge leading from one valve to the other, or from the injector nozzle to the exhaust port. Heavy cracks have frequently been observed close to the exhaust port where hot exhaust gases repeatedly rush over the surface, while relatively few cracks are to be found in the vicinity of the air inlet port where the head surface is repeatedly cooled by the incoming air.

"Craze cracks", indicating the presence of evenly distributed equal biaxial stresses, have been found in the centre of the piston crown. (1)

Cracks in liners usually start in the injector port wall and extend in both directions along the liner axis. The port is normally lined with a heat-resisting alloy insert as it is both a hot spot and mechanically weak.

1.1.2 Failure Mechanism

The failure of combustion chamber components can arise in two ways:-

1.1.2.1 Mechanical Loading

The components are subjected to the fluctuating gas pressure. Failures caused by this fatiguing action were reported starting on the cold water side of the cylinder head or at the horizontal junction of the crown and wall of the piston (2). Moving parts are subject to inertia forces and the liner, piston and rings experience frictional forces which may be increased by piston side thrust. Failures due to these latter forces are, however, comparatively rare.

1.1.2.2 Thermal Loading

Thermal stresses usually result from one or more of the following conditions:-

(i) Two connected parts having different expansion coefficients undergo a temperature change.

(ii) Two connected parts undergo different temperature changes.

(iii) The temperature distribution within a component is such that it cannot expand or contract to achieve a stress-free shape.

At least two of these conditions are continually present in diesel engine combustion-chambers during starting and stopping, running on full and part load, manoeuvring and of course each time the engine fires.

Investigations have shown that some of these cyclic thermal stresses cause fatigue cracking (3,4,5,6). Furthermore, thermal fatigue failure usually occurs fairly early in the engine's design life, sometimes after even less than 5000 start-stop cycles (3,7,8). In view of this it is important for designers to know the stress levels and thermal conditions which will give rise to fatigue lives in this range.

One mechanism of cyclic thermal stress failure arising from condition (iii) above has been described by Dearden (7) and others.

Consider a rod held between two massive immovable walls (Fig.1). If the rod is heated a compressive thermal stress will be set up within it as it is not free to expand. As its temperature rises so the compressive stress will follow the compression curve OA as shown in Fig.2. If the source of heat is removed and the rod allowed to cool, the compressive stress will diminish and since the point A was beyond the compressive elastic limit, i.e. plastic deformation had taken place, at zero strain there will be a small residual tensile stress OC; OC is often described as the operational residual stress. If OC is greater than the ultimate tensile strength the rod will break. If OC is below the ultimate tensile strength but above the elastic limit, on reheating the stress-strain curve will be as CDA, and further cycles of heating and cooling will cause the rod to be subjected to a typical high-strain cycling process.

If the rod is held for a time at a high temperature a complication arises. At high temperatures creep rates become significant and thus the induced compressive stress will tend to relax along AE. The rod is then cooled along EFG and the residual tensile stress is much greater than that with no hold time.

Therefore, in the investigation of resistance of metals to thermal fatigue it is extremely important to take into account not only the temperature range but the maximum temperature, the hold time at that temperature, and the cycling frequency.

The width of the hysteresis loop BD is a measure of the plastic strain occurring over the cycle. The metal fails when this strain can no longer be accommodated. It is important to note that the actual fracture must occur during cooling when a tensile stress is induced.

Another mechanism of cyclic thermal stress failure was considered by Walker (9) when investigating turbine shell materials. Under certain starting conditions the temperature of a hot spot is very much higher than that of the surrounding material; this results in compressive yielding of the hot material. Somewhat later, as the conditions even out, the temperature difference becomes smaller and high residual tensile stresses will develop in the plastically deformed area. These stresses will be reduced during running by creep relaxation processes. Subsequent starts will accumulate further creep deformation and lead eventually to creep-rupture. Walker concluded that creep rupture cracks would develop particularly in the steam inlet region during the long periods of time when the shell material is at operating temperature.

The failure mechanism described by Dearden (7) appears to be more important in CI engines as the cracks open when the combustion-chamber has cooled down.

1.1.3 Thermal Fatigue Failure in Engines

1.1.3.1 Load and Temperature Effects

When a compression-ignition engine fires, the gas temperature may rise to 2000°C or 2400°C and then fall again as cool air is drawn in for the next cycle. This fluctuation may be relatively slow, for example around 60 cycles/min in large marine diesels, or fast, up to

3000 cycles/min in a small high speed engine.

The actual temperature pulse is fairly small, of the order of 20°C to 50°C - it is greatest when starting from cold, and is dependent on the speed and maximum working temperature of the engine. The maximum temperature in the combustion-chamber walls is reached considerably after the peak pressure has passed. The actual layer affected by the pulse is normally about 0.1 in. for medium-sized engines. Service experience suggests that this temperature pulse is not a major cause of fatigue failures.

Apart from the cyclic variations described above there are also those effects related to the less frequent start-run-stop cycle, and to changes in engine output during running. In both cases there are variations in temperature gradient across the full thickness of the cylinder wall before the quasi-steady temperature of normal running is established. The frequency of starting-stopping and of load-changing depends upon the service for which the engine is required.

1.1.3.2 Notch Effects

Not only do changes in section and other discontinuities give rise to strain and stress concentrations in their own right but when heat flow is involved they may cause local variations of heat transfer rates and associated temperature gradients giving rise to thermal strain and stress. Thus thermal fatigue is most likely to occur at notches, and the nature of the notch can have a significant effect upon the fatigue endurance of service components and laboratory specimens.

Most materials strain more readily the higher the temperature (yield decreases with temperature increase).

Thus a hot spot in a component can give rise to a strain concentration (see 1.1.3.1 above) and may be regarded as a "thermal notch".

1.1.3.3 Effect of Material Structural Changes

No investigations of combustion-chamber failures have shown any evidence of material structural instability under normal running conditions, and from the available temperature measurements it would seem unlikely that the current surface temperature would be sufficiently high to cause a transformation. However, Gilbert (10) has shown from 60-week tests on some cast irons that iron carbide breakdown could occur under 500°C, although the process would be extremely slow.

1.1.4 Factors Influencing Resistance to Thermal Stress Failure

1.1.4.1 Cooling

The simplest method of reducing the tendency to thermal cracking is to cool efficiently, or its corollary, to keep flame-face temperatures as low as possible.

Cooling may be improved by reducing the thickness of the bottom deck, particularly in the vicinity of the valve ports; although this will inevitably increase the possibility of a failure due to gas pressure. It is also important to maintain sufficient cooling water throughput to ensure turbulent flow, which gives higher heat transfer coefficients than does laminar flow, and to keep output water temperature sufficiently low to avoid rapid scale deposition. Scale deposition may also be inhibited by a correct water treatment.

1.1.4.2 Thermal Shielding

Thermal cracking can also be reduced by thermal shielding. The surface to be protected is sprayed with alumina or other refractory to give the metal a fused coating of high thermal-shock resistance. The coating also reduces the heat loss and damps temperature fluctuation. However difficulties can arise in obtaining adequate adhesion between the coating and the metal surface.

These coatings are usually employed to protect piston crowns.

1.1.4.3 Material Properties

Dearden (7) and others have suggested that thermal stress failures are less likely to occur if the component materials have:-

(i) high thermal conductivity - to avoid steep temperature gradients;

(ii) low thermal expansion coefficient - to avoid steep strain gradients;

(iii) stress-strain characteristics such that the ratio of reversed plastic strain to total strain is as low as possible (in general this implies a low elastic modulus, a high elastic limit and a narrow stress-strain hysteresis loop);

(iv) low creep rate in compression;

(v) high fatigue strength under conditions of repeated plastic strain (leading to failure in less than 5000 cycles); and

(vi) high ductility which should not be significantly affected by repeated plastic straining.

When considering the resistance of cast materials to thermal stresses, the substantial influence of the elastic modulus should not be overlooked. The elastic modulus of flake iron E is considerably lower (approx. 18×10^6 lbf/in^2) than that of cast irons of nodular type. A comparative value for iron F is quoted as 25×10^6 lbf/in^2. This difference in modulus could account for approximately 30% lower thermal stresses in flake cast irons under similar testing conditions.

It is hardly possible to obtain the best values for all these properties in any one material and plainly some compromise must be made.

1.2 Previous Investigations of the Thermal Stress Problem for the British Ship Research Association

Three particularly interesting projects on the thermal stress problem have been carried out at Nottingham University under a British Ship Research Association (B.S.R.A.) contract.

(i)

Fitzgeorge and Pope (3) investigated the factors contributing to the failure of diesel engine pistons and cylinder covers. The nature of the stresses in the combustion-chamber components was investigated and the occurrence of cracks described. It was concluded that the cracks observed on the hot face were due to tensile residual stresses. Other cracks found on the cooled sides were thought to be due to fatigue action or repeated combustion processes combined with the mean stress resulting from wall temperature gradients.

Their analysis of the stresses in the piston showed that thermal stresses were dependent on its proportions. For low thermal stresses in the crown, the crown should be thin. For low thermal stresses in the wall, the wall should be thick, but a thick wall causes higher thermal stresses in the crown. As a result, various alternative designs to minimise the stresses were suggested.

(ii)

The above work was continued by Baker and Pope (4). The metallurgical, mechanical and thermal properties of eight different cast irons were investigated with a view to determining the extent of the contribution of each separate property to the production of residual stresses.

Conventional fatigue tests were performed on a high speed rotating beam machine and fatigue limits under 10^6 cycles for flake irons and over 10^6 cycles for nodular irons were obtained. It was found that the fatigue strength of flake irons increased with increasing temperature up to 400°C, thereafter decreasing, whereas that of nodular irons decreased continuously with increase in temperature.

Creep rate and creep relaxation tests were also performed and it was noted that the primary creep extension was very large between 400°C and 475°C. However, the relation between creep rate, stress and temperature could not be established. It should be noted that creep relaxation test results are especially important as these tests closely represent conditions in diesel engine components.

Expansion coefficients were also determined for each material.

Originally all the materials investigated were considered suitable for use in compression-ignition engine components - and indeed were employed in commercial engines - but increasing engine performance has resulted in many cases of cracks of the type described earlier occurring in the hot face. Thus an increasing selectivity has been forced upon manufacturers. From this and the earlier work (3) it was concluded that the order or merit for these materials was:-

1. Nodular irons.
2. Flake irons.

   And that cast steels would probably be superior to both types of cast-iron.

(iii)

On completion of the planned programme it was felt that further experimental work particularly in the high temperature region was necessary. Consequently Baker and Pope (11) designed two cyclic thermal-straining machines to induce residual stresses in cast iron specimens.

The construction of the thermal straining machine made it possible to measure the variation of the magnitude of the stress in the specimen with the temperature at any stage of the test. The test was considered superior to both creep and stress-relaxation tests in two respects, namely that the total plastic flow during the warming up as well as that during the soaking was measured and that the total plastic flow occurring was translated into tensile residual stress as the specimen cooled down.

The actual tests carried out were as follows:- $\frac{1}{4}$ in. dia. cylindrical specimens were slowly cycled between room temperature and 350°C incorporating a 24-hour hold time at the highest temperature. On cooling down tensile stresses were observed at approximately 200°C. Unfortunately the muffle furnaces used often failed before the test was completed and therefore only a limited amount of data was obtained.

One flake iron was found to have excellent resistance to primary creep, even in the vicinity of 475°C. This type was therefore particularly recommended as the desirability of employing a creep-resistant iron has been theoretically well established.

The creep properties of nodular graphite irons having a pearlitic matrix were inferior to those of flake irons, but the nodular irons performed better under cyclic thermal-strain conditions as would be expected from their superior tensile and fatigue properties. However they tend to have low thermal conductivity coefficients and high expansion coefficient.

At the conclusion of this work Pope suggested that further high strain fatigue tests either in thermal cycling or mechanical cycling at high temperatures should be carried out.

The execution and interpretation of true thermal cycling tests on constrained laboratory-size specimens is extremely difficult. Experimental difficulties arise particularly in strain measurement, the elimination of thermal gradients and the avoidance of specimen buckling. Fortunately there is some evidence that mechanical strain cycling at a constant temperature T_c somewhere between T_1 and T_2 is equivalent to thermal cycling between these limits providing significant metallurgical changes do not occur between them (see Chap. 2).

The object of the experiments described below is to show the influence of stress range, strain range, ambient temperature, strain concentration and hold-time on the mechanical strain cycling fatigue behaviour of a selection of cast irons and steels that might be considered as materials of construction for diesel combustion-chamber parts.

1.3 Present Test Programme

From the various testing methods available for the study of high strain fatigue properties (see Chap.2), fully reversed axial cycling was chosen as the most convenient.

(a) Apparatus

In the first part of the apparatus development programme two hydraulic high-strain fatigue machines were designed and constructed. One machine was developed exclusively for room temperature testing, while the other was adapted to allow testing at ambient temperatures up to 450°C.

In the second part of the programme the electronic controls for cycling, recording and temperature regulation were developed.

(b) Materials and Specimens

Six materials were chosen after careful scrutiny of the irons recommended for combustion chamber construction. The selected range included:-

two flake cast irons,
one nodular cast iron,
one austenitic cast iron, and
two cast steels.

Solid cylindrical specimens were used for the entire test programme. The effect of strain concentration was investigated using specimens of the same overall geometry but circumferentially notched.

(c) Testing

Both load and strain cycling were employed and the cycle frequency was kept at approximately 4 cycles/min throughout the programme. Cycling was applied within the endurance range 1 to 15000 cycles, the maximum load range was about 88 tonf/in^2 and the maximum diametral strain range was about 3%.

Strain cycling tests were peformed on plain and notched specimens at both room and 450°C temperatures. The effect of a short hold-time at maximum and minimum strains was also investigated for the high temperature tests on one flake iron and a cast steel.

At the beginning of the research programme it was realised that commercial organisations might wish to carry out similar low cycle fatigue comparisons on other materials. Since commercially available high strain fatigue machines at that time were almost without exception load controlled, it was decided to carry out a limited number of load cycling tests for comparison with the more realistic strain cycling tests. These were only performed on plain specimens at room temperature.

Auxiliary tests were also performed to provide information on:-

(i) the effect of specimen orientation,
(ii) the effect of variation in plate quality,
(iii) the effect of surface finish,
(iv) tensile tests,
(v) the relationship between diametral and axial strain.

2. LITERATURE SURVEY

2.1 Introduction

Fracture of metals caused by the cyclic application of the thermal strain is called thermal fatigue. Thermal fatigue or thermal cracking in C.I. engines most likely resulting from the accumulated effects of "Start" and "Stop" cycles was described in Chapter 1.

Various aspects of the mechanism of thermal stress failures have also been investigated in other fields. Coffin described many specific cases (12,13,14) and reviewed the subject in general (15).

In steam power plants an increasing number of thermal fatigue failures have been experienced with turbines which formerly ran continuously for months, but lately are being started and stopped frequently to accommodate load fluctuations. Also operating temperatures and pressures have been increased in order to obtain better efficiency. Fatigue cracks have also been observed in steam pipes.

In the steel industry thermal fatigue cracking of the cast iron ingot moulds is a major source of failures. The inside face of ingot moulds is initially heated very rapidly to about 700°C and the outer surface eventually reaches the same temperature. The stresses produced on the inner face initially compressive become tensile as the rest of the mould heats and expands.

Thermal fatigue cracks are also found in mechanical stokers, rolls used for hot rolling and in heavy-duty brake drums. "Checking" (cracking) (16) on the surface of a cast-iron brake drum is often connected with the transformation of cementite to martensite and is due to the volume change.

2.2 Thermal and Mechanical Cycling

2.2.1 Coffin

As stated previously the execution of laboratory thermal cycling tests is extremely difficult and there have been several noteworthy attempts to correlate thermal and mechanical cycling behaviour of materials to provide design data.

The first comparison of thermal and mechanical strain cycling fatigue strength was made by Coffin (17,18).

An apparatus was developed in which a thin-walled tubular specimen 0.5 in I.D. was alternately heated and cooled under axial constraint, the required temperature cycle being achieved by the regulation of an electric current passing through the specimen. Alternatively the specimen could be mechanically strain cycled by heating and cooling the main columns of the fatigue machine.

Both plain and notched (0.013 in diametral hole) specimens were used. The material employed was a heat-resisting stainless steel, AISI 347, and to investigate strain hardening and softening both annealed and cold-worked conditions were used.

The rate of cycling was 4 cycles/min and lives up to 20,000 cycles were investigated. At the higher strain ranges buckling caused considerable experimental difficulties.

A mean temperature of 350°C was used in the thermal cycling tests, although it might be considered that this was too low to reveal any appreciable time-dependent effects in the stainless steels.

The differences between the results obtained from mechanical and from thermal cycling were discussed in detail and it was shown that the two types of test should be equivalent in terms of the plastic strain range to cause failure, in a given number of cycles. Differences in material, specimen geometry, temperature distribution and other factors were also considered. The localization of plastic strain due to the diametral hole of the notched specimens was found to reduce seriously the fatigue life.

A linear relationship between the logarithms of the plastic strain range $\Delta\epsilon_p$ and the cycles to failure N of the form

$$\Delta\epsilon_p N^{\alpha} = \text{constant} \qquad (i)$$

was derived. The value of the index α was found to be close to 0.5.

Coffin suggested that in the region of higher temperatures where creep and other diffusional processes could occur, the relationship (i) might well be rather different and it was concluded that at any particular temperature a knowledge of the ductility and the cycling frequency was of prime importance.

2.2.2 Majors

Majors (19) performed mechanical load cycling tests at a steady high temperature 300°C and thermal cycling tests on titanium and nickel. Mean temperatures were 301°C and 274°C for titanium and nickel respectively. The frequency for mechanical cycling was 1 cycle/min, for thermal cycling 2 cycles/min. The log.-log. curves of ϵ_p - N were straight lines with negative slopes varying between 0.48 and 0.51.

It was found that the fatigue lives obtained from the two types of test were comparable when the steady strain-cycling temperature was the same as the maximum temperature in the thermal cycle.

2.2.3 Swindemann and Douglas

Swindemann and Douglas (20) tested Hastelloy B, beryllium and Inconel tubular specimens at temperatures of 700°C, 800°C and 875°C in thermal and mechanical strain cycling. The cycling frequency was $\frac{1}{2}$ cycles/min and the Coffin relationship between plastic strain and cycles to failure was confirmed. The values for α were 0.58, 0.81 and 0.76 for Hastelloy B, beryllium and Inconel respectively.

All three materials responded to plastic strain in the same manner, whether induced by thermal changes or mechanically imposed loads. No metallurgical changes were found during any of the tests.

Additional tests were performed at a frequency of 1 cycle every 30 min. This slow cycling was found to reduce considerably the fatigue endurances at the lower strain ranges. Comparable results were obtained from mechanical and thermal cycling. This phenomenon is apparently confined to higher temperatures and establishes the fact that plastic deformation is not the only factor controlling the fatigue life of a metal.

Since many metals have been found to have α values close to 0.5 at room temperature it was suggested that the increase in its value at higher temperatures is dependent upon the material behaviour and upon the deformation mechanism at the test temperature.

2.2.4 Taira et al.

Taira and others (21, 22) investigated the thermal fatigue behaviour of AISI 347 and Cr-Mo heat resisting steels over a range of temperatures up to 650°C using an apparatus similar to Coffin's. The authors introduced the concept of an equivalent steady temperature in order to relate thermal fatigue with high-temperature mechanical strain-cycling. According to their analysis this temperature is approximately equal to the mean of the upper and lower temperatures in a thermal fatigue test when strain amplitude is large and thus plastic strain is predominant, but is very close to the upper temperature when strain amplitude is small and elastic strain becomes significant.

In their thermal fatigue tests the temperature distribution along the specimen gauge length was uneven whereas a uniform distribution was obtained in the mechanical strain cycling tests. This uneven distribution tended to result in a localization of plastic strain and a correction factor had to be derived to enable valid comparisons to be made.

A steady frequency of 1 cycle/min was used for both types of cycling and throughout the investigation it was implied that metallurgical changes did not take place.

2.2.5 Forrest

The difficulties with specimen buckling encountered in the Coffin type of machine for thermal cycling have led the National Physical Laboratory to develop a reversed bending machine in which strain range and temperature can be varied independently. The specimen has the form of a rectangular bar, which is mechanically bent and heated by the electrical resistance method, thus allowing free access to and observation of its surface.

Forrest(23) reported a number of results obtained using this machine, which indicated that the resistance to alternating strain with temperature fluctuating in phase with the applied strain was about the same as that with temperature held constant at its maximum value.

2.2.6 Comparison between Thermal and Mechanical Cycling

From the investigations reviewed above three conclusions can be drawn:-

(a) Thermal and mechanical cycling can be directly related when the mechanical cycling temperature is close to the upper temperature of the thermal cycle, providing metallurgical stability is maintained.

(b) The Coffin relationship (i) can be applied to thermal cycling. In all cases the linear relation between the logarithms of plastic strain and cycles to failure was well established although there were some indications that the slope, the Coffin exponent α, might increase with rise in temperature limit.

(c) Finally, in all investigations no metallurgical changes were found - or assumed - to have occurred and thus could not be held responsible for any of the effects observed.

2.2.7 Other Thermal Cycling Investigations

Other methods of thermal cycling have been developed where direct comparison with mechanical cycling is less easy. For example, resistance to thermal shock is determined by alternately heating and cooling the tip of a long thin wedge or the rim of a discus-shaped specimen. Here it is impossible to measure stress or strain and thus only temperatures and cycles are recorded. The test is most valuable when a particular application is envisaged and a wide range of materials are to be compared.

Krempl (24) used cylindrical specimens 5 mm dia. to investigate the thermal cycling behaviour of Nimonic 80A between 200° and 925°C. Fatigue fractures were obtained up to 830°C and creep fractures at higher temperatures. Changes in plastic strain range during cycling were observed and plotted against cycles but a correlation with any other type of cycling was not attempted. In order to compare stress and strain for various endurances the author used the first-cycle values as a basis for comparison, although this might be a rather dangerous simplification as it is well known that considerable changes in shape of the hysteresis loop can occur in the first few cycles of a test.

Sachs and Weiss (25) studied thermal cycling with a constant mean load on two aluminium and two magnesium alloys between -195° and +316°C and described the process as closely related to intermittent creep. Cylindrical specimens 6.35 mm diameter were immersed in a liquid nitrogen bath and a special apparatus was developed for application of the constant load. Lives up to 500 cycles were investigated.

Graphs of plastic strain against thermal cycles on a log-log scale were plotted and linear relationships with slopes between -0.85 and -1.2 obtained. The effect of heating rate was found to be very inconsistent and in the author's opinion indicated material instability such as stress-ageing and cyclic-rate dependent ageing.

The successful correlation of thermal and mechanical strain cycling results has led investigators to concentrate on mechanical cycling and to study the effect of a number of variables on mechanical strain-controlled fatigue.

2.3 Mechanical Cycling

2.3.1 Type of Specimen

The basic forms of loading may be classified as those which produce direct stresses (axial tension or compression), bending, torsion or complex stress system. Specimens for axial cycling have usually a simple geometry. The measurement of load can be fairly easily accomplished. The critical measurement is that of strain and often an expensive instrumentation is needed (26).

Bend specimens vary considerably in geometry but can be extremely simple and easily manufactured. Instrumentation, however, is difficult and strain measurement, particularly at high temperatures, presents considerable problems. Failure criteria are not clearly defined and stress and strain state difficult to calculate because of the effect of transverse restraint (27).

Torsional specimens can be of solid cylindrical shape or more usually thin-walled tubes. Because of the tendency to buckle the latter are often mounted on a close fitting shaft or waisted to reduce the section liable to buckle (28).

2.3.2 Load Cycling

2.3.2.1 Constant Load-Amplitude Tests

In low-cycle fatigue the loads applied are usually sufficiently large to cause general plastic yielding. If in a low-cycle fatigue test the load limits are kept constant the strain limits will vary during cycling and vice-versa. Accordingly tests can be divided into two main groups, namely constant load and constant strain-range tests. In the conventional fatigue test where applied stress is below the yield stress this differentiation is unnecessary as load and strain are related through the modulus E throughout the test.

At very short fatigue endurances a large plastic strain variation corresponds to a comparatively small change in applied load. Therefore constant load-range tests are very difficult to perform with sufficient reliability. Some of the first investigations of load cycling by Hartmann and Stickley (29) have clearly shown this difficulty. Very flat S-N curves up to lives of 2×10^4 cycles were observed in tests on annealed and work hardened aluminium alloys. Similar results were reported by Hardrath (30) and Hardrath and Illg (31, 32) who used plain and notched specimens of aluminium alloys and stainless steels AISI 347 and AISI 403. Because of these difficulties strain cycling has been preferred by many later investigators.

2.3.2.2 Constant Stress-Amplitude Tests

A special type of load cycling can be termed the constant stress-range test. A small number of these tests was performed by Lin and Kirsch (33) on an aluminium alloy but the scatter of their results was abnormally large. Rolfe and Munse (34) reported the results of constant stress and constant load tests while investigating fatigue crack propagation. Linear crack growth was observed in constant nominal stress cycling at stress levels below the general yield of as-rolled ABS-C ship steel specimens with $\frac{3}{4}$" x 5" section tested at two temperatures, 25°C and -40°C.

2.3.2.3 Cyclic Creep

When ductile materials are subjected to cyclic loads, with or without a mean load, a small non-recoverable deformation may occur in each cycle. The effect has been more fully studied in copper (14) and other very ductile metals. Benham and Ford (35) have reported an absence of such deformation in aluminium alloy DTD 683; this is probably connected with its lack of ductility and high elastic range. These tests were conducted in axial cycling (35, 36) and reports on bending and torsional effects are also available (37, 38). There is relatively little information on cyclic creep in wrought steels and even less in cast steels and brittle cast irons.

The behaviour is attributed by Coffin (36) to the presence of a mean stress. Even when the mean load is zero the variation of specimen geometry through the load cycle results in there being a small positive mean stress. If the tensile load limit is slightly reduced it should be possible to eliminate this effect. However the adjustment is usually too coarse and the creep ceases to be tensile and becomes compressive (39).

Benham and Ford (35) described the progressive necking of copper specimens subjected to fully reversed cyclic loads sufficient to produce failures between $\frac{1}{4}$ and 50,000 cycles. They also measured the 'cyclic-strain-induced creep' for various levels of applied load, both under cyclic tension and fully reversed loads and reported that the direction of the induced creep was extremely sensitive to the mean load value.

Further investigations by Feltner and Sinclair (37) attempted to differentiate between cycle-dependent and time-dependent creep. Static and cyclic behaviour of copper, aluminium and cadmium subjected to repeated loading at room temperature and at $-196^{\circ}C$ were studied. Their results suggested that cyclic creep is cycle-dependent in the homologous temperature range $T/Tm < 0.25$, cycle- and time-dependent in the range $0.25 < T/Tm < 0.5$ and time-dependent in the range $T/Tm > 0.5$, where Tm is the melting point temperature. Transcrystalline fractures were observed during cycle-dependent creep while time-dependent failures were intercrystalline. Steels were not investigated.

Subsequently Wood (91) introduced creep into a high strain fatigue cycle and observed reduction in life with increased creep time per cycle. Low-carbon high-manganese pressure vessel steel was strain-cycled at 350°C with a range of creep periods between 1 min and 24 hrs in the tensile part of the cycle. The results confirmed that the failure was cycle- and time-dependent at T/Tm = 0.35.

Coffin (36) subjected specimens of annealed aluminium to push-pull loading at room temperature between fixed stress limits so that a constant mean stress was developed. The rate of shift of the loop with cycles was found to be an insensitive function of the mean stress, being practically constant. The shift of the loop was in the direction of the mean stress. For zero mean stress the hysteresis loop shift was extremely unstable, exhibiting a very wide scatter. It was noticed that the creep direction was not dependent on the direction of the first loading.

2.3.2.4 Changes in Plastic Strain Range

During load cycling the strain range is free to vary. The changes in total strain range and plastic strain range can be derived from the hysteresis loops recorded during the tests.

Both hardening and softening, decreasing and increasing strain ranges respectively, have been reported for mild steel by Benham and Ford (35). Dubuc (40) reported that for SAE 1030 and A 201 steels total strain range increased during cycling at higher stress levels but remained sensibly constant during cycling at lower stress levels.

2.3.3 Strain Cycling

Reversed axial strain cycling tests were first described by Liu, Sachs and others (41, 42, 43). Tests at large strain amplitudes - fatigue lives as short as 7 cycles were obtained - on 24 S-T aluminium alloy were performed. The authors found that very rapid hardening occurred in the first and second cycles but thereafter the hysteresis loop remained practically stable. The effect of pre-compression of 0.2% and higher immediately before cycling was also investigated and found to reduce endurances considerably.

Further tests on the same material were performed by D'Amato (44) and it was observed that a logarithmic plot of strain range/cycles to failure gave a straight line.

A very comprehensive investigation of the low-cycle fatigue behaviour of a heat-resisting stainless steel, AISI 347, an OFHC copper, and a 2S aluminium by Coffin and his associates (45, 46, 47, 48) confirmed that there was a relationship between plastic strain range and cycles to failure as described earlier (Section 2.2.1 equation (i)). This relationship was also derived independently by Manson (49).

As might be expected, when the total strain range $\Delta\varepsilon$ is large elastic component $\Delta\varepsilon_e$ may be neglected and the Coffin relationship becomes:

$$\Delta\varepsilon N^{\alpha} = \text{constant} \qquad \text{(ii)}$$

This has been confirmed experimentally (50).

Depending on the initial state of the material, softening or hardening can occur in strain cycling. As a specimen softens the stress or load range decreases and as it hardens the reverse occurs. The rate of hardening depends on the applied strain range; generally rapid hardening in the early cycles is followed by a levelling off of the hardening curve before final fatigue fracture.

Cyclic softening of prestrained material has been reported (45, 51). When the various degress of prestrain were compared, it was found that, regardless of the material's initial condition, the same stress range was eventually achieved in all tests. This phenomenon of a uniform cyclic condition was also reported by Dugdale (52).

Raymond and Coffin (53) have compared the change of stress-range for the same cyclic strain-range in an annealed and a hardened specimen of cold-drawn aluminium 1100. After approximately 200 cycles practically the same stress range was reached whatever the initial condition. The authors suggested that from these results it could be concluded that the nature of cyclic strain is quite different from that of monotonic strain and that strain cycling eventually wipes out the effects of prior deformation.

Smith et al. (54) have subjected a large number of different materials to reversed strain cycling tests in the fatigue range 0 to 10^6 cycles. The shape of the waisted specimens as well as their minimum diameter varied according to material availability. For the same reason separate buttonheads screwed on to the specimen bodies had to be used. Diametral strain was measured by Tuckerman optical strain gauges.

The materials were found to be metallurgically stable throughout their fatigue lives and the Coffin relationship was confirmed for all materials.

2.4 Influence of Various Parameters on Load and Strain Cycling Fatigue Behaviour

2.4.1 Mean Strain

Sachs (55) and his associates showed that equation (i) is only suitable for completely reversed strain cycling. Using the results of a number of tests on various pressure-vessel materials, the aluminium alloys 2024-T4 and 5454-O and the steels A 302 and A 225, Sachs showed that in general:

$$N = \left[\frac{\varepsilon_f^1 - \varepsilon_o}{\Delta\varepsilon}\right]^{\alpha'} \qquad \text{(iii)}$$

where $\varepsilon_o = \frac{1}{2}(\varepsilon_{max} + \varepsilon_{min})$ the mean strain or prestrain,

$\Delta\varepsilon$ is the total strain range,

ε_f^1 is the apparent fracture ductility, and

α' is close to 2.

The apparent fracture ductility is obtained by extrapolation of the log. $\Delta\varepsilon$/log. N curve to $N = \frac{1}{4}$ cycle and is not necessarily identical or even very close to the fracture ductility as measured in a monotonic tensile test.

It was shown experimentally that the effect of mean strain faded out rapidly for fatigue lives greater than 10^4 cycles.

Strain-controlled tests as originally suggested by Sachs (42, 43) and Pian and D'Amato (56) were developed by Sachs and Weiss (25). They found that the mean strain in the plastic range acts as a prestrain and reduces the fracture ductility of the material.

Subsequently Sessler and Weiss (57) conducted additional tests on the pressure-vessel steels A 302 and A 225, and confirmed that a positive mean strain or prestrain in tension lowered the fatigue life since the fracture strain available for strain cycling was reduced by the amount of the prestrain.

Coffin (53) later confirmed that the application of prestrain on an AISI 347 stainless steel had the effect indicated by equation (iii).

2.4.2 Biaxiality

Weiss et al. (58) conducted strain cycling tests in reversed bending on an A 302 steel and two aluminium alloys. Specimens of various width/thickness ratios were tested. Stress biaxiliaty, which is dependent upon this ratio, increased nearly linearly and reached a maximum when the width/thickness ratio was approximately 8. The number of cycles to failure decreased with increasing biaxiality. The effect was practically negligible at 10^4 cycles.

Various types of fatigue cycles were performed on plate-type cantilever specimens at Lehigh University (59). A uniform stress ratio of 2 to 1 was used throughout the programme. The Babcock and Wilcox Company (60) conducted a comparable programme of equibiaxial tests in a specially developed hydraulic machine using three typical pressure vessel steels, A 201, A 302 and T 1.

2.4.3 Stress Concentration

At a notch root the presence of the plastic deformation is particularly marked in low-cycle fatigue tests where applied stresses are very high. Plastic deformation influences the original stress concentration in the following ways:

(a) Notch geometry will alter during cycling;
(b) The original stress peak will be distributed; and
(c) Work hardening in the notch will result in non-uniformity of the specimen material and material properties will change during cycling.

In load cycling it is generally found (40, 61, 62) that the S-N curve for notched specimens starts on or slightly above the curve for plain specimens. The shallow sloping portion of the curve tends to be shorter than for the plain curve and divergence between the two curves increases with the number of cycles to failure, indicating the relative insensitivity to stress concentration in plastic cycling.

It should be noted that although a whole specimen may be subjected to load cycling the behaviour of the material close to the notch root may be closer to strain cycling due to the restraining influence of less highly stressed material away from the notch root.

Hardrath et al. (30) derived a formula for the stress concentration factor in the plastic range and showed experimentally that the effective fatigue strength reduction factor K_f and plastic stress concentration factor K_p converge at high stresses.

Weisman and Kaplan (61) in push-pull tests on SAE 4140, 4337 and 4340 steels found very little effect of stress concentration on high stress fatigue. They also pointed out that the unexpectedly large scatter observed in the test results indicated material property variation as much as variations in testing.

Sachs et al. (63, 64, 65) reported on the influence of notch geometry in a programme of comparative testing of high strength steels. It was noted that cracks appeared early in the life of the specimen and propagated at a nearly constant rate over the major part of that life.

Notches appear to have a more serious effect in strain cycling than they do in load cycling; the fatigue strength reduction is maintained much farther into the high strain region, sometimes even down to very low endurances.

Very little work has been done on the strain cycling of notched specimens in the plastic range. However Bowman and Dolan (66) tested the pressure vessel steels A 225 and

T-1 and reported reductions in applied strain range of up to 50% for notched specimens at an endurance of 2 x 10^4 cycles. For the same applied strain range they found that notching reduced the life from 10^5 to 6 x 10^3 cycles.

2.4.4 Surface Finish

Surface finish is not found to be as important in low-cycle fatigue as it is in conventional low-strain fatigue. In the presence of severe plastic deformation polishing may not delay the initiation of fatigue cracking. However in highly notch-sensitive material the influence of finish could be noticeable (67).

Mackenzie (68) found only a slight improvement in the life of En 25 in push-pull strain cycling tests when the specimen had been polished in an axial direction.

Maclintock (69) also reported negligible effect in a study of the influence of polished and ground surfaces on the strain cycling behaviour of pressure vessel steels.

2.4.5 Test Temperature

The interpretation of high-temperature low cycle fatigue tests is more difficult as mechanical properties show a considerable dependence on temperature and change of tensile strength, yield strength, strain-hardening characteristics and other properties need to be investigated. Creep effects become more significant with rise in temperature, decrease in frequency of cycling and the introduction of hold times.

The mode of deformation also depends on the temperature of the tested material at the time of straining. When the temperature is low relative to the melting point of the material, deformation is predominantly by reversed slip or twinning. At high temperature deformation is far more complex and includes such thermally activated processes as grain boundary sliding and dislocation climb; such modes are strongly time dependent.

The influence of temperature and cycle frequency can be observed in the type of fracture surface obtained. At low temperatures and high frequencies transgranular fractures are obtained while at high temperatures and low frequencies the fractures become intergranular. The change in mode of fracture to one typical of long time creep-rupture tests offers an evidence that creep mechanisms play an important part in the fatigue failure process at high temperature (9, 70, 71).

A majority of materials show a decreasing fatigue life with increasing temperature just above room temperature; a minority show increasing fatigue life. This behaviour is attributed to the effects of strain ageing and stress relaxation. In the minority case the fatigue life first increases and then decreases as temperature rises further.

Johansson (72) tested three steels in alternating bending at 20°C, 300°C and 500°C. Rather unexpected results were obtained for the 18% Cr 8% Ni steel; endurances at 300°C were better than at 500°C but room temperature endurances were lower than both. For high strains at low frequencies additional effects due to creep had to be considered and curves showing the load relaxation at constant strain were presented. This relaxation was at first rapid but generally settled down to a steady rate after a number of cycles.

Weiss et al. (58) investigated the effect of test temperature on A 302 steel and 5454-0 aluminium in bend strain cycling(in free bending and bending over circular dies.) Three different temperatures were employed. The aluminium alloy registered practically no change from room temperature when tested at 200°C. The steel's fatigue life increased up to 200°C but fell off rapidly thereafter and at 430°C was considerably below the room temperature value.

2.4.6 Testing Frequency

Investigations of the cyclic rate effect have shown that for cycle frequencies less than 1000 cycles/min fatigue strength generally increases with the increase in cyclic rate. At higher frequencies however considerable heating of the specimen may occur and cause reduction of the life thus masking the true effect of the cyclic rate.

Smith et al. (73) compared fatigue results at room temperature and at frequencies of 7, 12 and 1000 cycles/min on aluminium alloy sheet. The range covered lives up to 10^7 cycles. Special guides were used to prevent buckling in compression. All the results at lower frequencies clearly showed shorter lives than at 1000 cycles/min; some tests at 7 cycles/min did not reach even 50% of the lives obtained at higher speed.

Similar results were reported by Oberg and Trapp (74) on magnesium, aluminium and steel alloys at 90 cycles/min and 3450 cycles/min. Lives up to 10^8 cycles were investigated.

Continuation of this work by Oberg and Ward (75) with cycling speed of 2200 cycles/min on steels SAE 4340, 8630 and 2330 ran into trouble with specimen heating during the test. A method of keeping the specimen at room temperature by immersing it in a liquid bath could be objected to on account of environmental influence.

Cycling frequencies up to 63 cycles/min were used by Illg (76) in the study of steel 4130 and aluminium alloys.

Lives between 2 and 10^7 cycles at room temperature were investigated. A special hydraulic testing machine capable of producing sinusoidal and saw-toothed fatigue cycles was developed. The results clearly showed reduced fatigue strength with the decrease in frequency.

Similar general conclusions were drawn by other investigators using reversed bending, rotating bending (65) and at higher temperature in axial strain cycling (77).

Benham (62) recommends cycling speeds between 50 and 100 cycles/min for low cycle investigations for the following reasons:

(a) the generation of excessive heat in the specimen is avoided;

(b) the testing time is kept within reasonable limits; and

(c) frequency effect is minimised.

Taira (21, 22) reported on the effect of two frequencies (1 cycle/min and 0.1 cycle/min) in thermal cycling. Shorter lives were obtained at the lower frequency.

Considerable reduction in life with decreasing frequencies was also reported by Swindemann and Douglas (20) who performed mechanical and thermal cycling at 0.5 cycle/min and 1 cycle in 30 min at high temperature.

Kooistra (27) investigated two pressure vessel steels A 201 and A 302. $2\frac{1}{2}$ in. wide cantilever beam plate specimens were loaded at three frequencies, 12000, 75 and 7 cycles per hour. Constant strain ranges up to 2% were used and considerable reduction in the life with lower frequencies obtained.

Valluri (78) found that the increase of life with rising frequencies was greater at high stresses than at low stresses.

2.4.7 Hold Time

As the time-dependent effects will influence the deformation as well as the resistance of the material to fracture, hold time becomes an important factor at high temperature testing. Significant decreases in the number of cycles to failure have been reported.

Coles and Skinner (70) introduced a hold time at maximum strain during strain cycling at 565°C and found considerable reductions in life. Beyond a certain critical hold time creep effects became dominant causing further reduction; change in the fracture mode was also observed. The results on Cr-Mo-V steel indicated that the Coffin relationship (i) overestimates endurances both at room temperature and 565°C. The expression

$$t\ f^{m} = \text{const.} \qquad \text{(iv)}$$

where f is the cycle frequency,
t is the test duration and
m is a constant for the material (less than 0.5 for creep and close to 1.0 for fatigue),
was found to be in good agreement with the test results.

The effect of hold time has also been discussed by Coffin (12, 47) who used mean temperature 350°C to compare the results of thermal stress cycling with mechanical cycling at a steady temperature (350°C, 500°C and 600°C).

Four hold-times from 6 sec to 180 sec were employed; and applied both at the tension and at the compression ends of the cycle. It was found that the number of cycles to failure decreased with lengthening hold time. Coffin concluded that ductility changes could influence low cycle fatigue test results when the time to failure was comparable with the time to produce significant loss of ductility.

Walker (9) evaluated the influence of hold time in tension only at 510°C in an investigation of various cast steels used for steam turbine shells. Cracks found in some shells had appeared to be caused by the repeated effects of high tensile stresses arising during turbine start-ups as a result of the temperature gradients generated at such times.

A buttonhead specimen, 0.18 in. diameter, was subjected to uniaxial cycling. Specimen strain was calculated from the displacement of the testing machine jaws and it is felt that such an arrangement may have reduced the precision of the measurement. There was also some danger of uneven temperature distribution since the furnace did not wholly enclose the specimen gauge length.

When hold time was increased from 15 sec to 12 hours the cycles to failure dropped by two-thirds. The mode of crack initiation and early propagation also changed from transgranular to intergranular. This modal change suggests that creep plays an important role in high temperature strain cycling when the hold time is long.

In similar tests at present being performed at the C.E.G.B. laboratories at Leatherhead (79) observations of mode of cracking indicate that for hold times longer than 5 hours creep fracture can be obtained.

Tests at the National Gas Turbine Establishment (71) on Nimonic 90 and 11% Cr steel have shown that failures at low temperatures are cycle-dependent and at high temperatures time-dependent. The change from intergranular to transgranular with increasing frequency at high temperatures was again reported. The differences between hold time effects for various types of cycle were also considered.

2.4.8 Geometrical Effects

Effects associated with the necessary slight differences in specimen geometry between the tension and compression ends of a fatigue cycle were investigated by Raymond and Coffin (53).

Annealed and prestrained aluminium 1100 was strain-cycled and changes in hardening and softening studied. From the hysteresis loop measurements the authors concluded that the second order geometrical effects grow in importance during cycling and therefore must be considered. Unequal loads in tension and compression resulting in equal but opposite strains at the minimum diameter produce a stress bias at larger sections of the specimen and lead to progressive increases in diameter at these locations. The progressive change in geometry results in sharper necking and to overcome this the specimens were periodically remachined to restore the original curvature diameter ratio. This led to a considerable extension of the fatigue life.

2.4.9 Metallurgical Effects

Deformation processes involved in the individual grains were investigated by Thompson and Wadsworth (80). They described the process as reversed slip in concentrated bands. If plastic flow takes place in each cycle the process is irreversible and the grain will not be restored to its original shape after the completion of a cycle; temperature and strain rate will contribute to this effect (15).

The effect of grain size was investigated by Baldwin, Sokol and Coffin (81) using an AISI 347 stainless steel. Cylindrical specimens and sheet specimens were strain cycled in push-pull at room temperature. In the cylindrical specimens increase in grain size lowered the fatigue life; in the sheet specimens increase in grain size increased fatigue life. Similar tests were performed by Swindemann and Douglas (20) who confirmed decrease in life for coarse-grained cylindrical specimens.

3. MATERIALS AND SPECIMENS

3.1 Materials

Four cast irons and two cast steels were chosen for the present tests after a number of discussions between B.S.R.A., B.C.I.R.A. and member firms of B.S.R.A. Tables I and II give their code letter, compositions, heat treatment and metallographical reports.

Only two of the eight cast irons previously tested by Pope et al. (4,11) were included in the present test programme: type E as it was most promising flake iron and the nodular graphite iron F as it appeared to have high thermal fatigue strength which might compensate for its low thermal conductivity. The composition of irons E and F was kept almost the same as in Baker and Pope's work. The nickel content of iron F was reduced from 2 to 1 per cent to improve its ductility; the composition of iron E was adjusted to be suitable for the manufacture of large components (iron F is not considered to be section sensitive). These cast irons have very different fracture ductilities and a comparison of their high strain fatigue hebaviour is therefore of considerable academic interest.

A material recommended by B.C.I.R.A. was the brake-drum iron B, which is a large flake graphite iron of a high carbon content (3.8% T.C.) considered particularly suitable for combustion-chamber parts as it can withstand high surface temperatures. This iron has been used in more than 200 small sized engines.

A special austenitic iron A having a 36% Ni content was chosen for its high tensile strength and ductility. This has a low thermal expansion coefficient because of the high nickel content. Small cylinder heads with sections as thin as 3/16" have been successfully cast in it at the B.C.I.R.A.

After discussions with B.S.R.A. member firms it was decided to test a cast chrome-molybdenum steel C which is used for centre sections of tripartite assemblies and a cast mild steel S corresponding to BSS 592 grade B.

All the materials except A and S were supplied in the form of hollow octagonal castings, Fig.3, which were broken up into slabs 18 x 12 x 2 inches. The total weight of each casting, Plate 1, was 9 cwt. Cast iron A was cast in smaller slabs 12 x 8 x $1\frac{1}{4}$ inches to avoid blow holes and cast steel S in slabs 14 x 9 x 2 inches.

The detailed cutting diagram is shown on Fig.4. Every plate was cut into blanks on a band saw and each blank marked according to the position in the plate. The top part of the plate was discarded because of the possibility of blow holes.

Two specimens could be obtained from the thickness of all slabs except material A. Although the specimens were normally cut with their axis parallel to the longest side of the slab, Fig.4A, a few specimens were cut with their axes in the transversal direction, Fig.4B, to investigate the effect of orientation on the fatigue behaviour, Section 6.3.4.

3.2 Specimens

3.2.1 Design Considerations

The advantages of using simple tension-compression specimens are:-

a) A relatively clearly defined uniaxial stress state in the test cross section.

b) The specimen geometry can be chosen to allow continuous measurement of strain in the test section.

c) A failure criteria, such as complete separation of the specimen can be easily defined and observed.

d) The specimen facilitates the study of fatigue and creep, because the testing machine can be made to follow a programmed cycle and long hold times with minimum difficulty.

Two types of axial specimens are generally encountered in high strain fatigue testing: a cylindrical specimen incorporating a finite gauge length and an hour glass shape (waisted) specimen. The shape of the reduced diameter region of the cylindrical specimen is such that the stress concentration is almost non-existent and thus failure occurs in the gauge length. Strain measurement and recording are fairly easily accomplished. This type has been used by many investigators (9, 20, 54). It is also used for conventional tensile testing, c.f. BS 1452: 1965, BS 18: 1962, BS 3688: 1963 standards. The hour glass shaped specimen is without a finite gauge length and only the change of the minimum diameter is recorded. The design of the specimen also aims to eliminate the stress concentrations at the minimum diameter or to reduce them to very low values.

The hour glass specimen is particularly suitable for tests involving larger strains in order to avoid buckling (12, 15, 39, 53, 56). However, buckling can readily be detected from an X-Y plotter trace; it can be observed in Fig.91 during the last few cycles when a large crack developed.

Buckling can be prevented and the rigidity of the axial cycling device improved by the design of a special guiding fixture as used by Weiss and others (57, 82, 83).

There are also certain disadvantages connected with the use of axial specimens, two of these may be mentioned. Plain cylindrical specimens may have plastic strain limited to a certain localized area and thus give an erroneous strain reading over the whole gauge length. On the other hand, the hour glass specimen could give a certain degree of stress concentration in the region of the minium diameter caused by its geometric shape (53).

The ends of the specimen are usually provided with a suitable head, such as buttonhead or threaded cylindrical shank. Special heads can be screwed on (54) or butt-welded on the test section if a shortage of material or an insufficient diameter prevents the manufacture of specimens from one piece.

3.2.2 Specimen Shape

The recommendations in the British Standard BS 1452: 1956 were used as a guide when developing the shape of the present specimens.

The specimen used at room temperature tests is shown in Fig.5, for high temperature testing in Fig.6. The specimen has conical ends. When the grip nuts 5 in Fig. 9 are tightened, the collets 4 which are screwed on the specimen ensure that the specimen sits axially in the holder cones 3.

Both types of specimen have a 1 inch parallel gauge length. It was necessary to use longer specimen, Fig.6, to accommodate a muffle furnace for high temperature tests. This was accomplished by simply extending both shanks, otherwise keeping the geometry of the specimen unaltered.

For the investigation of the stress concentration effects the specimen was provided with a circumferential

Izod V-notch with a sharp radius 0.25 mm, see insert on Fig. 5.

Machining was performed with carbide tipped tools. For grinding the surface between shoulders an aluminium oxide grinding wheel was used for all materials. The notch was also cut with tipped tools and the shape and flank angle checked on a Vickers projection microscope.

4. APPARATUS

4.1 Introduction

In view of the programme outlined earlier the requirements imposed on a low-cycle high-strain fatigue testing machine were:

a) low frequency of cycling (less than 20 cycles/min).

b) push-pull operation ($\pm$ 15 tons).

c) continuous measurement of stress and strain while controlling one or the other.

d) specimen temperature control (up to $450^{\circ}C$).

e) automatic hold time control (0 to 30 min).

It was decided to develop two machines with associated instrumentation satisfying the above requirements, one being suitable for high temperature work.

4.2 Testing Machine (Room Temperature Testing)

Although a considerable amount of experience of low-cycle fatigue testing on a mechanical horizontal straining-frame machine was available (Schenck, Avery), it was decided to explore the possibility of a hydraulic vertical straining-frame machine, Plate 2, for the reasons outlined below.

Although a mechanical machine has the advantage of high stiffness, it has the disadvantages of mechanical backlash, a strictly limited stroke (in commercially available models) and the possibility of clutch slip, etc. An hydraulic machine does not suffer from these disadvantages although it does have the drawbacks of low stiffness and a long 'warm-up' period.

As the cast irons selected for the test programme include completely brittle ($\frac{1}{2}$% fracture strain) and extremely ductile (30% fracture strain) types, the greater adaptability of an hydraulic machine is an overwhelming advantage.

The horizontal specimens testing position has no intrinsic advantages over the vertical position except that it is convenient to hang an extensometer on an horizontal specimen whereas it is necessary to provide some support for it on a vertical specimen. However, it is very important to avoid stress concentration at the point of contact of the extensometer on the specimen in low-cycle fatigue testing (particularly if high temperatures are involved) and the vertical specimen position offers the best hope of keeping the contact load to a minimum. The arrangement for effecting this will be described later.

The vertical position also has the advantage over the horizontal in that observation of all sides of the specimen is much easier.

Fig.7 shows the block diagram of the final arrangement of the machine. It is convenient to consider this in two parts, the straining frame and the hydraulic system. Basic scheme of the hydraulic system is shown in Fig.8.

4.2.1 Straining Frame

The straining frame, Fig.9, consists of two heavy crosshead plates 8 and 9 joined by two extremely rigid columns 6. The lower crosshead plate 8 is carried on the base unit which is constructed of heavy duty angle-irons welded together. The columns 6 are ground to the same length to ensure parallelism of the crossheads; this was checked during assembly both before and after tightening the four main nuts. A double-acting hydraulic cylinder is bolted to the underside of the lower crosshead plate 8.

Each end of the test piece 11 is held in the machine jaw 2 and 3 by a ring collet 4 and a heavy duty nut 5. By tightening the nut the conical end of the specimen is firmly pressed into the female cone of the jaw. The collets are provided with two dowels to prevent turning during clamping.

The lower jaw cone 3 is screwed to the piston rod and the upper jaw 2 to the load cell 1 which is in turn screwed to the centering plate 7.

Great care was taken in the machining of the threads and centering surfaces to maintain concentricity and axiality. The axiality of the upper and lower jaws was achieved in assembly by adjustment of a centering plate which was dowelled after alignment. All the parts are locked in position by auxiliary plates or grub screws.

4.2.2 Hydraulic System

The arrangement of the hydraulic system is illustrated in Fig.10.

All the hydraulic equipment apart from the cylinder is housed in a single control cabinet, Plate 3, in order to keep the length of pipework and number of fittings to a minimum. The oil reservoir 105 stands on $\frac{1}{2}$ in. thick rubber blocks in the base of the cabinet; it has no rigid connection with the cabinet. The reservoir has a large inspection cover, an oil-level indicator and drain plug, and an internal baffle plate. A combined filler-cap and breather 104 is provided on top of the reservoir.

The oil pump 101 and electric motor 103 are mounted on the top plate of the reservoir. The pump is bolted to a heavy angle-iron base which is shimmed to align the pump and motor shafts. Although the coupling 102 (Reynolds chain coupling No.2) can accommodate a certain degree of misalignment, the pump construction is such that even small lateral loads can cause excessive wear of the bearings and gland packing.

Oil is drawn to the pump through a cylindrical microfilter 4 in. below the reservoir low level and a $\frac{1}{2}$ in. n.b. pipe. The pump inlet is threaded $\frac{1}{2}$ in. BSP as, although the flow of oil is extremely small, to avoid suction depression the inlet velocity should not exceed 4 ft/sec.

The Denison Deri pump 101 delivers approximately 3/4 gall/min up to 2000 psi and is driven by a totally-enclosed Brooks motor (3 H.P. 1430 r.p.m.). The pump is of the balanced-vane type, based on the principle that twin wave displacements 180° out-of-phase combine to give a straight-line flow. The pump has two double-lobed rotors, displaced by 90°, rotating in circular stators. Each stator has two diametrically-opposed spring-loaded vanes continuously brushing the rotors and separating the inlet and outlet ports. The construction is such that only one direction of rotation is allowable. The pump must not be allowed to run dry as it relies upon self-lubrication.

On the first machine the pump was found to be too vigorous for some tests and has therefore been modified by providing an external bleed on the delivery returning to the oil reservoir.

A slightly smaller pump was provided on the second machine because of its intermittent operation (to be used for high-temperature and hold-time testing). This pump is driven by an English Electric motor ($1\frac{1}{2}$ H.P. 1430 r.p.m.).

On both machines a long length of pipe is fitted between the pump and the rest of the system to cut down noise and vibration transmission. A pressure relief valve 106 and gauge 108 are attached to the pump delivery pipe to protect the tension side of the system.

The line to the compression side of the cylinder is also fitted with a pressure relief valve 112 and gauge 111. These valves can be adjusted to relieve at anywhere between 500 and 2000 psi. In fact the working pressure was never below 500 psi. and shock waves developed at reversals did not appear to influence the pumping.

Beyond the pressure relief valve is the flow control valve, 119. This valve can adjust the flow between 5 and 1000 in^3/min, and also allows for temperature and pressure variation. The valve can be locked in position.

A further length of pipe follows the flow control valve to provide a second barrier to vibration transmission.

Pressure is applied alternately to the tension and compression sides of the hydraulic cylinder through a solenoid-controlled pilot-operated four-way valve, 109. Although the solenoids are designed for constant operation, frequent switching presents a high performance demand and a considerable temperature rise was noted. The initial surge current was measured and found to be 4.9 amperes while the hold current was only 0.74 amperes. The high surge current was found to have a disruptive effect on the electronic instrumentation and had to be partially suppressed.

The four-way valve also has a connection back to the reservoir and a neutral position (reached when neither solenoid is excited) enabling the cylinder piston to be stopped in any desired position.

Finally sequence valves 113, 114 are fitted in both tension and compression lines as a protective loop in a position close to the cylinder to eliminate 'kick back' on stroke reversal or at the moment of fracture. The action of the sequence valve is to allow flow through its line only when the pressure in the other line has fallen to some predetermined level. The valve is counter-balanced, has a reversed flow and is adjusted by a screw projecting through the control panel. The valve also prevents pressurizing both sides of the cylinder simultaneously through malfunction of the four-way valve.

For the final speed adjustment and smoothing of the stroke reversals a fine needle cone valve 117, 118 in parallel with a capillary tube 116 is provided in each line. Bleed points are provided at high points throughout the system for initial air purging. All pressure gauges are connected to the system through capillary tubing to prevent possible damage from pressure shock waves. The double-acting cylinder 115 has a 6 in. diameter piston and is flanged at the rod end.

All tests were performed at approximately 4 cycles/min. Frequency is controlled by a precision flow control valve and a fine needle valve. The control obtained was found to be precise enough to give zero movement of the piston and maintain any desired load without fluctuation for an indefinite period.

4.2.3 Oil

The hydraulic oil used for both machines was Shell Tellus 27. This oil is highly treated with additives to prevent oxidation and inhibit corrosion. The maximum allowable temperature is 60°C, but in practice the temperature never rose above 44°C.

4.3 Instrumentation (Room Temperature Testing)

4.3.1 Introduction

As outlined earlier the instrumentation has two functions: firstly to control the machine operation in both load- and strain-cycling; and secondly to automatically record the hysteresis loops throughout the specimen life.

It was decided to use electronic equipment for the following reasons:-

(a) high signal magnification and instantaneous range change are readily achieved,

(b) backlash and friction loss can be reduced to a minimum

(c) permanent records are simply obtained by the use of an X-Y plotter, and

(d) relay circuitry can be employed to give completely automatic control.

Signals from a strain gauged load cell or a strain measuring inductance type transducer are fed to a transducer meter for amplification and then to a Messcontactor control meter which operates the four-way solenoid valve when the signal reaches preset limits. The control and recording system is shown in block diagram form in Fig. 11 and the detailed connections given in Fig.12, are described in sections 4.3.2 and 4.3.3. General view of the instrumentation can be seen on Plate 8.

One potential drawback to electronic instrumentation is the long term drift that can occur. Plainly this is a problem in fatigue testing where it may be necessary to run a machine continuously over long periods. However, it was found that the system developed was essentially stable over periods up to three weeks (the length of the longest test undertaken). Stability of the oscillator output of the transducer meter is better than 0.1%.

4.3.2 Load

A course measurement of specimen load can be obtained from the hydraulic system pressure gauges. The main gauge is fitted to the pump delivery pipe and the other two to the tension and compression oil lines. However, for accurate measurement and for control and recording purposes a load cell employing electrical resistance strain gauges was designed and constructed and is mounted in series with the specimen (Fig.13).

The cell's overall length is 6 in. and its base diameter 3 in. It is made of En24 steel (composition 1½% Ni, 1% Cr, 0.3% Mo) which has had a heat treatment consisting of holding at 830°C for one hour, quenching in oil and tempering at 240°C. The cell was machined all over and the central 'waisted' section ground. The heavy cell base, ground at 90° to its axis, rests on the centering plate. A sleeve is fitted as a protection for the strain gauges and associated wiring.

Four 400-ohm matched Tinsley gauges are bonded to the cylindrical central portion. Two, the active gauges, are mounted longitudinally and two, the dummy gauges, transvessely. The four gauges were wired to form a 4-arm bridge, and both gauges and their immediate connections are completely sealed in Araldite to prevent moisture access. The cell is fully compensated for changes in ambient temperature as the gauges in all four arms of the bridge are mounted on an essentially isothermal surface, the wall of the cell.

The calibration curve for the load cell is shown in Fig.14. This was obtained after some preliminary cycling and testing of the gauges and circuitry. A 5-ton proving ring mounted in the straining frame was used for the calibration of both cells. The calibration shows very satisfactory linearity; in fact the linearity is as good as the $\pm$ 1% of full scale deflection quoted by manufacturers of commercial load cells. The calibration was checked at frequent intervals and no significant deviations found. The cell sensitivity is 1.3 mV/V.

The load cell is connected to the transducer meter through a screened cable to eliminate noise and pick-up that might interfere with the smooth working of the control and recording system. The amplified load signal is also fed to the Y-axis of an X-Y plotter, thus giving a continuous record of each load cycle throughout the test.

4.3.3 Strain

As some of the metals tested have a very small fracture elongation the strain measuring system has to be highly sensitive and have a very large magnification. The extensometer has to stay in firm contact with the specimen during the test, and yet not influence the test result by causing local stress concentrations. It must be of a robust construction to withstand a fracture shock.

These requirements are satisfied by an extensometer based on a displacement transducer. The transducer used consists essentially of two small coils surrounding a moving ferromagnetic core. These coils form the two active arms of a bridge energised by 5V at 1 Kc/s.

Movement of the armature changes the inductances of the coils, causes an inbalance of the bridge and produces an output signal proportional in phase and magnitude to the displacement of the armature from its central position. The circuit is shown in Fig.12.

As bought the transducer probe travel was limited to $\pm$ 0.035 in. but a small modification to the internal construction resulted in extending the travel to +0.060 in. to -0.065 in. After recalibration the linear range was found to be $\pm$ 0.055 in. The sensitivity is 1.7 mV/V input per 0.001 in. and linearity within 0.5% of full scale deflection. The transducer characteristics were checked at intervals through the test programme. The calibration curve for transducer No.I. is shown in Fig.15.

The transducer armature is supported by a leaf spring assembly ensuring frictionless travel. This feature is particularly important for measurements of extremely small strains. Many standard transducers employ an ordinary coil spring to support the armature; this is an unsatisfactory design as relatively minute side loads can deflect the probe tip and cause bridge inbalance.

The weight of the complete transducer is approximately 4 oz. It is held in an aluminium-alloy frame, Fig.16, incorporating a spring system to maintain positive contact with the specimen. The frame is in turn supported by a soft spring suspension fastened to the load cell sleeve, Plate 5. The transducer is connected by a flying lead to the second transducer meter and control unit as described earlier (section 4.3.2); with the armature in its central position the force exerted by the probe tip is approximately 3 oz. This was found to be insufficient to significantly influence the test results, no specimen fractured under the probe tip and even after prolonged testing there was no discernible specimen marking.

4.3.3.1 Transducer Meter

The four-arm load cell bridge as well as the transducer half-bridge are connected into the Boulton-Paul Transducer Meter, C 51. These meters energise the bridges at 5 volts and 1 Kc/s. Each bridge output is fed through the appropriate attenuator and a stable-gain amplifier into a phase-sensitive detector, the reference-voltage of which is derived after conversion to D.C. from the 1 Kc/s source energising the bridge circuit meter. Accuracy is 1% of full scale deflection for any value between 0.01% and 100% bridge supply.

The D.C. output of the detector is $\pm$ 5.0 mA into 300 ohm load and is fed to an X-Y plotter and either a moving-coil meter or the Messcontactor control meter.

For faithful reproduction of a dynamic signal a carrier wave should be approximately five times the frequency of the signal. As the bridge operates at 1 Kc/s it is possible to cycle at up to 200 c/s without distortion of the signal. The frequency response of the sharp cut-off filter is 0-200 c/s.

4.3.3.2 An Ekco E 193 - Recorder

The plotter characteristics impose the principal limits on the maximum load and strain rates that can be recorded.

The maximum carrier and pen speeds are respectively:

(i) X-axis full scale deflection, 500 milli-seconds;
(ii) Y-axis full scale deflection, 200 milli-seconds.

For satisfactory operation load and strain rates should not exceed values corresponding to 20% of the above speeds.

As the X-Y plotter employs a 50 c/s chopper input amplifier it is necessary to obtain a fully smoothed D.C. signal. To this end a filter was incorporated in the circuit as shown in Fig.17. The D.C. input to the plotter is recorded as a voltage drop; 50 and 100 mV/in. were the most frequently used input ranges. The input leads are screened to minimise 50 c/s hum pick-up.

Microswitches were mounted on either end of the carrier track to cut out the plotter should the strain be sufficient to cause the carrier to travel to either end. By this arrangement the plotter will automatically switch off when the specimen fails, and so prevent damage to the carrier.

4.3.3.3 Automatic Cycling

Automatic cycling is achieved by feeding the load or strain signal to a transistorised Messcontactor controller which in turn controls the 4-way solenoid valve in the hydraulic circuit.

The Messcontactor controller comprises two units, a moving-coil meter and a relay device. The meter range is the same as that of the transducer meter from which the signal is fed and is ± 5.0 mA. The desired control limits are set up on the meter scale by means of adjustable pointers. These pointers can be positioned anywhere over the whole scale.

The actual switching is initiated by photocells to eliminate the need for any mechanical contact with the indicating pointer, thus there is no danger of interference with the measuring function. The indicating pointer is fitted with a shield which cuts off the light to the photocell when the control limit is reached. The change in resistance of the photocell is used to fire a cold-cathode thyratron which in turn energises a relay controlling the solenoid valve. The two limit photocells have separate thyratron, transistor amplifier and relay circuits. Switching accuracy is better than ±1% full scale deflection and the response time is of the order of a few milli-seconds. A cycle counter is attached to the relay unit.

4.3.3.4 Safety Devices

Automatic cut-outs were fitted in series with the solenoid valve to operate on fracture in tension or in compression. Although it is not normally to be expected that specimens will fail in compression, it is possible (and was occasionally observed) for the specimen to fail at the maximum cyclic load just as the piston movement is reversed.

A third cut-out is fitted on the base of the testing frame to switch off the pump motor should the piston drive to its lowest position.

4.4 High Temperature Equipment

4.4.1 Introduction

The second machine was designed for high temperature testing. Apart from the actual heating equipment certain modifications were found to be necessary to adapt the machine and instrumentation as described above.

Although it had originally been hoped to use a single oil pump for both machines, preliminary trials showed that specimen failure in one machine could transmit a shock wave through the hydraulic system and influence the loading on a specimen in the second machine. In consequence two pumps were used although it was not thought necessary to have more than a single oil reservoir. The steady state temperature of the oil was found to be 50°C with two machines working at maximum pumping pressure compared with 44°C with one machine.

4.4.2 Testing Machine

Although the design of the machine is basically the same as described in section 4.2.1, it was found necessary to incorporate a forced-circulation water cooling system to protect the load cell and piston rod from excessive temperatures. A special distance piece is inserted between the load cell and the top jaw and provided with 6 coils of $\frac{3}{8}$" n.b. copper tube. A slightly elongated lower jaw is provided with 2 coils of copper tube. The coils are connected in series and permanently attached to the cold water supply by a reinforced plastic hose. With this arrangement the temperature of the upper end of the piston rod was 45°C maximum and of the load cell was 37°C maximum. A 1 in. diameter hole is provided in the centre of the top crosshead to give access to the inside of the load cell. This could be used to give additional cooling of the load cell should a higher temperature test be attempted.

To accommoate the extra cooling equipment it was found necessary to extend the columns from 20 in. to 26 in. The hydraulic cylinder has a 8 in. travel (5 in. travel on first machine) and is fitted with a tail rod, but is otherwise of identical construction to that used in the first machine. This tail rod resulted in a slight simplification in the hydraulic circuit since tension and compression oil volumes were equal and only one valve, 112, was necessary to regulate the flow.

4.4.3 Heating Equipment

It was required to hold the specimen temperature at 450°C throughout the test and to have zero temperature gradient over the whole gauge length.

A recently developed heating tape was used in the preliminary trials. It is claimed that flat tapes give a heat transfer efficiency twice that for conventional round wire heaters. Correct application, which is extremely simple, will eliminate hotspots. It had been hoped to wind this tape around the specimen and so economise on space and give excellent access for the extensometer. However, it soon became apparent that the large masses of the jaw nuts were acting as heat sinks and the best tape presently available could not raise the specimen temperature above 340°C.

In consequence a cylindrical furnace with heating elements placed parallel with the specimen gauge length was developed (Fig.18). The elements are double-wound, the pitch diminishing towards the lower end, and inserted in silica tubes to give an even radiation. The furnace is made in two halves each having resistance of 32.5 ohms, and is provided with appropriate openings for the extensometer probes and thermocouples, Plate 6. The outside of the furnace is covered with aluminium foil and the space between the wall and the silica tubes is filled with asbestos wool. A thick asbestos sheet covers the ends of the furnace.

A thermocouple is firmly fixed to the bottom part of one silica tube to serve as a temperature controlling element. Two other thermocouples are attached to separate points on the specimen surface. All three are NiCr/NiAl and have 4 ft leads. This type of thermocouple gives a high output, yields accurate readings and is suitable for temperatures not exceeding 1100°C. As the steady temperature was $450^{\circ}C$ it was unnecessary to give the thermocouples protective sheaths.

A standard potentiometric recorder is used to continuously record the output of one specimen thermocouple. This instrument operates on an automatic null balance system; the unbalance current is applied to the winding of a motor which drives the slide wire contact so as to reduce the unbalance. A 0°-$600^{\circ}C$ temperature range corresponds to 25 mV; sensitivity is 0.1% and calibration accuracy is 0.5% of full scale deflection (FSD). The chart speed is 1 in. per hour.

The second specimen thermocouple is attached to a Cambridge indicating controller used solely as an indicator. It was originally intended to use the Cambridge controller for temperature control but the on-off action and 10 second delay between each sensing caused excessive temperature fluctuation. Therefore it was replaced by a Ether Transitrol controller and a saturable core reactor which operates on a stepless control method Fig.19. In particular the signal from the furnace thermocouple is fed into a sensitive galvanometer and displayed as temperature. The indicator-pointer of this galvanometer is fitted with a flag which can pass freely between a light bulb and a photocell which are mounted on a control-arm. The control arm can be pre-set to the required temperature. When the flag passes between the light bulb and the photocell, the output of the photocell is gradually reduced. This output is amplified by the magnetic amplifier which in turn controls the degree of the saturation of 1 KVA saturable core reactor. The output of the reactor controls the supply of power to the furnace.

The sensitivity of the galvanometer is 100 μA F.S.D. and that of the temperature control is 0.1%. A constant voltage transformer stabilizes the mains supply to the

Magnetic Amplifier and the Ether controller. The amplifier gives a maximum output of 30 watt at 160 V DC across a 850 ohm load. To reduce the time taken to reach equilibrium, the mains voltage input of the reactor was reduced from 200 V at the start-up to about 155V. This reduction was achieved with a Variac connected in series with the furnace heater and another resistance R which was required to keep the current at an acceptable value. The furnace temperature of 567°C corresponded to the specimen temperature of 450°C. The temperature variation during testing was found to be less than ± 1°C. A typical temperature-time record is shown in Fig.20. During running-in of a new furnace which lasted about two days, the temperature was slowly increased up to the maximum to avoid cracking of the furnace walls. A simple operational check of the reactor was developed and periodically repeated. When the flag was passed upscale between the light bulb and the photocell, the saturable core reactor should reduce the furnace voltage from 160V D.C. to 16V. This reduction which is required to maintain a stable control can be adjusted with the resistance R, Fig.19.

4.4.4 Load Measurement

Although the original load cell (see 4.3.2) had a satisfactory performance it was decided to develop a new cell with higher sensitivity. To obtain this a semiconductor gauge made from a single silicon crystal was used. Silicon has a very high piezo-resistance and therefore exhibits a gauge factor up to 200. This eliminates the need of amplification of conventional resistance strain gauges.

As there was little information on the behaviour of semiconductors as load-cell elements or on their reaction to tensile or compressive cycling the development of this cell offered the opportunity of gaining much valuable experience.

The physical design of the cell is similar to that of the earlier one and a full bridge circuit is used. The gauge resistance is approximately 130 ohms and the experimental gauge factor is 110. The length of the silicon crystal is 5 mm; and connections are made through nickel strips. The soldering of the nickel strip connections must be undertaken with great care as the nickel itself is joined to the silicon by gold wire. The gauges were stuck to the cell surface with Araldite which was cured at 100°C for 24 hours. The whole gauge and connection assembly was covered with more Araldite as a waterproofing. It was necessary to avoid temperature fluctuation during operation so tests were never started before steady state had been achieved. If this is not done serious zero shift can occur as silicon gauges are very sensitive to temperature change. These temperature changes could also influence the gauge factor. For the change of 20°C the gauge manufacturers, Langham and Thompson quote 2% change in sensitivity. The maximum measured temperature difference between the loadcell and the room temperature was 12°C. Additional compensation of the thermal effect was achieved by appropriate matching of 2 positive and 2 negative gauges in the full bridge network. This arrangement combines maximum strain sensitivity with minimum temperature sensitivity. The sensitivity of this load cell was found 50 times higher than that of the original one.

4.4.5 Strain Measurement

The strain-measuring equipment used in the high-temperature tests, Plate 6, was the same as that used in the room-temperature tests with the following exceptions:-

(i) The steel probe tip of the extensometer is replaced with $1\frac{3}{4}$" long ceramic tip passing through the furnace wall.

(ii) A heavy asbestos sheet is placed in front of the transducer to protect it from the heat of the furnace.

(iii) Extension arms are fitted to the transducer holder to clear the furnace sides.

(iv) A compression spring between the holder and the furnace ensures positive contact of the transducer and the specimen surface.

4.5 Hold-Time Equipment

4.5.1 Machine Modification

The high-temperature testing machine was modified to enable specimens to be held at maximum or minimum strains during cycling, Plate 4.

A $1\frac{1}{4}$ in. thick steel plate was attached to the end of the piston rod and held in position by the bottom jaw screwed down on to it. Four one inch diameter studs were screwed into the machine base plate; and two nuts screwed on to each. As shown in Fig.9 the position of these nuts on the studs governs the maximum and minimum strain positions of the piston.

4.5.2 Instrumentation

The hold-time instrumentation is shown in Fig.21.

Two process timers are incorporated in the control circuit; one for tensile and one for compressive load hold-time. The timers' range is 30 min. and the desired hold time is set on a one-way dial. Repeat accuracy is claimed to be 0.25%. The minimum setting is 60 sec.

Each timer, Fig.22, consists of a synchronous motor driving a friction clutch ring. When the strain limit is reached the motor is energised through a relay. Simultaneously the clutch ring engages the elapsed time indicating pointer which is then driven towards the zero position. When this is reached the pointer operates an actuator connected through the amplifier to the solenoid, and the oil flow is reversed in the usual manner.

A double-pole double-throw switch is fitted in the circuit to enable the timer to be cut out without stopping cycling. The two timers are provided so that the maximum and minimum strain hold times can be separately set. If the two hold times were always to be the same a single timer could be used.

It would be possible to restart the timer before the set hold time has elapsed because of minute strain fluctuations. This danger is avoided by shorting the circuit as marked in the wiring diagram Fig.21.

5. EXPERIMENTAL PROCEDURE

5.1 Calibration Methods

The testing machines and instrumentation were calibrated after assembly and periodically thereafter. All calibration values are shown in Table VI.

5.1.1 Axiality

Two sizes of plain specimens, 0.564 in. and 0.75 in. diameters, were used. Three wire strain gauges were attached to the specimen axially and 120° apart and the specimens loaded elastically. No difference was detected in the separate readings taken from each gauge. The check was repeated after turning the piston through an arbitrary angle; the readings were again identical.

5.1.2 Load Cell

The load cell was calibrated firstly in a 50-ton Denison testing machine and then with a proving ring *in situ*. The resulting calibration curve is shown in Fig.14.

The non-linearity to full scale deflection is well within 0.5%. Apart from zero setting at the beginning of the test no external balancing was necessary.

5.1.3 Transducers

The displacement transducers were calibrated against a Zeiss drum micrometer head and slip gauges, Fig.15. Temperature in the laboratory automatically controlled to between 20°C and 25°C did not affect appreciably the results of room temperature tests. The high temperature extensometer was mounted on an unstrained specimen as shown in Plate 7 for a period of one week. The observed transducer movements of 1.5×10^{-5} in. including drift are very small compared with the lowest diametral strain range of 0.1%. A quick check calibration was performed before each test.

The non-linearity of both probes was not more than 0.5% full scale deflection (F.S.D.). Also stability checks were performed over the period of 24 hours. The drift at room temperature amounted to 0.1% F.S.D., at 450°C it increased to 0.6% F.S.D. Similar tests on the X-Y plotter over the same period did not show any appreciable amount of drift, which was to be expected in view of a comparatively low range of sensitivity used. The movement of the carrier is 0.5 sec for F.S.D. and the pen response in the Y direction 0.2 sec. The calibration of both axes was performed periodically, and adjusted as and when necessary to the prescribed value of 4.1" deflection at 200 m V/inch.

During the cycling, the overall control of the load and strain ranges was better than 0.8%.

The effect of large capacitive out-of-balance was also checked. This kind of disturbance could occur for certain positions of the probe tip and when longer leads were used. Under such a condition the bridge output signal could contain a large quadrature component. The effect can be partially nullified by readjustment of the measuring equipment or by connecting a small condenser in parallel with the appropriate bridge arm. The maximum tolerable inbalance is 1000 pF for 50 ohm gauges.

5.1.4. Connecting Leads

The insulation resistance of the system was as high as possible to minimise pick-up of other currents (particularly the solenoid current pulses). To this end the leads were taken away from the machine as directly as possible.

The actual lead resistance was low in comparison with the strain gauge resistance. The leads between the gauges and the meter were as short as possible. A PVC-covered 3-core cable with 14/.0076 conductor was adopted; and the lead resistance was measured as 0.37 ohms over 10 yards. Although this resistance was negligible compared with the 400 ohm gauges used, the cable length was limited to 2 yards with the meter placed close to the machine. For the high temperature machine the siting of the additional equipment necessitated a 4 yard cable.

The leads could also introduce a fixed series resistance into the active arms of the bridge causing an apparent reduction in gauge factor. Recalibration *in situ* allows for discrepancy as well as for the correction necessary to account for the X-Y plotter scale.

5.2 Testing Methods

5.2.1 General

Since materials subjected to cyclic plastic deformation may strain harden or soften (12,40) particularly during the first few cycles, it was necessary to develop a procedure for setting the strain or load limits before any force was supplied to the specimen. The influence of irregular loading, change of frequency, etc. could impair the test results. Machines operated by limit switches with indirect triggering require a number of adjustments during the test (35).

As the machines were designed for both load and strain cycling, it was necessary to control the hydraulic system either from the load or from the strain limits according to the type of test. A few preliminary tests were carried out in order to determine overshoot on reversals, time delay, and speed of cycling. In view of the low cycling speed a minute amount of overshooting was easily adjusted by the appropriate advancing of the limit pointers. The time delay at the reversal points was considered negligible.

5.2.2 Procedure for Setting up and Running the Test

The specimen was examined visually and measured with a micrometer. It was then mounted in the bottom jaw and firmly locked in position. The transducer meter in the load cell circuit was then switched to the maximum sensitivity and the specimen was moved hydraulically into the position with the top jaw. The top nut was tightened and a careful check was made to insure zero load on the specimen.

The extensometer was mounted and adjusted to the middle of its mechanical and electrical ranges. A large range of the zero setting provided on the transducer meter enabled easy compensation. To simulate loading of the specimen the transducer meter was unbalanced by moving a potentiometer and the output of the meter was fed into the messcontactor-controller and X-Y plotter. When the signal on the X-Y plotter reached the required limit, the messocontactor was adjusted to give reversal. The same procedure was used for compression and tension. The appropriate valves were then adjusted to produce oil pressures in tension and compression, sufficient for the machine to reach these preset limits. The stress-strain hysteresis loops were continuously recorded on the X-Y plotter.

The life of a specimen was taken as the number of cycles to break the specimen in two parts. When complete fracture occurred, the machine was switched off by a microswitch which was mounted below the lower jaw. Microswitches were also mounted at the extremes of the table travel (X, i.e. strain axis) to switch off automatically the X-Y plotter when the specimen fractured. The detailed operational instructions are given in the Appendix.

5.2.3 High Temperature Testing

The method of inserting the specimen in the jaws was the same as for room temperature tests. Two thermocouples were clipped on the gauge length, one of them as near as possible to the probe tip. The furnace was then placed in position and the extensometer adjusted, taking into account the necessary compensation for thermal expansion which amounted approximately to 0.012". Since the setting of the strain limits is very sensitive to the temperature changes, a good temperature control is essential. The saturable core reactor allowed for the control within a very narrow band of $\pm$ 1°C (BSS1686:1950).

The temperature control is operated in the following manner:-

1. Set the instrument set-point to the desired temperature.
2. Set the instrument proportional band to maximum width.
3. Switch on.
4. Full voltage will be applied to the windings and the temperature will begin to rise. When the instrument pointer passes the set-point the instrument will begin control.
5. When the system has reached a steady state (within approx. 3 hrs), the proportional band is gradually reduced until the minimum bandwidth at which stable control can be maintained, is obtained.
6. Final adjustment is made to the set-point to bring the indicating pointer to the desired temperature. The reason for obtaining the smallest possible bandwidth is because this corresponds to the minimum 'offset' that can follow a load change.

5.2.4 Hold-Time Tests

Hold-time tests are set up in the following manner:-

1. The strain limits are set in the same way as for ordinary strain cycling.
2. The solenoid valve is energised and pressure slowly built up, compressing the specimen.
3. When the messcontactor-controller reaches the limit pointer the first timer is started automatically. The four upper nuts are then screwed down to prevent the $1\frac{1}{4}$ in. plate, and thus the piston, moving higher and increasing the compressive strain.
4. When the predetermined hold-time has elapsed the load is reversed and the piston and plate move down to the maximum strain position.
5. When the messcontactor reaches the other limit pointer the second timer is started and the bottom four nuts adjusted in similar manner.

When the two sets of nuts are correctly set the minimum pressure to hold the piston plate against each set of nuts during the hold-time is adjusted on the relief valves.

6. RESULTS

6.1 Static Tensile Tests

A series of tensile tests was performed at room temperature and at 450°C on fatigue type specimens, Figs. 5 and 6, on the previously described fatigue machines using the standard diametral extensometer. The aim of these tests was to obtain monotonic tensile stress-strain curves under the same conditions as applied during fatigue tests. The influence of machine stiffness and instrumentation response was thus kept unchanged. The load-extension diagrams were recorded on the X-Y plotter, see Fig.23. A certain degree of postyield instability was observed on cast steels C and S during high temperature static tests, Fig.24.

A limited number of static tensile tests was also performed on a 50 tons Denison universal machine using a Lindley extensometer on iron E. The diameter of the specimen was 0.564 in. with 2½ in. parallel gauge length and the strain rate was of the order of 0.005 in/in/min. The ultimate tensile strengths (UTS) of 20.1 tonf/in^2 obtained compares fairly well with the value of 21.0 tonf/in^2 reported by previous workers (4) when it is remembered that the materials were from different melts and the specimens of different geometry.

Although the strain rate in these tests was 0.005 in/in/min as compared with 0.1 in/in/min in the tests on fatigue-type specimens, there was no significant difference in the stress-strain curves.

The results of the tensile tests at room temperature and at 450°C summarised in Table III represent an average value of two or three tests. Curvesof nominal stress plotted against diametral strain are compared at room temperature in Fig.25 and at 450°C in Fig.26. It can be seen that at 450°C the tensile strength of all the materials is reduced, yet the materials follow the same order as at room temperature tests. Larger reductions in the UTS were noticed for cast steels; for nodular cast iron F and both flake cast irons these reductions were comparatively smaller.

Fracture ductility ϵ_f defined as $\log \frac{A_o}{A_f}$ where A_o is the initial specimen area and A_f is the fracture area, increased considerably at 450°C for all materials. Ductility of nodular iron F was about twice that at room temperature, and a smaller increase was observed for flake cast irons B and E. Two different scales are used in the presentation of the diametral strain of cast irons E and B to enable an easier comparison.

The curves for cast irons B and E, Figs. 25, are typical of irons containing flake graphite. They show some degree of curvature from the start of straining which can be attributed to the deformation of the voids containing the graphite flakes (84). The voids represent considerable stress concentration in the matrix because of their shape and corresponding low tensile strength.

On the other hand, nodular irons contain graphite in the cavitities of approximately spherical shape. Stress concentration caused by these cavities is much lower than that caused by graphite flakes and the tensile strength is considerably increased, for example, cast iron F in Fig.25. Quantitatively, the nodular cast iron F shows the highest tensile strength of all tested materials, namely 49 tonf/in^2, followed by steels C, S and iron A in decreasing order. Flake cast irons E and B have the lowest tensile strength of 20 and 9.7 tonf/in^2 respectively.

6.2 Load Cycling

6.2.1 Load Cycling of Plain Specimens

Load-cycling tests were carried out on plain specimens at room temperature. The graphs of nominal stress range (tonf/in^2) against cycles to fracture are given in Fig.27. The values obtained for the static tensile strength are used as starting points for these load cycling graphs.

The shape of these S-N curves is similar to that found by other investigators (39). The "minimum life" reported by some workers (30,31,40) was not observed.

To illustrate typical load-cycling behaviour at very high strain ranges, Figs. 28 and 29 show the first and last cycles (N=50) of a load-cycling test on cast iron A. The diametral strain in this instance was 2.15%. Another three load-cycling tests were performed with identical load limits. Although the load range was kept within 1%, there was a 40% variation in diametral strain between the tests.

As the load limits are kept constant during the whole test, the strain is free to vary due to strain hardening or softening. The form of the hysteresis loop recorded during these tests on cast steel C is shown in Fig.30 and 31. (Other examples of load cycling of nodular iron F can be observed in Figs. 141 and 142; last few cycles of iron E in Fig.143.)

The cycle-dependent deformation behaviour during load cycling is conveniently described under two headings as follows:

(a) the change in width of the hysteresis loop (Section 6.2.2)

(b) the movement of the hysteresis loop along the strain axis (Section 6.2.3)

6.2.2 Change in Width of the Hysteresis Loops

Close examination of the separate hysteresis loops reveals a continuous change of their shape during the test. These changes in the plastic and total strain ranges are presented in Figs. 32-37 for materials A to S respectively. Fig.30 shows a test performed on cast steel C with a nominal stress range of 73.6 tonf/in^2; the failure occurred in 46 cycles, Fig.31. A distinct yielding can be observed in the compression part of the first cycle. Examination of the width of the loops shows a slow increase during cycling.

Some materials show slightly more complicated behaviour during the early part of their cyclic life. Steels C and S as well as the austenitic iron A show initially a large decrease of the strain range, while the nodular iron F shows a rapid increase. In general, the graphs indicate either a steady state or a very slow increase of the strain range, total as well as plastic, during the main part of the life. Failure is characterized either by rapid increase of the strain range (steel C) or by the material failing in a brittle fashion without observable change in the strain range (nodular iron F).

6.2.3 Cyclic Creep

The effect of the gradual movement of the hysteresis loop along the strain axis is shown in Figs. 38-43. Two different scales for cycles (N) were used for some materials to simplify the comparison. The curves describe the shift of the loop along the strain axis as the diametral contraction against cycles to failure.

The results obtained for the cast mild steel S are typical of the cyclic creep behaviour. There is a close similarity between the cyclic creep of this material and a wrought mild steel investigated by Benham and Ford (35). Cast steel C and cast irons E and F show a steady linear increase in strain nearly to the fracture point.

The somewhat different behaviour of austenitic iron A and flake iron B can be observed in Figs. 38 and 39. The maximum value of diametral contraction was reached in the first cycle. In the subsequent cycles the strain range remained unchanged and increased slightly only in the last few cycles before fracture.

Values of the compressive and tensile stresses for a number of tests are shown in Table VII.

6.3 Strain Cycling

6.3.1 Strain Cycling of Plain Specimens at Room Temperature

All the reversed strain cycling tests were started in compression and were carried out at approximately zero mean stress and at a frequency of 4 cycles/min. The results of tests on plain specimens at room temperature are shown in Fig.44 and at 450°C in Fig.45. These graphs show mean curves only for easy reference and present the relationship between the total diametral strain range and number of cycles to failure. Experimental points for each material are shown on Figs. 46-51. Strain values from the static tensile tests were used as starting points for these curves.

Typical hysteresis loops recorded by the X-Y plotter during strain cycling are shown in Figs. 52 and 53. Fig.52 shows the first six cycles of a test carried out on austenitic iron A; strain hardening can be observed during each cycle. A number of cycles immediately preceding the fracture of flake cast iron B can be seen in Fig.53. (A gradual change of the hysteresis loop of cast steel C can be seen in Fig.144.)

The total strain range was set at the beginning of cycling and was controlled from the diametral extensometer. Since the shape of the hysteresis loop changes during cycling, the stress limits and the ratio of the elastic/plastic strain can alter. Fortunately the change of this ratio is extremely small and therefore can often be ignored.

However, stress-range changes are considerably larger. The variation of nominal stress range/cycles is shown in Figs. 54-59. The hardening rate of iron A and mild steel S is comparatively slow, while other materials reach their maximum stress range within the first few cycles. Similarly at failure irons A and S show a slow decrease of the nominal stress range. The values of stress amplitudes obtained from the stable hysteresis loops at half life during strain cycling were used in the construction of cyclic stress-strain curves, Figs. 60 to 65. Similarly half life strain amplitudes from load cycling tests were included for comparison. All the curves are distinctly above the monotonic stress-strain curves obtained in tensile tests at room temperature and at $450^{\circ}C$. These cyclic stress-strain curves illustrate the strain-hardening ability of these cast materials.

The values of the nominal stress range obtained at $\frac{1}{4}$ cycle, $\frac{3}{4}$ cycle and at half life were superimposed on the load cycling curves in Figs. 66 to 71 for comparison with the load cycling results. The stress range data obtained from the high temperature strain cycling were also included; these curves lie considerably below the room temperature results.

Similarly load cycling data can be compared with strain cycling data, Fig.44. Diametral strain range of the hysteresis loops derived from load cycling tests, Figs. 32 to 37, superimposed in Fig.44 gives the same order of merit for all materials; however the converted values are lower than experimental curves because of the cyclic creep which occurs during load cycling.

6.3.2 Strain Cycling of Plain Specimens at High Temperature

The results of strain cycling of plain specimens at 450°C are shown in Fig.45. All materials show a slight improvement in their endurances; this difference is more pronounced for cast irons E and B.

The change of the nominal stress range against cycles is shown in Figs. 72 to 77. Somewhat different behaviour than that at room temperature can be observed. Iron A showed a noticeable increase in the stress range during the main part of the test. Mild steel S failed in a brittle fashion, while at room temperature the fracture was ductile. On the other hand, no sudden failure of the flake cast irons B and E was observed, while at room temperature both irons failed in a brittle manner. Cast steels C and S showed a limited amount of postyield instability in the first cycle, which can be compared with similar behaviour during static tensile test. (A number of representative hysteresis loops is shown in Figs. 145, 146, 147 and 148.)

6.3.3 Notched Specimens

Specimens provided with a notch (Fig.5) were mounted in a similar way to the plain specimens. The extensometer was adjusted on the gauge length well away from the notch.

The effect of notching the flake cast irons E and B is far less prominent than in the case of the other materials as can be observed in Fig.78. It is also interesting to note that the superiority of the cast mild steel S is considerably reduced by stress concentration and for endurances over 10^3 cycles lower values of strain range are obtained than for the flake cast iron E.

The results of tests at 450°C are plotted in Fig.79. All materials show slightly improved endurances over those obtained at room temperature, except for cast steel C where the changes are marginal.

6.3.4 Influence of Orientation

The influence of orientation was studied on one plate of flake iron E. Two series of standard specimens were made, one series cut in the longitudinal direction, the other in the transverse direction of the slab, Fig.4. Tests were performed in strain cycling at room temperature. The testing conditions were kept unchanged for each pair of longitudinal and transverse specimens. Practically identical results were obtained from both types of specimens, Fig.49.

It was therefore concluded that, at least for the flake cast iron E the orientation of the specimen does not exercise any noticeable influence.

6.3.5 Variation between Plates

Generally the tests were planned in such a way, that only specimens made from a particular plate were used for a specific part of the testing programme. However, it was realised that with the growing number of tests more than one slab would be needed to cover completely any part of the investigation.

Three plates of iron E were chosen for comparative testing. Identical tests were carried out on specimens cut from the same plate position in different plates. All the results confirmed adequately that there was no appreciable variation in the qualities of different plates, Fig.49.

A number of tests was also repeated on other materials. This was considered particularly necessary for the austenitic iron A, in view of the smaller size of plates. No significant difference in the results of comparable tests was observed.

6.3.6 Polishing

A number of specimens made from plate No.7 of the flake graphite iron E was chosen to investigate the influence of the polished surface. A Morrison specimen polishing machine with automatic feed was used. A set of standard polishing emery papers up to the grain 400 was applied without coolant. A satisfactory surface finish of the whole gauge length including the shoulder transition was obtained in approximately 30 min. for a specimen.

The results subsequently obtained in the strain cycling tests were essentially the same as those obtained for standard ground specimens. It appeared that any difference in the finished surface as produced was not sufficiently large to influence the results of the tests. In addition, it was realised that the surface of the engineering parts was only polished in very special circumstances. It was therefore decided not to include the polishing in the testing programme. To generalise the above findings, it would be necessary to undertake additional tests on all other materials. However it was felt that iron E was, if not the representative, one of the most important types used.

6.3.7 Start of Cycling

All tests were started in compression. Compression could be considered to represent more realistically the situation in practice, particularly in thermal cycling in C.I. engines.

Again it was much easier to start a test in compression because the natural increase of the cross-sectional area during compressive flow reduces the required sensitivity of the initial load control, whereas the reduction of the area associated with tensile deformation increases the required sensitivity. Furthermore, after yielding in compression, the subsequent half cycle does not show the sharp knee of the virgin stress-strain curve; this again makes the control of the tensile strain easier. Higher fatigue resistance obtained by starting in compression was reported by Dubuc (40), who found longer lives with 2 annealed copper alloys; other materials, comprising steels and Al-alloy did not show any difference. It was therefore considered appropriate to check the influence of the starting direction on the endurance. Some comparative tests starting in tension are shown in table VIII; they indicate only very minor differences. Fig.80 shows the first few loops of the two identical tests on cast steel C, one started in compression, the other in tension. (Another strain cycling test with start in tension on flake iron E is shown in Fig.139 and on nodular iron F in Fig.140.) Specimen life was defined as the number of cycles causing complete separation of the test section.

6.4 Hold-time Tests

Two materials, namely flake iron E and cast steel C were chosen for hold-time tests. The results of a few comparative tests with hold time of 5 min and 10 min, Fig.

81, do not show any substantial difference and it was therefore decided to use 5 min hold times in tension and compression. The tests were started in compression and the conditions closely similar to those at high temperature strain cycling were applied.

The results are again plotted as total diametral strain $\Delta \varepsilon_d$ against cycles to fracture N, c.f. Figs. 81 and 82. Previous results obtained in high temperature strain cycling are included for easy comparison. Lives up to 1800 cycles were investigated. Variation of stress range for cast steel C is shown in Fig. 110, for iron E in Fig. 111.

The hold-time tests on iron E show improved endurances in the whole investigated region. When comparing the results of cast steel C with those from standard strain cycling at 450°C it can be observed that the endurances are better only at very high strains, being noticeably lower at lives longer than 125 cycles.

6.5 Ratio of Diametral to Axial Strain

In high strain fatigue investigations, diametral strains are often measured (15, 39). It is possible to convert the total diametral to total axial strain range $\Delta \varepsilon_{ta}$ by using the equation

$$\Delta \varepsilon_{ta} = 2 \Delta \varepsilon_{td} + \frac{\Delta \sigma}{E} (1 - 2\nu) \qquad (5)$$

where E is Young's Modulus and ν is Poisson's ratio. The derivation of this equation is given in Appendix 10.1, and is based on the assumptions of constant volume in the plastic range, constant values of E and ν and no change in the axial stress range during a test. Although this might be acceptable for materials with a fairly homogeneous structure, cast irons present the problem of a complicated behaviour of dispersed graphite in the matrix. It was therefore considered important to check the relationship of the diametral to axial strain. General view of the instrumentation arrangement for this test is shown in Plate 8.

Standard fatigue specimens of the long type (Fig.6) were used. The diametral strain was measured with the inductance probe fitted with the extended tip to allow free access to the gauge length. For the axial strain a miniature inductance transducer with a free armature assembly was used, Plate 7. The outputs of both transducers were fed to the X-axis of two identical X-Y plotters. Both Y-axes were connected in parallel to the load cell.

Hysteresis loops for diametral as well as axial strains were obtained for all materials for a number of loadings. One representative pair of these loops is shown in Fig.83. The ratio of the diametral to axial strain was readily obtained from calibration curves, Figs. 84 and 85 and plotted against load in Fig.86. It is thus immediately observed that in tension this ratio is generally lower than that measured in compression. Coarse brake drum iron B shows the lowest value of the ratio in compression 0.25; higher values are found in iron E containing medium flake graphite.

The hysteresis loops, Fig. 83, were also used to plot the axial against diametral plastic strain range for all materials at room temperature, Fig.87. Some results of the tests on En25 are also included; they were performed as a check on accuracy of the instrumentation.

6.6 Fracture Appearance

6.6.1 Macroscopic observations

Two typical fracture surfaces were easily distinguished.

Flake cast irons were characterized by a flat fracture in the transversal plane. The surface had a bright appearance and showed a complete absence of any visible plastic deformation. This type of fracture occurred during both load and strain cycling at room and high temperature.

The second type of fracture was observed on some specimens of the more ductile materials, Plate 10. An initiation region in a plane perpendicular to the axis of the specimen could be distinguished from the propagation part and the third part consisting of a necked out portion. This latter part could be well compared with the familiar failure occurring in the monotonic tensile test. The initiation region showed usually a very smooth and regular surface.

6.6.2 Microscopic Observations

It is well known that the fatigue failures of ductile materials change from transcrystalline to intercrystalline and from cycle dependent to time dependent as the ambient temperature is increased. In view of this the fracture surfaces of typical specimens were examined.

The flake cast irons show fractures which follow the graphite flakes, c.f. Plate 9 & 15 in a typical manner of grey cast iron failures. The crack proceeds along the centre line of graphite flake. The same type of fracture occurred for high temperature. The actual path of failure of nodular iron was invariably difficult to determine, Plate 13. In all the observed cases some evidence of a cleavage failure was shown by the subsidiary cracks behind the main fracture path. This type of failure is often observed in nodular irons. Both types of cast steel as well as the austenitic iron have shown clearly defined fractures along the grain boundaries at both room and high temperature.

Microstructures of all the tested materials are shown on Plates 12 to 19 and described in Table II.

7. DISCUSSION

Before discussing the fatigue results, it will be convenient to consider the effect of cyclic loading on the stress-strain behaviour of the test materials.

7.1 Differences in the Properties of Cast Irons in Tension and Compression

The number of materials showing distinctly different properties in tension and compression is very limited. Volumetric changes and different stress/strain behaviour in tension and compression closely connected with the structure of cast materials, particularly flake cast irons, therefore deserve some additional comment.

7.1.1 Tension

The ultimate tensile strengths of all the materials tested are shown in Table III. It is interesting to note that the values at 450°C are lower than those obtained at room temperature. The decreasing order of merit for the materials is F, C, S, A, E and B.

Thum and Ude (86) proposed that as the graphite flakes would not transmit tensile stress, they should be regarded as discontinuities or voids in a steel-like matrix.

Later Gilbert (84) suggested that these voids increase in size when strained in tension. During the his tests the specimen was placed alternately between compression plates and in grips for tensile loading. Approximately 10 discontinuous loading cycles were applied during each test. The programme covered loading in tension as well as reversed loading and the results may be summarized as follows:

The total strain was separated into four components:

1) pure elastic deformation of the matrix
2) plastic deformation of the matrix
3) recoverable strain due to the opening of the voids
4) permanent strain due to volume change of the voids.

At low and medium stresses the lateral strains were not affected by graphite volume changes; they represented mainly purely elastic and plastic deformation of the matrix. At the relatively high stresses the spacesoccupied by graphite were thought to be elongated in the longitudinal direction and the permanent strain was found to be the largest component. The voids caused a decrease of the ratio of lateral/longitudinal strain with increase in longitudinal tensile stress.

On unloading, the recoverable strain is partly elastic and partly due to void closure. The recoverable strain curve is therefore not a straight line.

7.1.2 Compression

It has been shown by various investigators (86) that failure in compression occurs at a stress three to four times the tensile stress; and that the proof stress is much higher in compression.

The investigations of Gilbert (84) suggest that the compressive strains are comparatively unaffected by the presence of voids and the recoverable strain curve is a close approximation to a straight line. In cast iron subjected to alternating tension and compression the voids opened up in tension can be closed again in compression and the original recoverable strain characteristics restored.

Gilbert (85) measured the ratio of total diametral strain to total axial strain of a selection of cast irons and found an approximate value of 0.26. After subjecting the specimen to a number of increasing load cycles in tension followed with similar series in compression, it was observed that this ratio increased in compression but showed a slight decrease in tension.

To summarize: in tension the ratio of diametral to axial strain decreases slowly with increasing stress, mainly due to the growth of voids; in compression the ratio increases with increasing stress and can even exceed a value of 0.5 in the region of very high stresses.

7.2 Cyclic Plastic Deformation

7.2.1 Reversed Cycling

Since the behaviour in tension and compression can differ considerably, the cycling tests described in section 6.5 were performed to obtain the ratio of axial to diametral strain range. The curves of total diametral and axial strain, Fig. 84 and 85, have been prepared from hysteresis loops of the form shown in Fig.83. Each pair of these loops represent changes of the axial and diametral strains with incrementally increasing or decreasing load at room temperature.

These loops were also used to check the assumption of constant volume in the plastic range as implied in Equation (5) Section 6.5. Fig.87 is a plot of the axial $\Delta\varepsilon_{pa}$ against diametral plastic strain range $\Delta\varepsilon_{pd}$ for all tested materials and steel En 25 ($2\frac{1}{2}$% Ni-Cr-Mo) in the as-rolled condition is included for comparison. As explained in section 6.5 the instrumentation presents considerable difficulties, but even if an appropriate allowance is made for experimental error, Fig.87 shows clearly that an assumption of constant volume in the plastic range is not justified for cast irons B, E and F. The most serious deviations are shown by iron B ($\Delta\varepsilon_{pa}/\Delta\varepsilon_{pd}=4$) and, to a lesser extent, iron E ($\Delta\varepsilon_{pa}/\Delta\varepsilon_{pd}=2.64$). Cast steels and En 25 are not far off the ratio 2:1 and the use of constant volume assumption would not be seriously in error.

There are two particularly striking effects of cyclic plastic deformation behaviour. The first is the marked change in nominal stress range (cyclic hardening or softening) which may occur under conditions of strain cycling. The second effect is the large accumulation of plastic strain (cyclic creep) which can occur during the reversed load cycling.

7.2.2 Cyclic Hardening

When a metal is subjected to cycles of plastic deformation between strain limits, the stress range may change significantly after only a few cycles. The terms cyclic strain, hardening and softening are used to describe such increases and decreases in stress range since they are accompanied by corresponding changes of indentation hardness. Generally annealed materials show hardening, while cold worked materials soften.

Kemsley and Paterson (87) and others have shown that single crystals respond to cyclic deformation in a similar way to polycrystals, the rate of hardening depending on the number of available slip systems. Their investigations suggest that the amount of hardening in high-strain fatigue is controlled by the interaction of dislocations with the stress field, while in low-strain fatigue hardening is due to point defects. Wadsworth (88) investigated the saturation of hardening in annealed materials and saturation of softening of work-hardened materials; he suggested that saturation was reached on attaining a balance between newly created and annihilated dislocations.

All test materials showed a certain degree of cyclic hardening at room temperature and at 450°C. Figs. 60 to 65 compare static and cyclic stress-strain curves. The derivation of cyclic stress-strain curves was described in section 6.3.1. Although all the curves are above the respective monotonic stress-strain curves, brittle materials B, E and F show comparatively smaller increase of the stress range than the ductile materials, A, C and S. Cyclic stress-strain curves which are lower than the monotonic curves have been reported by Benham and Ford (35) for cold worked copper. Similar curves, to Figs. 60 to 65 have been constructed by Smith et al. (54) using an incremental step method; Morrow (89) applied another technique consisting of cycling within a gradually increasing and decreasing strain range until a stabilized curve was reached.

It was observed in the present tests that the rate of hardening was significant, particularly during the first few cycles. However, it decreased rapidly and the hardening was virtually complete within approx. 10% of the total life. Examples of the actual X-Y record are shown in Fig.52 for the austenitic iron A and Fig.88 for cast mild steel S at room temperature. Strain hardening of nodular iron F at 450°C is shown in Fig.89. An apparent softening was recorded just prior to fracture for most metals, c.f. Fig. 90, also at high temperature Fig.91. An extremely slow decrease of load was observed in mild steel, Fig.92, which could be attributed to the formation of large cracks during the last few cycles.

It is interesting to compare the above observations of cyclic behaviour of the present materials with the investigations of Benham and Ford (35) who found in particular that:

1) Regardless of control conditions, most of the fatigue life was spent at essentially constant load or strain.
2) After initial transient adjustment nominally same hysteresis loop was obtained for strain or load cycling.
3) The change in hysteresis energy per cycle was investigated in order to find a satisfactory index for hardening but a simple correlation was not found.

In 1952 Polakowski (90) suggested that under cyclic conditions and for a given strain amplitude a metal will reach a particular cyclic hardness value either by work hardening or softening. This has been verified by actual hardness tests on the fatigued specimens. The effect was shown by Benham (39) on cold worked and annealed copper which was respectively softened and hardened to very nearly the same cyclic conditions; similar results were reported by Coffin (47) for a 347 stainless steel.

The applicability of the suggestion of Manson and Hirschberg (54) that metals with $\sigma_{ULT}/\sigma_{YS} > 1.4$ cyclically harden and $\sigma_{ULT}/\sigma_{YS} < 1.2$ cyclically soften, was investigated for all test materials and the results are summarised in Table V. A 0.01% proof stress was used instead of yield stress for the flake cast irons. Since the behaviour of these materials is different in tension and compression, both values are listed in the table. It can be seen that the ratio for all materials is above 1.4. This satisfactory correlation existing between the parameter σ_{ULT}/σ_{YS} and cyclic stress/strain curves, Fig. 60 to

65 may serve as a guide for estimating from tensile tests as to whether hardening or softening may be expected when the required fatigue data is absent. However the actual amount of hardening could not be estimated from the absolute value of the parameter σ_{ULT}/σ_{YS} as can be seen from the presented data in Table V and more complicated relationship would have to be sought.

7.2.3 Cyclic Creep

The phenomenon of cyclic creep was first noticed by Bairstow more than fifty years ago, but considerable interest was only aroused in recent years with the development of low cycle fatigue research. Some investigations performed on ductile materials were referred to in section 2.3.2.3 but there is very litte information available on brittle materials.

Benham (39) described the progressive necking in copper when subjected to fully reversed cyclic loads and measured creep strain for various levels of applied load under cyclic tension and in reversed cycling. He reported on the extreme sensitivity of direction of the creep strain with the mean load; the creep direction was found to be consistent with the sign of the mean stress.

Coffin (36) studied aluminium 1100 in repeated cycling at selected tensile and compressive mean stresses. Starting in tension or compression did not influence the shift direction which was dependent only on the direction of mean stress. For zero mean stress the shift of the loop was extremely unstable, the method of testing being probably one of the causes. Each test was continued for 15 cycles. Improvements of the instrumentation particularly in the region of very low mean stresses were found desirable.

Creep observed during the present load-cycling tests was described in section 6.2.3 for all test materials. A number of true stress values obtained in these tests in reversed load cycling is given in Table VII. The values are greater in tension than in compression. The cyclic creep recorded in Figs. 38 to 43 can be therefore attributed to the presence of a small mean tensile stress. It was shown that even a very small bias occurring during the loading was sufficient to change the creep from tension to compression. A compressive creep curve, Fig.93, was obtained from a test on iron B cycled between load limits +8.1 T/in^2 and -8.2 T/in^2. The diametral contraction decreased steadily from the maximum value reached in the first cycle to the end of the test.

Another test on cast steel C was performed with a slight load bias on the compression side of the cycle. The start of cycling with a distinct yield point and a number of final loops just before failure are shown in Fig.94. At the start true stress in compression was 35.40 T/in^2 and in tension 34.60 T/in^2. Fig.95 shows the movements of the strain limits, total as well as plastic strain range plotted against cycles. Increase of the specimen diameter measured after the failure was 0.0015", the same as the value of diametral strain shown on the X-Y plot.

It can be concluded that very sensitive instrumentation is required for cyclic creep investigations with a small stress bias. Two sources of error may have influenced the accuracy of load measurement in the present tests; one was the drift in the strain-gauge load-cell and the extensometer during the time of the test; the second was a slight difference which might have occurred in sensitivity of the load-cell between tension and compression. Mean stress of 100 lbf/in^2 in tension or compression of the total range of 20,000 lbf/in^2 was found to cause a noticeable shift of the loop (36). If the mean stresses are 0.5% of the maximum stress range, drift and calibration errors can be expected to be of the order of 0.1% of load range, and there can be a 20% error in the mean stress.

An interesting aspect of cyclic hardening was observed during load cycling tests of austenitic iron A, Fig.28. Maximum contraction occurred during the first cycle after which the hysteresis loop quickly stabilized. Accordingly the cyclic creep curve, Fig.38, showed an unexpected sharp peak at the end of the first cycle. Further cyclic creep was not observed until just before fracture. Large initial hardening decreasing to a constant value is shown in Fig.32 where diametral strain range is plotted against cycles. It can be therefore concluded that a large amount of cyclic hardening in the first cycle completely stopped subsequent cyclic creep. This behaviour is not only limited to ductile materials; flake cast iron B, Fig.39, shows also a sharp peak on the creep curve, although the effect is smaller.

In cyclic creep investigations it is also necessary to distinguish between the above described cycle-dependent deformation effect and time-dependent creep. This can be achieved by comparing static creep results with those from cycling at various temperatures and speeds. Work of this type was reported by Feltner and Sinclair (37) and Wood (91) c.f. section 2.3.2.3.

7.3 Comparison of Load and Strain Cycling

No distinction is made between load and strain (deflection) cycling at long endurances, since cyclic stress and strain at below yield values are directly proportional.

However, at short endurances where cyclic plasticity occurs, the type of cycling plays an important part. Although strain cycling is the more realistic type of test it would be extremely useful to be able to relate data for load cycling to those of strain cycling and vice versa. One of the objects of the programme was therefore to compare load and strain cycling for cast materials, for which little data exists.

The decreasing order of merit in which load cycling places the six materials, Fig.27, remains unchanged throughout the tested region and is F, C, S, A, E, B. This order of merit correlates reasonably well with the static tensile strength of the materials, Table III. On the other hand, strain cycling results correlate with ductility rather than with static strength and give an order of merit of the materials as S, C, A, F, E and B. However, if the strain measurements recorded during load cycling tests are used to construct graphs of diametral strain/cycles, then these tests give the same order of merit as strain cycling tests, although load cycling results are slightly lower than strain cycling values. These lower results are thought to be due to the cyclic creep which occurs during load cycling, see Section 7.2.3. It is also interesting to replot strain cycling results on a load basis, Figs. 66 to 71. Although the stress ranges measured in strain cycling are slightly higher than those obtained in the load cycling, the order of merit is the same.

The above tests show conclusively that there is very little to be gained by carrying out load cycling tests unless strain records are taken.

The hysteresis loops show that the load range changes during strain cycling, Fig.52, and that the strain range changes during load cycling, Fig.96. These changes of the shape of the hysteresis loop are rapid and often considerable in magnitude in the first few cycles of the test, say in 10% of the total life. Thereafter a steady condition of stress or strain is reached, and this may be described as a "cyclic condition". The presented results suggest that this could be achieved either by constant load or constant strain cycling.

Finally, it is interesting to compare also the last few cycles before fracture. During load cycling usually only one crack appeared on the gauge length. As the cross section area is reduced as the crack propagates, the cyclic stress is rising and thus speeding the crack growth. The fracture might occur unexpectedly in a catastrophic fashion, Fig.97, or a certain amount of necking could be observed for more ductile materials. On the other hand the initiation of a crack during strain cycling would relax the load and thus decelerate the crack growth. A number of very small cracks was usually observed on the surface of the specimen during strain cycling and the fracture is not catastrophic. A certain amount of load relaxation was recorded for brittle materials, such as shown during the last part of the test on flake iron B, Fig.53. Ductile materials showed a large load relaxation, c.f. Fig.92, of mild steel S.

7.4 Strain Cycling

7.4.1 High Temperature

Although the increase in temperature to 450°C produces significant changes in ductility and ultimate tensile strength (UTS) in most of the materials, c.f. Table III, the order of merit in which strain cycling tests on plain specimens place materials is only slightly modified, Fig. 45.

The only material showing a marginal decrease in the fatigue strength results at 450°C was cast mild steel S, Fig.51. Steels frequently exhibit reduced ductility within a certain range of test temperatures. These changes in the ductility and UTS with temperature are attributed to the strain ageing, and distinct regions of brittleness can be observed. The reduction in endurance is therefore not wholly unexpected. Sachs and Weiss (25) reported similar decrease of the fatigue strength below the room temperature value for an annealed mild steel A302 at 427°C, although a better fatigue strength was found at 204°C, than at room temperature. When comparing this behaviour for similar materials it should be noted that the embrittlement range may considerably vary with strain rate.

Another aspect of the high temperature tests is a comparatively larger improvement of the fatigue strength of cast irons than that of more ductile materials which again will be most probably influenced by the ductility changes. Considerably different behaviour in the failure of flake cast irons at high temperature might be also connected with the increase in ductility. At room temperature tests, irons B and E fractured in a distinctly brittle manner, Fig.55, while at 450°C the failure was progressive, Fig.73.

Nodular graphite cast irons have fairly high tensile strength and higher ductility than flake graphite irons. It was hoped that nodular iron A with the austenitic matrix which favourably reduces the modulus of elasticity would be particularly suitable at high temperature. However, Fig.45 shows clearly that at 450°C the nodular iron F remains superior to the austenitic iron from about 50 cycles up to the lives of 5×10^3 cycles.

7.4.2 Effect of Notches

Mechanical or thermal strain cycling fatigue at low endurances is most likely to arise at sources of strain concentration, which can be found wherever there is a discontinuity of geometry, structure or temperature. That a presence of strain concentration can reduce the fatigue strength very considerably was shown for strain cycling by Bowman and Dolan (66). The effects of plastic deformation in the root of the notch are described in Section 2.3.3. Of particular interest is the work hardening introduced in the vicinity of the root, which will cause non-uniformity of the material and complicate the results.

The introduction of a notch, Figs. 78 and 79, modifies the order of merit in which the strain cycling tests place the six materials, Figs. 44 and 45. A particularly large drop in fatigue strength is shown by the conventional nodular cast iron F when notched, whereas the austenitic nodular iron A is relatively insensitive to notches. The notch sensitivity of both nodular irons decreases when the ambient temperature is increased to 450°C.

This notch behaviour and the fact that iron F has lower thermal conductivity (4) than iron E helps to explain why engine cycling tests (3) indicate that iron E is the better material of the two for cylinder heads.

The differences in strain cycling between plain and notched specimens are shown in graphs of plastic strain range/cycles, Figs. 98 to 103. Although the extensometer was positioned well away from the notch, it is interesting to note that each pair of lines are parallel except for iron F. This and the low notch sensitivity of all materials other than F suggest that cracks initiate at the root of the notch very early in the cyclic life. It could be argued that the strain concentration is relatively insensitive to the strain range within the limits of the present tests.

7.4.3 Hold Time

A medium flake cast iron E and a cast steel C were the two materials chosen for 5 min. hold-time tests at 450°C. They have widely different structure as well as physical properties and the test results could therefore offer some indication on the behaviour and differences between the brittle and ductile groups of materials. The effect of the hold time at maximum strains on the shape of the hysteresis loop of flake cast iron E is shown in Fig.104. A loop obtained during a simple strain cycling test is included for comparison. Both tests were performed with 0.4% total diametral strain range. A representative loop of a hold time test on cast steel C at total diametral strain range of 1.8% is shown as Fig.105.

Creep relaxation taking place at maximum strains can be observed. Ideally the loop should follow the line of constant strain on reaching the point of reversal during the hold time period. This type of cycling could be realised only with a constant strain-holding instrumentation, for which the electronic equipment would be extremely costly. With a simple mechanical arrangement, Section 4.5, the strain holding was not perfectly rigid and consequently the reversal points are slightly rounded.

The effect of 5 minute hold times at maximum and minimum strains on the behaviour of the flake cast iron E can be observed in Fig.81; the hold-time results are consistently above those obtained with simple strain cycling. Fig. 101 shows that the plastic strain range is larger than that measured during standard strain cycling at 450°C; this reflects the influence of creep relaxation at maximum strains. It is interesting to note that the (negative) slope of the hold time curve is close to 0.3, widely different from all other types of cycling, which were near to 0.5.

The hold-time results for cast steel C, Fig.82, suggest better endurances for very high strains than those obtained during standard high temperature strain cycling. However, for lives longer than approx. 125 cycles, lower results were shown. Thus for instance, for the tests performed at the total diametral strain range of 0.5%, the endurance during a hold time test showed a reduction of the value measured in a standard test in the ratio of 3:2. Although the differences in the plastic strain range for the two types of cycling are small, Fig. 100, the tendency of a faster decrease of the plastic strain range with cycles for the hold time tests can be observed, the slope of $\log \Delta\varepsilon_p / \log N$ changes from 0.5 to a value of close to 0.6. A similar even more clearly observable trend is shown in the total strain range results.

The above results suggest that for a given life the permissible strain range is dependent on material ductility if creep is not important, i.e. if the ductility increases with the temperature, then the permissible strain range increases. At higher temperatures with hold time the creep effect tends to reduce fatigue life. The present results suggest that the increase of life produced by the increase of ductility outweighs the decrease of life produced by creep if the hold time is very short. At longer lives and at longer hold times than those tested, the creep effect could well outweigh the increase in ductility.

To summarise, the tests performed on materials E and C at 450°C suggest that there may be a marked change in the number of equivalent strain cycles to failure when a dwell time is incorporated at maximum and minimum strain reversals. Room temperature tests with the same 5 min. hold time, did not show any difference in endurances from those obtained at normal cycling speeds of 4 cycles/min. This suggests that the plastic strain cycling is not the sole mechanism controlling the failure of a metal. The tests with longer hold time (up to 8 hrs) at present conducted by C.E.G.B. Leatherhead (92) suggest that long dwell periods in tension part of a cycle are particularly damaging. Similarly, other investigations (9,20) have also shown that it might be necessary to consider longer lives; the present tests covered endurances only up to 1750 cycles.

It is interesting to compare the results with those of other investigators. The slopes of log $\Delta\varepsilon_p$/log N equal to 0.5 in strain cycling without hold time at room and elevated temperatures were reported by Tavernelli and Coffin (93). Swindemann and Douglas (20) found a tendency towards increasing slope at high temperature and with decreasing cycle frequency. Although the effect of frequency may not be directly comparable with that of hold time, it could serve as an approximation while comparable tests are scarce. Walker (9) used Cr-Mo steel of not very different composition from the cast steel C with hold time incorporated in the tension part of cycle and found again a steeper slope of log $\Delta\varepsilon_p$/log N.

Also Coles and Skinner (70) conducted investigations described in Section 2.4.7 on a Cr-Mo-V steel similar to the steel C and observed reductions in cyclic life and change in the fracture mode from transcrystalline to intercrystalline with increased hold time. Later Barnes and Tilly (71) pointed out that the method of applying hold time is of particular importance and could considerably influence the result of the test. Residual stresses resulting from the plastic deformation during the initial heating period will be redistributed in the subsequent hold time. A testing technique following closely actual temperature and strain cycles should be used.

It can be therefore concluded that further investigations should cover the effect of longer hold times, hold times incorporated in the compression side of the cycle and tests at higher temperature to ascertain the limits beyond which creep phenomenon seriously influence the fatigue resistance of combustion-chamber materials.

7.4.4 Scatter of Results

It is interesting to note comparatively small scatter of results observed during all tests. Scatter of fatigue results has always constituted a serious problem; it could be of considerable magnitude particularly at low strain levels. Noticeably lower scatter in the high-strain fatigue test results than in the conventional low-strain fatigue was reported by some investigators (39). Weissman and Kaplan (61) collected results from a number of low-endurance tests for a variety of steels and found very small scatter. Forest (67) reported on lower scatter in crack propagation than in crack initiation.

The present results support the evidence of a small scatter band in high-strain fatigue testing.

It may be that there is a correlation between plastic strain range and the degree of scatter in the fatigue results. The brittle materials B, E and F have a narrow plastic strain range and small scatter of results while the more ductile materials A, C and S with a higher plastic strain range exhibited a greater degree of scatter. Also crack propagation covering the main part of cyclic life could reduce scatter. Finally, although the non-homogeneous nature of cast materials is well known, it was interesting to observe that fractures occurred invariably in the gauge length and failures in the shoulder transition in the threaded shank or due to the blowholes were not experienced. McClintock (83) investigated scatter by comparing the position of the fracture on the specimen. He was able to estimate the part due to the material non-homogeneity and by improvements in the specimen preparation and testing procedure, noticeable scatter reduction was achieved.

7.5 Basic Considerations

7.5.1 Coffin-Manson Relation

A number of investigators (15) has demonstrated that many materials when subjected to strain cycling conform to the relationship (often referred to as "Coffin's relation", Chapter 2)

$$\Delta \varepsilon_{pa} N^{\alpha} = C \tag{1}$$

where $\Delta \varepsilon_{pa}$ = axial plastic strain range
N = cycles to failure
α, C = constants.

Orowan (107) considered a small element subjected to cycles of plastic strain surrounded by a large volume of elastically cycled material and suggested that a product of plastic strain and number of cycles was a constant. On attaining the critical value of plastic strain the material would fracture. Orowan's theoretical expression was modified by Gross and Stout (108) to εN^{α} = constant.

This work was followed by Coffin who arrived at the relationship (1) while attempting to show that the total plastic strain to failure was constant. The experiments described in Section 2.1.1 were conducted at the Knolls Atomic Power Laboratory (12) on ductile metals for comparatively low endurances and under such conditions that time and temperature effects could be neglected. It was suggested that coefficient α is strongly frequency dependent (47), and that total rather than plastic strain range could be used at very low life.

Independently the same form of relationship (1) was developed by Manson (49). Later Manson (95) related fatigue life to the elastic as well as plastic strain range components of the total mechanical strain range, thus producing a relation suitable for cyclic lives up to 10^6 cycles. Smith, Hirshberg and Manson (54) investigated a selection of engineering alloys in strain cycling up to 10^6 cycles. In this region ~~a~~ straight line relationships of cyclic life against plastic strain and cyclic life against elastic strain were obtained.

Similar relationships of total and plastic strain range against cycles can be observed for tested materials in Figs. 98 to 103. The curve of the elastic component $\Delta\varepsilon_e$ was included in Fig.103 for simple strain cycling of cast steel S at room temperature. The cross-over point between the curves of the elastic and plastic component is in the vicinity of 10^4 cycles which was also observed by Manson for other materials. It is interesting to note that flake cast iron E does not behave in the same fashion and the elastic strain range curve is displaced above its plasticcounterpart, Fig.101.

It is interesting to note that Sachs (55) investigated very short endurances and experimentally verified substitution of the plastic strain range in the relationship (1) by the total strain range.

At room temperature or at a sufficiently low temperature when time-dependent effects do not occur to any appreciable extent the value of α is very close to 0.5. A number of results were summarised by Tavernelli and Coffin (13), Pian and D'Amato (56) and Majors (19) for titanium. Slightly higher values were obtained by Majors for nickel.

Coffin suggested that the constant C could be approximated by means of a tensile test. As the failure occurs at $N = \frac{1}{4}$ and the plastic strain equals to the fracture ductility ε_f, the constant C becomes equal to $\varepsilon_f/2$. In subsequent investigations Coffin (13) concluded that the use of fracture ductility from a simple tension test was conservative in nature.

Using an energy criterion, Martin (28) derived an identical equation to (1). However, he evaluated the constant C by setting the total damage energy absorbed in N cycles equal to the work used in a static tensile test and found this method in better agreement with room temperature strain cycling data than when fracture ductility was used. From strain energy considerations the constant

$$C = \frac{\varepsilon_f}{\sqrt{2}}$$

and at $N = \frac{1}{2}$

$$\Delta \varepsilon_{pa} = \varepsilon_f .$$

Martin also suggested that a parabolic hardening law could further improve the results of his damage energy concept which was originally based on a linear work-hardening law.

Later Langer (94) used relationship (1) to generalize low cycle fatigue data obtained by various organisations for the ASME Boiler and Pressure Vessel Committee, with the aim of applying strain fatigue data to the design of components subjected to a limited number of cycles. Experimental data were provided by Tavernelli and Coffin (13) from the strain cycling tests on twelve structural materials.

7.5.2 Application of Coffin-Manson Relation to Brittle Materials

It is important to see whether the relationship (1) holds also for the present materials which cover a wide ductility range; to the best of our knowledge these are the first tests on cast irons.

The diametral plastic strain range was determined from the width of hysteresis loops at half life in the strain cycling tests for all materials. The experimental points for both total and plastic diametral strain range are plotted against cycles to failure on a log-log basis in Figs. 98 to 103. Results obtained in load cycling, strain cycling at 450°C and in the hold time tests were also included.

The curves of log $\Delta\varepsilon_{pa}$ against log N were plotted in Fig.106 only for room temperature tests on plain specimens. The values of axial plastic strain were obtained by multiplying diametral plastic strain by the appropriate factor taken from the calibration curves Fig.87.

Fig.106 suggests that there is a linear relationship between log $\Delta\varepsilon_{pa}$ and log N for at least four materials, S, C, E and B. Some deviation was observed for both nodular irons F and A, particularly for very short lives of the order of only 10 cycles, which although worth noting, may not be very significant. The values for C and α taken from Fig.106 are listed in Table III together with fracture ductilities. The table shows clearly that there is no simple connection between fracture ductility ϵ_f and the constant C for all tested materials. However the slope α is close to 0.5 as suggested by Coffin.

Since it was not possible in the time available to obtain calibration curves for conversion of diametral strain to axial strain at high temperature, the high temperature results are compared with room temperature results on the basis of diametral plastic strain, Figs. 107 and 108.

This comparison shows that although the high temperature results show a linear relationship between log $\Delta\epsilon_{pa}$ and log N for all materials, the slope α increases slightly, c.f. Table IV, and the intercept on the Y axis (called C_1 to differentiate it from C) is slightly higher than at room temperature. The increase in the value of C_1 bears no simple relationship to the increases in fracture ductility which these materials show with the increase in temperature. However, it is interesting to note the division of test materials into 3 distinct groups according to the permissible diametral plastic strain range which for the flake cast irons, nodular irons and cast steels are respectively 0.004%, 0.02% and 0.1% for a life of 10^4 cycles.

Although Baldwin et al. (81) did not find any change in the exponent α with temperature, other investigators reported values of α from 0.58 to 2.0, (40, 55, 72). Values less than 0.5 were found by Majors (19) for nickel at a temperature of 274°C. Also fracture ductility was studied by some investigators. Coffin (13), Martin (28) and others suggested that the correlation between fracture ductility and the constant C in relation (1) may be due to the close association of the static behaviour and fatigue at very high strain levels. A reduction in ductility after cycling was noted by a number of investigators (12, 28). An experimental investigation of the ductility exhaustion was reported by Sessler and Weiss (82) who proposed following empirical relation between the ductility and number of cycles

$$\varepsilon_{fr} = \varepsilon_f \left[1 - \left(\frac{N_x}{N_f} \right)^{\frac{1}{2}} \right] \tag{6}$$

where ε_{fr} is the remaining fracture ductility after N_x strain cycles of a material having an original fracture ductility ε_f. N_f is the number of cycles to failure which the specimen would have sustained under constant strain cycling. Tests on 24 ST aluminium performed by Sachs et al. (41) were found to be in relatively good agreement with the above relation. However, the data later obtained by Sessler and Weiss on pressure vessel steels A 302 and A 225 were far from the values predicted by Eq.(6).

In the present investigation a limited number of $\frac{3}{4}$ cycle tests (Fig.109) was performed on materials A, C and E, in order to indicate the trend of the ductility change after a load reversal. In all cases the ductility was below the values of the monotonic tensile tests. An additional test on iron A after 4 cycles resulted in a 20% reduction of the original ductility. However, mild steel S showed a slight improvement from 38.8% to 41.5%.

7.5.3 Energy Approach of Morrow

A criterion for failure based on a constant critical amount of plastic work suitable for high strain fatigue was proposed by many investigators. Pardue, Melchor and Good (96) tested a number of materials in bending and observed that the total energy increased with decreasing load. Tests were performed at room temperature and covered a region between 10^2 and 10^5 cycles. Similar results were obtained by Martin and Brinn (97) in high temperature tests on stainless steel 347. Tavernelli and Coffin (13) evaluated total absorbed energy for various materials and concluded that this energy might not be a meaningful measure of fatigue failure since fatigue is a very localized phenomenon and a crack could be considered as an energy sink absorbing more energy than the undamaged portion of a specimen.

Feltner and Morrow have pursued the energy approach with some success and in 1959 postulated an energy criterion (98) stating that the energy required to cause a fatigue fracture was constant and equal in the first approximation to the area under the static true stress-strain curve. In a later investigation on steel SAE 4340 Morrow (89) observed a distinct increase of the total energy to fracture with the increase of fatigue life. The average plastic strain energy per cycle was considered to be a measure of the fatigue damage and monotonic stress-strain curves were replaced by cyclic stress-strain curves.

In the investigations on damping properties Lazan (99) and other suggested that the total energy consisted of two parts: one associated with the plastic strain and the other connected with the anelastic strain. Only plastic strain is responsible for the damage; it can be evaluated from the cyclic stress-strain curve and is dominating at very high stresses. At very low stresses the strains are anelastic and considered non-damaging from the fatigue point of view.

From the continuous records of hysteresis loops obtained in the present investigation the graphs of energy

/cycles were constructed, Figs. 112 to 131. It was noticed that the variation of energy with cycles was related to the variation of stress range during strain cycling or, similarly, to that of strain range during load cycling. This marked similarity particularly for longer lives can be observed in Fig. 149 showing comparative values of energy and strain range for a number of load cycling tests on cast mild steel S.

From the data reported by Morrow (89) the slope of the total plastic strain energy plotted against cycles to fracture on a log-log basis for steel SAE 4340 appears to be 0.35 while the value of 0.40 was obtained for the cast mild steel S, cf. Fig. 132. A similar linear relationship, starting fairly closely from the value of total energy in monotonic tension, is shown by all other materials, Figs. 133 to 138. It is interesting to note that there is practically no difference in the toal energy values obtained in strain or load cycling. The high temperature results suggest only slightly slower increase of total energy with cycles in both strain cycling tests, with and without hold time. Morrow pointed out comparatively slow increase of the total strain energy with decreasing stress. From the presented results, the total energy required to cause fracture in 10^5 cycles is only about 100 times larger than that needed in the monotonic tensile test. Data of 1200 tests compiled by Halford (100) are compared with the present results in Fig. 132. Although the test conditions must have been widely different, the same trend can be observed. It could be concluded that there exists a basic linear relationship for total plastic strain energy against cycles to fracture for all tested materials, commencing in monotonic tension and applicable in load or strain cycling.

7.6 Fatigue Damage and Crack Propagation

7.6.1 Fatigue Damage

Sessler and Weiss (82) suggested that two interdependent processes, namely the loss of available ductility due to strain hardening and the formation and growth of cracks, were responsible for the damage. Both processes are reflected in the retained fracture ductility after cycling. Tests were performed on the pressure vessel steels A 302 and A 225 and after reversed strain cycling at room temperature for a predetermined number of cycles specimens were fractured in a -196°C monotonic tension test.

The authors divided a typical specimen's life up as follows:

(a) 0-10% : No cracks; strength increased to a peak.

(b) 10-25% : First small cracks form; strength decreases to initial value.

(c) 25-75% : Many other small cracks form; strength decreases fairly slowly due to stress relief from multiple notch effect.

(d) 75-100% : Small cracks join up to form long cracks eventually crossing whole section; rapid loss in strength to ultimate fatigue failure.

Weiss et al. (83) have also reported on cumulative fatigue damage studies of A 302 and A 225 steels and 5454-O aluminium alloy. They concluded that ductility loss due to strain hardening alone would probably allow a substantially longer life. Furthermore only the final part of the rapid crack growth occurring after a sufficient amount of ductility loss was considered responsible for failure.

Limited studies of the complex cumulative damage problem indicated that subsequent cycling at a strain level higher than the level of a prior precycle resulted in failure at shorter lives than would be predicted by a linear damage assumption.

Recently Grosskreutz (101) derived a mathematical model of crack extension and found the rate of crack growth proportional to the square root of the crack length. He concluded that high strain fatigue can be considered as crack propagation and the Coffin relationship (1) as crack propagation law.

7.6.2 Crack Propagation

It has been suggested by a number of investigators (102) that cracks initiate early in the life of a specimen. Subsequent propagation was described by various theories in which the rate of crack growth was related to the stress range and the crack length.

From their fractographic observations of intrusions and extrusions, Forsyth and Ryder suggested a mechanism by means of which a crack extension per cycle occurs by localized brittle fracture ahead of the crack tip in the region of a high triaxial stress, followed by ductile necking of the bridge material between external and internal cracks. Laird and Smith (103) subsequently enlarged this hypothesis by considering work hardening of the crack tip during the tensile part of the cycle. During tension the crack is extended and blunted, while in compression it is resharpened. It was suggested that this process is necessary to restore the stress concentration factor for repetition of the cycle. The crack propagation was described as a miniature double cup-cone separation repeated every cycle. Orowan's original suggestion that the crack becomes stationary during several cycles while material hardens and then fractures, was not confirmed.

In the present investigation it was possible to observe crack propagation on a limited number of specimens of cast mild steel S which had failed during strain cycling tests. Plate 10 shows one of the fractured specimens 1 SB 10 which was strain cycled at room temperature in the total diametral strain range of 2.55% with the resulting endurance of 10 cycles. Several small cracks were visible on the surface after the second cycle, only one of these propagated to fracture. The fracture surface can be considered to have three different regions. The first is a small lentil-shaped dark area of crack initiation which is comparatively smooth and distinctly in a transversal plane. The second is the propagation area on which a number of concentric lines could be observed. It is suggested that these ripples indicate subsequent positions of the crack front during cycling. The final ductile tear covers over 50% of the cross section and has a moon-like shape. It has the bright appearance of a shear fracture. Fatigue crack propagation in cast steel C is shown in Plate 11.

These tests would suggest that crack propagation forms a large part of the specimen life. It should however be emphasised that ripple marks were not observed on every specimen and more tests would be required to confirm the described behaviour. Further, it is possible that the grain structure could be an important factor in the visual observation of the surface ripples.

Similar tests on medium strength steels are in progress at the C.E.G.B., Leatherhead. Preliminary results show some correlation between the number of ripples and cycles to failure at short lives.

Irwin (104) investigated crack propagation in pressure vessels and suggested that linear fracture mechanics laws could be applied when considering the progressive extension of a crack during fatigue. In the present tests where an overall plastic deformation occurred, this method could not be used. However, in most structures it is almost impossible to avoid some kind of a notch, the tip of which will undergo a certain amount of plastic deformation. If the Coffin relationship is really a reflection of crack propagation, it is pertinent to consider the behaviour of such a member which is elastically constrained but contains a small plastic zone adjoining the tip of the crack. The radius of this plastic zone is given as

$$r = \frac{K^2}{2\pi\sigma_y^2} \tag{7}$$

where K is fracture toughness (stress intensity factor) and σ_y is the yield stress of the material. McClintock (105) discussed plastic strains near a crack in a perfectly plastic material. The plastic strain on the boundary of the plastic zone is given by the equation

$$\varepsilon = \gamma_y \frac{2r\cos\phi}{d} \tag{8}$$

where d and ϕ are coordinates measured from the tip of the crack and γ_y is the shear strain at the boundary where $d = 2r\cos\phi$. From the Coffin-Manson relation which may be used in the small plastic zone, the number of cycles is inversely proportional to the square of plastic strain

$$N = \frac{\text{const.}}{\varepsilon^2} \tag{9}$$

Now consider a small segment of material adjacent to the tip of the crack. The number of cycles to fracture N will be proportional to the inverse $(2r)^2$ from eq.(8) & (9)

$$N = \frac{\text{const.}}{(2r)^2} \tag{10}$$

and therefore the rate of crack growth would be proportional to r^2 or to K^4, i.e.

$$\frac{da}{dN} = \text{const. } K^4 \qquad (11)$$

It is interesting to note that the relationship of this form was also derived by Paris (106) when investigating the application of fracture mechanics to fatigue problems. He analysed a number of crack propagation laws and concluded that their validity might be questioned in view of a very limited range of test data applied. It was suggested that a large testing programme covering very wide range of crack growth rates would be necessary.

Rolfe and Munse (34) measured crack growth during cycling of notched mild steel plates just below general yield. In their constant load cycling tests the crack growth rate increased continuously. However, the constant stress tests provided some evidence of the relation between the rate of crack growth and nominal stress σ_{nom}. In these tests, Rolfe and Munse gradually reduced the maximum tensile load as the crack grew so that the stress based on the remaining area was constant. The rate of crack growth was reasonably constant for most of the life of the specimens tested in this way and was expressed by the equation $\frac{da}{dN} = k\,\sigma_{nom}$ (12)

where k is a coefficient depending on material, geometry and test temperature.

7.7 Design Considerations

The discussion so far has centred on the reaction of the six materials to mechanical strain cycling. However their resistance to thermal fatigue and cracking in service must also depend on thermal conductivity K, and linear coefficient of expansion, α. Representative values of K and α for the six materials are given in Table IX. The ability of a material to withstand thermal stress is sometimes gauged in terms of Eichelberg (109) "quality factors" such as $\frac{(1-\nu)K}{E\alpha}$ or modified to include strength giving $\frac{(1-\nu)K\sigma_u}{E\alpha}$ where σ_u is the tensile strength at an appropriate temperature. In the present work an analogous quality factor might be written as $\frac{K\varepsilon_t}{\alpha}$ or $\frac{K\varepsilon_p}{\alpha}$ using either the total or plastic strain range obtainable for a particular endurance N and temperature T, cf. Table X. Values for the above factors have been calculated for the six materials at $N = 10^2$, 10^3 and 10^4 cycles at $T = 20^\circ C$ and $450^\circ C$ and tabulated in Table XI. As far as thermal fatigue is concerned rather than simply mechanical strain cycling fatigue it is seen from Table XI that the cast steels are considerably superior to the irons in all cases. Since the values used in preparing these tables were with the exception of ε not obtained in the present work, small differences revealed in the Table XI between cast irons are probably not meaningful; however flake cast irons B and E are again at the bottom of the list. Similar tables to Table X and XI have not been prepared for notched specimens since there is a considerable doubt as to the interpretation of results obtained by measuring diametral strain range away from the notch rather than axial strain across the notch. Unfortunately time did not permit to carry out this type of strain cycling tests.

It has been shown in the previous sections that the Coffin-Manson rule (1) applies to the present test materials at both room and high temperature (cf. Figs. 98 to 103). The justification for its use in the high strain fatigue test on a uniaxial push-pull specimen having a reasonably uniform strain field is discussed in section 7.6.2. As pointed out in section 7.6.1 a simple crack propagation model suitable for low endurance fatigue was developed by Grosskreutz (101) who used relation (1) in describing the propagation of very small cracks in a plastic field until they reach a critical size.

The designer could find such a simple model very attractive. The methods of computing the stress and strain distribution in a structure as developed by Marçal and Turner (110) could be used for finding maximum plastic strains. High strain fatigue data obtained from a simple laboratory specimen at the relevant strain ranges and described in the previous sections or Coffin-Manson relation (1) could then be used for the estimation of the number of cycles required to produce a very small crack in the structure. It is possible that the concept of linear fracture mechanics would then enable to calculate whether and when this small crack will grow to a critical size.

It is perhaps interesting to point out that Marçal and Turner (110) used a simpler concept than above by assuming that the endurances of a specimen and a structure are similar while defining the endurance as the first appearance of a crack (by eye).

8. CONCLUSIONS

1. The present mechanical strain-cycling tests on plain specimens suggest that cast steels C and S and nodular cast irons A and F will have better thermal fatigue properties than flake graphite cast irons E and B.

2. The superiority of the cast steels and nodular cast irons is not so marked when a strain concentration (notch) is present. This and the fact that nodular iron F has a lower thermal conductivity than medium flake iron E partly explains why engine cycling tests (7) indicated that iron E was the better material for cylinder heads.

3. The mechanical strain-cycling behaviour of the test materials can be predicted by the Manson-Coffin law $\Delta\varepsilon_p N^{\alpha} = C$ in the endurance range 50 - 10,000 cycles.

4. Significant errors can be introduced by using the equation

$$\Delta\varepsilon_{ta} = 2\Delta\varepsilon_{td} + \frac{\Delta\sigma}{E}(1 - 2\nu)$$

which assumes constancy of volume, to convert diametral to axial strains for cast materials E, B and F. However, only very small deviations were observed for more ductile materials, A, C and S.

5. Increasing the ambient temperature from room temperature to 450°C has very little effect on the reversed-strain-cycling behaviour of all the materials tested, except nodular iron F. However preliminary tests on materials E and C at 450°C show that hold-times at maximum and minimum strains are likely to influence fatigue behaviour.

6. The increase in fatigue strength shown by flake iron E for hold time of 5 min. can probably be attributed to the increase in ductility produced at 450°C and its low elastic modulus.

7. All test materials cyclically hardened and therefore follow the rule suggested by Manson according to which metals with $\sigma_{ULT}/\sigma_{YS} > 1.4$ cyclically harden and $\sigma_{ULT}/\sigma_{YS} < 1.2$ cyclically soften.

8. The phenomenon of the cyclic-strain-induced creep observed on ductile materials was found to be operative also during load cycling of brittle metals.

9. It was generally observed that the strain range during load-cycling and the stress range during strain-cycling, after the initial period of strain hardening remained relatively unchanged throughout the major portion of the specimen life.

10. High-strain fatigue failure of cast irons follows the path of graphite flakes. Failure of other cast materials is intergranular and not temperature dependent at room temperature and at 450°C, with or without short hold times.

11. It will be necessary to investigate the effect of longer hold-times at maximum and minimum strains, hold-times in compression only and other ambient temperatures (up to 550°C) to ascertain the limits of temperature and cycling rate beyond which creep phenomena seriously influence the fatigue resistance of combustion-chamber materials.

12. The performance of the six materials in complex thermal strain cycling conditions in engines will be a function of thermal conductivity K, and coefficient of expansion α, as well as strain cycling fatigue resistance. Orders of merit based on quality factors $\frac{K\varepsilon_t}{\alpha}$ and $\frac{K\varepsilon_p}{\alpha}$ show that the cast steels in all situations are likely to have the best thermal fatigue resistance. There is not such a clear distinction between the different irons when K and α are taken into account, although generally one or other of the nodular irons follows the cast steels.

9. RECOMMENDATIONS FOR FURTHER WORK

There is a number of suggestions emanating from the present investigation with particular reference to brittle materials as well as other work which deserves some further attention. The factors, which have not been examined in the present tests and may affect the resistance that cast materials offer to cycles of thermal strain are:

1) Hold times covering the whole range of the investigated materials, at other ambient temperatures, hold times in the compression part of the cycle and longer hold times, approaching more realistically the engine cycle. These tests would ascertain the limits of temperature and cycling rate beyond which creep phenomenon would seriously influence the low-cycle fatigue resistance of combustion-chamber materials and structural changes would take place.

2) Influence of change in the notch geometry with particular attention to the notch sharpness, and its connection with fracture toughness.

3) Influence of roughness and surface polish covering other materials.

4) Influence of other cycling speeds and their correlation with hold-time periods.

5) Cumulative effect of cyclic thermal strains and those produced by the fluctuating gas pressure.

6) Influence of mean stress and strain particularly with incorporated hold time. The combustion chamber components are subjected to strain cycling about compressive mean stress and strain and these may improve the low cycle fatigue behaviour of cast metals.

7) Investigation of cyclic crack propagation.

8) Investigation of size effect on cyclic straining.

10. APPENDICES

10.1 Conversion of Total Diametral to Total Axial Strain Range

Restricted access, particularly at high temperature work, short gauge length to eliminate the buckling, eccentricity problems and other complications make it sometimes extremely difficult to employ an axial extensometer to measure axial deformation directly. For these reasons a diametral extensometer was used in the present work. This is quite common practice in the high strain fatigue research (15, 39, 54).

The total (elastic and plastic) axial strain is computed as follows (cf. Fig. 150)

$$\Delta \varepsilon_{ta} = \Delta \varepsilon_{pa} + \Delta \varepsilon_{ea} = \Delta \varepsilon_{pa} + \frac{\Delta\sigma}{E} \qquad (13)$$

where $\Delta \varepsilon_{ta}$ = total axial strain range
$\Delta \varepsilon_{pa}$ = plastic axial strain range
$\Delta \varepsilon_{ea}$ = elastic axial strain range
$\Delta \sigma$ = axial stress range
E = Young's Modulus.

Creep and anelastic strains are negligible. Stress range is measured at a steady state, after the completion of strain hardening or softening.

Now:

$$\Delta \varepsilon_{pa} = 2 \Delta \varepsilon_{pd} \qquad (14)$$

if constant volume in the plastic range is assumed

value $\Delta \varepsilon_{pd}$ = plastic diametral strain range
$\Delta \varepsilon_{td}$ = total diametral strain range
ν = Poisson's ratio

Therefore $$\Delta \varepsilon_{p_d} = \Delta \varepsilon_{t_d} - \frac{\nu \Delta \sigma}{E} \qquad (15)$$

and $$\Delta \varepsilon_{p_a} = 2\Delta \varepsilon_{t_d} - \frac{2\nu \Delta \sigma}{E} \qquad (16)$$

$$\Delta \varepsilon_{t_a} = 2\Delta \varepsilon_{t_d} - \frac{2\nu \Delta \sigma}{E} + \frac{\Delta \sigma}{E}$$

$$\Delta \varepsilon_{t_a} = 2\Delta \varepsilon_{t_d} + \frac{\Delta \sigma}{E}(1 - 2\nu) \qquad (5)$$

Relationships for $\Delta \varepsilon_{pa}$ and $\Delta \varepsilon_{ta}$ are those which are required. The instrumentation system which records hysteresis loops makes equation (16) unnecessary for the evaluation of $\Delta \varepsilon_{pa}$, since $\Delta \varepsilon_{pa}$ can be obtained from equation (14) where $\Delta \varepsilon_{pd}$ is the width of the hysteresis loop at zero load. However, $\Delta \varepsilon_{ta}$ can only be found using an axial extensometer, or from equation (5) if using a diametral extensometer. In the latter case, the values of ν and E are involved for each material. If these were constant and the same in tension and compression then there is no problem. However, cast irons were expected to show some variation in Poisson's ratio and Young's modulus which would impair the use of equation (5). A separate series of calibration tests were therefore performed to measure diametral and axial strains and the results are reported in the Section 6.5.

10.2 Instructions for Operation of the Machine

As the method of setting up of the machine and the recalibration prior to the test became rather unwieldy it was advantageous to design an order of operations according to which the apparatus was to be prepared for the use. Wrong order would influence the degree of precision or result in the damage of the machine or specimen.

1) motor switched on
2) both relief valves open
3) flow valve and both needle valves closed
4) all electronics switched on, X-Y plotter disconnected from the circuit
5) transducer meter switched on. Warm up time required 15 minutes, minimum.
6) set load cell meter to the highest magnification
7) fasten specimen in both jaws by inserting first the bottom end
8) mount the transducer mechanically
9) set the a) attenuation factor
   b) gauge factor
   c) range selector
   d) X-Y plotter sensitivity.

The required values for both load and strain cycling are in Table VI.

10) Rotate "set zero" control in approximate mid position
11) adjust probe mechanically so that meter reading is in the range of electrical zero
12) adjust "set zero"
13) set range to 1
14) readjust "set zero"
15) set range to "Calibration", readjust and return to the range required
16) check quadrature component
17) plug in messcontactor-controller and X-Y plotter
18) mark on the graph paper zero and limiting positions for cycling as calculated.
19) Turn by hand "set zero" knob until the pen reaches the marks on the paper starting with compression, repeat the cycle and return to zero. Check whether zero reading is identical with the original setting.
20) Read cycle counter.

21) Switch on solenoid valve.

22) Bring pressure to the required value, check the cycling speed.

23) Readjust pressure and speed.

The test will then proceed until fracture.

REFERENCES

1. NORTHCOTT L. and BARON H.G. 1956 "The Craze Cracking of Metals", Journ. Iron and Steel Inst. 184, No.111, p.385.

2. FLYNN G. and THOMPSON F.D. Fatigue testing of engine parts for thermal and dynamic loading. Inst. Mech. Eng. London. Symposium on Thermal Loading of Diesel Engines, October 1964.

3. FITZGEORGE D. and POPE J.A. "An investigation of the factors contributing to the failure of diesel-engine pistons and cylinder covers". B.S.R.A. Report No. 123 (RB871) 1953.

4. BAKER S.G. and POPE J.A. "Investigations of the mechanism of failure of I.C. Engine components exposed to combustion conditions". B.S.R.A Report No.227 (RB1373), 1957.

5. BROCK E.K. and GLASSPOOLE A.J. "The Thermal loading of cylinder heads and pistons on medium speed oil engines". Inst. of Mech. Engrs. London. Symposium on Thermal Loading of Diesel Engines. Oct. 1964.

6. WHITEHOUSE N.D., STOTTER A. and GRAY C. "Piston thermal loading". Ibid, ref.3.

7. DEARDEN A. "Residual thermal stress in compression Ignition Engines". Proc. Inst. Marine Engrs. Jan. 1962.

8. FUGITA H. "Service Records of Mitsubishi Nagasaki Diesel U.E. Type Engines and Improvements made on Engines". Proc. Inst. Marine Engrs. Vol.73, No.2, Feb.1961.

9. WALKER C.D. "Strain-fatigue properties of some steels at 950°F with a hold in the tension part of the cycle". Joint International Conference on Creep, Inst.Mech. Eng. 30th Sept. 1963.

10. GILBERT G.N.J. The growth and scaling characteristics of cast irons in air and steam. BCIRA Journal, Vol.7, No.10, 1959.

11. BAKER S.G. and POPE J.A. "The creep, stress-relaxation and thermal-strain properties of several high-grade cast irons". B.S.R.A. Report No.363 (RB1915) 1961.

12. COFFIN L.F., Jr. "A Study of the Effects of Cyclic Thermal Stresses on a Ductile Metal". KAPL 853 Knolls Atomic Power Laboratory June 3, 1953.

13. TAVERNELLI J.F. and COFFIN L.F. "Experimental Support for Generalized Equation Predicting Low Cycle Fatigue" Trans. ASME, Vol.84, p.533, 1962.

14. COFFIN L.F. Journal of Basic Engineering. Trans. A.S.M.E. Series D. Vol.82, 1960, p.671.

15. COFFIN L.F. Low cycle fatigue: a review. Applied Materials Research, Vol.1, No.3, p.129, 1962.

16. GILBERT, G.N.J. Private Communication.

17. COFFIN L.F., Jr. Trans A.S.M.E. 76, 923, 1954.

18. COFFIN L.F., Jr. and WESLEY R.P. Trans. A.S.M.E. 76, 931, 1954.

19. MAJORS H. Thermal and mechanical fatigue of nickel and titanium. Trans. A.S.M. 51, 421-437, 1959.

20. SWINDEMAN R.W. and DOUGLAS D.A. "The failure of structural metals subjected to strain-cycling conditions". Trans. A.S.M.E. June 1959 - <u>82</u> - 203.

21. TAIRA S, OHNAMI M., MINATA H. and SHIRAISHI T. Thermal fatigue and cyclic mechanical strain fatigue at elevated temperature of 18-8 Cb stainless steel and 2.5 Cr-1Mo steel. Bulletin of J.S.M.E., 1963, Vol.6, p.169, Tokyo.

22. TAIRA S., OHNAMI M. and KYOGOKU T. Thermal fatigue under pulsating thermal strain cycling. Bulletin of J.S.M.E. 1963, Vol.6, p.178, Tokyo.

23. FORREST P.G. and PENFOLD A.B. New approach to thermal fatigue testing. Engineering 192, p.522, 1961.

24. KREMPL E. Ueber Die Zeitfestigkeit von Nimonic 80A bei Beanspruchung durch Waermespannung. Materialpruefung, 1963, No.7. pp. 274-283.

25. SACHS G. and WEISS V. Beitrage zur Kurzzeitermüdung. Zeitschrift für Metallkunde, 1962, Vol.53, p.37.

26. Final Report, Pressure Vessel Research Committee, Fabrication Division. Reports of Progress of the Welding Research Council, Vol.19, July 1964, pp. 58-63.

27. KOOISTRA L.F. Effect of plastic fatigue on pressure vessel materials and design. Weld. Journ., Vol. 36, p.120, 1957.

28. MARTIN D.E. "An Energy Criterion for Low-Cycle Fatigue", Jnl. Basic Engrg., Trans ASME (April 1961).

29. HARTMANN E.C. and STRICKLEY G. The Direct Stress Fatigue Strength of 17s-T Aluminium Alloy Through the Range of $\frac{1}{2}$ to $5x10^9$ cycles of Stress (NACA TN 865), Nov.1942.

30. HARDRATH H.F., LANDERS B.C. and UTLEY E.C., Jr. Axial-Load Fatigue Tests on Notched and Unnotched Sheet Specimens of 61S-T6 Aluminium Alloy, Annealed 347 Stainless Steel, and Heat-Treated 403 Stainless Steel (NACA TN 3017), Oct.1953.

31. HARDRATH H.F. and ILLG W. Fatigue Tests at Stresses Producing Failure in 2 to 10,000 Cycles (NACA TN 3132), Jan. 1954.

32. ILLG W. and HARDRATH H.F. Some Observations on Loss of Static Strength Due to Fatigue Cracks (NACA RM L55D15a), 1955.

33. LIN H. and KIRSCH A.A. An Exploratory Study on High-Stress Low-Cycle Fatigue of 2024 Aluminium Alloy in Axial Loading (WADC TN 56-317), Aug.1956.

34. ROLFE S.T., and MUNSE W.H. Fatigue Crack Propagation in Notched Mild Steel Plates. Welding Res. Suppl. Vo.42, No.6, June 1963, p.252.

35. BENHAM P.P. and FORD H. Journal Mechanical Engineering Science, Vol.3, No.2, 1961.

36. COFFIN L.F. A.S.M.E.Paper No.63-WA-109, presented at Winter Annual Meeting, 1963.

37. FELTNER and SINCLAIR. USAF Contract No. AF33(616) - 8177. Project No.1 (80-735) Task No.73521. Report No. RTD-TDR-634149.

38. MOYAR G.J. and SINCLAIR G.M.
(a) Joint International Conference on Creep. 1963. A.S.M.E. and Institution of Mechanical Engineers.
(b) Journal of Basic Engineering, March 1963. P.105.

39. BENHAM P.P. Journal of Institute of Metals. Vol.89. 1960-61. p.328.

40. DUBUC J. "Plastic Fatigue under Stress and Strain with a Study of Bauchinger. Montreal Ph.D. 1961.

41. LIU S.I., LYNCH J.J., RIPLING E.J. and SACHS G. "Low-Cycle Fatigue of the Aluminium Alloy 24S-T in Direct Stress". Metals Technol. (Feb.1948).

42. LYNCH J., RIPLING E.J. and SACHS G. Trans. A. Inst. Min. Met. Eng. 1948, 175, 435.

43. LIU S.I. and SACHS G. Ibid, 1949, 180, 193.

44. D'AMATO R. A Study of the Strain-Hardening and Cumulative Damage Behavior of 2024-T4 Aluminium Alloy in the Low-Cycle Fatigue Range (WADD TR-60-175), April 1960.

45. COFFIN L.F., Jr. and WESLEY R.P. Trans. Amer. Soc. Mech. Engrs. 76, 931 (1954).

46. COFFIN L.F., Jr. Effect of cyclic heating and stressing of metals at elevated temperatures. STP 165, 31 (American Society for Testing Materials, 1954).

47. COFFIN L.F. Trans ASME 76, 923 (1954).

48. COFFIN L.R., Jr. Trans. Amer. Soc. Mech. Engrs. 78, 527 (1956).

49. MANSON S.S. NACA, TN 2933, 1953. "Behaviour of Materials under Conditions of Thermal Stress".

50. COFFIN L.F. Proc. Symposium on Internal Stresses and Fatigue of Metals, 1959, 363, Elsevier, N.Y.

51. POLAKOWSKI N.H. and PALCHOUDHURI A. Proc. Amer. Soc. Test. Mater. 54, 701 (1954).

52. DUGDALE D.S. J.Mech. Phys. Solids, 7, 135 (1959).

53. RAYMOND M.H. and COFFIN L.F. Jr. Geometric and hysteresis effects in strain-cycled aluminium. Proc. Int. Conference on Mechanics of Fatigue in Crystalline Solids. Nov.1962 Orlando, Florida.

54. SMITH R.W., HIRSCHBERG M.H. and MANSON S.S. "Fatigue behaviour of materials under strain cycling in low and intermediate life range." NASA TN D-1574 (1963).

55. SACHS G., GERBERICH W.W., WEISS V. and LATORRE J.V. "Low-Cycle Fatigue of Pressure-Vessel Materials", Proc. ASTM, 60, 512 (1960).

56. PIAN T.H.H. and D'AMATO R. Low-Cycle Fatigue of Notched and Unnotched Specimens of 2024 Aluminium Alloy under Axial Loading (WADC TN 58-27), 1958.

57. WEISS V. and SESSLER J.G. Strain-controlled Fatigue in Pressure-vessel Materials. ASME 63-WA-226, Sept. 1963.

58. WEISS V., SESSLER J.G. and PACKMAN. Effects of Several Parameters on Low Cycle Fatigue Behaviour. Proc. Int. Conference on Mechanics of Fatigue in Crystalline Solids. Nov.1962, Orlando, Florida.

59. GROSS J., GUER D. and STOUT R. "The Plastic Fatigue Strength of Pressure-Vessel Steels. The Welding Journal, 33, Res.Suppl. 31-39, 1954.

60. IVES K. Equibiaxial low cycle fatigue properties of typical pressure vessel steels. Report No. 7548, The Babcock Wilcox Co., Alliance, Ohio, 1964.

61. WEISMAN M.H. and KAPLAN M.H. "The Fatigue Strength of Steel Through the Range from ½ to 30,000 Cycles of Stress", Proc. ASTM, 50, 649 (1950).

62. BENHAM P.P. "Fatigue of Metals Caused by a Relatively Few Cycles of High Load or Strain Amplitude," Metallurgical Reviews, 3, 11 (1958).

63. MURDI B.B., SACHS G. and KLIER E.P. "Axial-Load Fatigue Properties of High Strength Steels," Proc. ASTM, 57, 655 (1957).

64. SACHS G. and SCHEVEN G. "Relation Between Direct Stress and Bending Fatigue of High Strength Steels", Ibid. 57, 667 (1957).

65. SCHEVEN G., SACHS G. and TONG K. "Effects of Hydrogen on Low-Cycle Fatigue of High Strength Steels, Ibid. 57, 682 (1957).

66. BOWMAN and DOLAN T.J. Further studies of biaxial fatigue properties of pressure vessel steels. Weld. J. Res. Suppl. 34, 1955, pp.51-59.

67. FOREST P.G. Fatigue of Metals. Pergamon Press 1962.

68. MACKENZIE Colin. Private communication. Low cycle fatigue research at the Imperial College.

69. McCLINTOCK F.A. Private communication.

70. COLES A. and SKINNER D. Assessment of Thermal Fatigue Resistance of High Temperature Alloys. Journ. Royal Aero. Soc. Jan. 1965, p.53.

71. BARNES J.F. and TILLY G.P. Assessment of Thermal Fatigue Resistance of High Temperature Alloys. Journ. Royal Aero. Soc. May 1965, p.343.

72. JOHANSSON A. "Fatigue of Steels at Constant Strain Amplitude and Elevated Temperatures". Stockholm. Colloquium on Fatigue (IUTAM), 1956.

73. SMITH F.C., BRUEGGEMAN W.C. and HARWELL R.H. "Comparison of Fatigue Strength of Bare and Alclad 24S-T3 Aluminium Alloy Sheet Specimens Tested at 12 and 1000 Cycles per Minutes" (NACA TN 2231).

74. OBERG T.T and TRAPP W.J. "High Stress Fatigue of Alloy Steels", Prod. Engrg. 22 (1), 159 (1951).

75. OBERG T.T. and WARD E.J. U.S.Atomic Energy Comm. Pub. 1953 WADC-TR-53-256.

76. ILLG W. Fatigue Tests on Notched and Unnotched Sheet Specimens of 2024-T3 and 7075-6 Aluminium Alloys and of SAE 4130 Steel with Special Considerations of the Life Range from 2 to 10,000 Cycles (NACA TN 3866), 1956.

77. ECKEL J.F. The influence of frequency on the repeated bending life of acid lead. Proc. ASTM, Vol. 51, p. 745, 1951.

78. VALLURI S.R. Effect of frequency and temperature on fatigue of metals. NACA TN 3972, Febr. 1957.

79. C.E.G.B. Leatherhead. Private communication.

80. THOMPTON N. and WADSWORTH N. Advances of Physics 7, 84, (1958).

81. BALDWIN E.E., SOKOL G.G. and COFFIN L.F. Jrn. "Cyclic Strain Fatigue on AISI Type 347 Stainless Steel", Proc. ASTM, 57, (1957).

82. SESSLER J. and WEISS V. Low cycle fatigue damage in pressure-vessel materials. ASME 62-WA-233 Nov. 1962.

83. WEISS V. and SESSLER J. and PACKMAN P. "Low cycle fatigue of pressure-vessel materials. Report Met. E. 575-662-F. Syracuse University Research Institute, 1962.

84. GILBER G.N.J. An Evaluation of the stress/strain properties of flake graphite cast iron in tension and compression. BCIRA Journal, 1959, Vol.7, p.745-789.

85. GILBERT G.N.J. Stress/strain properties of cast iron and Poisson's ratio in tension and compression. BCIRA Journal 1961, Vol.9, No.3, p.347-363.

86. THUM and UDE. Giesserei. 1929, Vol.16, p.501.

87. KEMSLEY D.S. and PATERSON M.S. Acta Met. 8, 453 (1960).

88. WADSWORTH N.J. Work hardening of copper crystals under cyclic straining, Acta Metallurgica Vol.11, No.7 July 1963.

89. MORROW J.O.Dean. Cycle Plastic Strain Energy and Fatigue of Metals. ASTM Materials Science Symposium on Internal Friction, Damping and Cyclic Plasticity Phenomena in Materials. Chicago. June 1964.

90. POLAKOWSKI N.H. Proc. ASTM 1952, 52, 1086.

91. WOOD D.S. The effect of creep on the high-strain fatigue behaviour of a pressure vessel steel. UKAEA, 1965. TRG Report 993 (C).

92. ELDER W.J. CERL, Leatherhead. Private communication.

93. TAVERNELLI J.F. and COFFIN L.F. "A compilation and interpretation of cyclic strain fatigue tests on metals" Trans ASM 1959 - 51 - 438.

94. LANGER B.F. "Design of Pressure Vessels for low-cycle Fatigue". Paper. 61-WA.-18. A.S.M.E. 1961.

95. MANSON S.S. Thermal Stresses in Design, Machine Design, Vol.32, No.13, June 1960 and Vol.32, No.14, July 1960.

96. PARDUE T.E., MELCHOR J.L. and GOOD W.B. "Energy Losses and Fracture of Some Metals Resulting from a Small Number of Cycles of Strain." Proc. SESA 7 (2), 27 (1960).

97. MARTIN D.E. and BRINN J. "Some Observations on the Plastic Work Required to Fracture Stainless Steel under Cyclic Loading", Proc. ASTM 59, 677 (1959).

98. FELTNER C.E. and MORROW J. Micro-Plastic Strain Hysteresis Energy as a Criterion for Fatigue Fracture (TAM Report No.576) Urbana: University of Illinois (1959).

99. LAZAN B.J. and WU T. "Damping Fatigue, and Dynamic Stress-Strain Properties of Mild Steel", Proc. ASTM, 51, 649 (1951).

100. HALFORD G.R. The fatigue toughness of metals; a data compilation. TAM Report 265, University of Illinois, May 1964.

101. GROSSKREUTZ J.C. A Theory of Stage II Fatigue Crack Propagation. Midwest Research Institute, Kansas City, Missouri, Dec. 1964.

102. FROST N.E. and DUGDALE D.S. The propagation of fatigue cracks in sheet specimens. Journal of Mechanics and Physics of Solids, Vol.6, No.2, p.92, 1958.

103. LAIRD and SMITH. Crack propagation in High Stress Fatigue. Phil. Mag. Vol.7, p.847, 1962.

104. IRWIN G.R. Metals Eng. Quart. 1963, 3 (1) 24.

105. McCLINTOCK F.A. and HULT J.A. Proc. of the 9th Internat. Congress on Applied Mathematics, Brussels, 1956, Vol. VIII, p.51.

106. PARIS P. Fracture mechanics approach to fatigue. Fatigue, Xth Sagamore Conference, August 1963.

107. OROWAN E. "Stress Concentrations in Steel under Cyclic Loading," The Welding Journal, 31 (6), Research Suppl. 273-s to 282-s (1952).

108. GROSS H.J. and STOUT R.D. "Plastic Fatigue Properties of High-Strength Pressure-Vessel Steels", The Welding Journal, 34 (4) Research Suppl. 161-s (1955).

109. Eichelberg G.: Temperaturverlauf und Wärme-spannungen in Verbrennungsmotoren. Forsch. Arb. Ing. Wes. No.263 1923, p.3.

110. P.V. Marçal and C.E.Turner, 'Limited life of shells of revolution subjected to severe local bending'. J. Mech. Eng. Sci., Vol.7, 4, 408, 1965.

Code Letter	TC	Si	P	S	Mn	Ni	Cr	Mo	Al.	Heat Treatment
A	2.16 to 2.21	1.73 to 1.92	0.026 to 0.040	0.005 to 0.011	0.25 to 0.48	34.4 to 35.4	-	-	-	None (As Cast)
B	3.62	1.55	0.018	0.066	0.49	-	-	0.90	-	None (As Cast)
C	0.265	0.38	0.026	0.012	0.64	0.31	1.19	0.29	0.080	Anneal 925°C Furnace Cool. Normalise 880°C Air cool. Temper 700°C. Air Cool.
E	3.29	1.10	0.12	0.088	0.69	1.18	-	0.39	-	6 hrs at 500°C
F	3.51	2.64	0.019	0.01	0.36	1.26	-	-	-	4 hrs at 950°C Air Cool 2 hrs at 625°C Air Cool
S	0.215	0.37	0.024	0.013	0.70	0.16	0.14	0.06	0.052	Anneal 925°C Furnace cool.

Table I. COMPOSITION AND HEAT TREATMENT OF CAST IRONS AND CAST STEELS

Table II

Plate No.	Material Code Letter	Metallographical Report	Supplier
4	A	Predominantly nodular graphite in an austenitic matrix small amounts of carbide at the grain boundaries.	B.C.I.R.A.
5	B	Medium/coarse flake graphite in a matrix containing about equal amounts of ferrite and pearlite.	B.C.I.R.A.
6	C	Moderately coarse feathery bainite with segregation banding at the grain boundaries.	Clyde Alloy Steel Co. Ltd.
7	E	Medium flake graphite in a completely pearlitic matrix containing very small amounts of phosphide eutectic.	Vickers Ltd.
8	F	Well formed nodular graphite in a pearlitic matrix with small ampunts of ferrite associated with the graphite.	Sheepbridge Equipment Ltd.
9	S	Fine lamellar pearlite in a ferritic matrix.	Clyde Alloy Steel Co. Ltd.

<u>TABLE III</u>

CODE LETTER	At room temperature					At 450°C		
	U.T.S.	% RA	ε_f	C	α	U.T.S.	% RA	ε_f
A	27.2	13.7	14.5	15.0	0.54	15.6	17.3	17.6
B	9.7	0.31	0.3	1.7	0.48	8.7	0.52	0.46
C	43.6	23.5	26.1	31.0	0.50	34.8	35.0	44.2
E	20.8	0.45	0.7	1.9	0.54	17.0	0.59	0.92
F	49	1.58	2.5	17.5	0.50	44.8	5.36	5.66
S	32.6	32.0	38.8	40.0	0.48	20.0	41.3	53.0

TABLE IV

Code Letter	At Room Temperature		At 450°C	
	C_1	$\propto$	C_1	$\propto$
A	16	0.54	30	0.54
B	1.0	0.48	1.25	0.48
C	35	0.50	39	0.50
E	1.6	0.54	2.2	0.54
F	12	0.50	16	0.50
S	33	0.48	40	0.48

TABLE V

CODE LETTER	UTS σ ULT T/IN^2	YIELD STRENGTH σYS T/IN^2	RATIO σ_U/σ_{YS}	COMMENTS
A	30	20	1.5	
B	11	3 8*	3.5 1.3	*In compression BM 13
C	46	32 31*	1.45 1.55	*In compression CB 14
E	21	7 19*	3 1.1	EM5 - L *In compression 2E 3MH
F	49	36	1.4	
S	36	15	2.4	

TABLE VI.

CALIBRATION TABLE

	Rig I (Room temperature)		Rig II (High temperature)	
Transducer No.	318		392	
Transducer sensitivity	2.13mV/0.001"/V input		2.02 mV/0.001"/V input	
Filtered output	Deflection X	Load Y	Deflection X	Load Y
gauge factor (direct connection)	2.70	2.84	2.54	2.96
gauge factor (via contactor)	2.50	2.60	2.27	2.76
Attenuation factor	4	8	4	2
X-Y plotter (mV/1")	200	100	200	200
Range for load (1 TON=10mm)	-	0.25	-	25
Range for strain (scale =100mm)	As Required	-	As Required	-

TABLE VII

CYCLIC CREEP

CODE AND SPECIMEN	Cycles to fracture	No. cycle	σ_c T/IN^2	σ_T T/IN^2	
A AB6	106	1^{st} 105	24.0 24.5	25.0 25.1	
B BB7	12	1^{st} 11	8.98 8.98	9.0 9.0	
C 1CM8	46	1^{st} 45	36.5 37.5	37.1 38.0	
E 2E11M	166	1^{st} 165	16.0 16.0	16.05 16.05	
F FM10	148	1^{st} 147	40.7 40.7	41.6 41.5	
S 1SB2	28	1^{st} 27	22.0 23.5	24.0 25.0	

TABLE VIII

	Cycles to Failure			
START IN	E	F	C	S
COMPRESSION	16	45	18	78
TENSION	17	46	21	71

TABLE IX

Material Code	^{o}C Test	$E\times10^{-6}$	$\alpha\times10^{6}$ per ^{o}C	K cal/gm sec ^{o}C
A	20 450	15 12	14 16	0.03 0.044
B	20 450	19 16	12 14	0.12 0.11
C	20 450	30 26	12 14	0.1 0.09
E	20 450	20 18	11 13	0.11 0.10
F	20 450	25 23	12 14	0.08 0.07
S	20 450	30 25	12 13.5	0.124 0.10

TABLE X

Material Code	Total Diametral Strain Range $\mathcal{E}_t$ for $N=10^2$	10^3	10^4	Plastic Diametral Strain Range $\mathcal{E}_p$ for $N=10^2$	10^3	10^4
A	0.65 0.7	0.25 0.32	0.2 0.3	0.3 0.5	0.09 0.2	0.03 0.06
B	0.1 0.13	0.08 0.09	0.05 0.08	0.029 0.04	0.009 0.015	0.004 0.007
C	1.25 1.35	0.5 0.65	0.15 0.3	0.9 0.95	0.3 0.4	0.09 0.1
E	0.15 0.18	0.12 0.15	0.11 0.13	0.03 0.04	0.008 0.01	0.0025 0.0035
F	0.75 0.88	0.4 0.5	0.2 0.25	0.35 0.3	0.1 0.1	0.025 0.025
S	1.4 1.35	0.6 0.55	0.25 0.23	1.0 1.07	0.35 0.35	0.11 0.125

TABLE XI. Modified Quality Factors

Material Code	°C Test Temp.	$\frac{K}{E\alpha}\cdot 10^6$	$\frac{K\varepsilon_t}{\alpha}\cdot 10^6$ for $N=10^2$	10^3	10^4	$\frac{K\varepsilon_p}{\alpha}\cdot 10^6$ for $N=10^2$	10^3	10^4
A	20	145	1420	540	440	640	195	65
	450	230	1950	900	830	1360	540	165
B	20	530	1000	800	490	290	90	40
	450	490	1050	690	620	310	117	54
C	20	280	10500	4200	1250	7500	2500	750
	450	240	8300	4000	1850	6050	2650	640
E	20	500	1500	1200	1100	300	80	25
	450	425	1370	1150	1050	310	76	27
F	20	360	6800	3650	1800	2350	660	165
	450	220	4000	2550	1260	1500	500	125
S	20	350	14960	6350	2550	10400	3650	1140
	450	300	10050	4150	1700	8000	2600	970

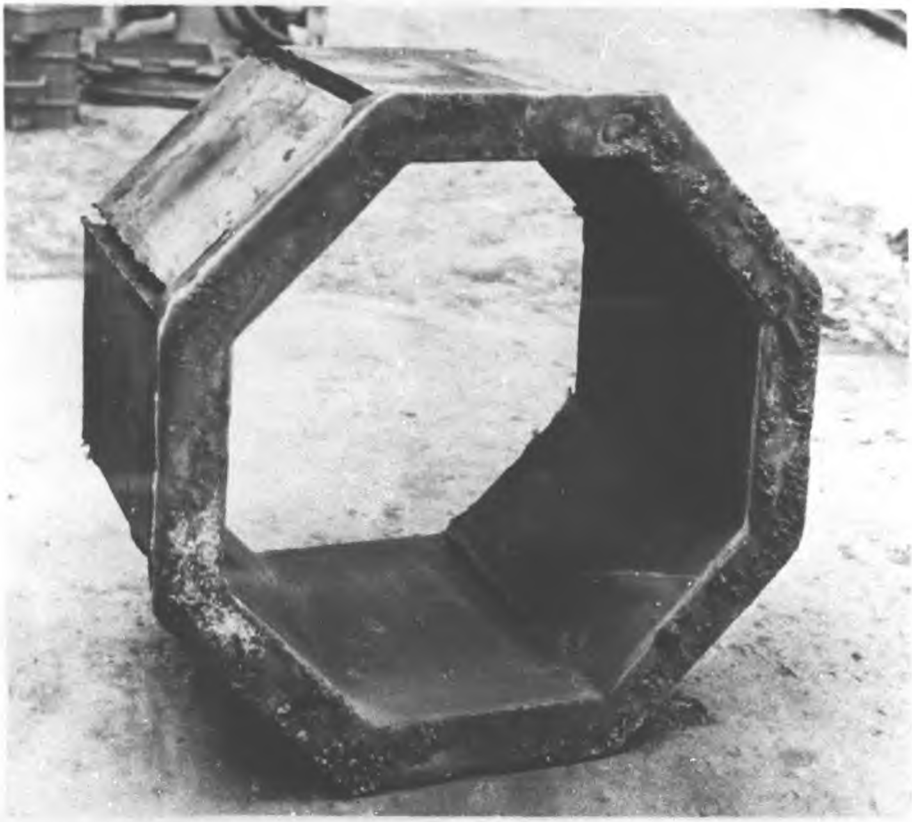

PLATE 1. GENERAL VIEW OF TEST CASTING.

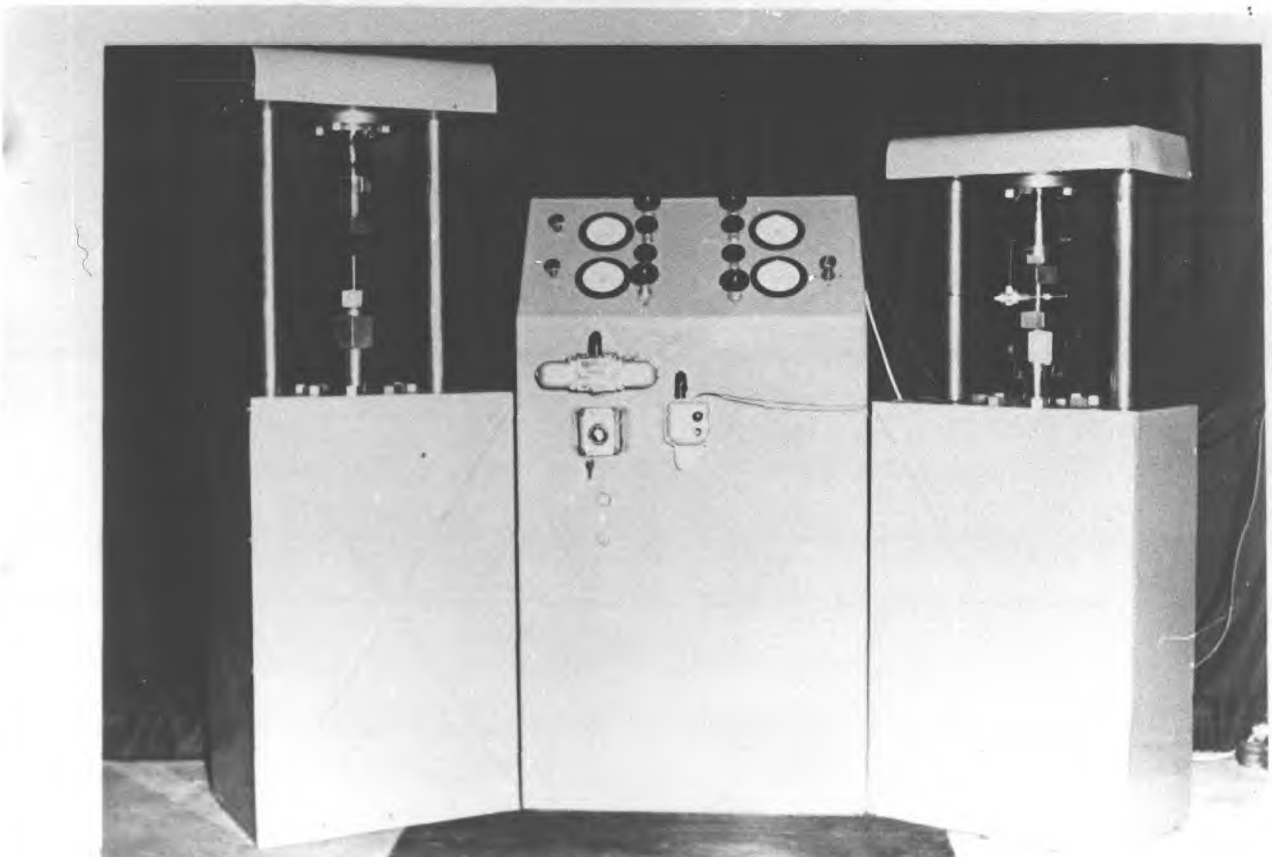

PLATE 2. HIGH STRAIN FATIGUE MACHINES.

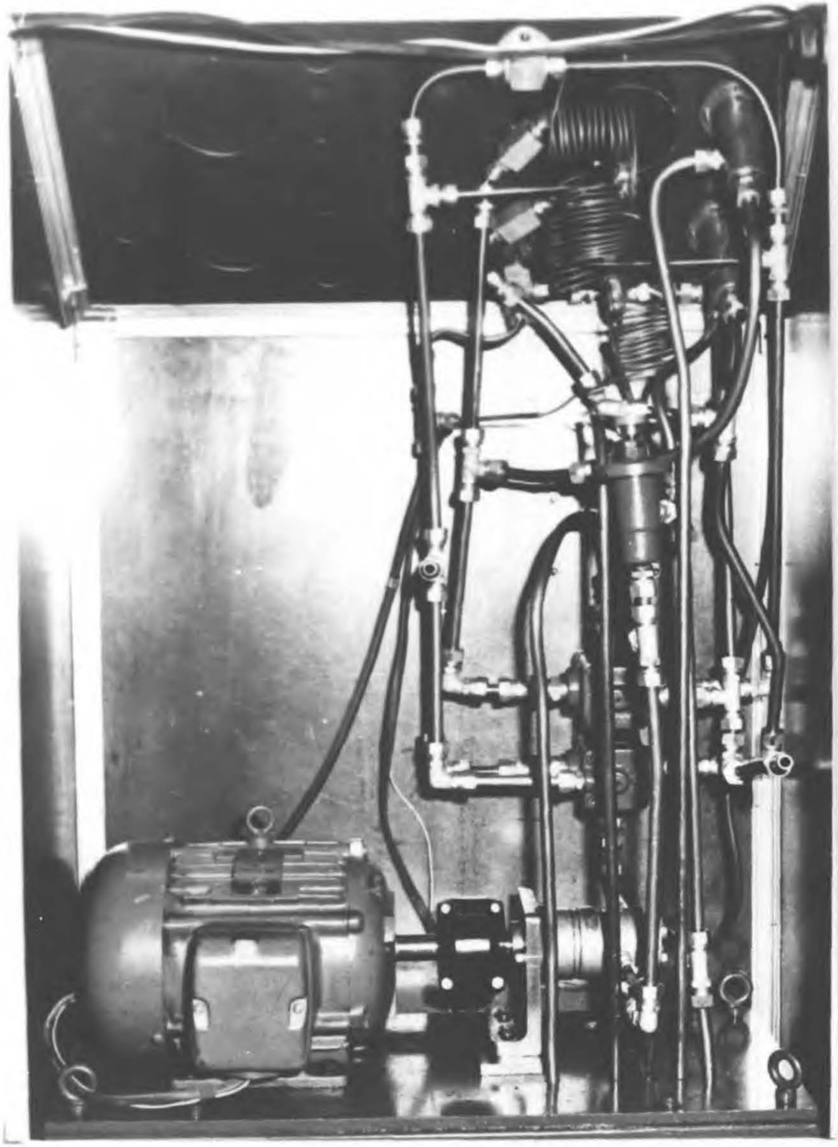

PLATE 3. HYDRAULIC SYSTEM

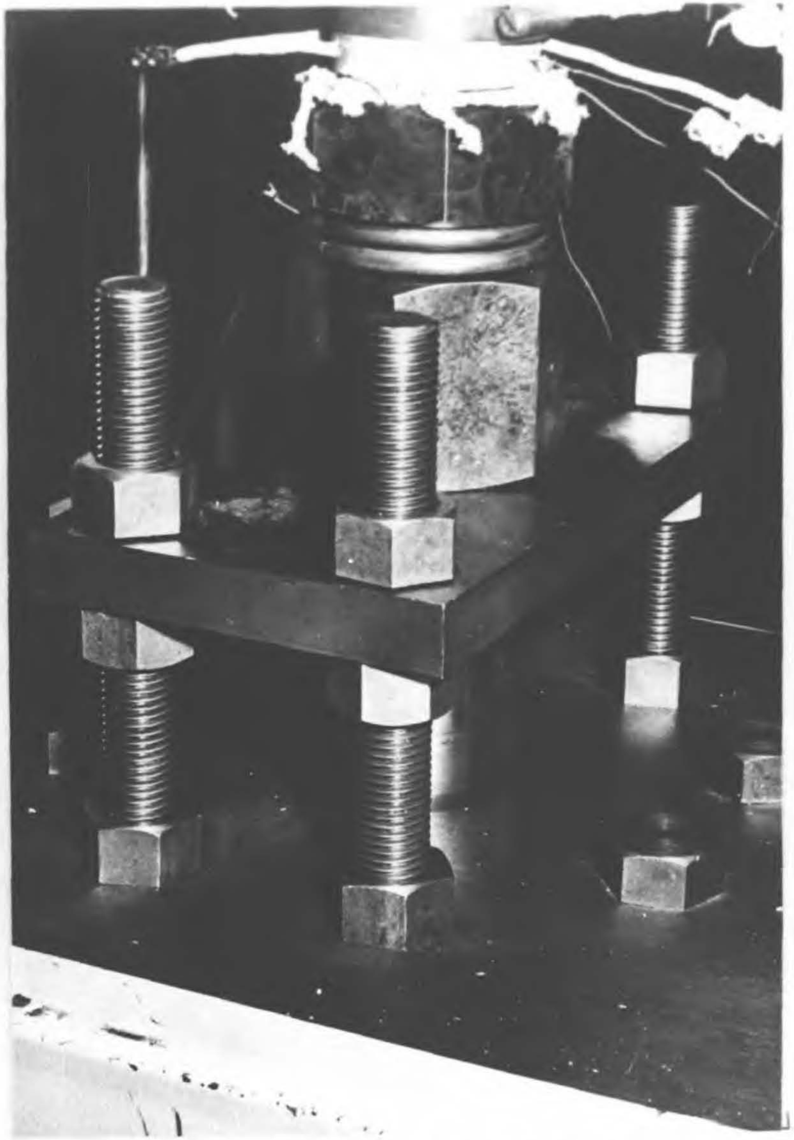

PLATE 4. MACHINE ADAPTATION FOR HOLD - TIME TESTS.

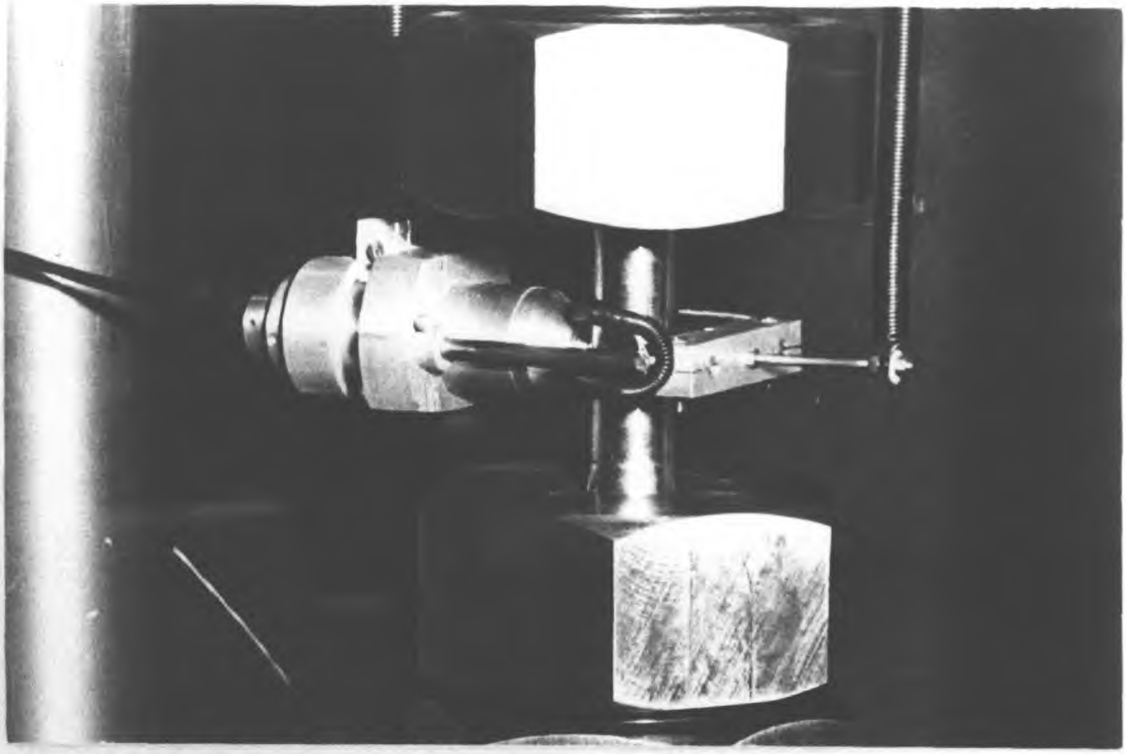

PLATE 5. DIAMETRAL EXTENSOMETER
FOR ROOM TEMPERATURE TESTS.

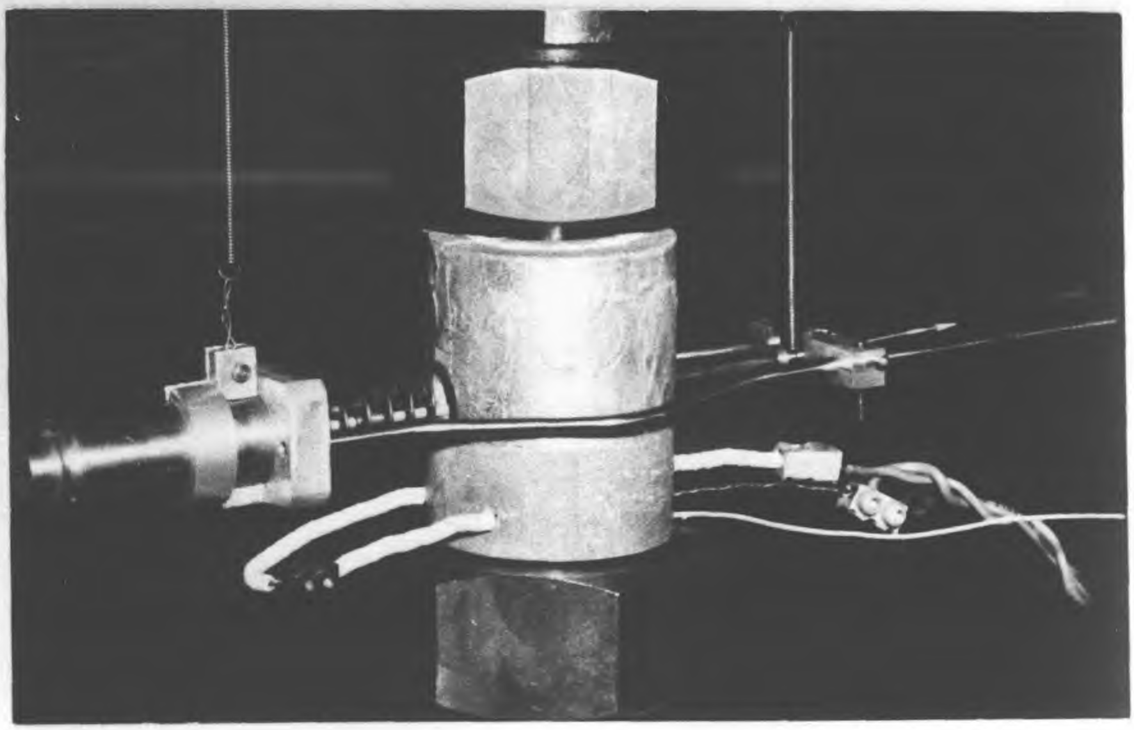

PLATE 6. DIAMETRAL EXTENSOMETER
FOR HIGH-TEMPERATURE TESTS WITH
MUFFLE FURNACE.

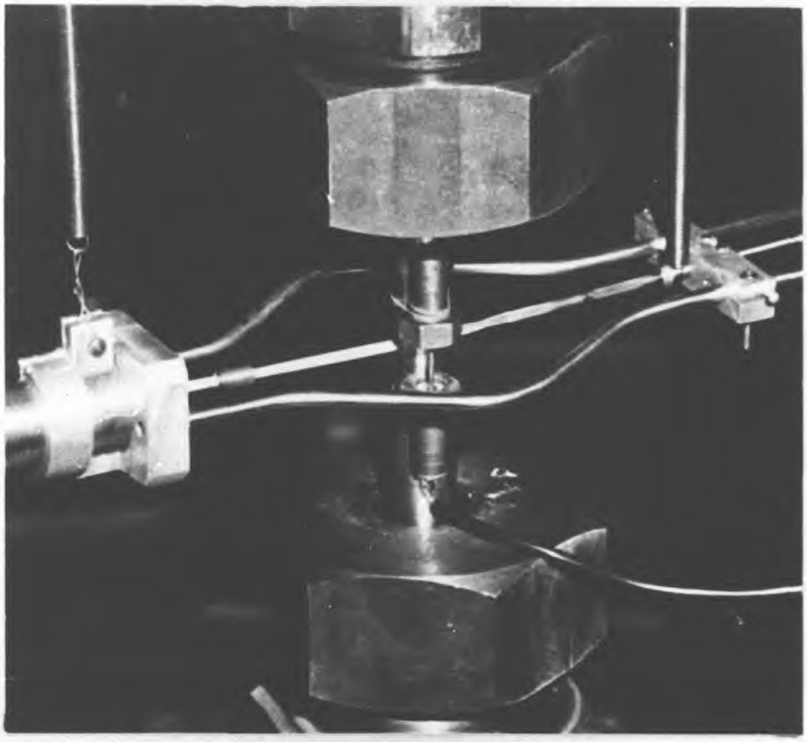

PLATE. 7. DIAMETRAL AND AXIAL EXTENSOMETERS FITTED TOGETHER FOR CALIBRATION.

PLATE 8. GENERAL VIEW OF A CALIBRATION TEST.

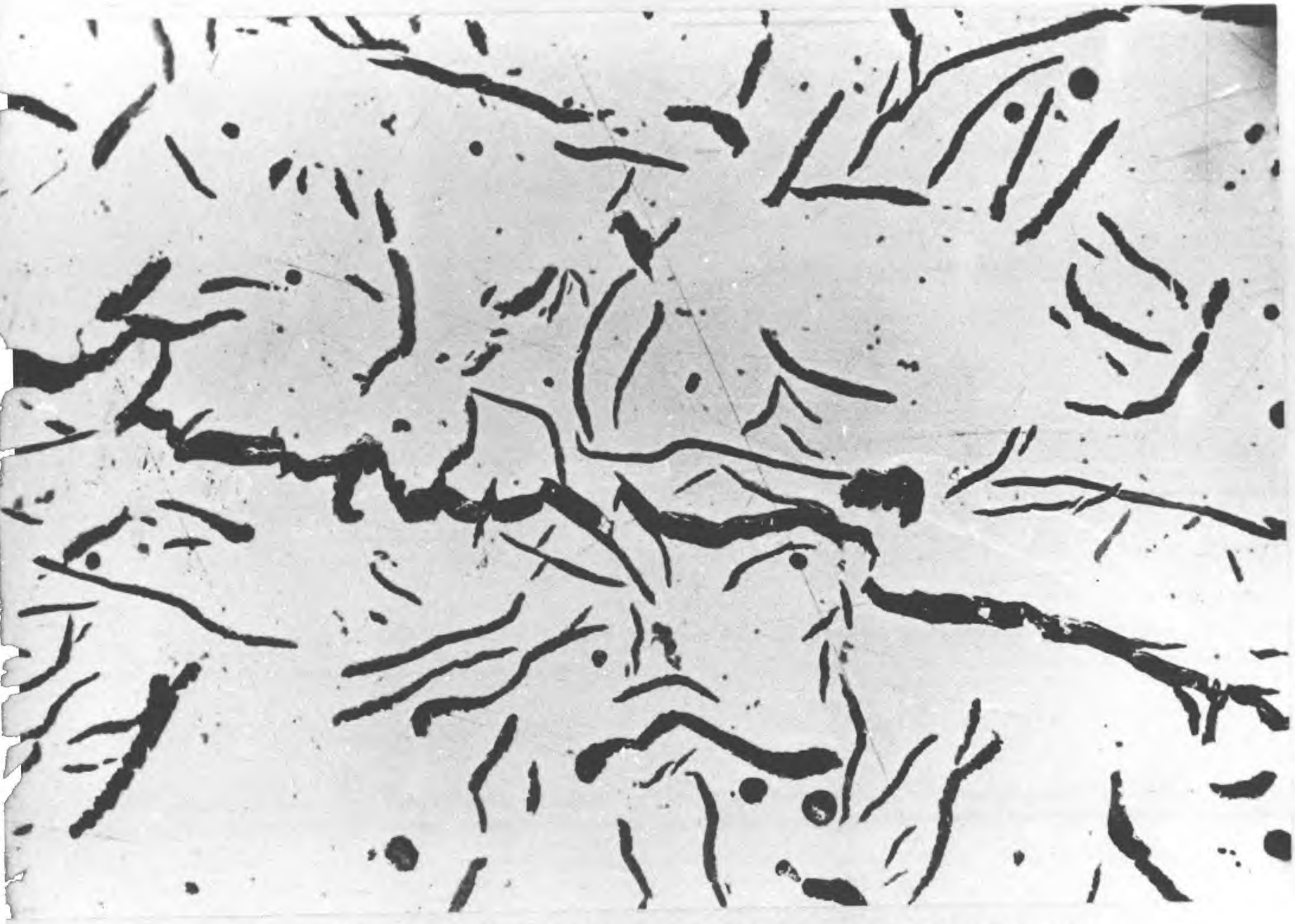

PLATE 9. FRACTURE OF FLAKE CAST IRON

7EB. 8. (X60.)

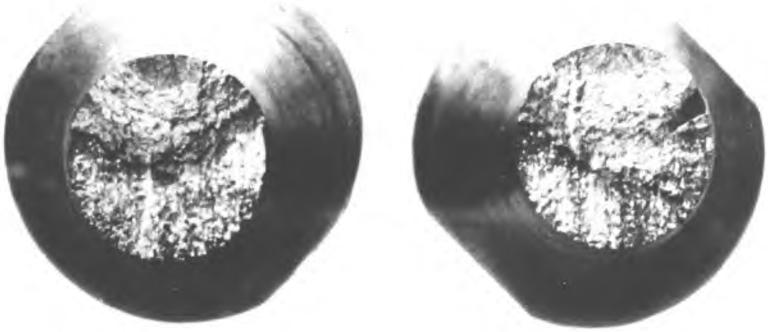

PLATE. 10. CRACK PROPAGATION IN CAST MILD STEEL.
ISB 10

PLATE 11. CRACK PROPAGATION IN CAST Cr-Mo STEEL.
CB 7.

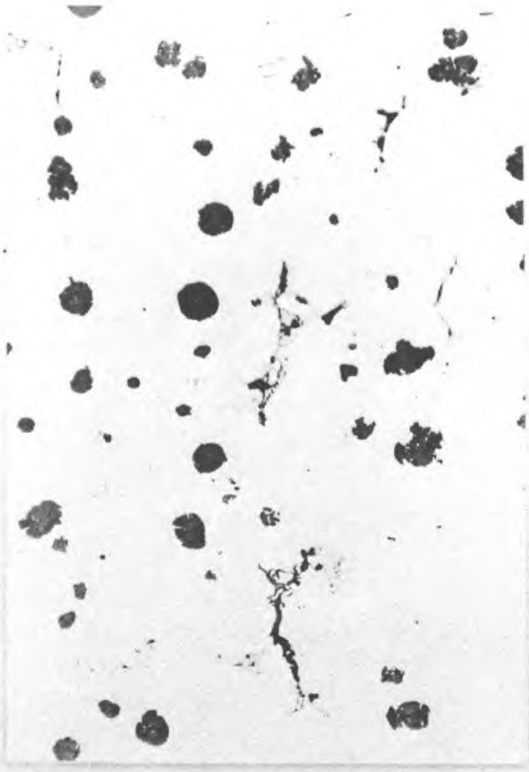

PLATE 12. AUSTENITIC CAST IRON A (x 60)

PLATE 13 AUSTENITIC CAST IRON A (x 100)

PLATE 14. COARSE FLAKE CAST IRON B'' (x 60)

PLATE 15. COARSE FLAKE CAST IRON B (x 600)

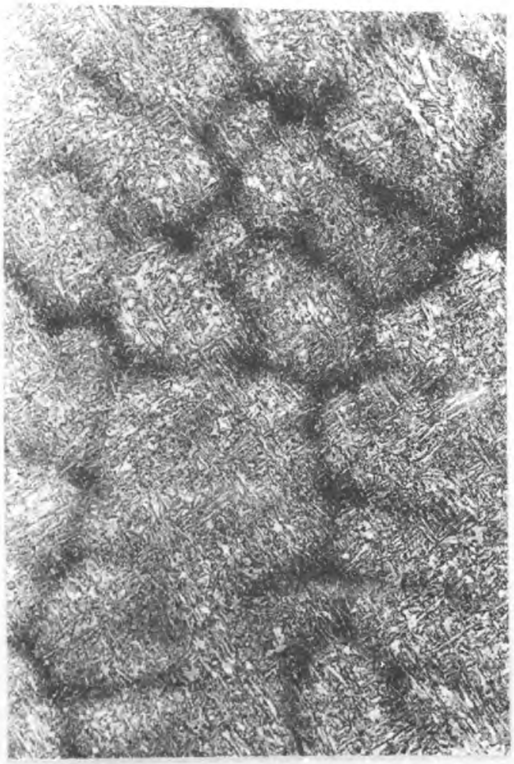

PLATE 16. CAST Cr-Mo STEEL C (X 60)

PLATE 17 MEDIUM FLAKE CAST IRON E (X 60)

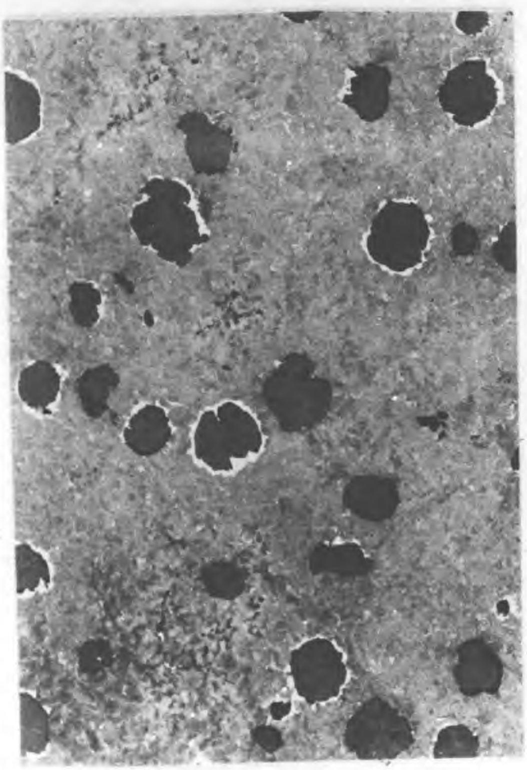

PLATE 18. NODULAR CAST IRON F (X 60)

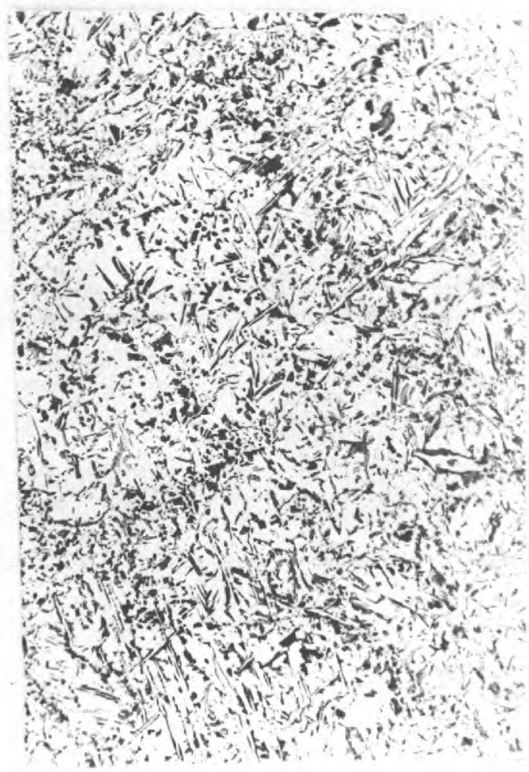

PLATE 19. CAST MILD STEEL S (X 60)

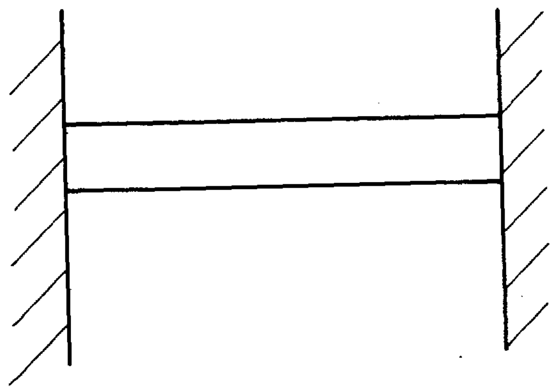

FIG. 1. Constrained bar

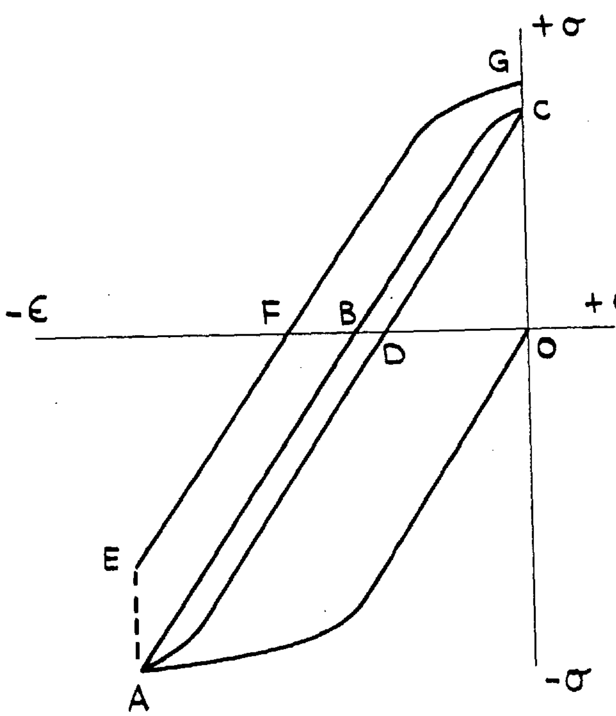

FIG. 2. Idealized stress-strain cycle produced by heating and cooling of a bar in Fig.1.

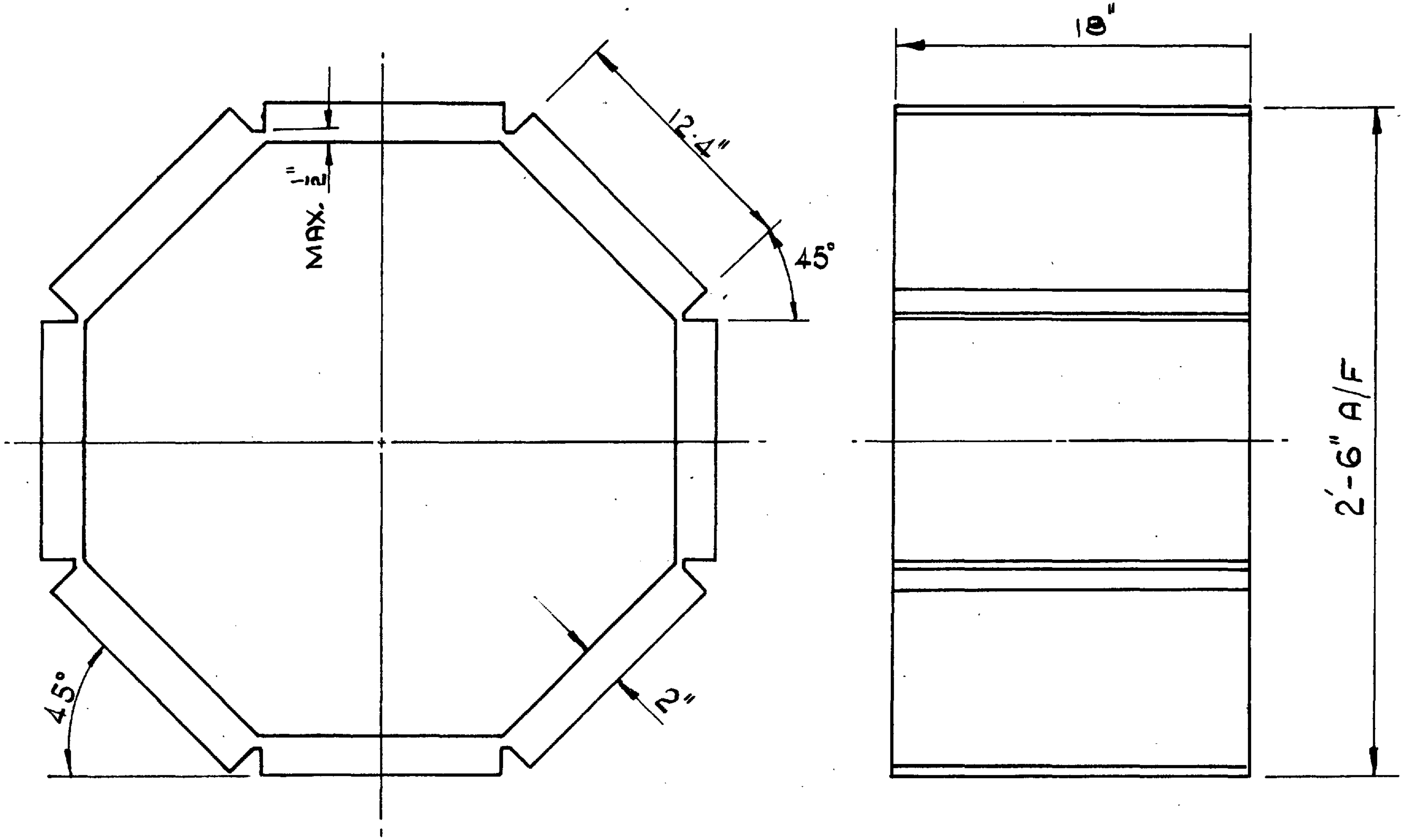

FIG.3. Octagonal casting

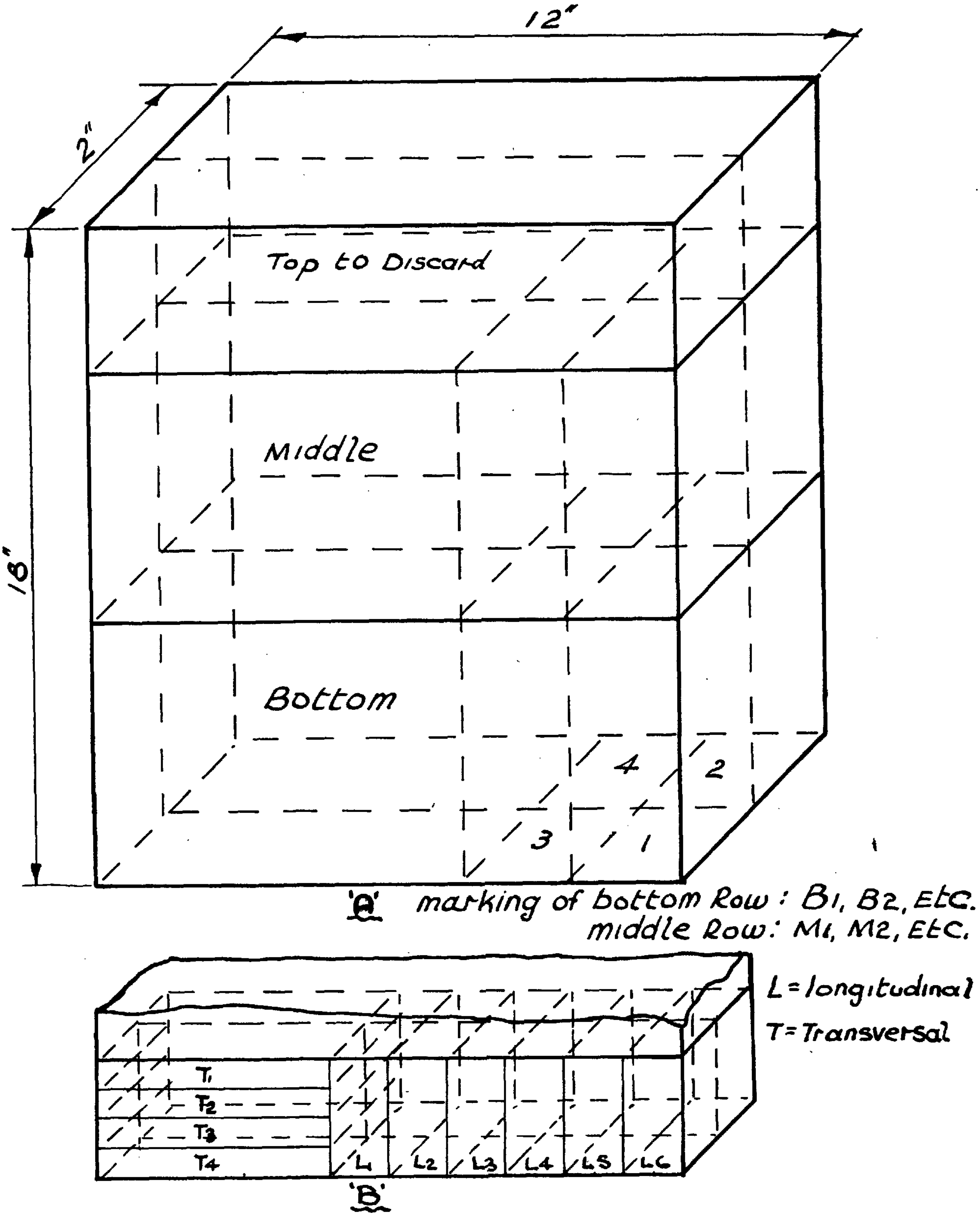

FIG.4. Cutting plan

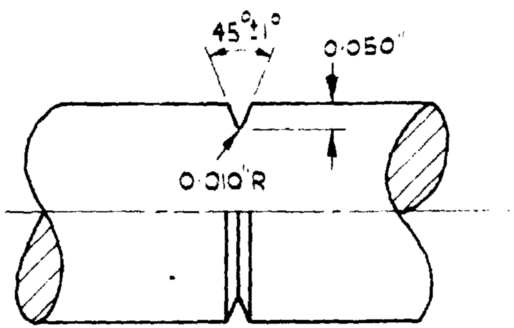

DETAIL FOR NOTCHED SPECIMENS

SCALE - TWICE FULL SIZE.

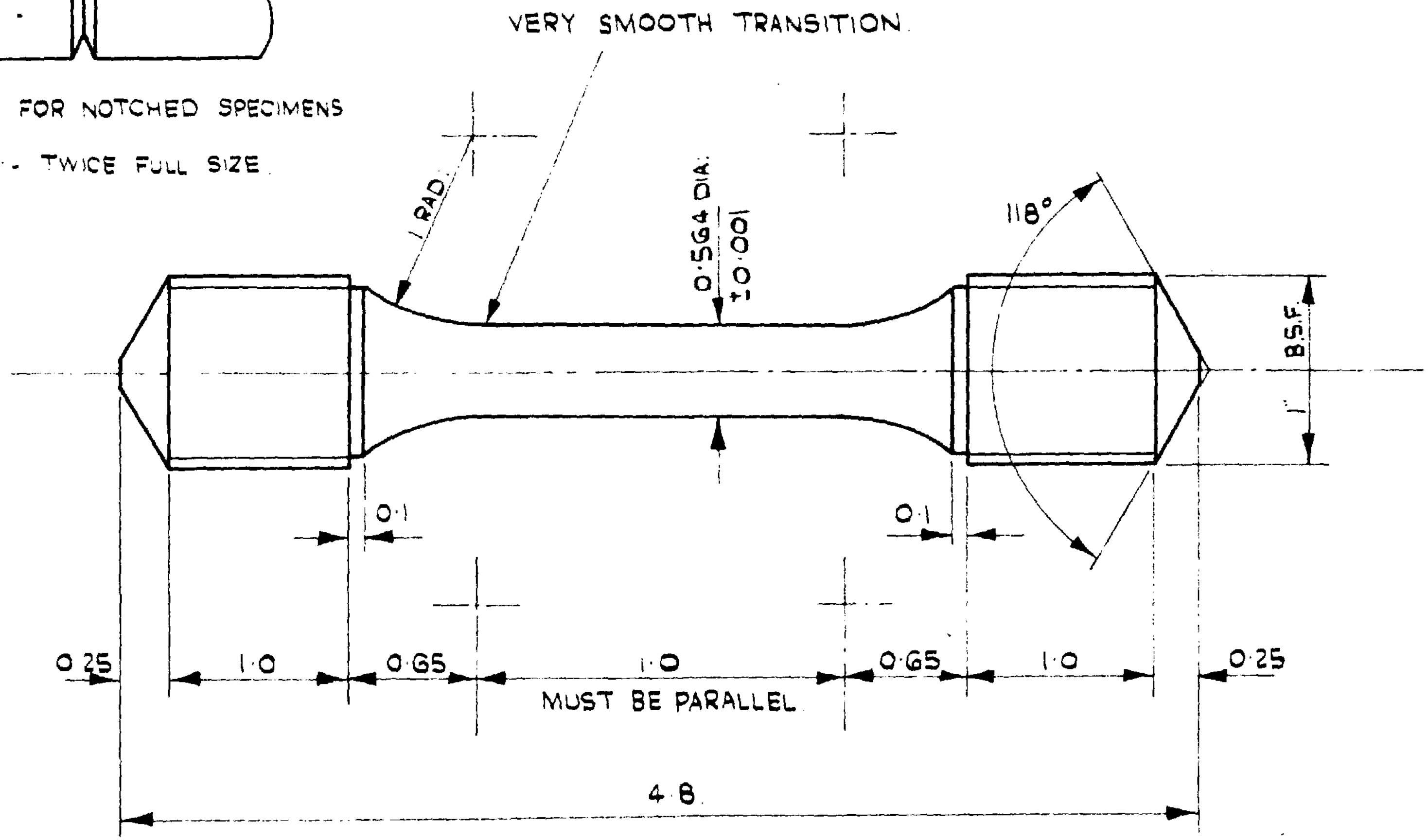

FINE POLISH BETWEEN THREADED ENDS.

ALL TURNED SURFACES MUST BE CONCENTRIC.

SMOOTH ALL EDGES.

FIG. 5. SPECIMEN FOR B.S.R.A. RIG.

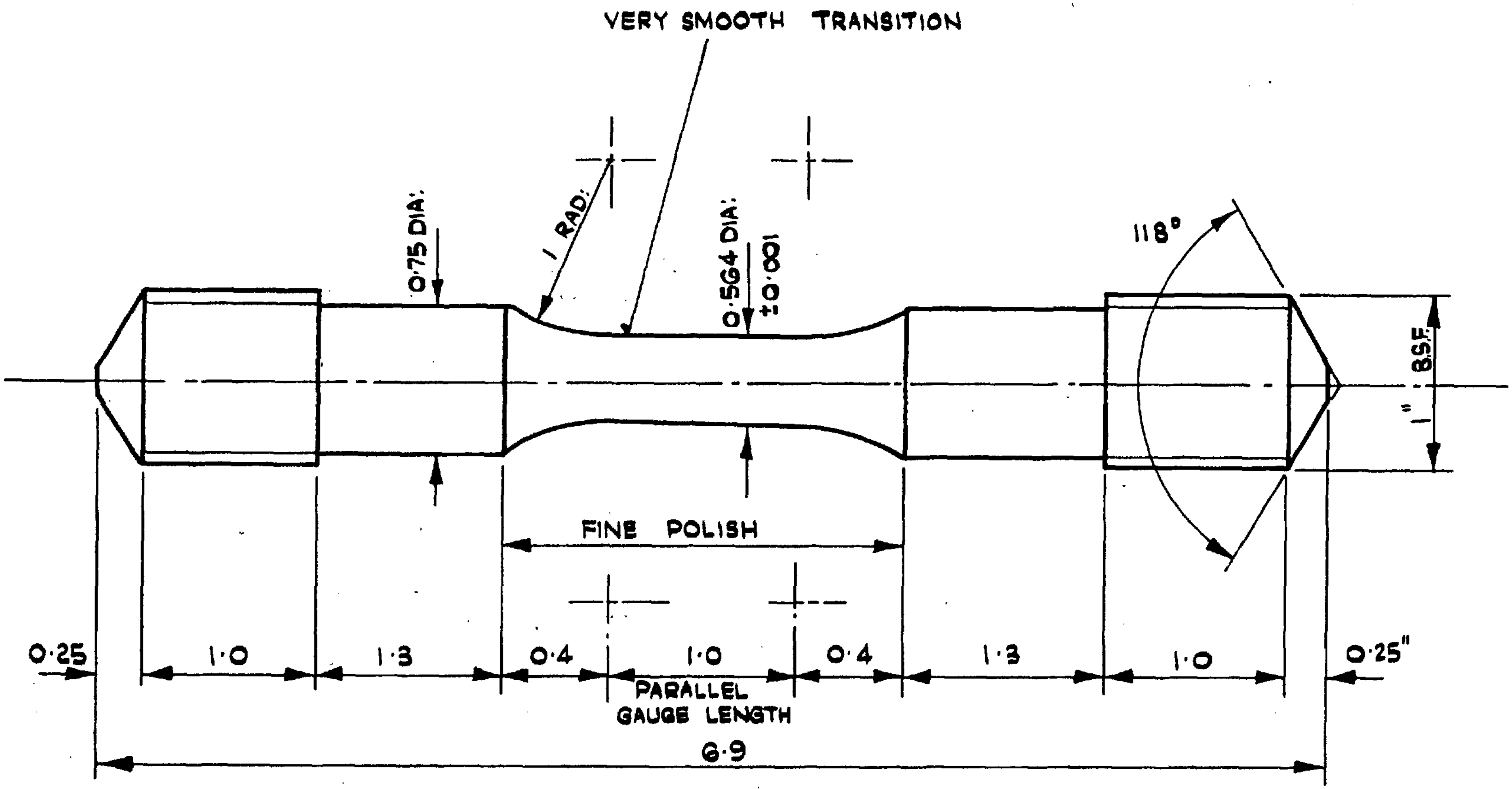

ALL TURNED SURFACES
MUST BE CONCENTRIC.

SMOOTH ALL EDGES.

FIG. 6. HIGH TEMP. SPECIMEN. B.S.R.A.

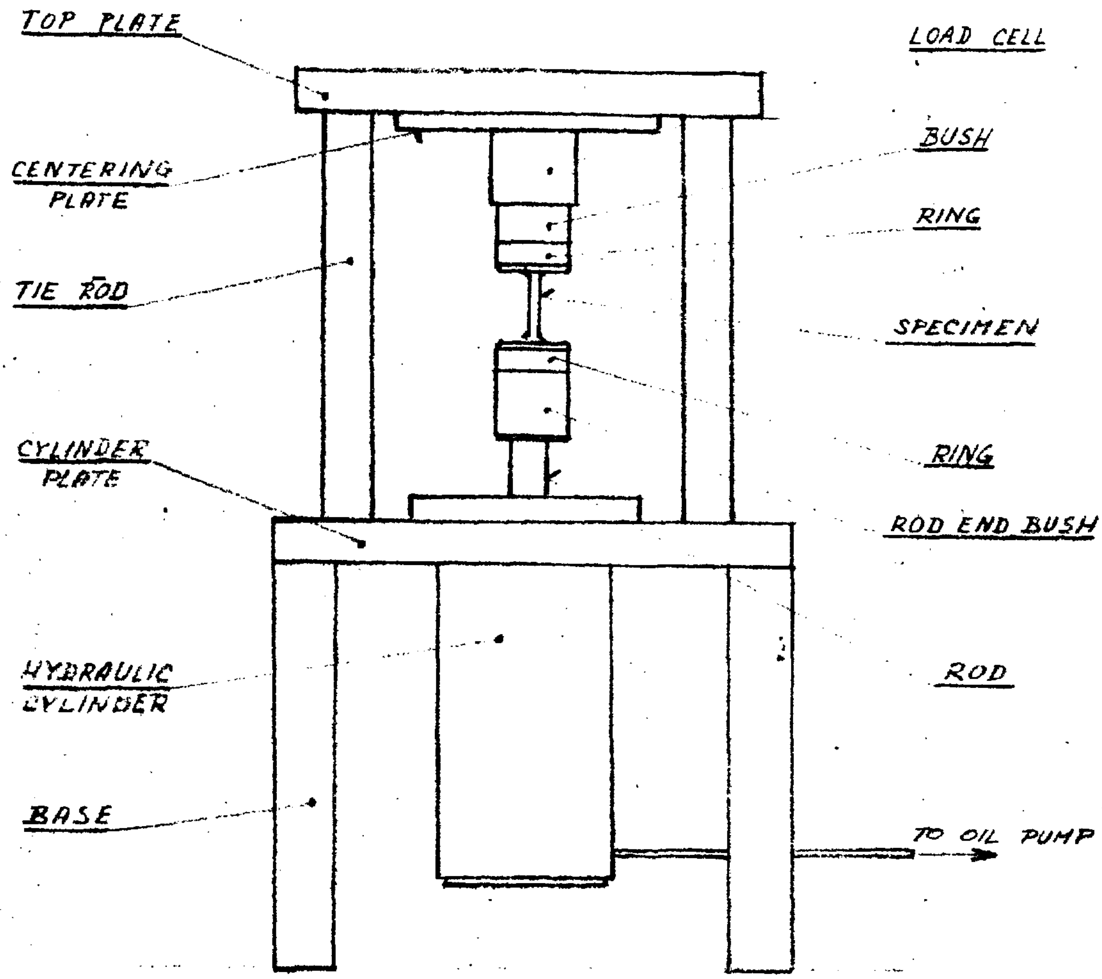

14TH FEB 62		
BSRA RIG - BASIC DIAGRAM		RN- 13

FIG. 7.

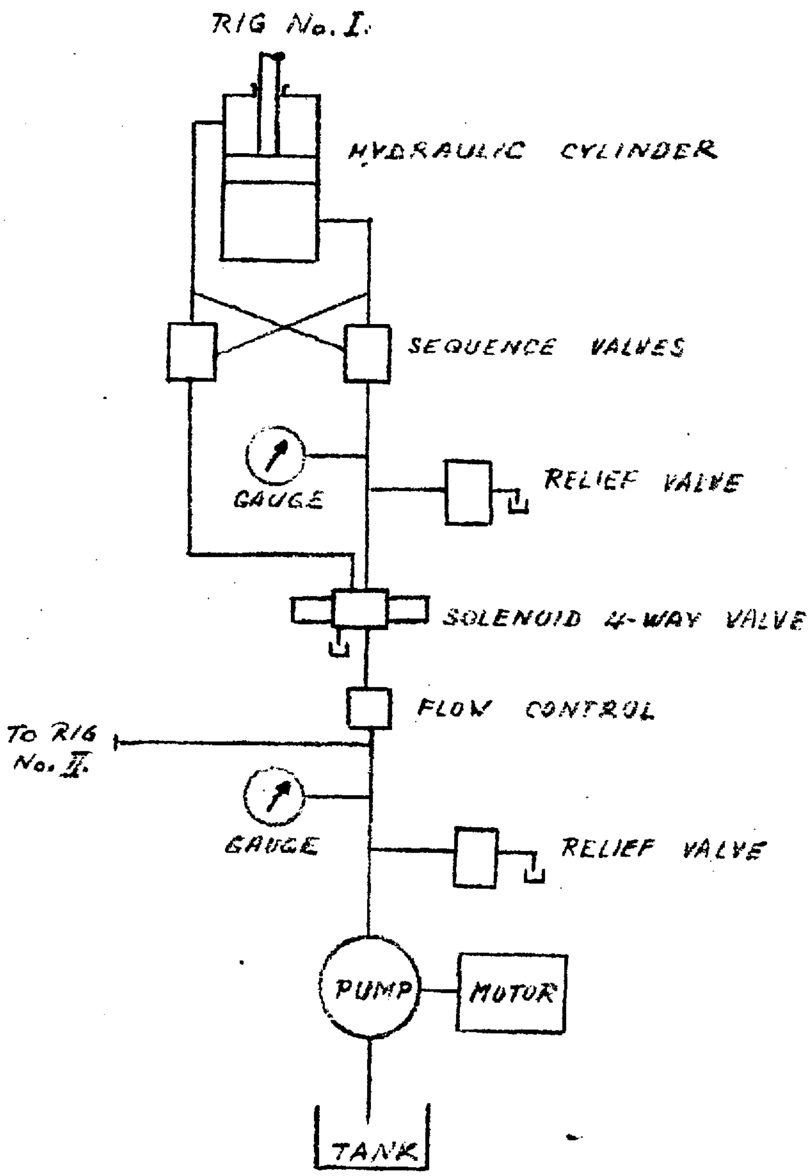

14TH FEB 62

FIG. 8. BSRA RIG - HYDRAULIC SCHEME

RN-15

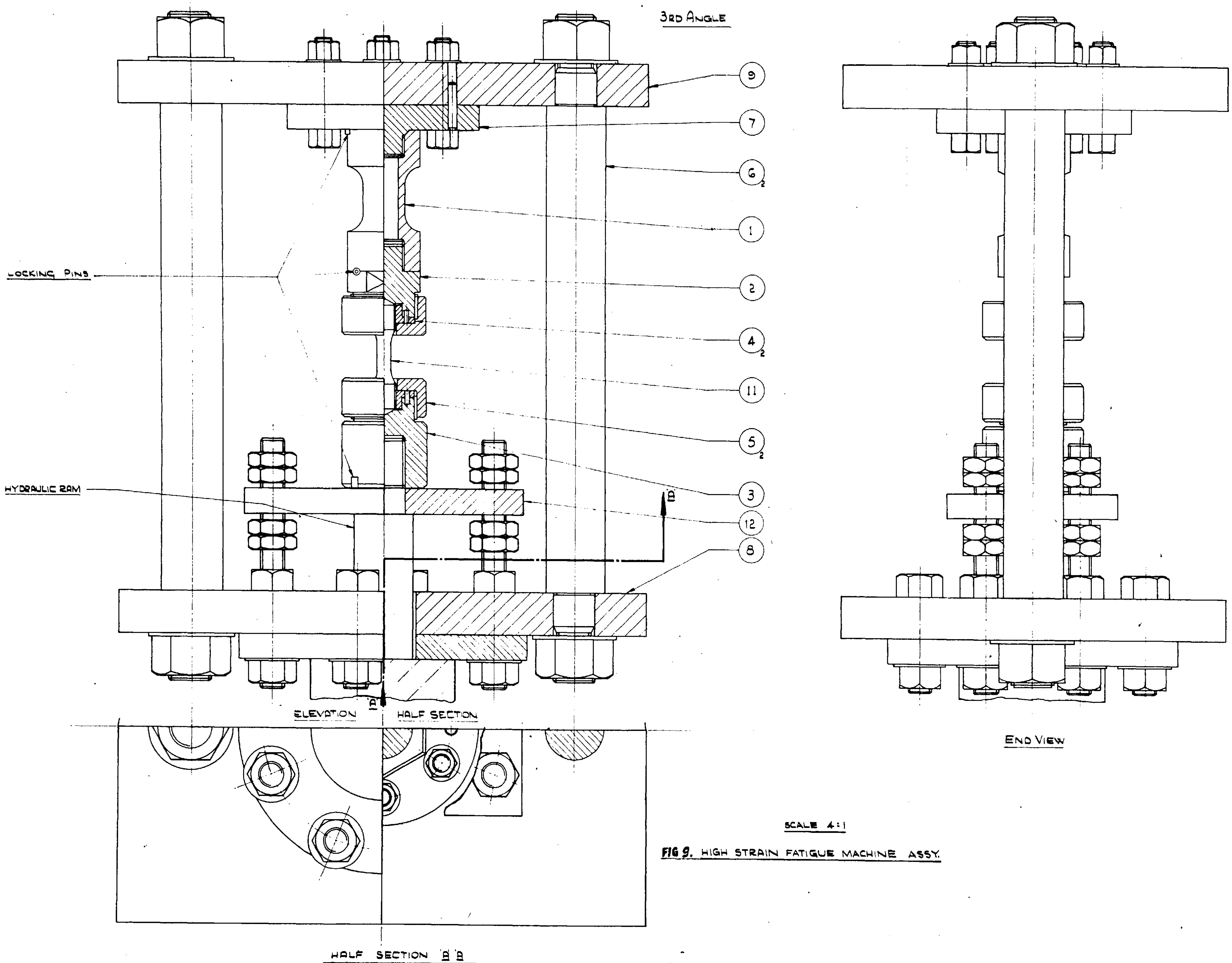

SCALE 4:1

FIG 9. HIGH STRAIN FATIGUE MACHINE ASSY.

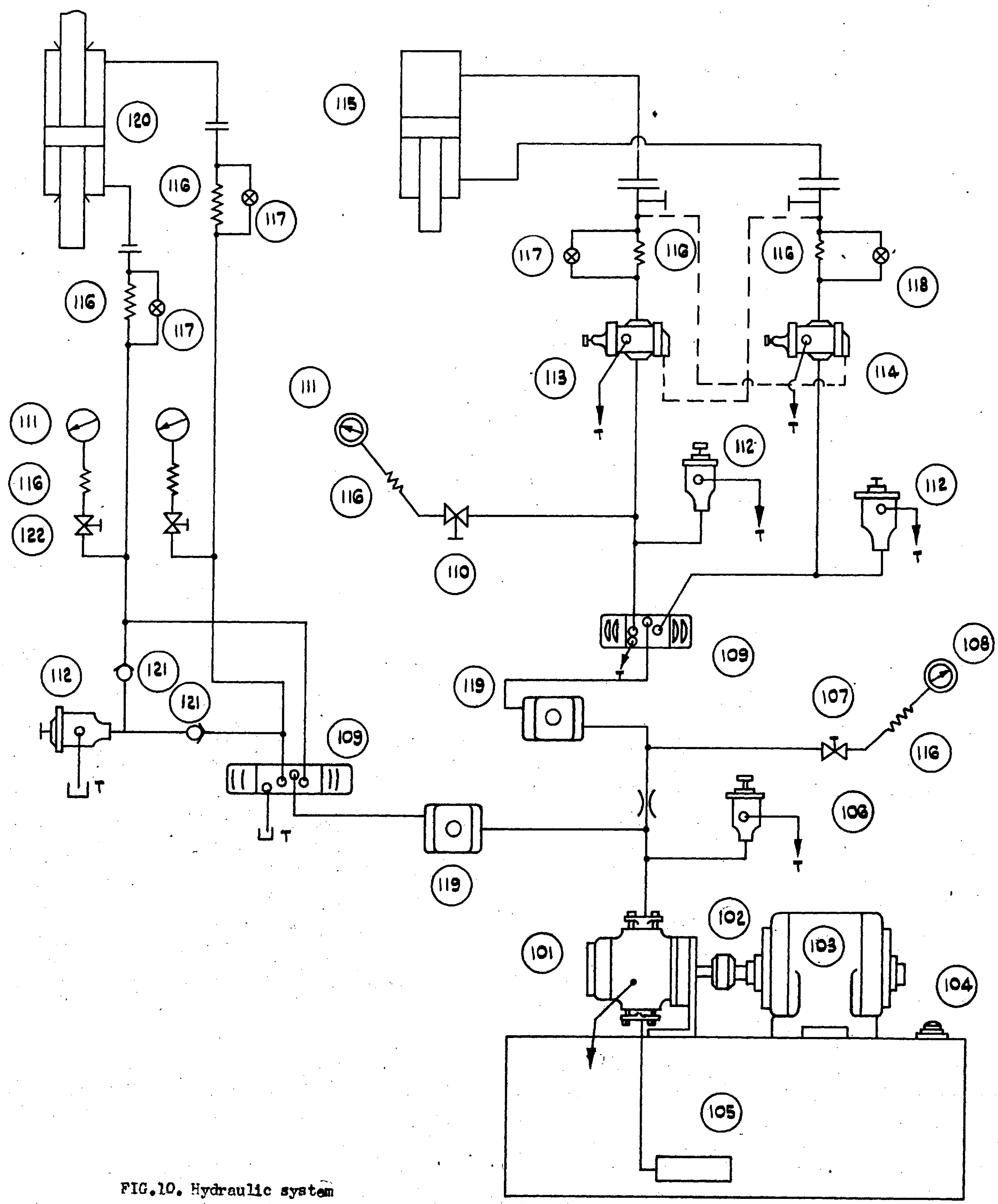

FIG.10. Hydraulic system

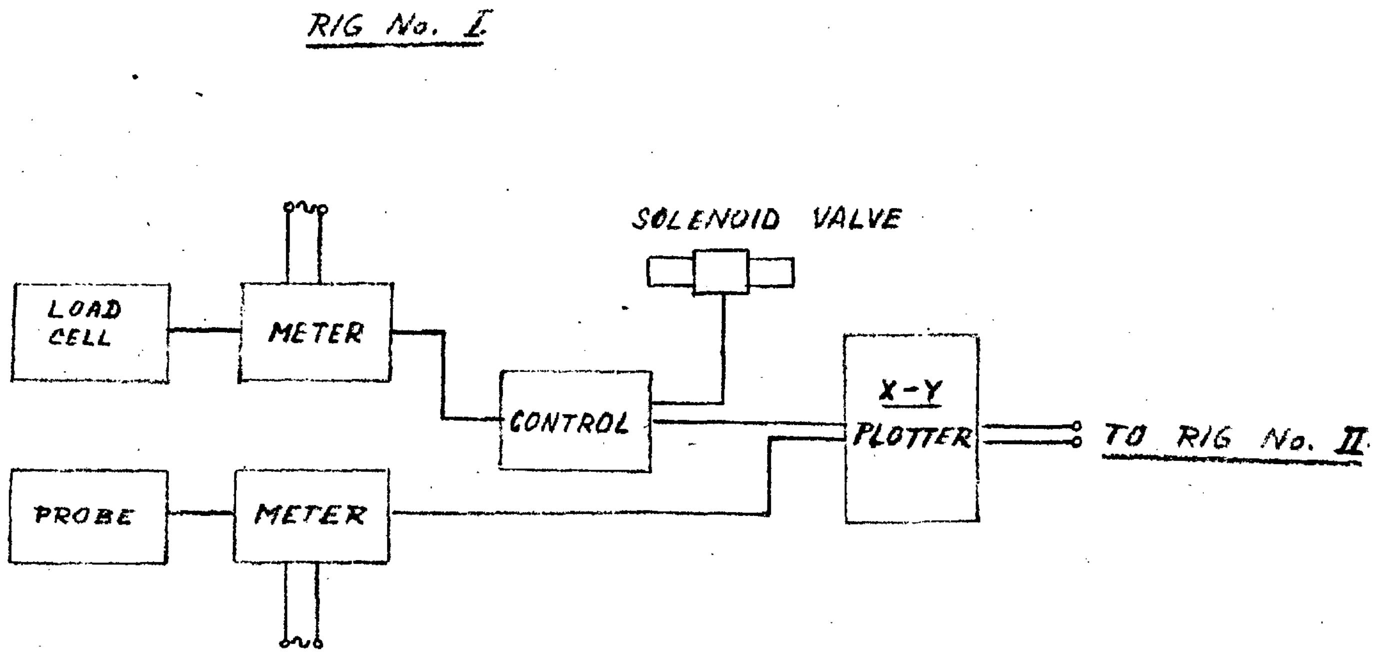

FIG. 11.

14TH FEB 62		
BSRA RIG - INSTRUMENTATION		RN - 14

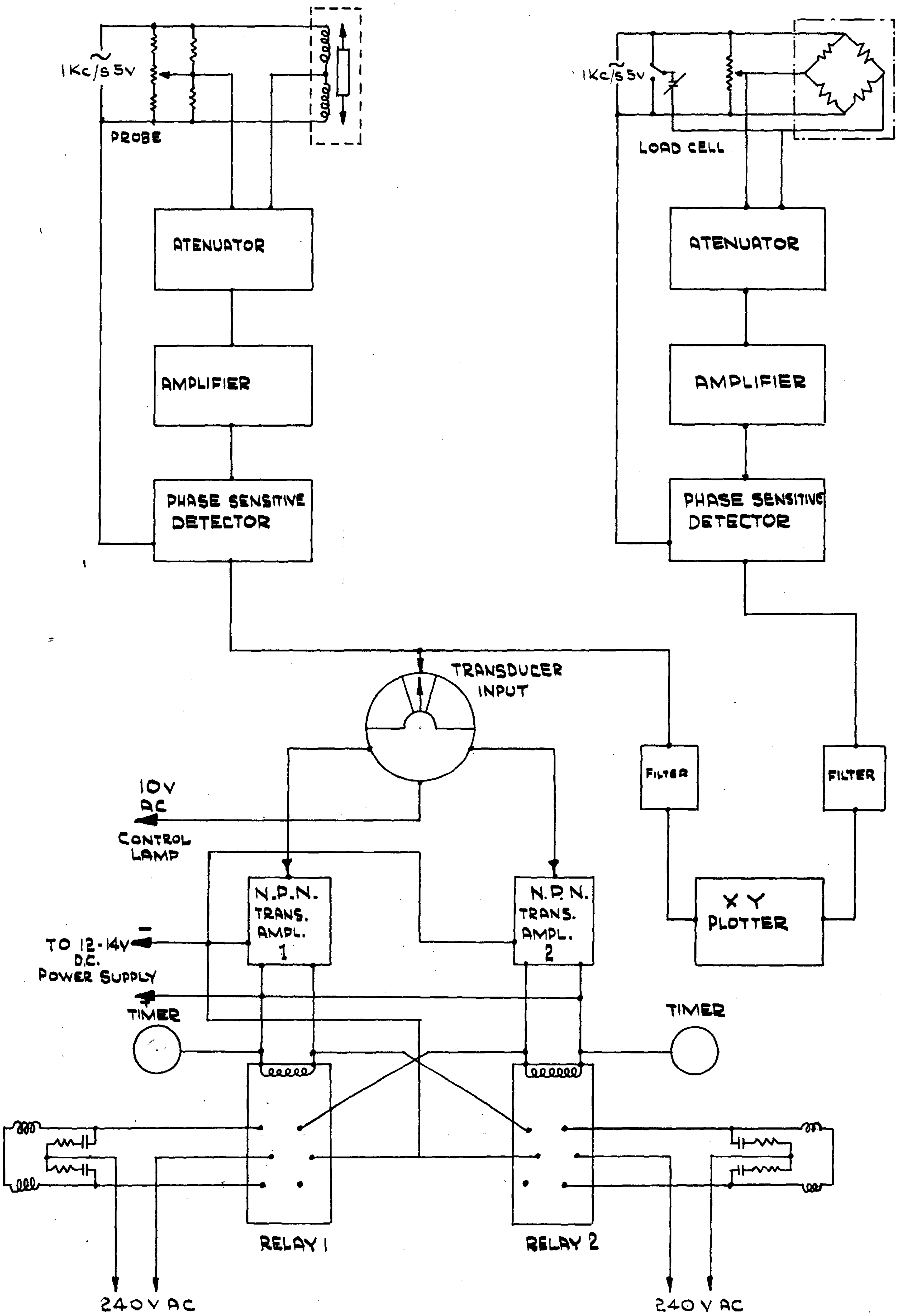

FIG.12. Cycling control

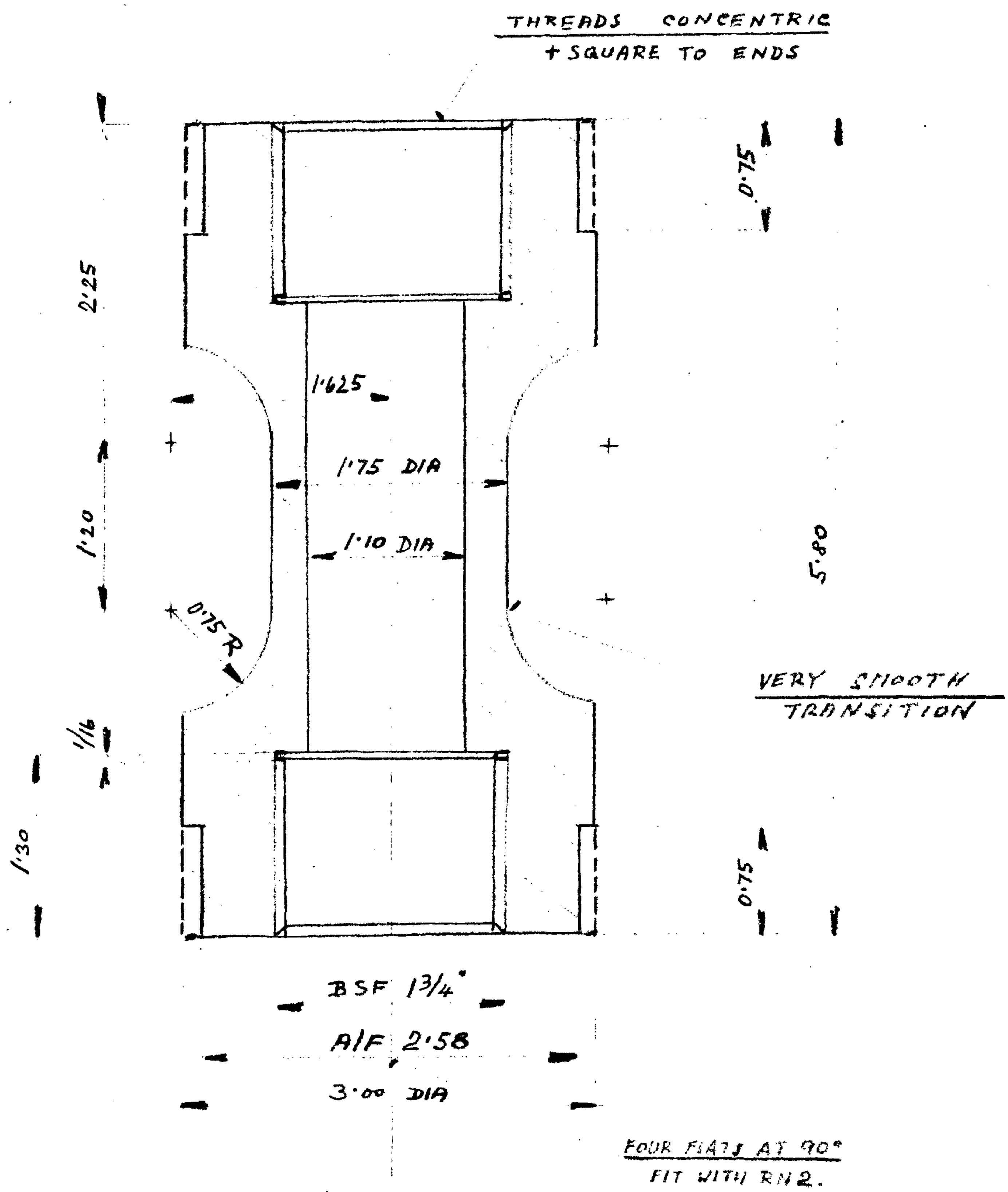

1- OFF

30th NOV. 61	MAT. EN24	HARDN.	GROUND + TEMP.
LOAD CELL			RN-1

SMOOTH ALL EDGES **FIG. 13.**

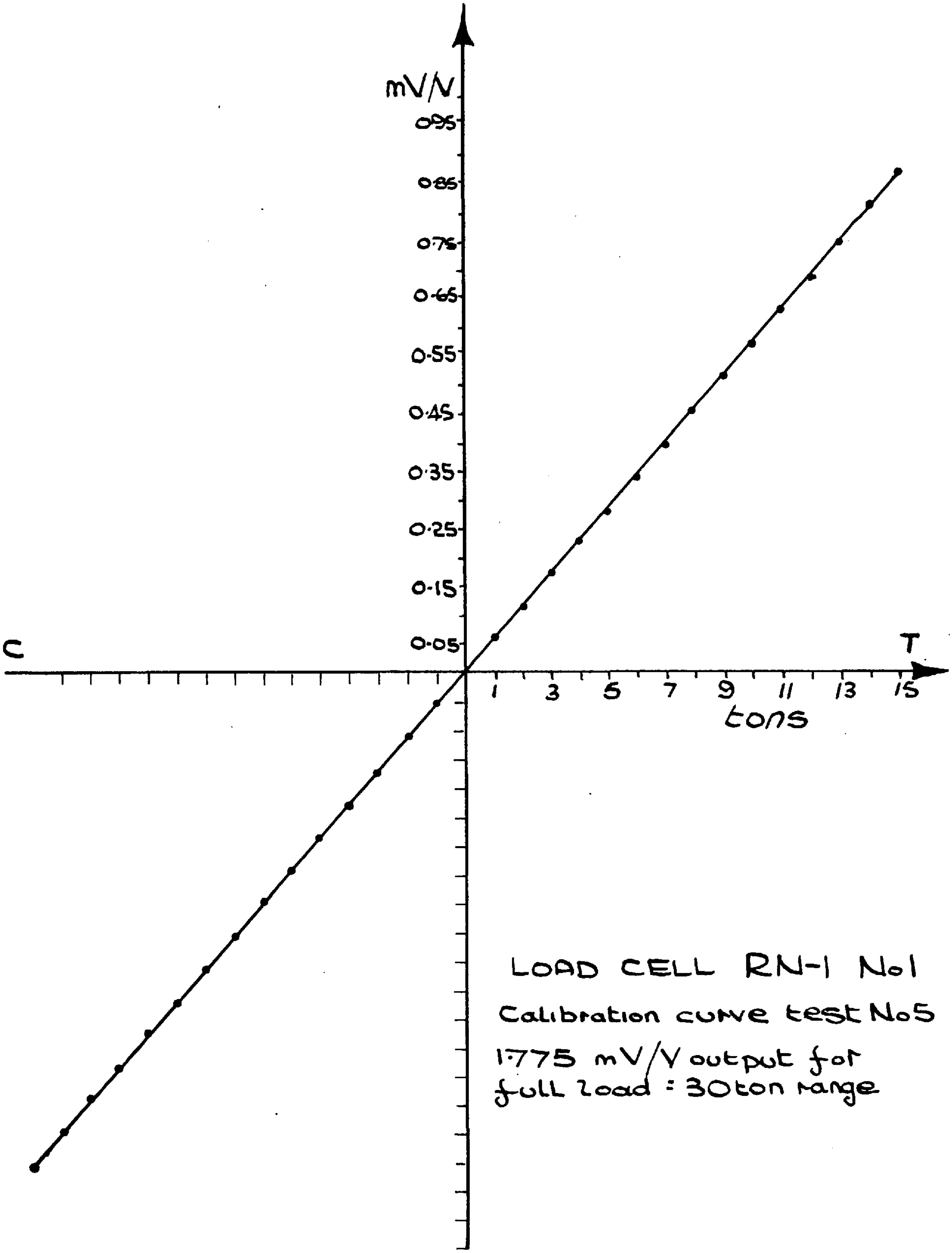

FIG.14.Calibration of load cell

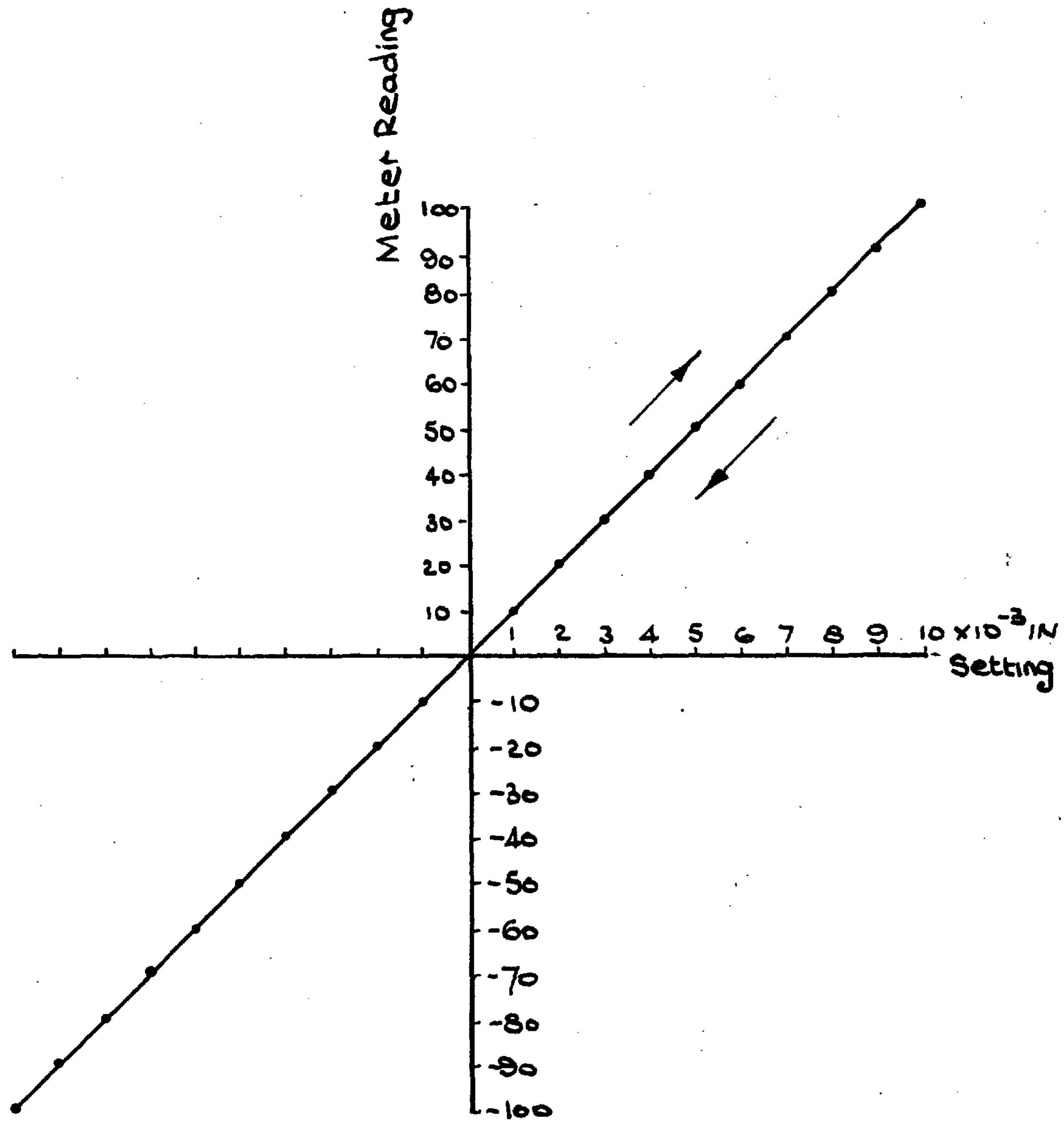

PROBE I CALIBRATION CURVE TEST No 3

Meter reading against
ZEISS micrometer screw

Scale ±100 Gaugefactor: 2·13
Attenuation factor 4

FIG.15. Calibration of probe

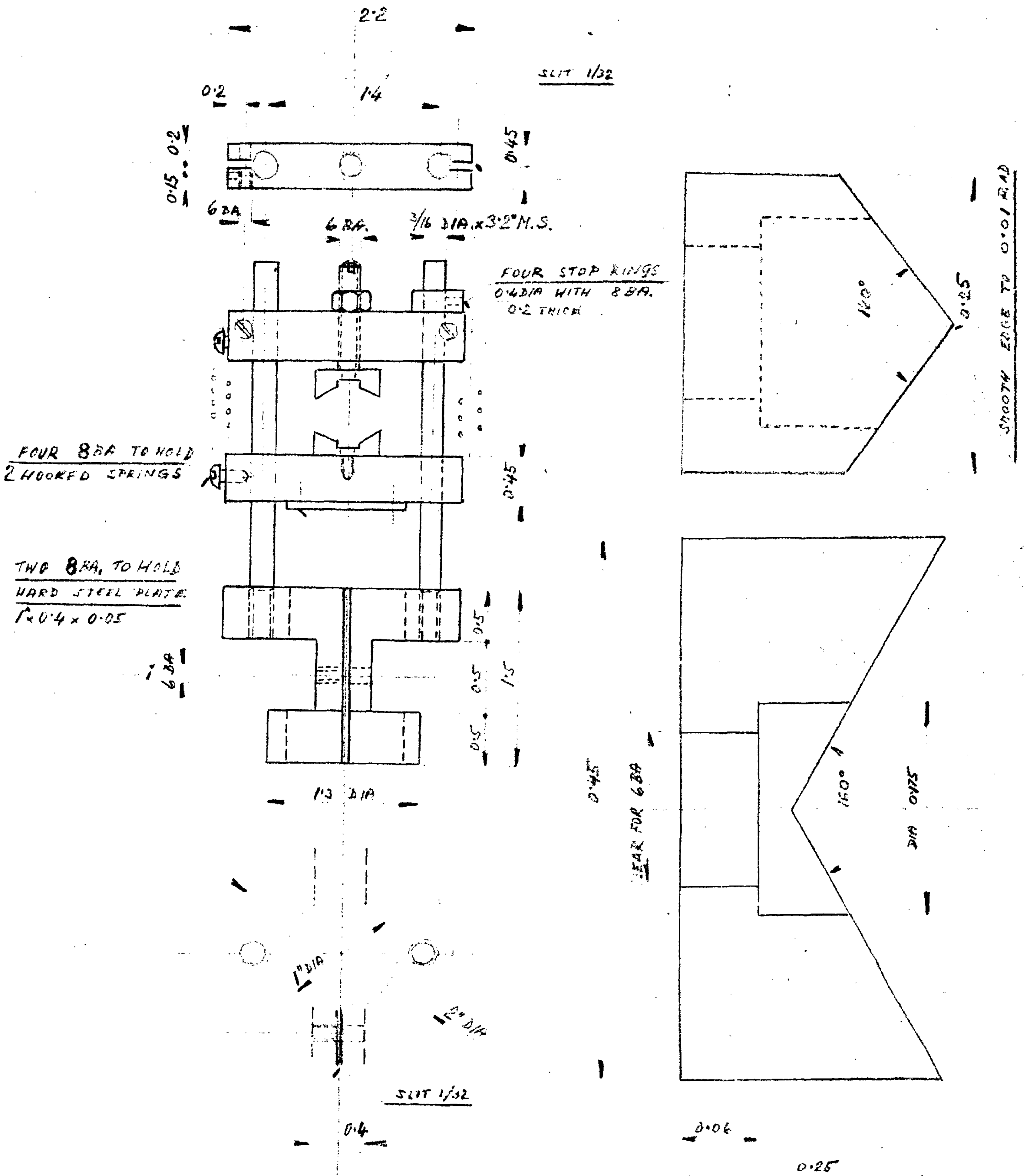

2-OFF TOOL STEEL
HARDN^D + GROUND EDGE
SCALE 10:1

NOTE: VEE BLOCKS
MUST BE AXIAL

1-OFF

FIG. 16.

2ND FEB 62	MAT. DURAL	
PROBE HOLDER		RN-12

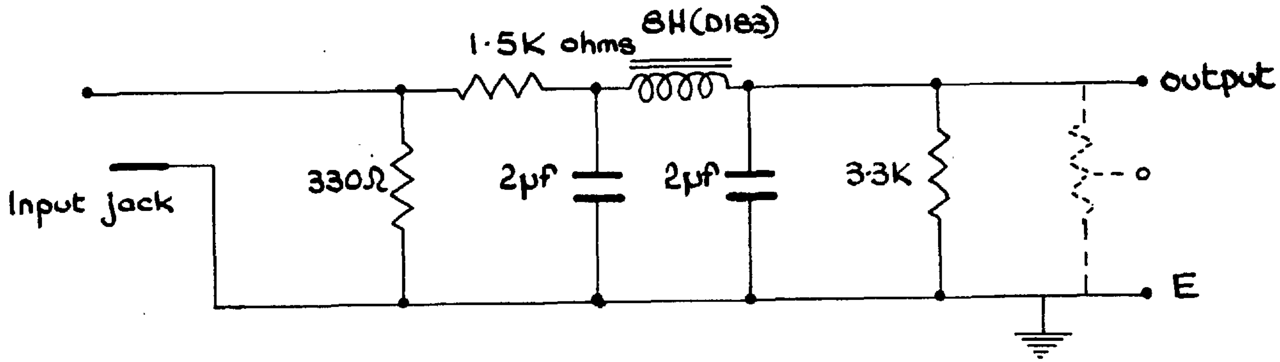

FIG.17. Filter circuit

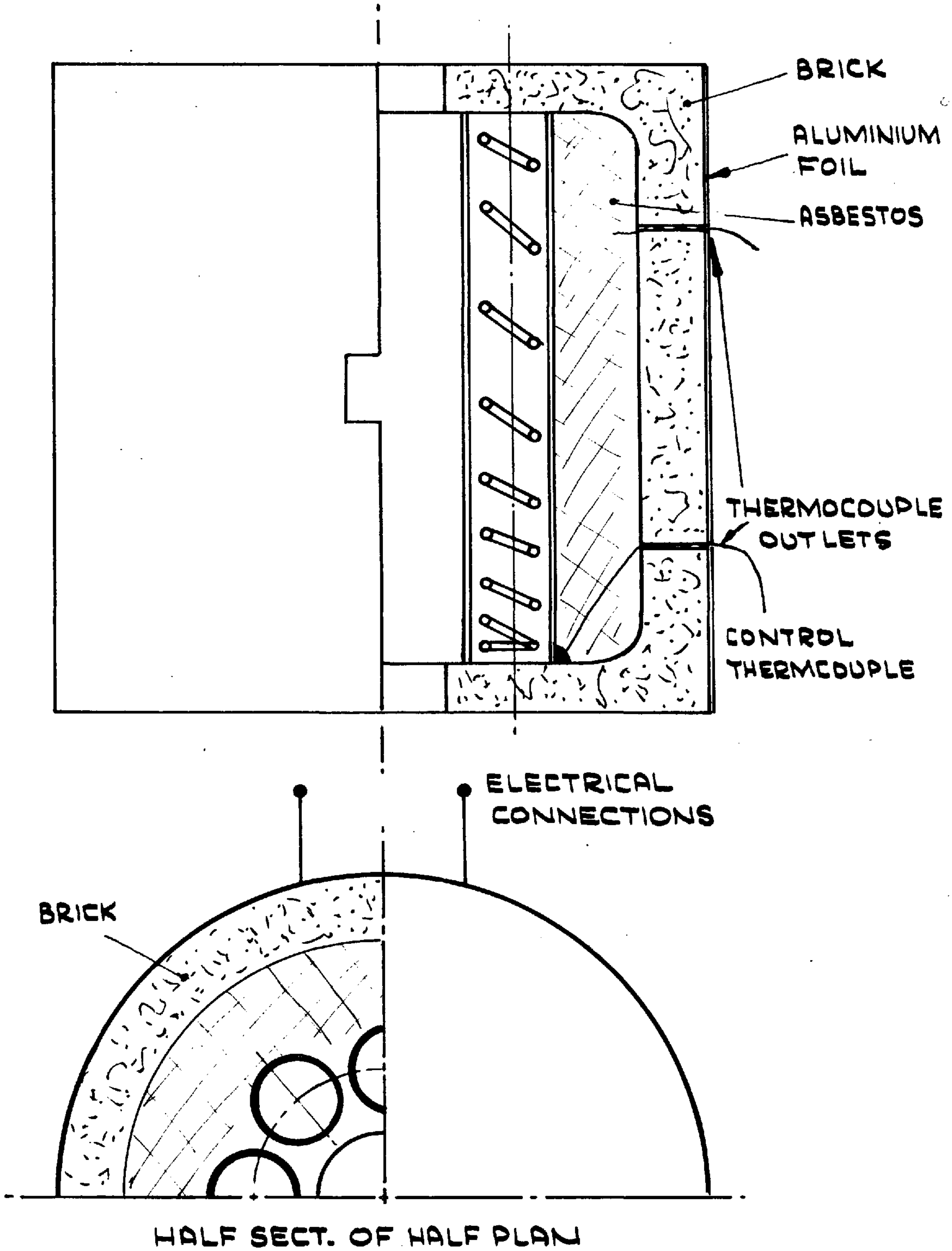

FIG.18. El. Furnace

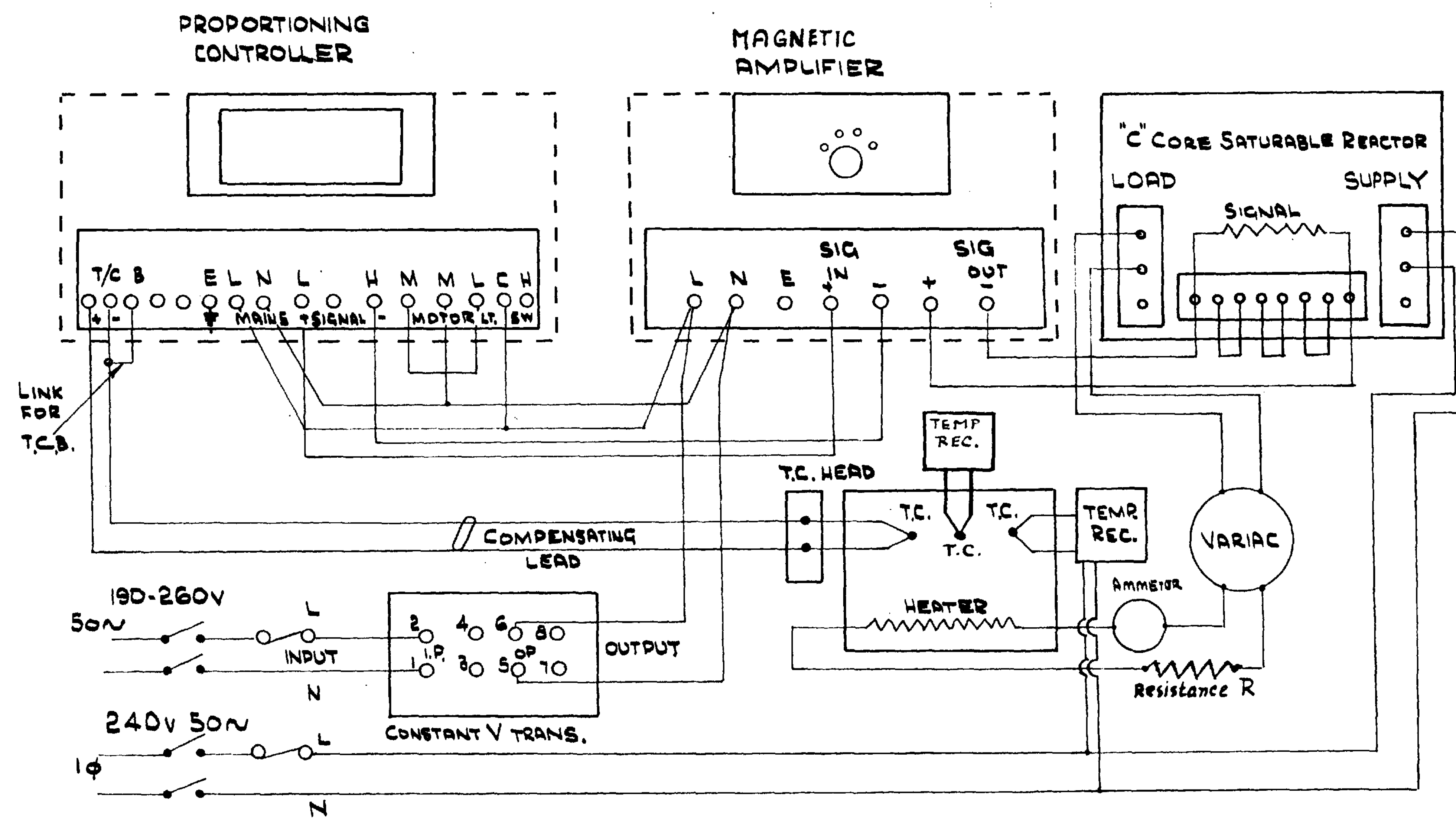

FIG.19 Temperature control

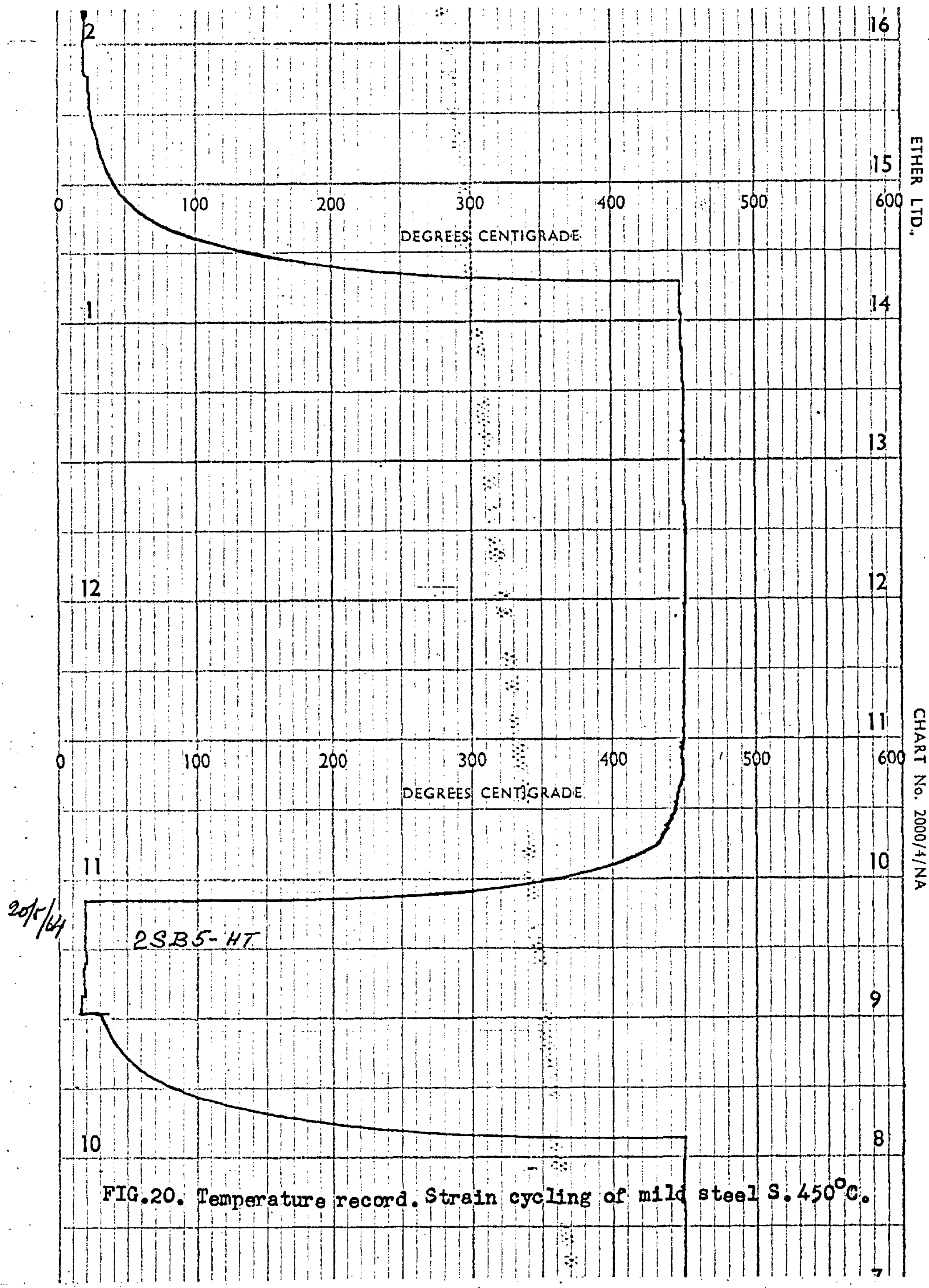

FIG.20. Temperature record. Strain cycling of mild steel S. 450°C.

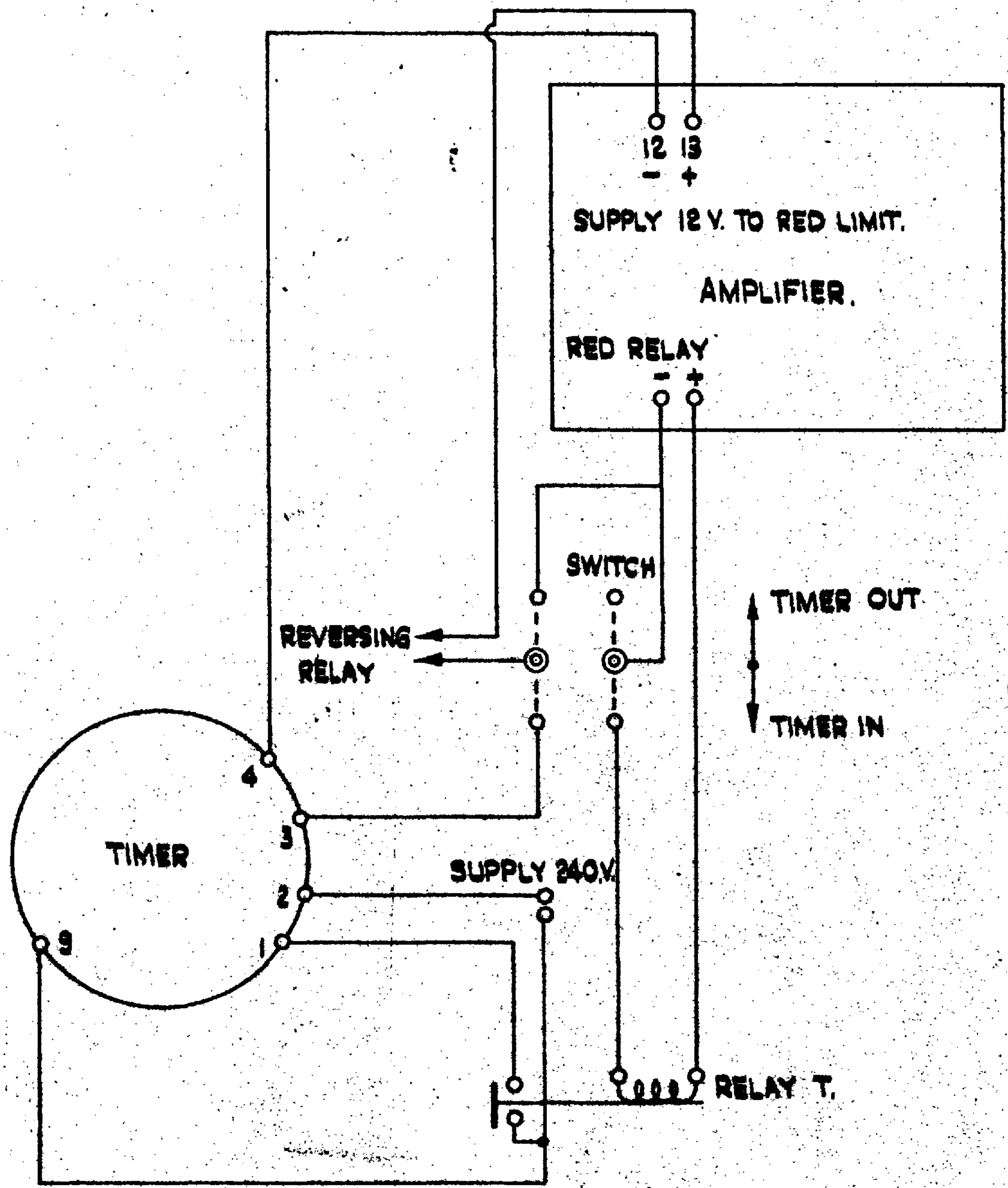

FIG.21. CONNECTIONS TIMER - AMPLIFIER.

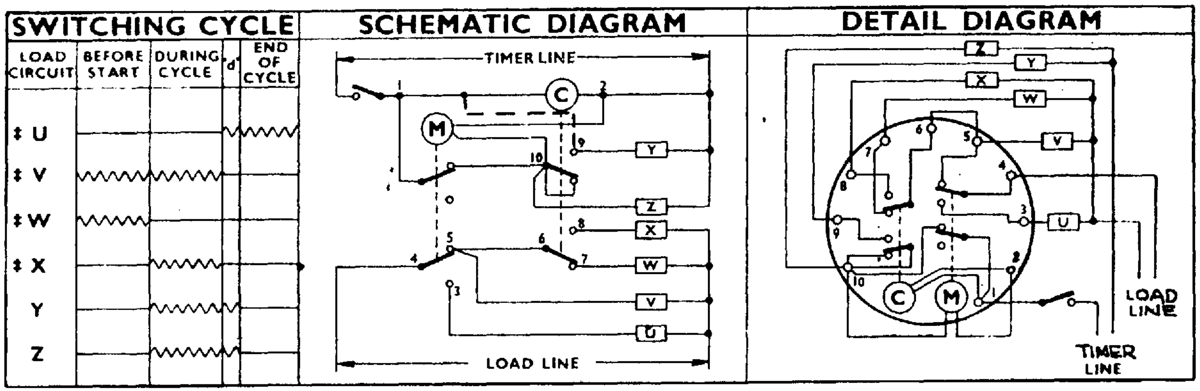

FIG.22. Timer diagram

1S B1

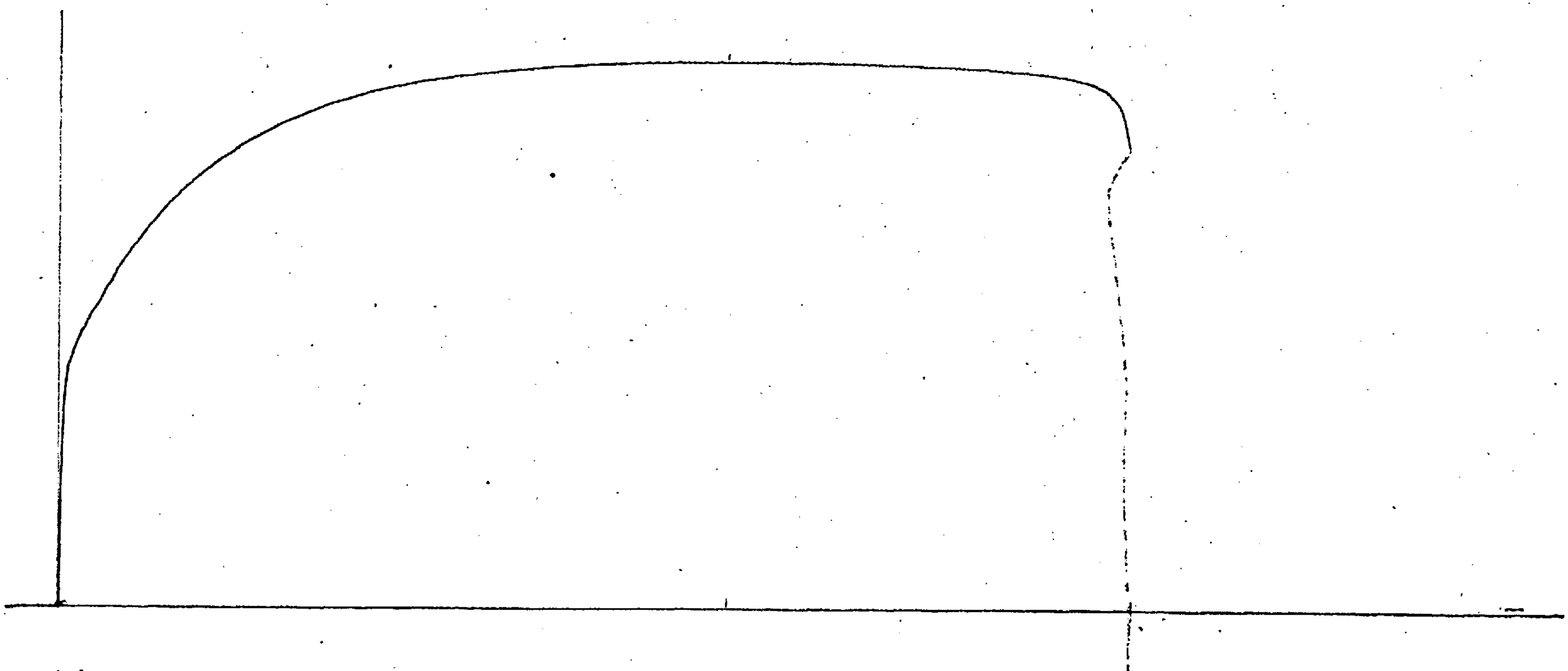

λ 1 Ton

• > 0·005"

$\varepsilon_{FD} = 14{\cdot}4\%$

Fig.23. Cast mild steel S.Load v. deflection at room temp.

2SB1- HT

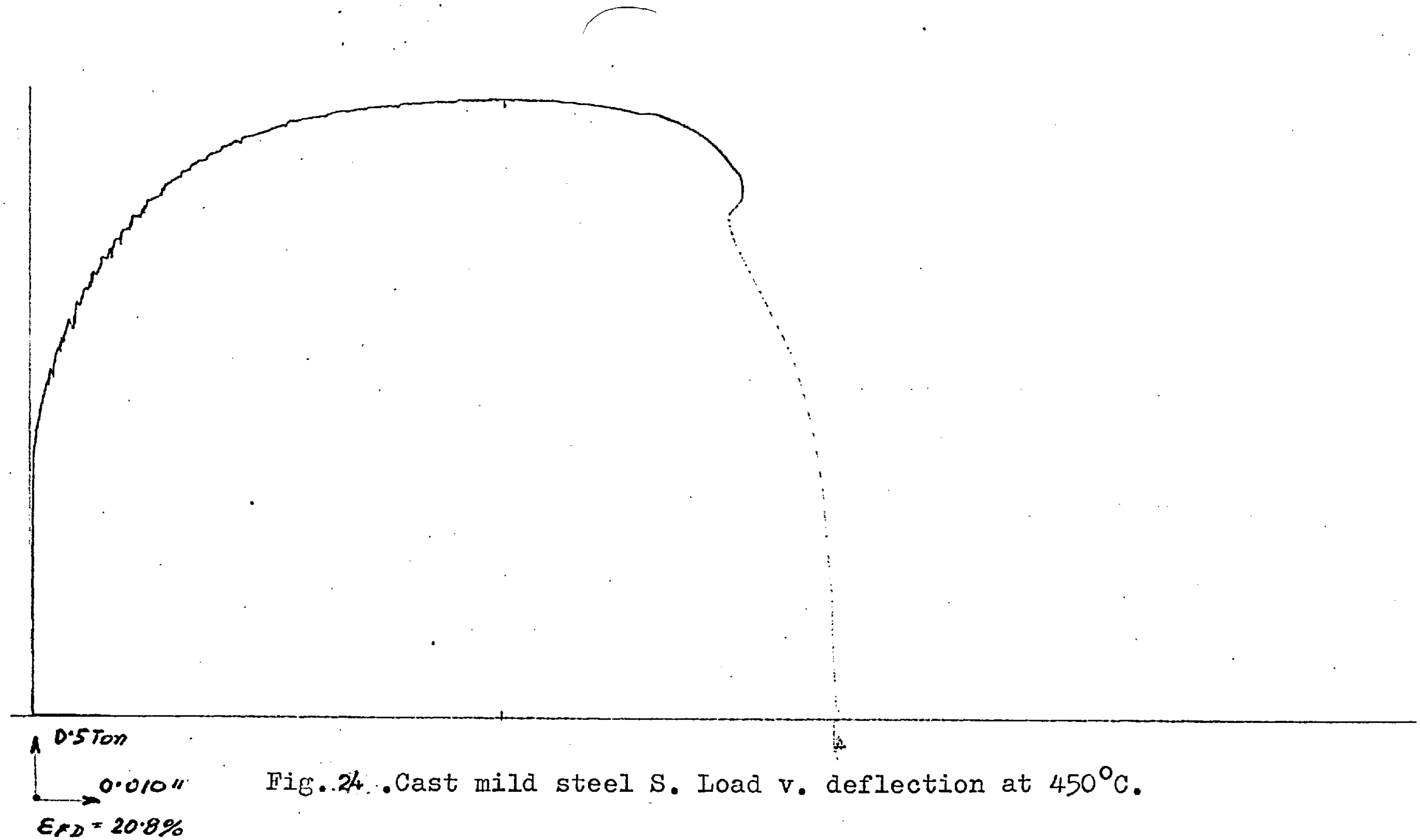

Fig. 24 .Cast mild steel S. Load v. deflection at 450°C.

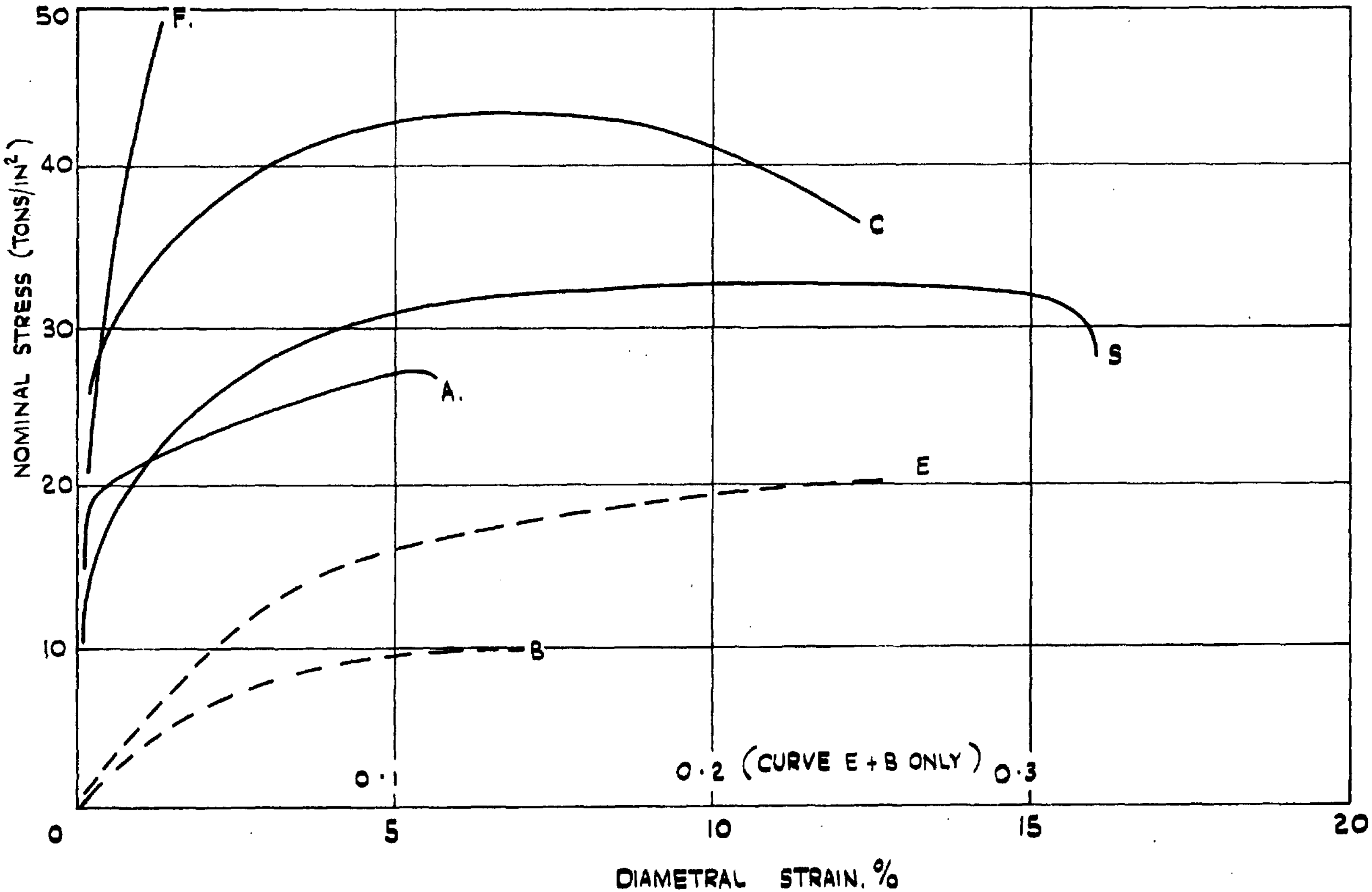

FIG.25. Static stress-strain curves at room temperature

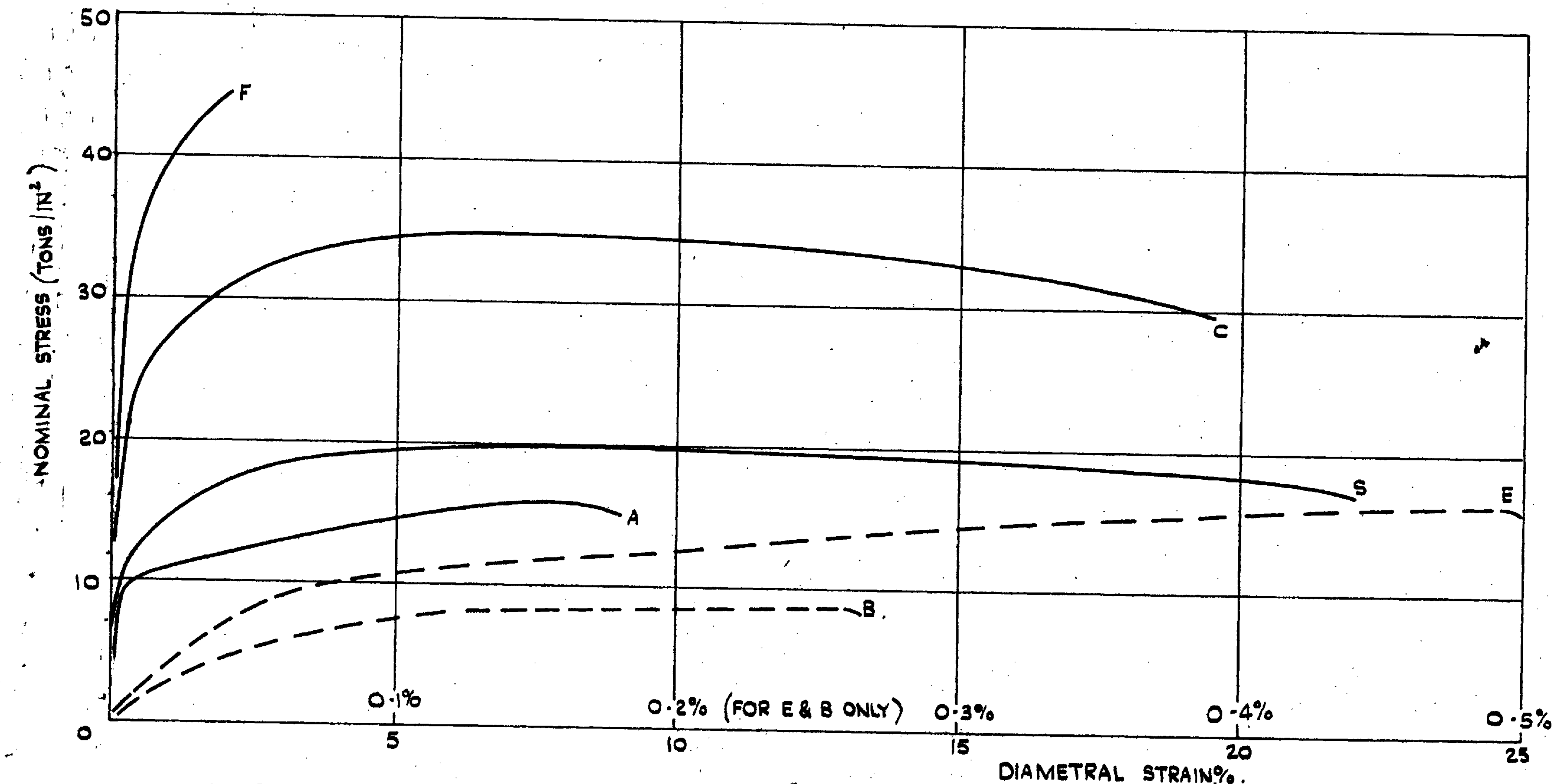

FIG. 26. Static stress-strain curves at 450°C

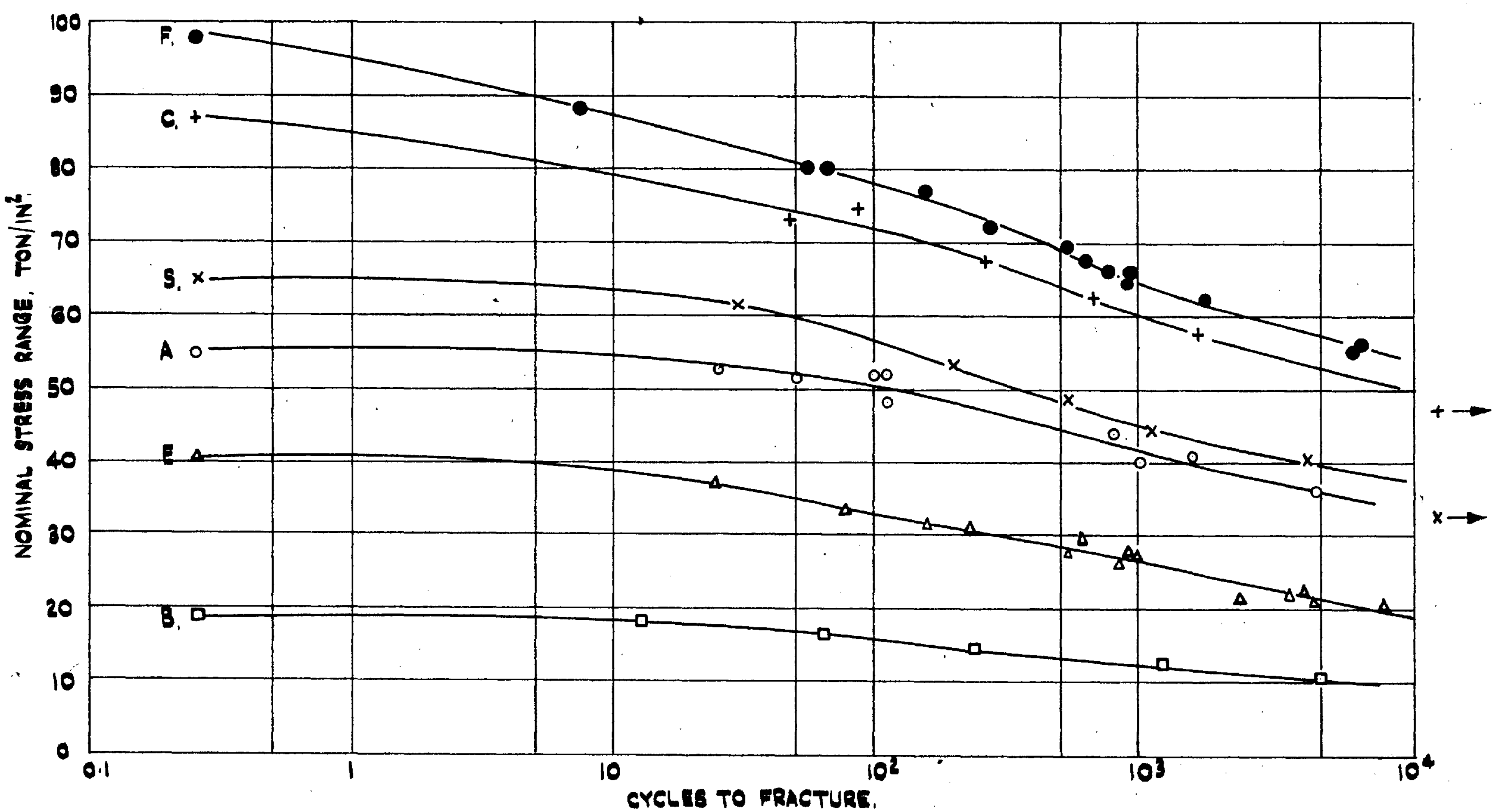

FIG. 27. LOAD CYCLING OF PLAIN SPECIMENS.

/AT2

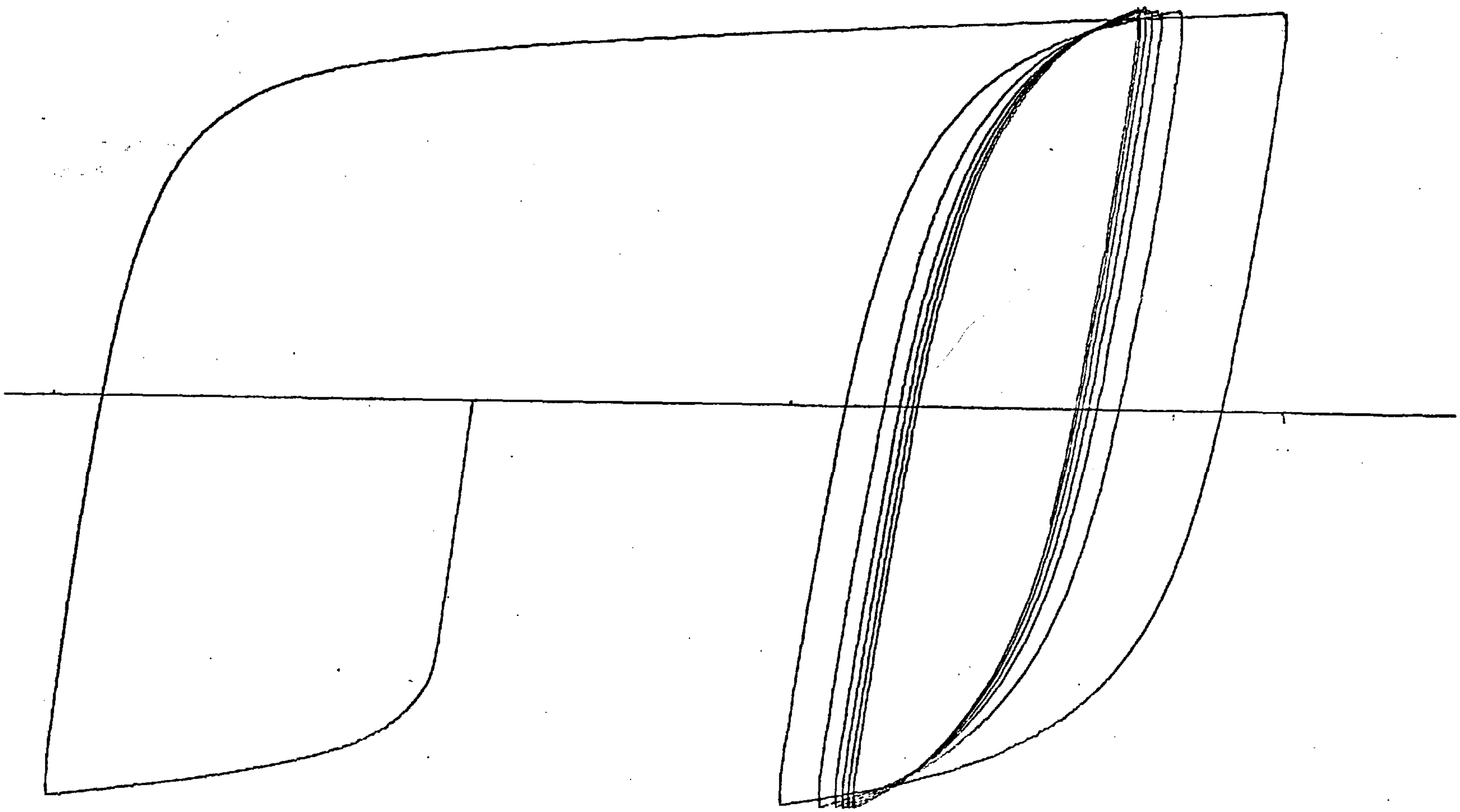

CYCLE Nos. 1 ÷ 7 (N=50)

1 Ton $\Delta\sigma = 48^T/_{in^2}$

0·001"

Fig. 28 .Cast iron A.Load cycling, first 7 cycles.

1AT2

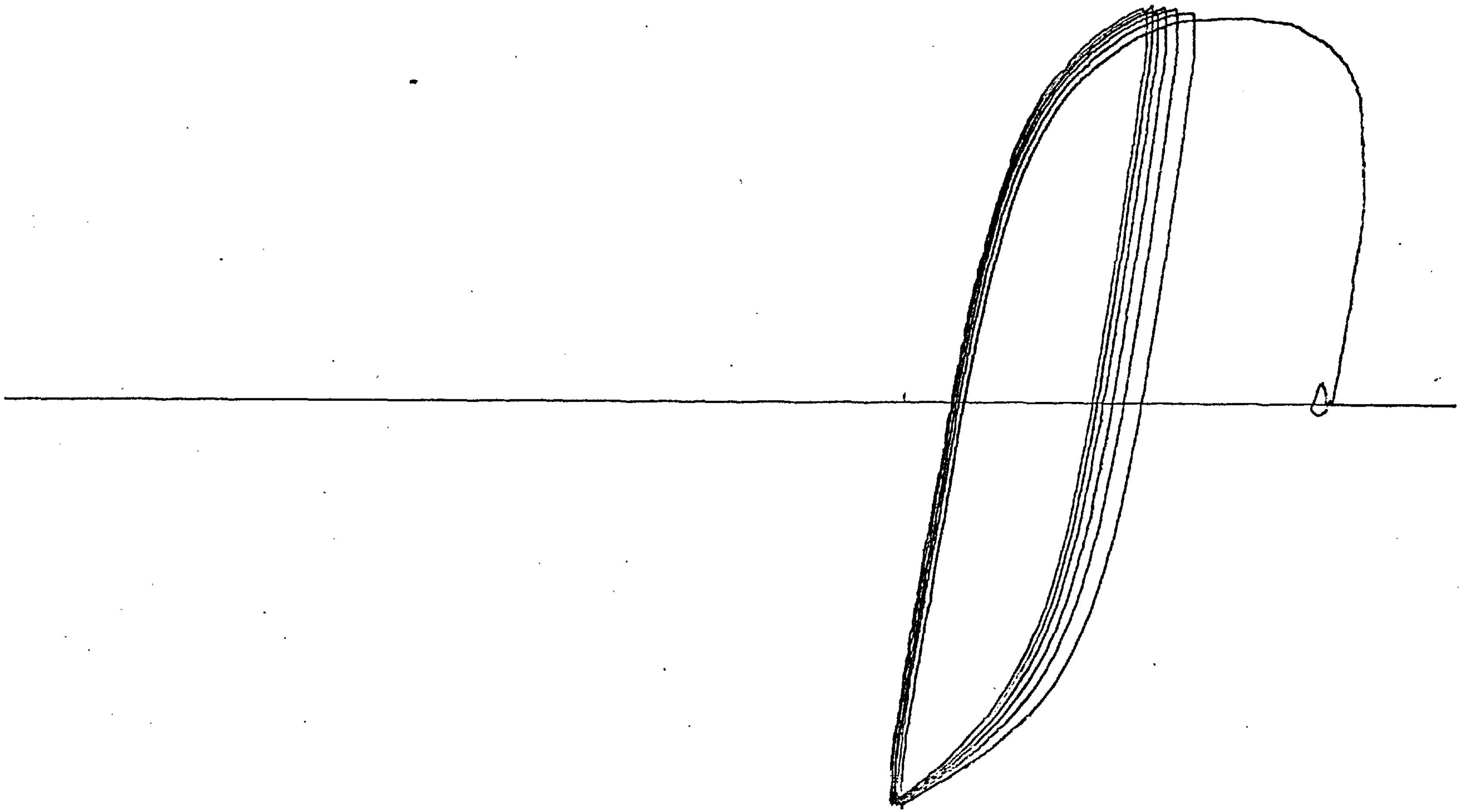

CYCLE Nos. 44 ÷ 50
9688-
1 Ton $\Delta\sigma = 48 T/IN^2$
0·001"

Fig. 29 . Cast iron A. Load cycling, final 6 cycles.

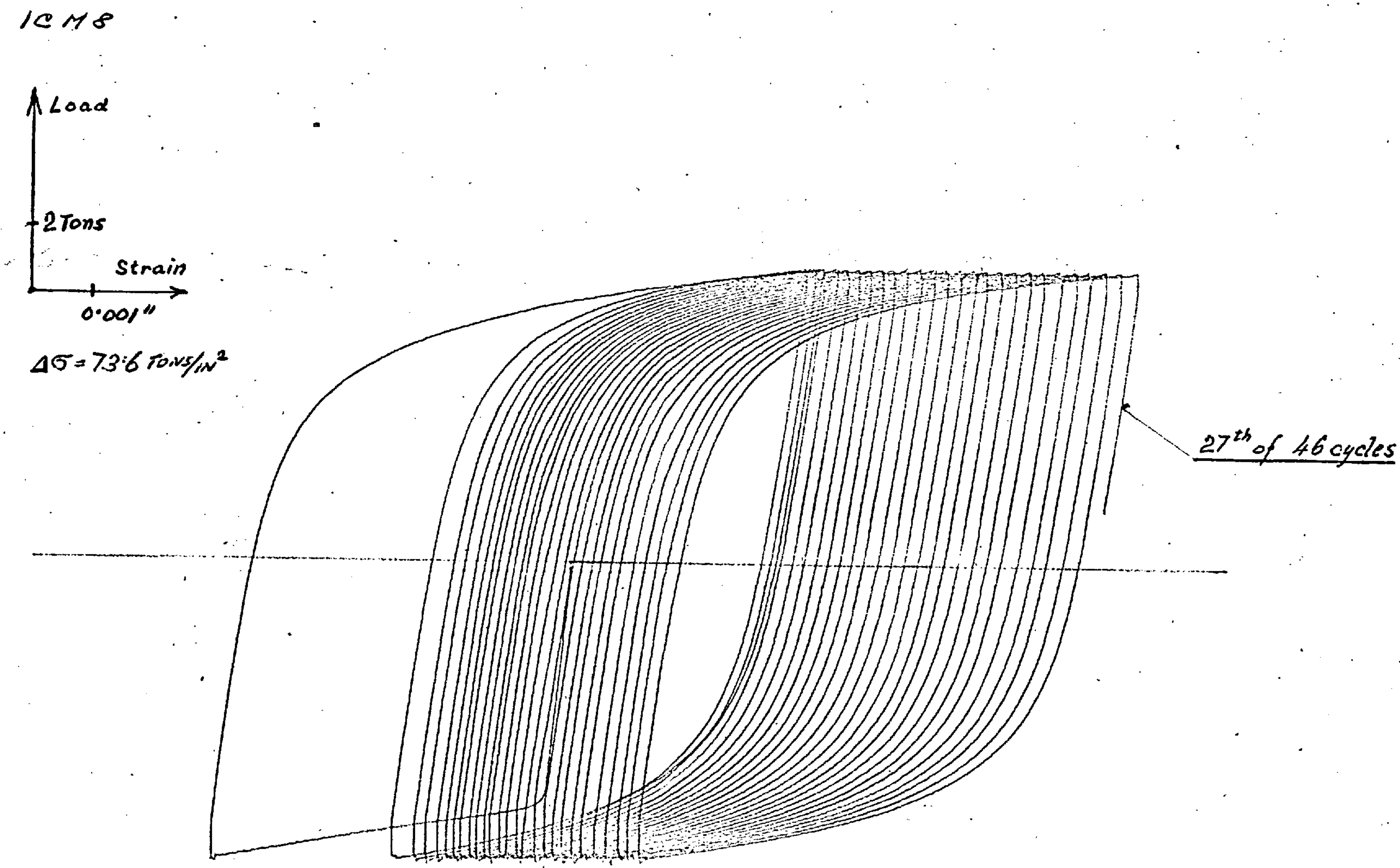

Fig. 30. Cyclic Creep of Cast Steel C during Load Cycling.

ICM8

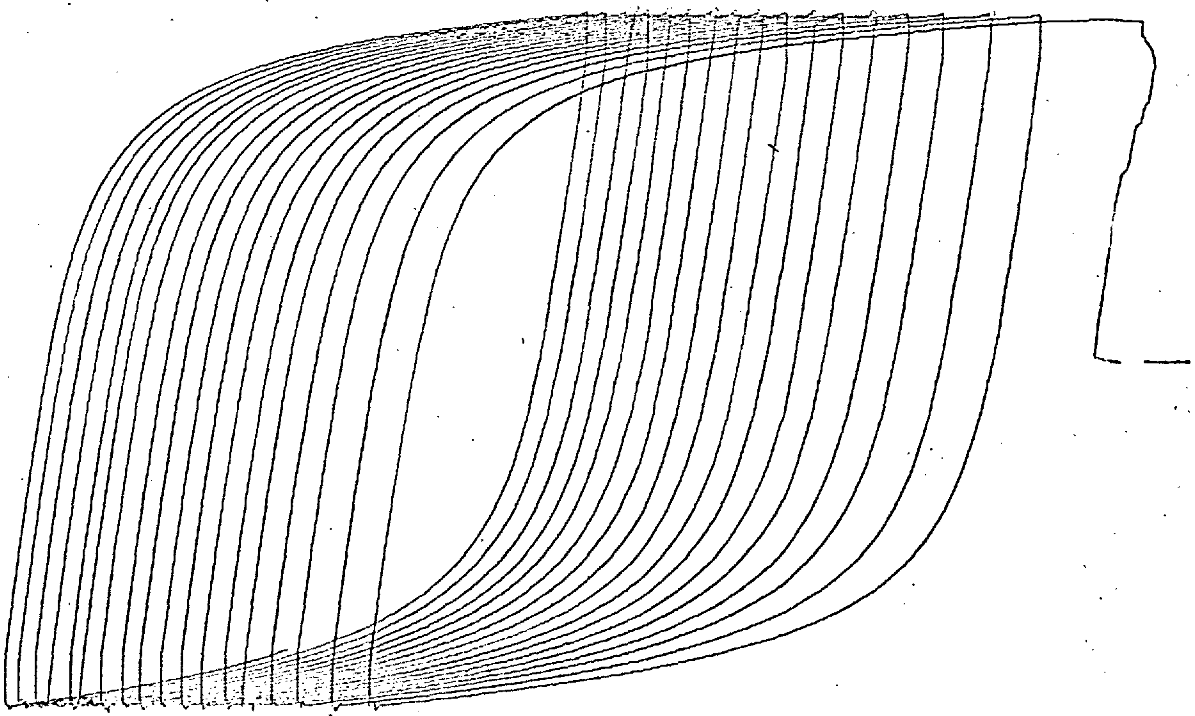

2 Tons $\Delta\sigma = 73.6\ T/IN^2$

0·001"

CYCLE Nos. 27-46

Fig. 31 .Cyclic creep of cast steel C.(Continuation) 4589 - 4635 Rupture

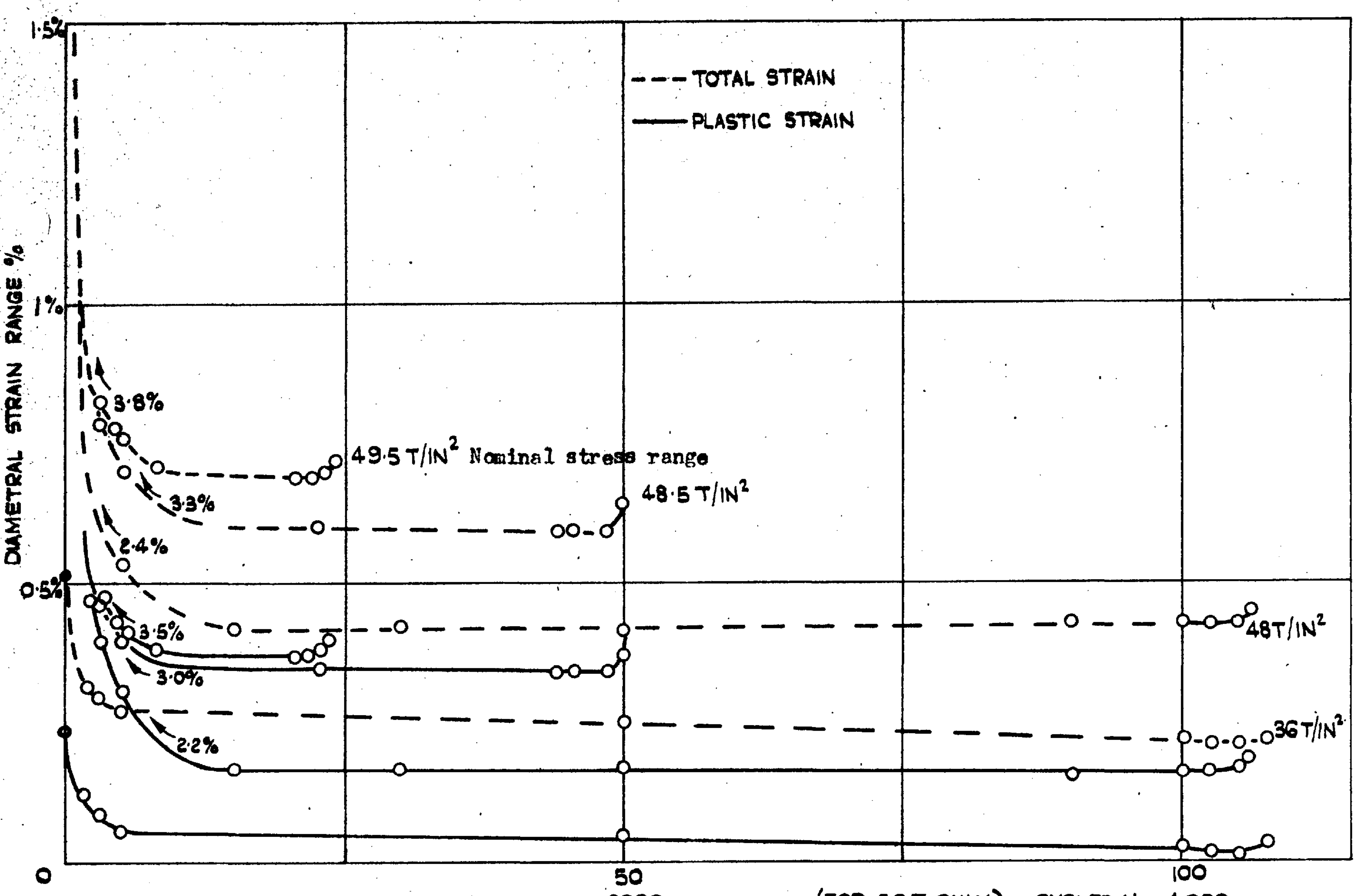

FIG.32. Variation of strain range during load cycling of cast iron A

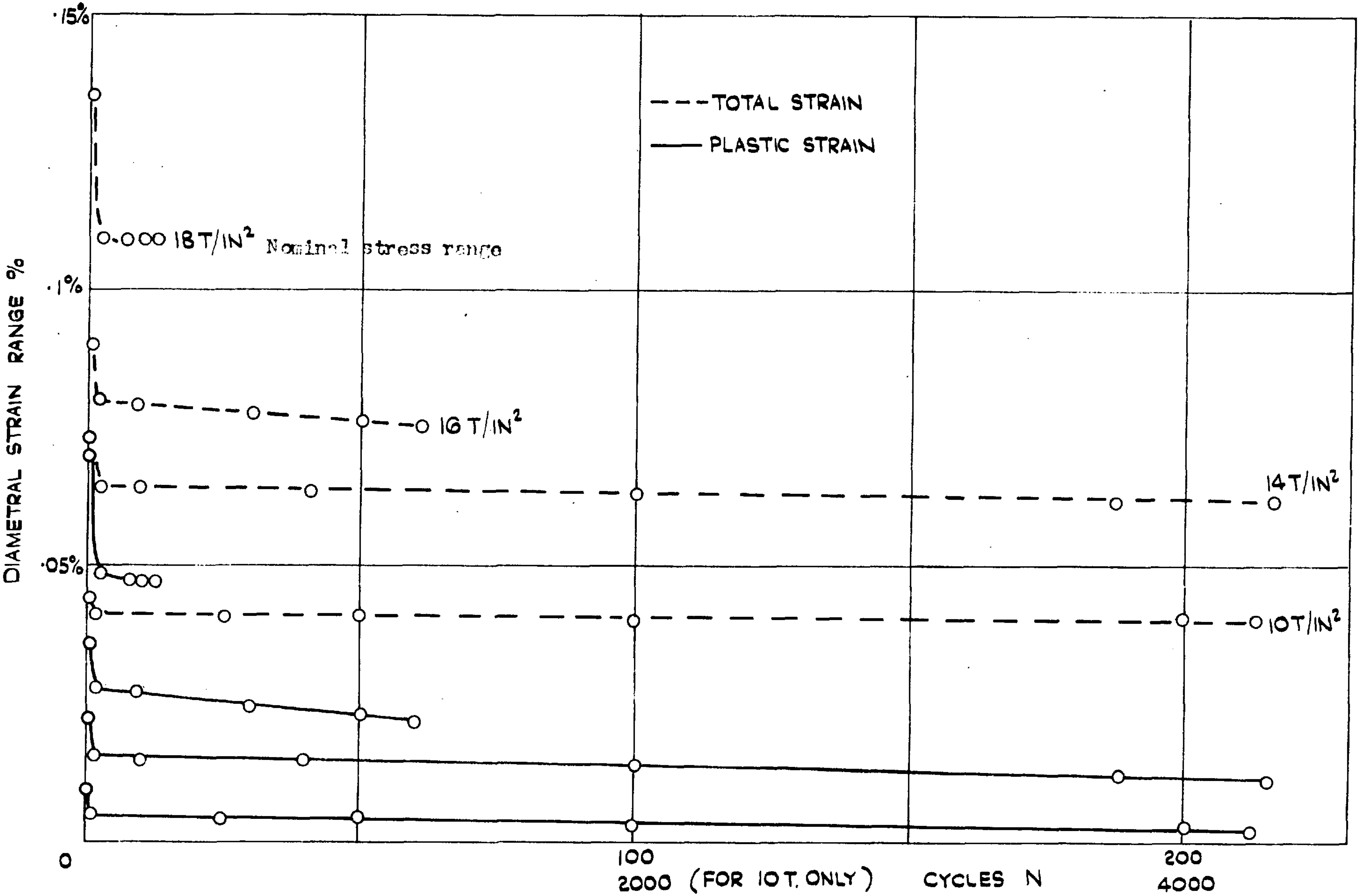

FIG. 33. Variation of strain range during load cycling of cast iron B

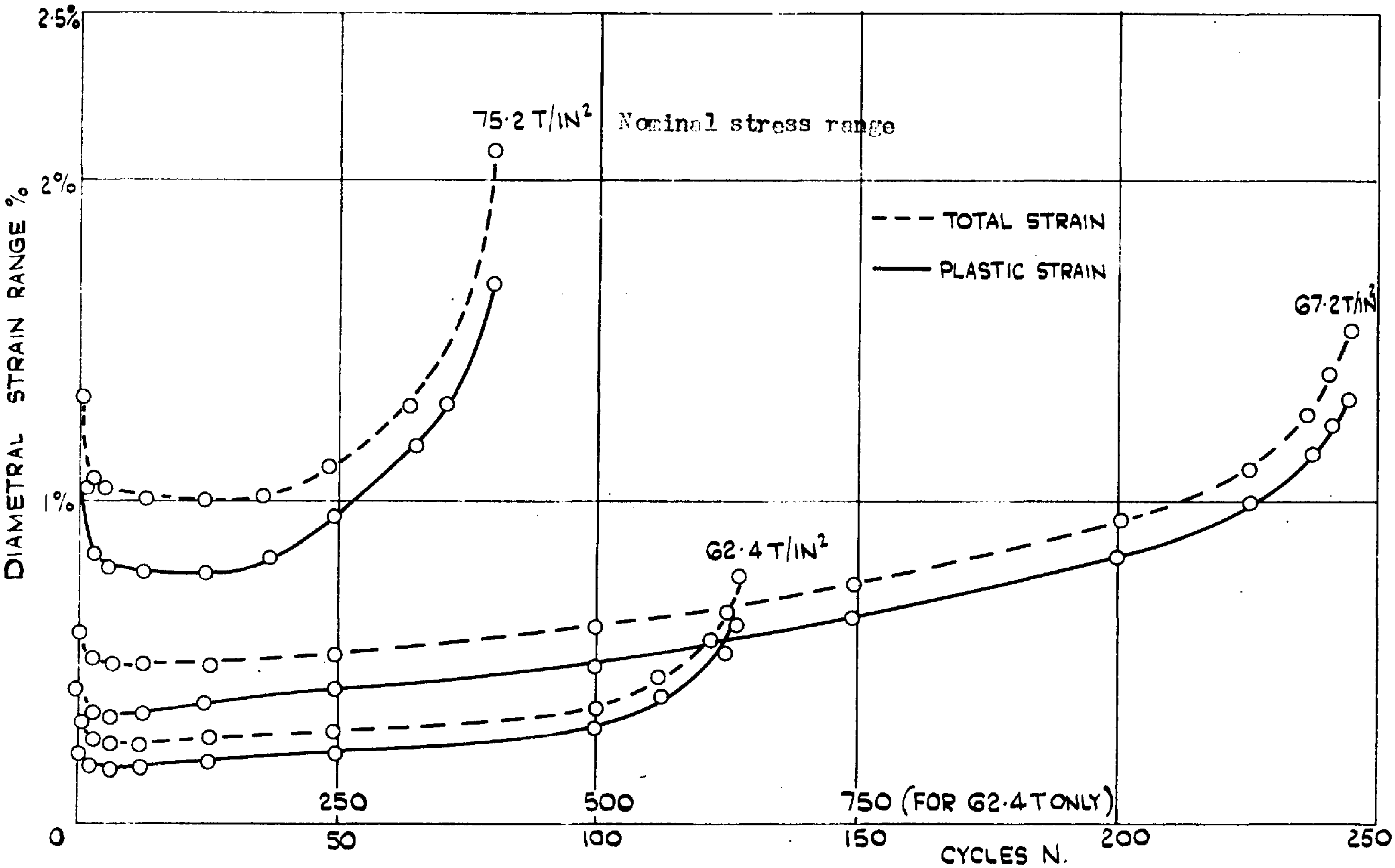

FIG.34. Variation of strain range during load cycling of cast steel C

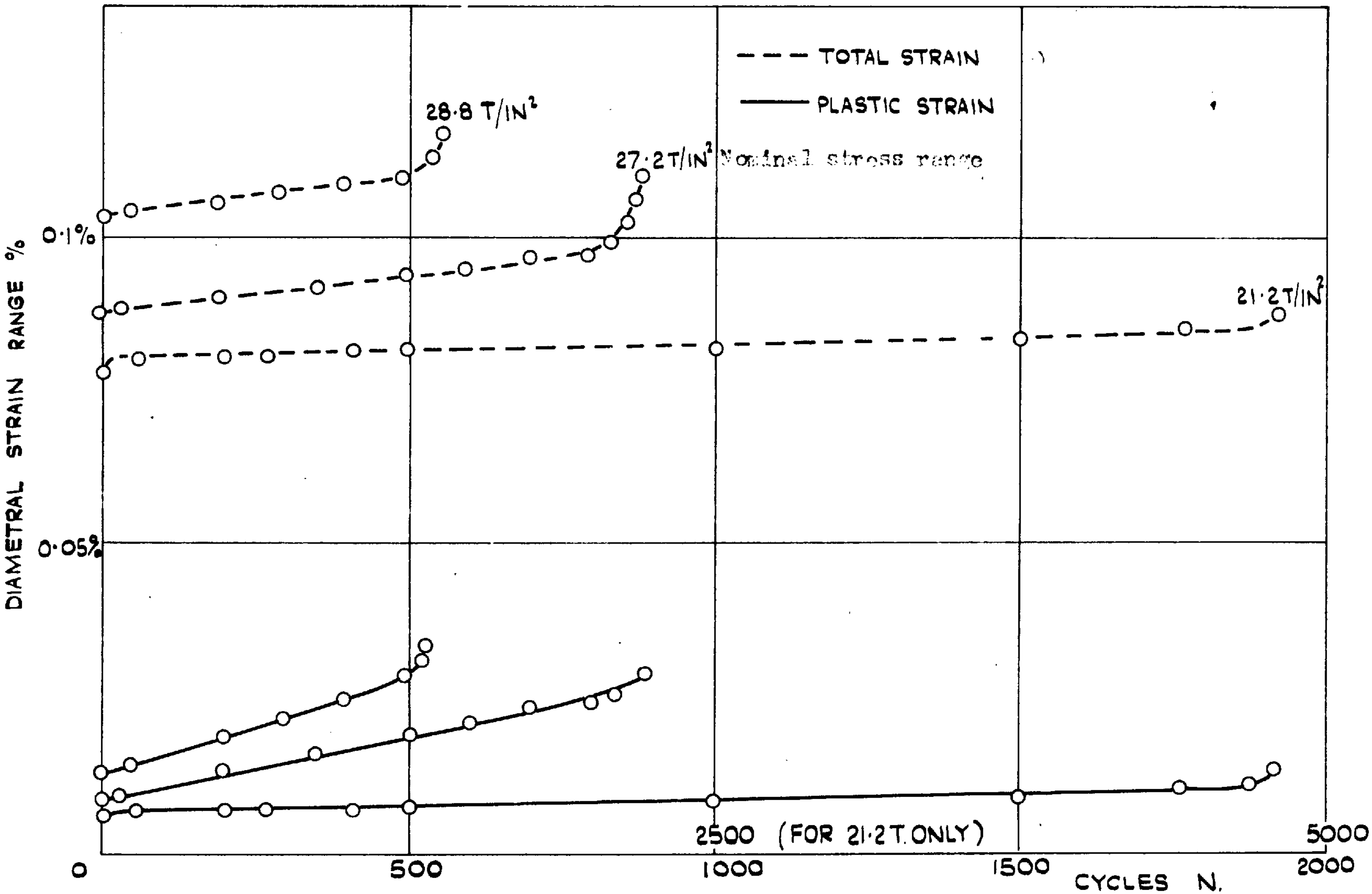

FIG.35. Variation of strain range during load cycling of cast iron E

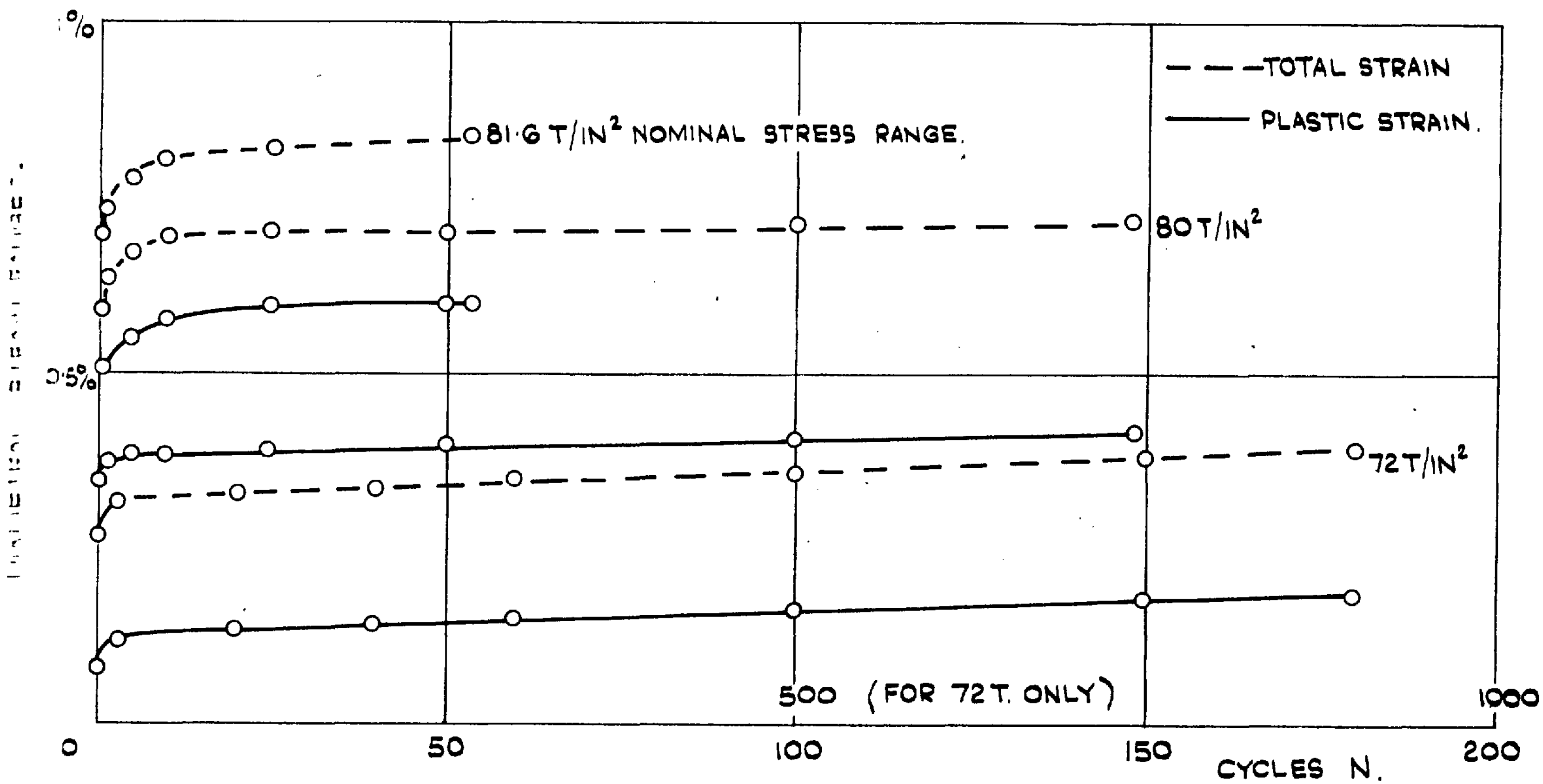

FIG. 36. Variation of strain range during load cycling of cast iron F

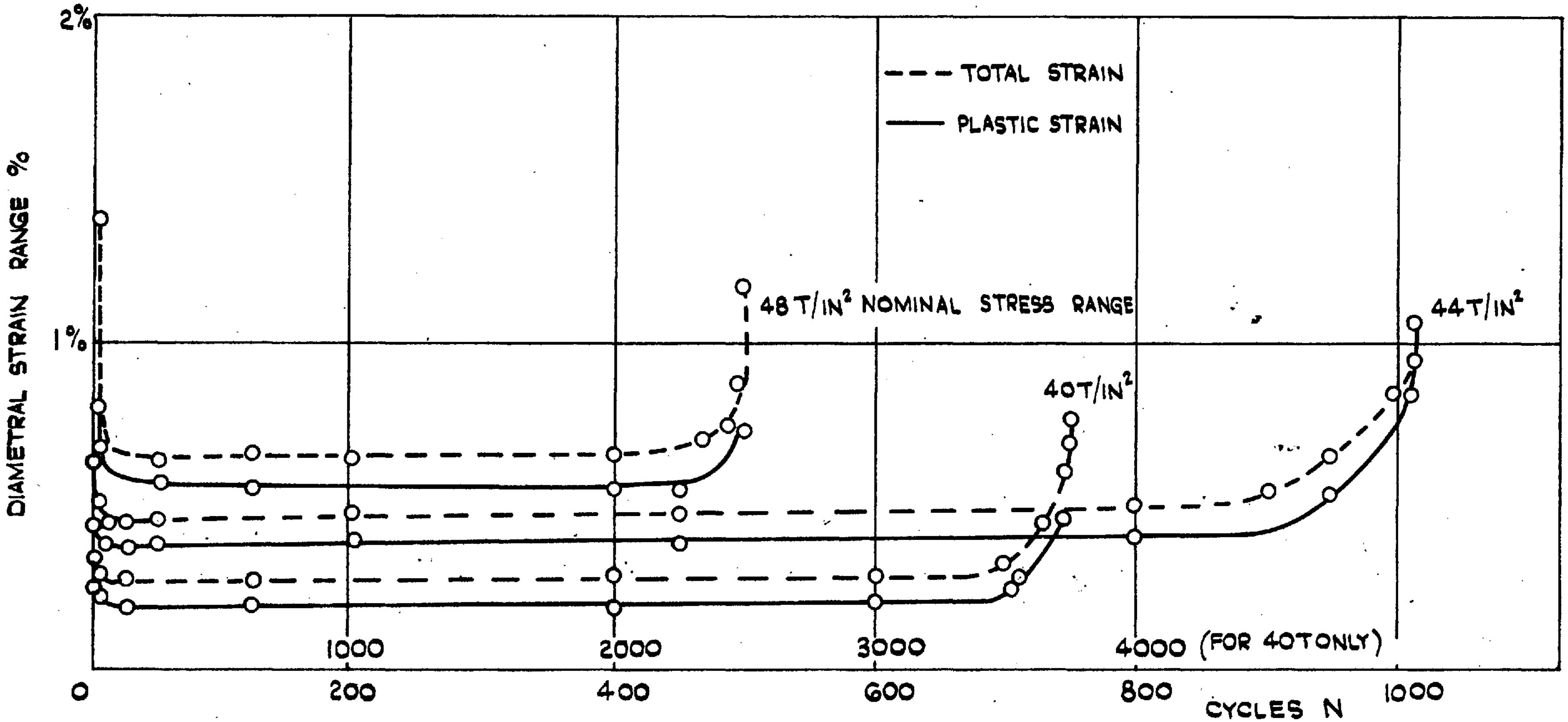

FIG.37. Variation of strain range during load cycling of cast steel S

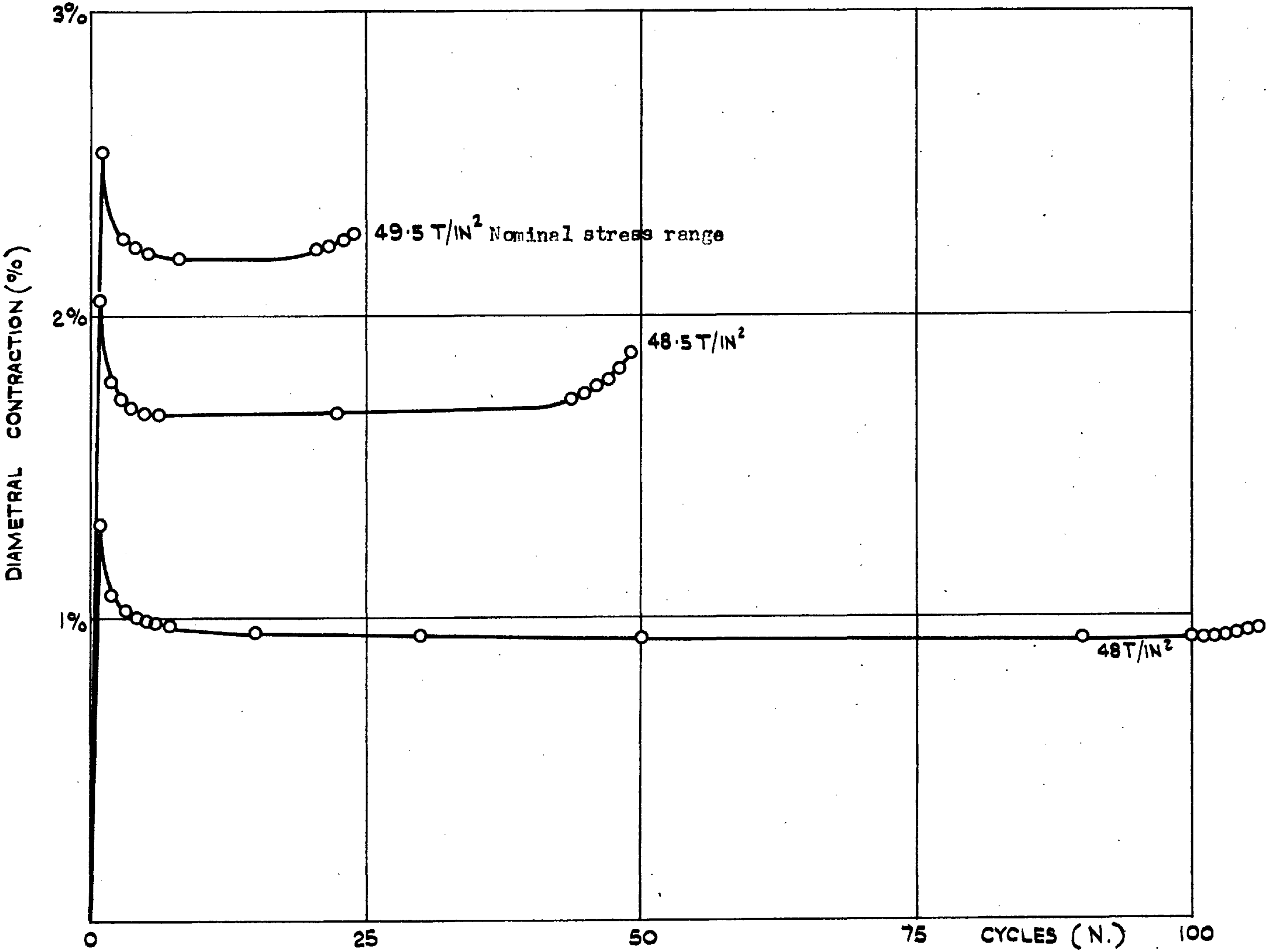

FIG. 38. Cyclic creep of cast iron A

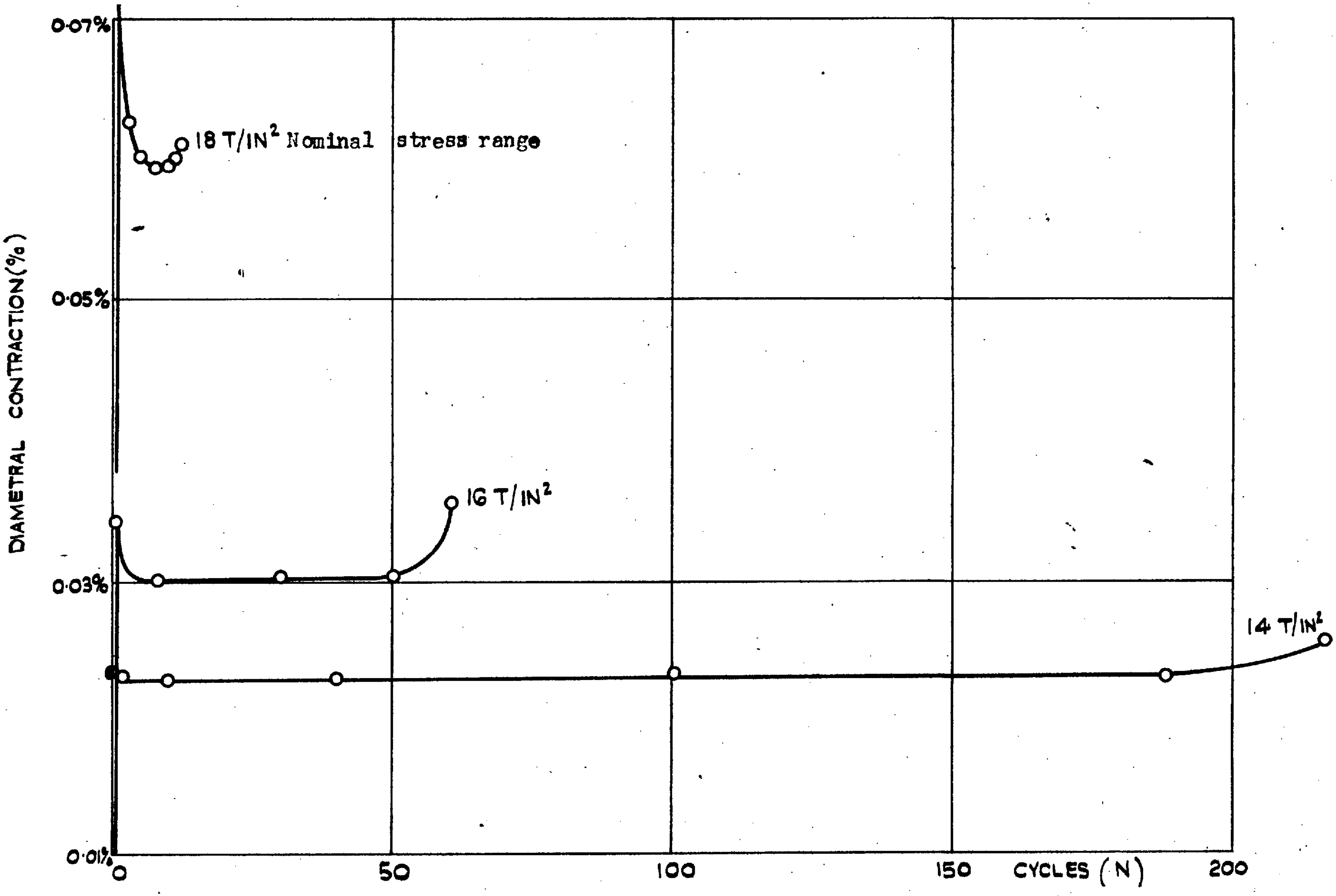

FIG.39. Cyclic creep of cast iron B

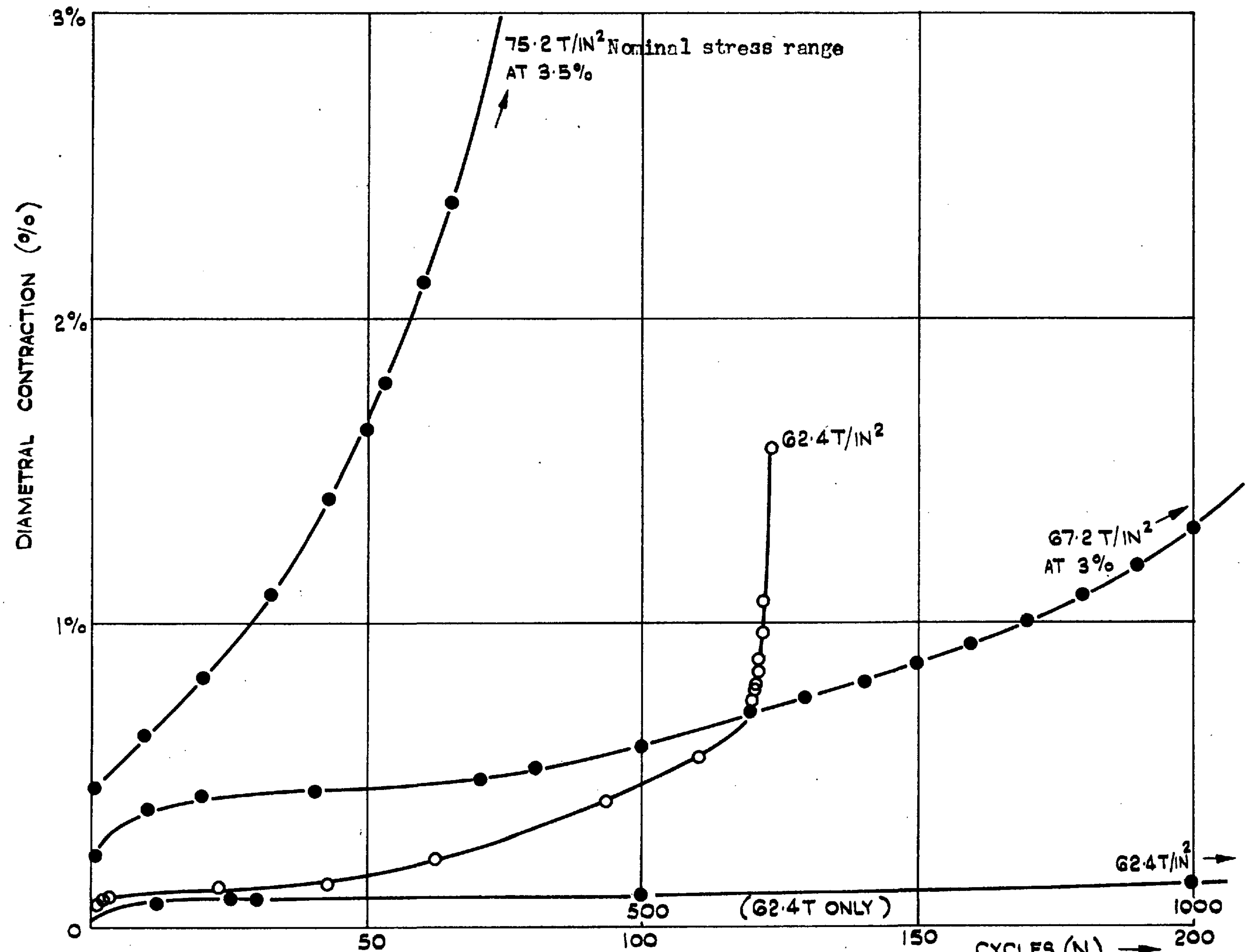

FIG.40. Cyclic creep of cast steel C

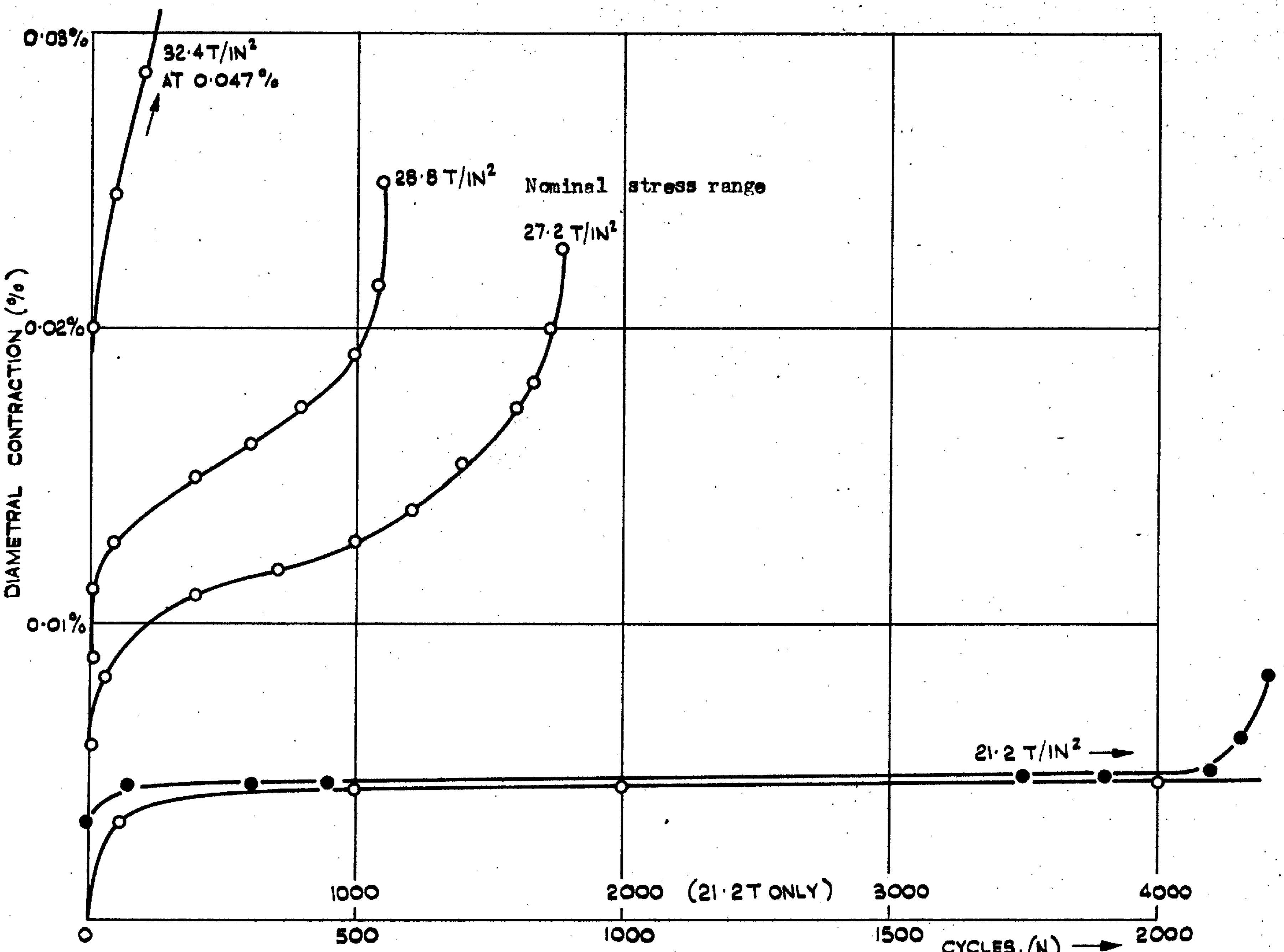

FIG.41. Cyclic creep of cast iron E

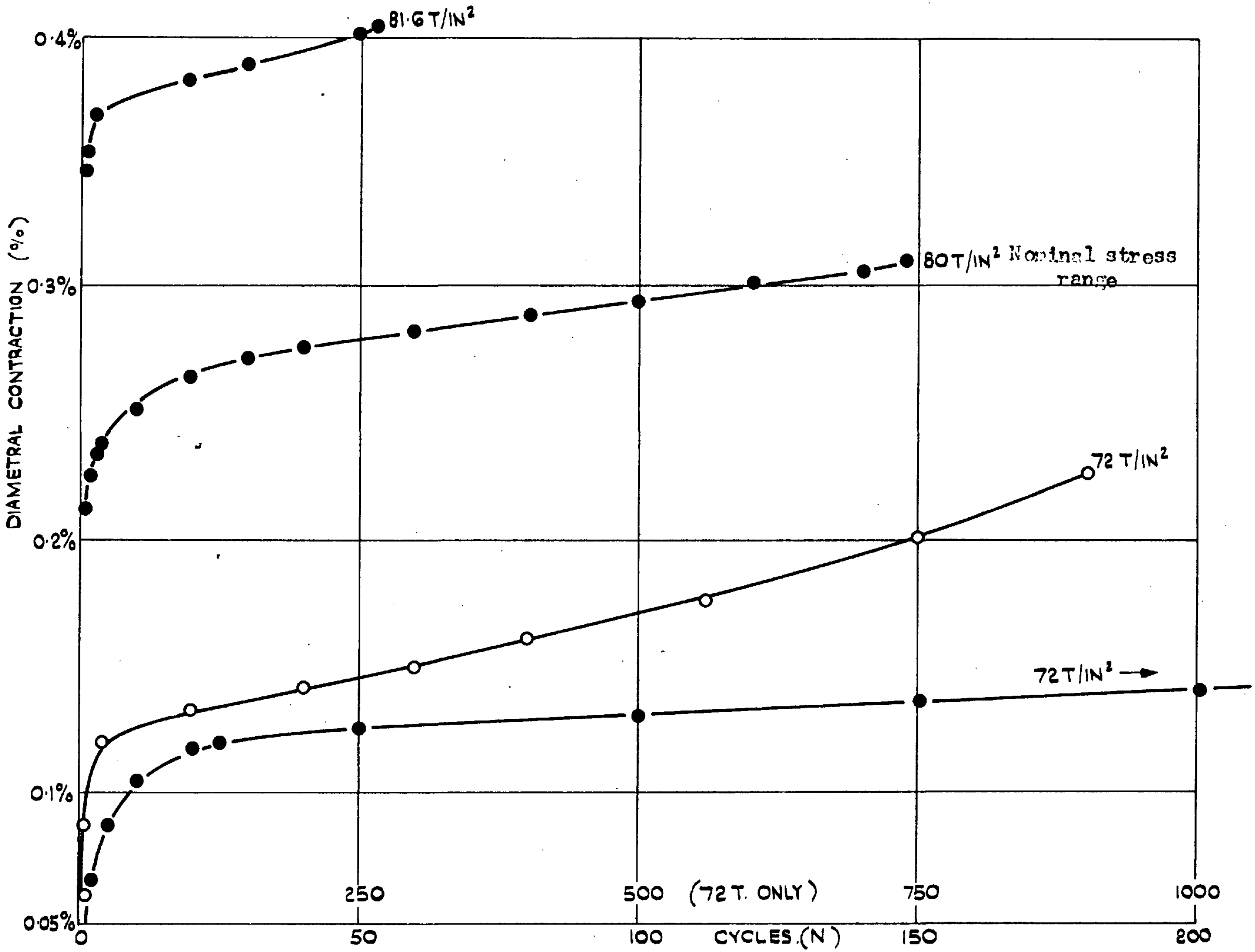

FIG.42. Cyclic creep of cast iron F

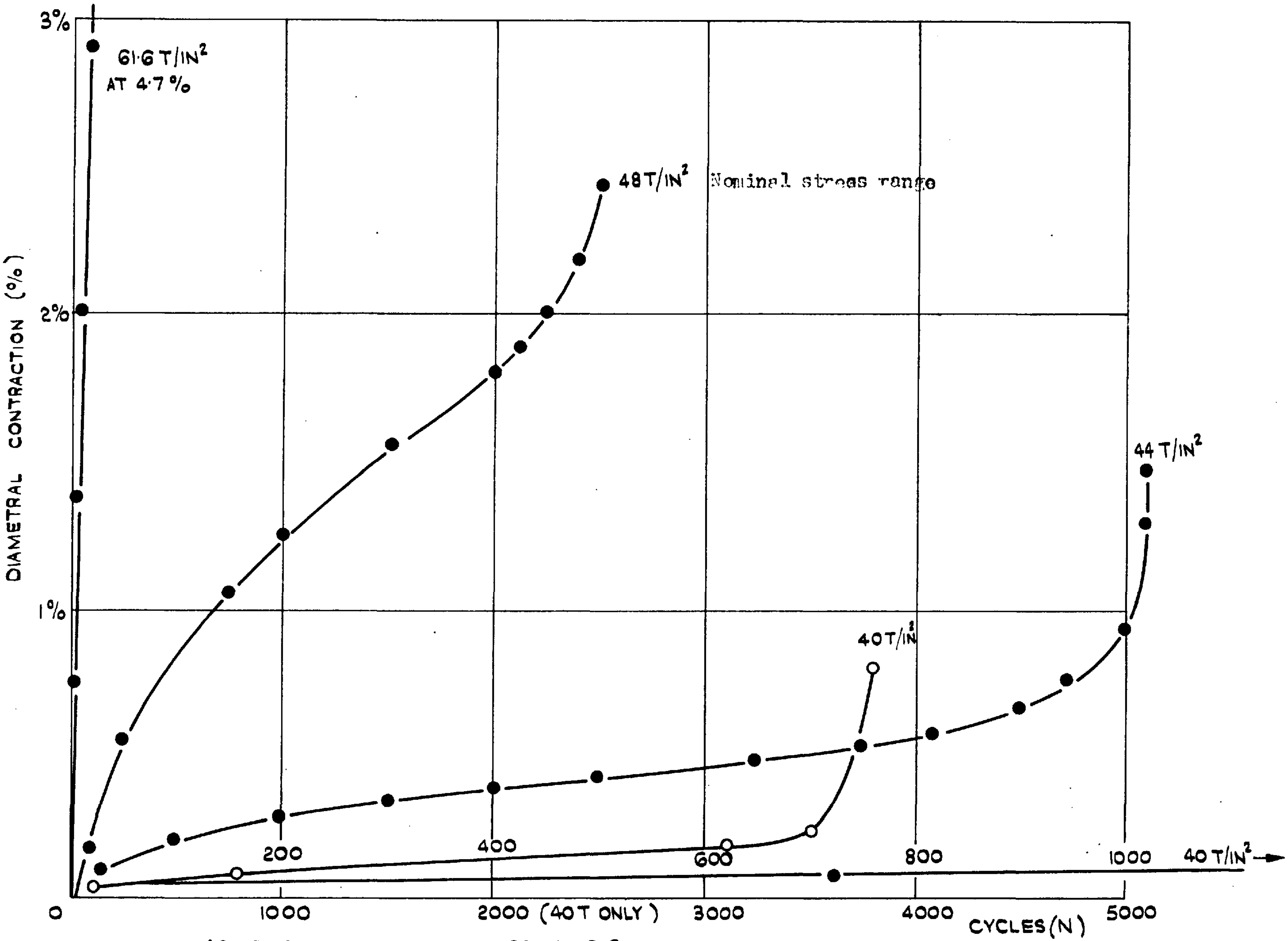

FIG.43. Cyclic creep of cast mild steel S

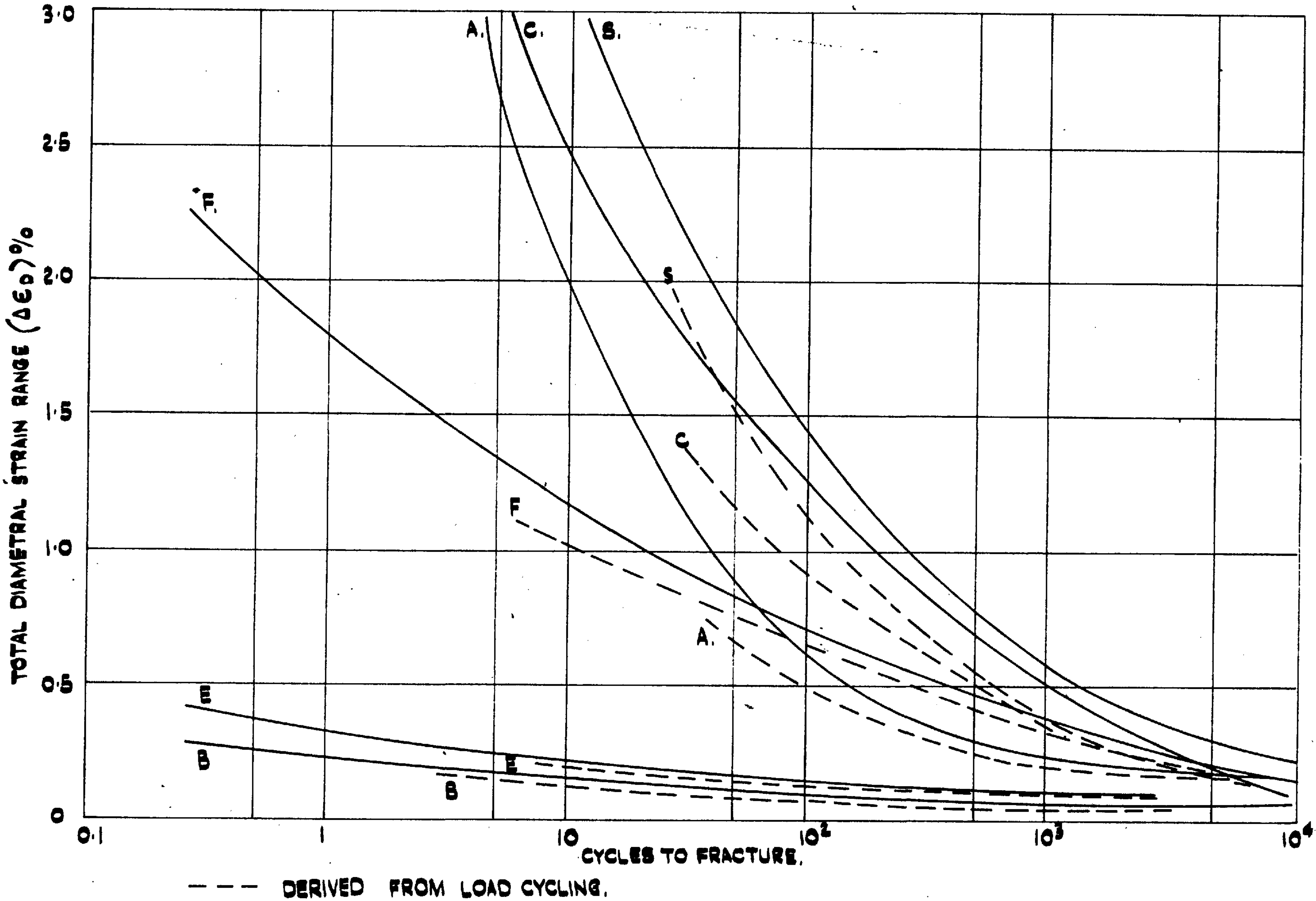

FIG. 44. STRAIN CYCLING AT ROOM TEMPERATURE OF PLAIN SPECIMENS.

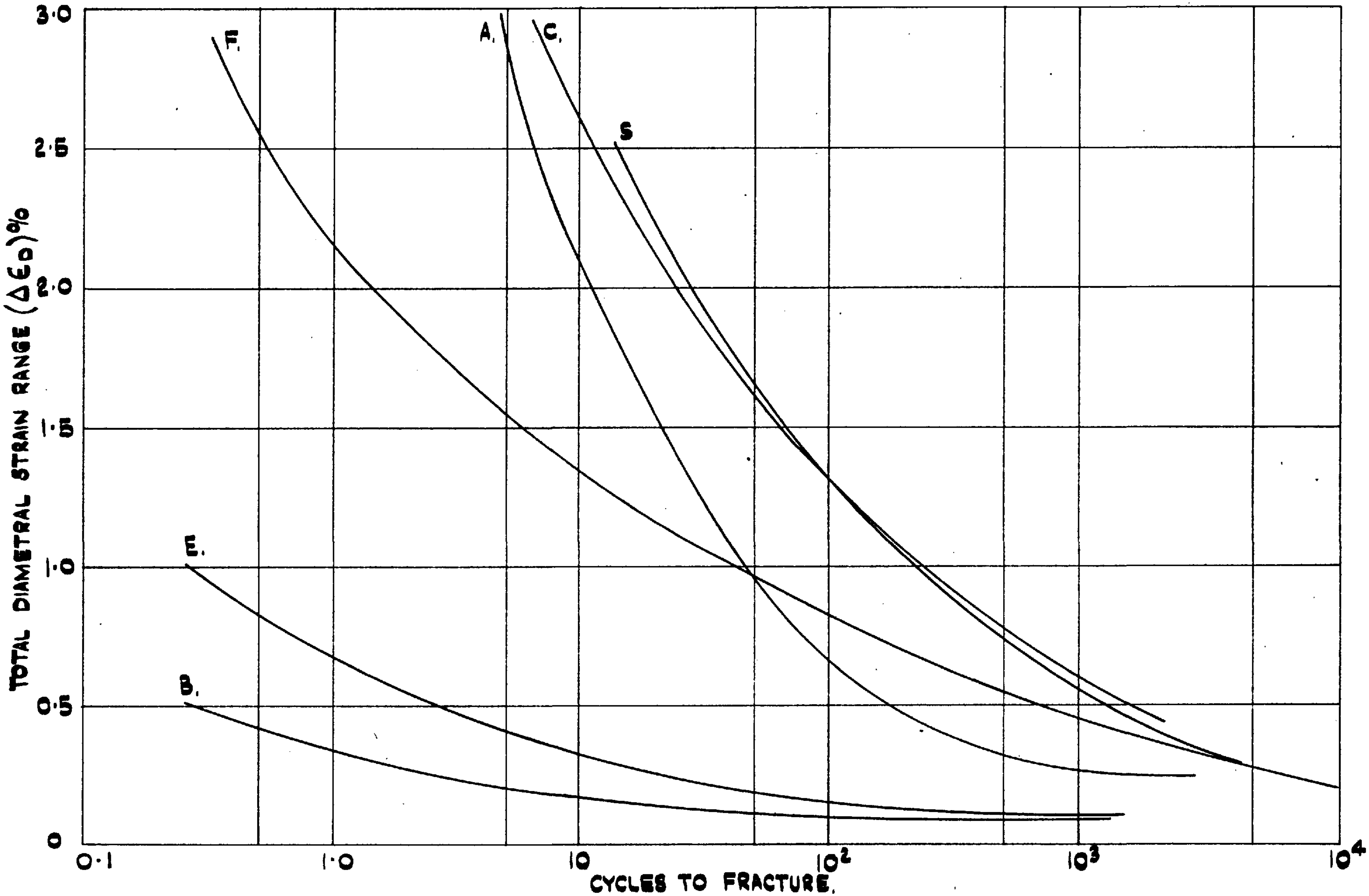

FIG. 45. STRAIN CYCLING AT HIGH TEMPERATURE OF PLAIN SPECIMENS. (450°C.)

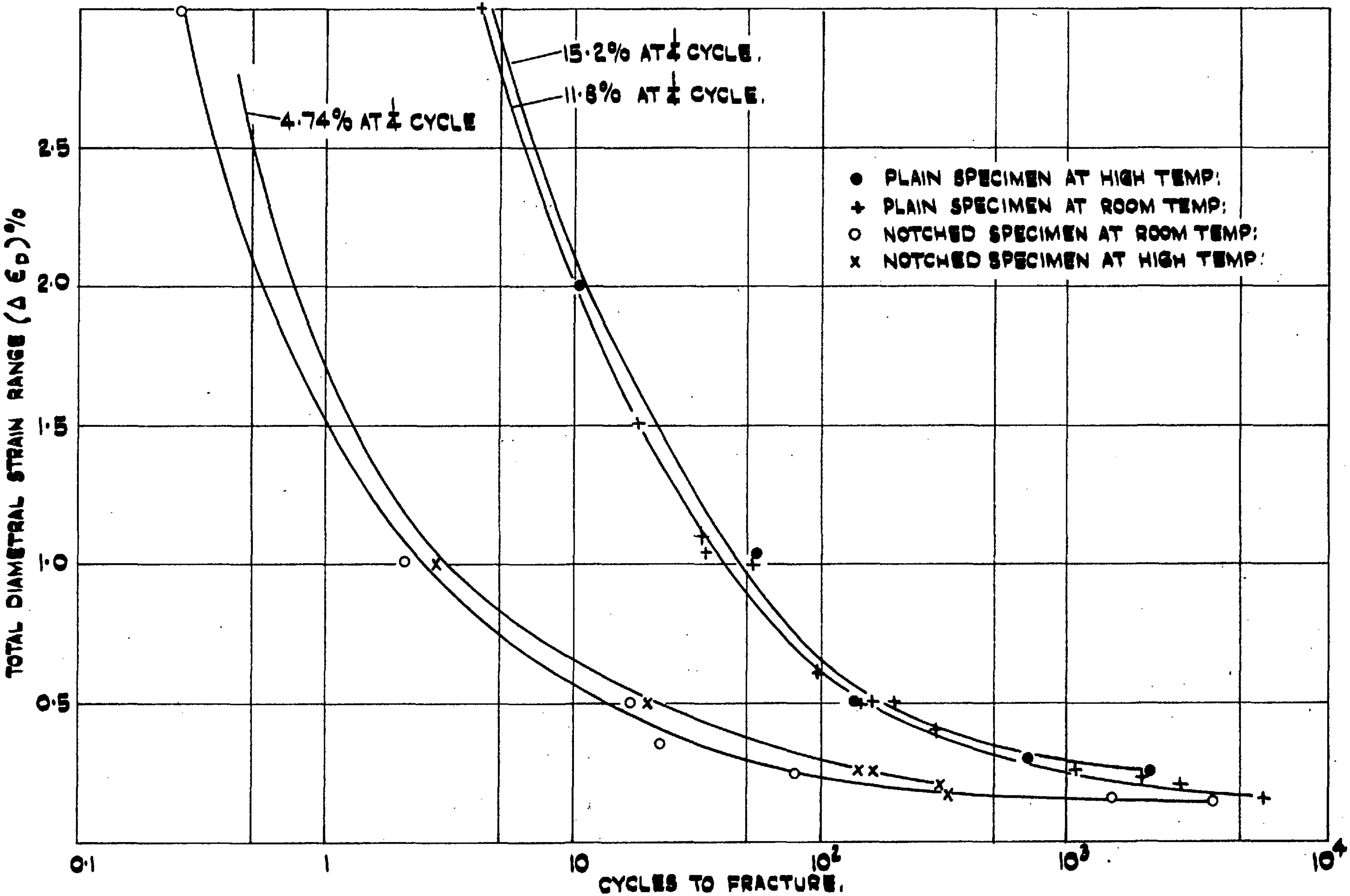

FIG. 46. STRAIN CYCLING OF "A" CAST IRON.

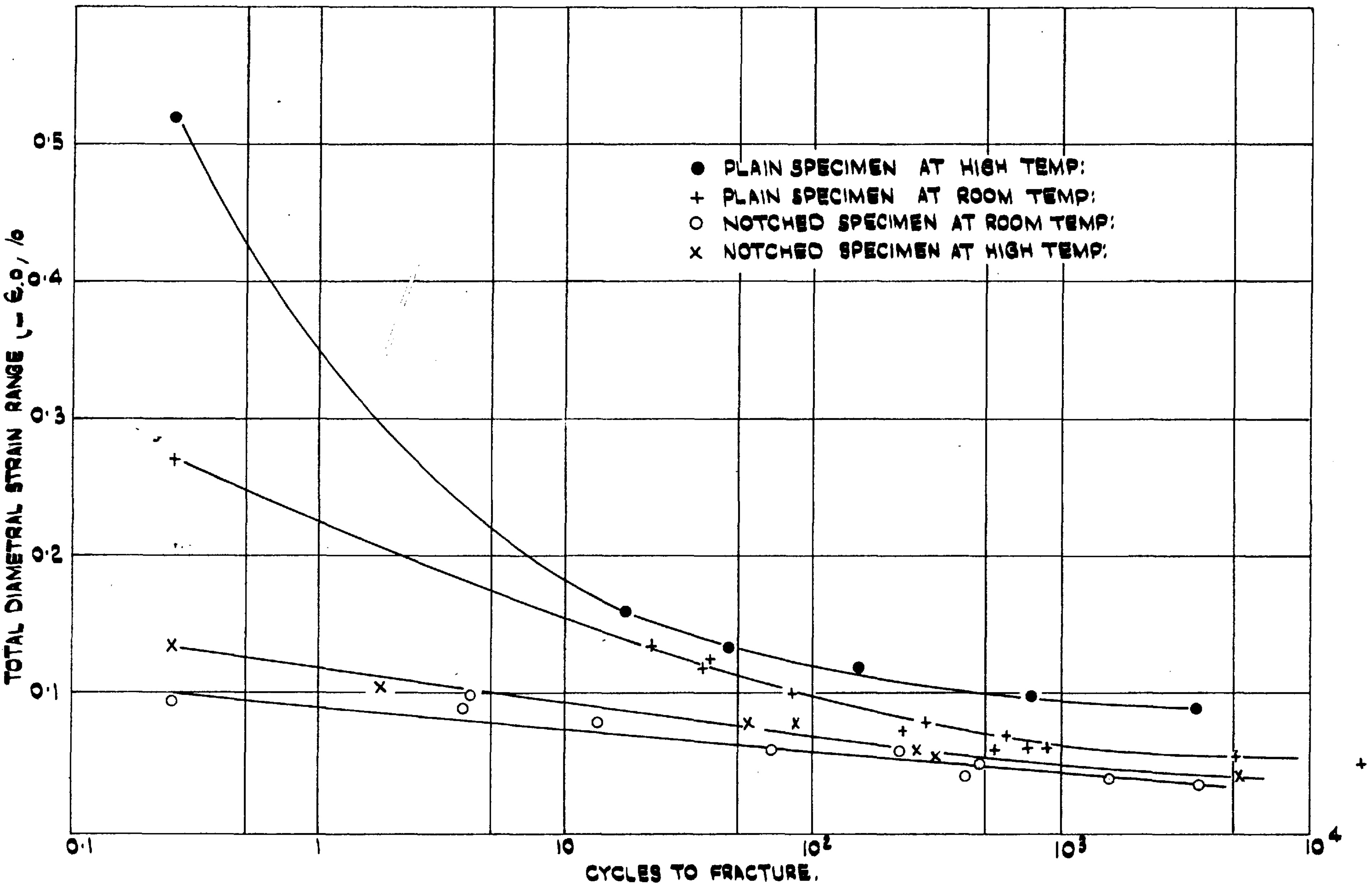

FIG. 47. STRAIN CYCLING OF "B" CAST IRON.

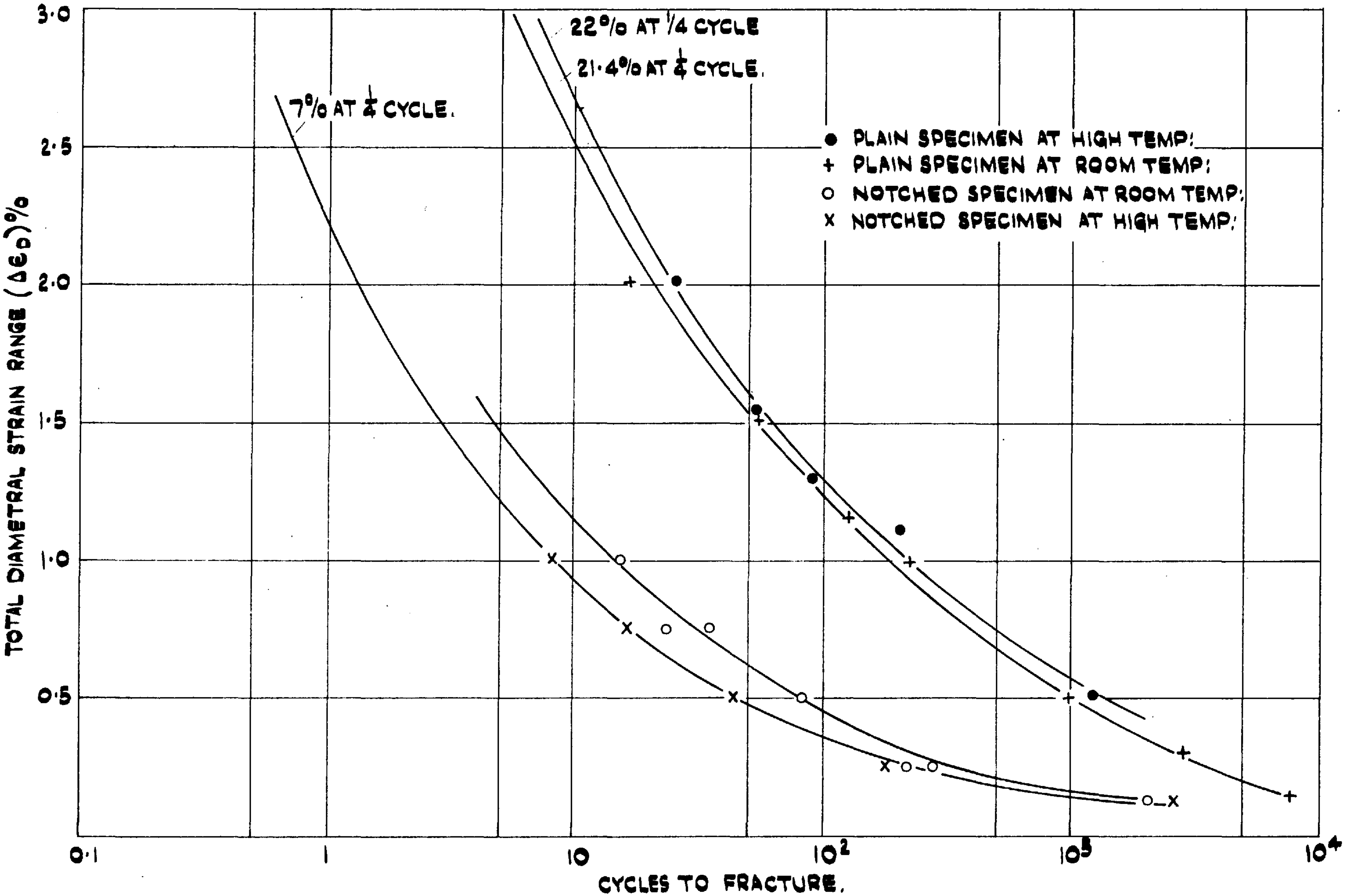

FIG. 48. STRAIN CYCLING OF "C" CAST STEEL.

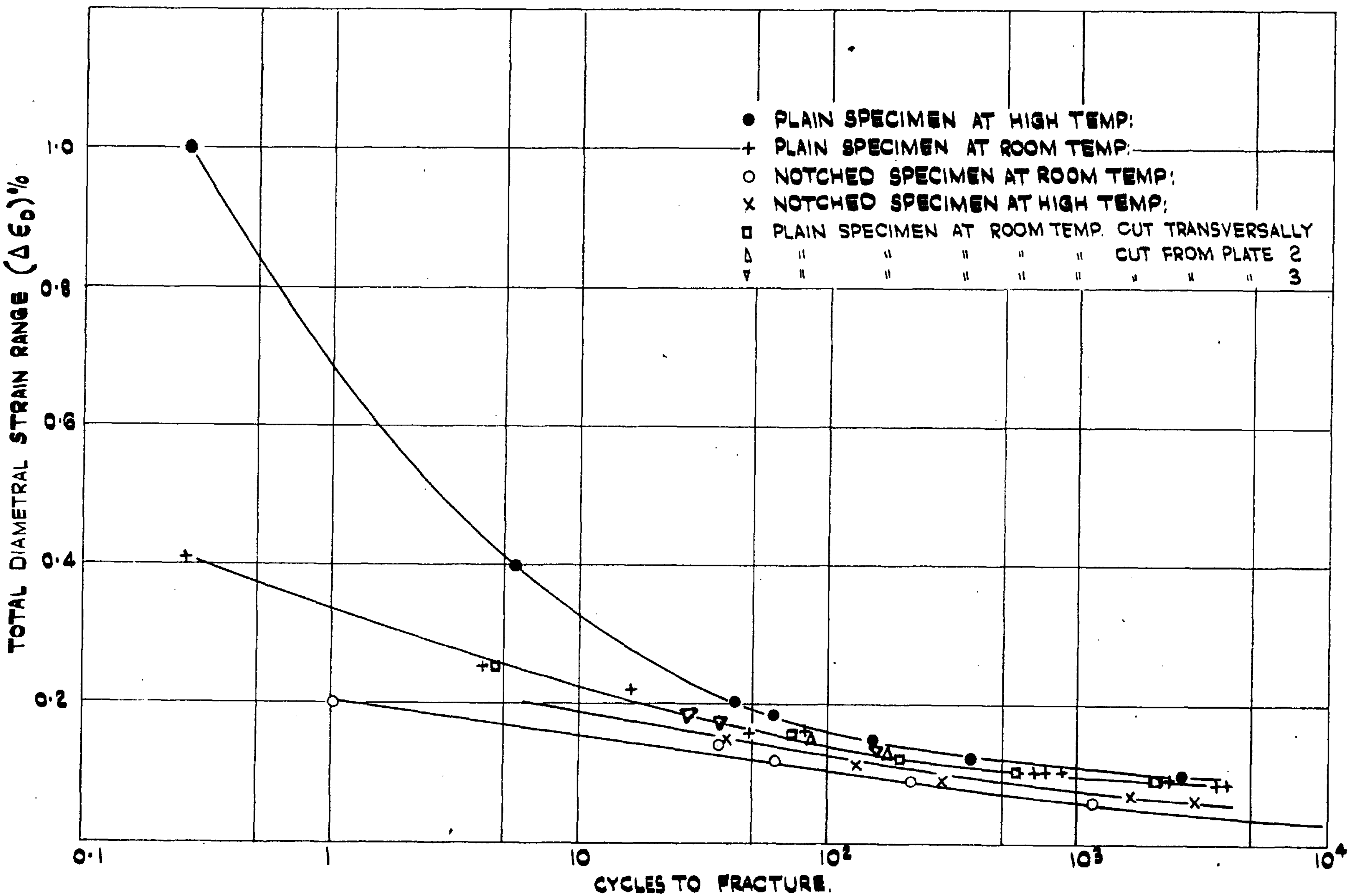

PLAIN SPECIMEN AT HIGH TEMP;
PLAIN SPECIMEN AT ROOM TEMP;
NOTCHED SPECIMEN AT ROOM TEMP;
NOTCHED SPECIMEN AT HIGH TEMP;
PLAIN SPECIMEN AT ROOM TEMP. CUT TRANSVERSALLY
" " " " " CUT FROM PLATE 2
" " " " " " " " 3
TOTAL DIAMETRAL STRAIN RANGE ($\Delta \epsilon_D$)%
1·0
0·8
0·6
0·4
0·2
0·1
1
10
10^2
10^3
10^4
CYCLES TO FRACTURE.

" "

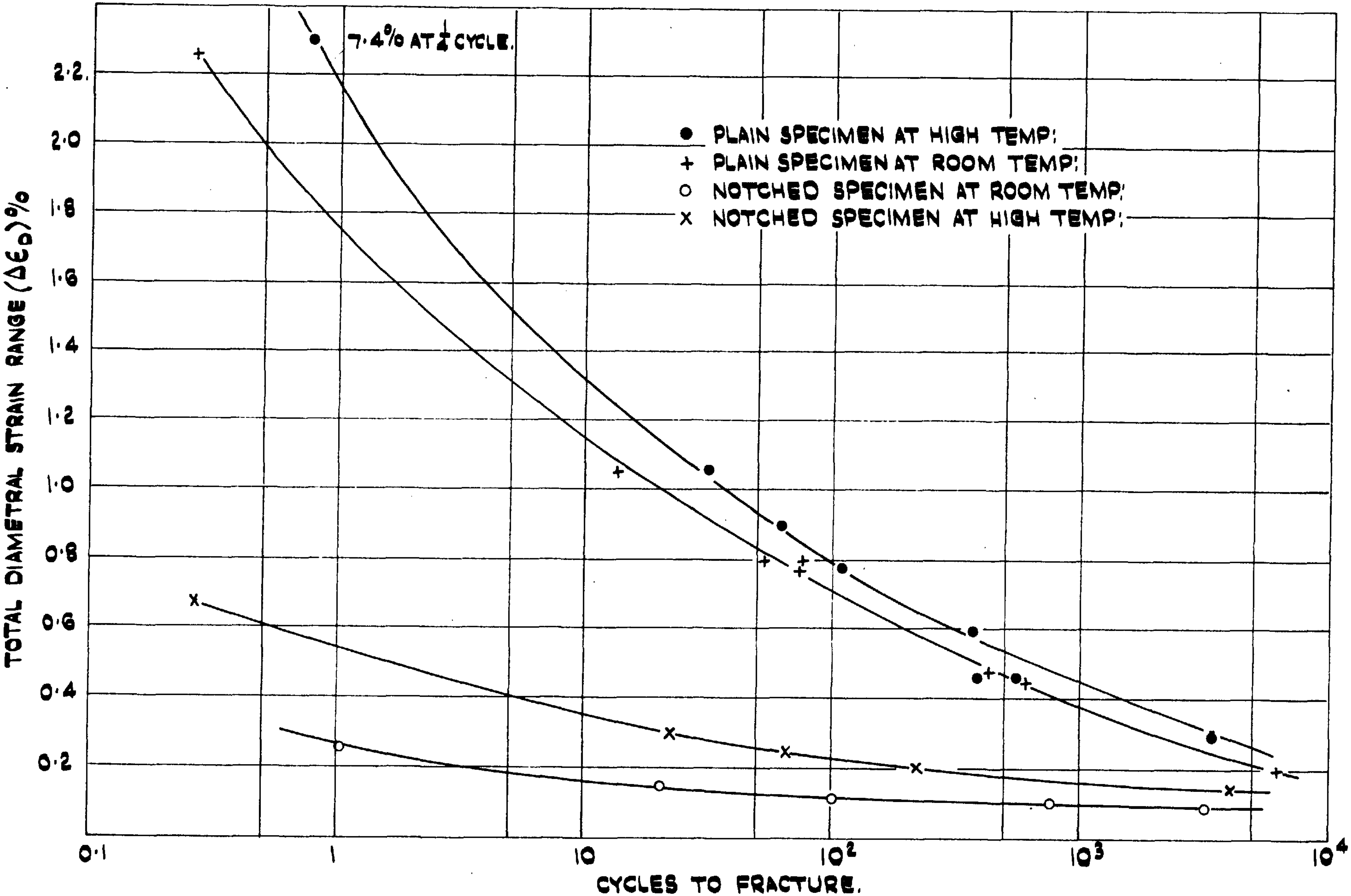

FIG. 50. STRAIN CYCLING OF "F" CAST IRON.

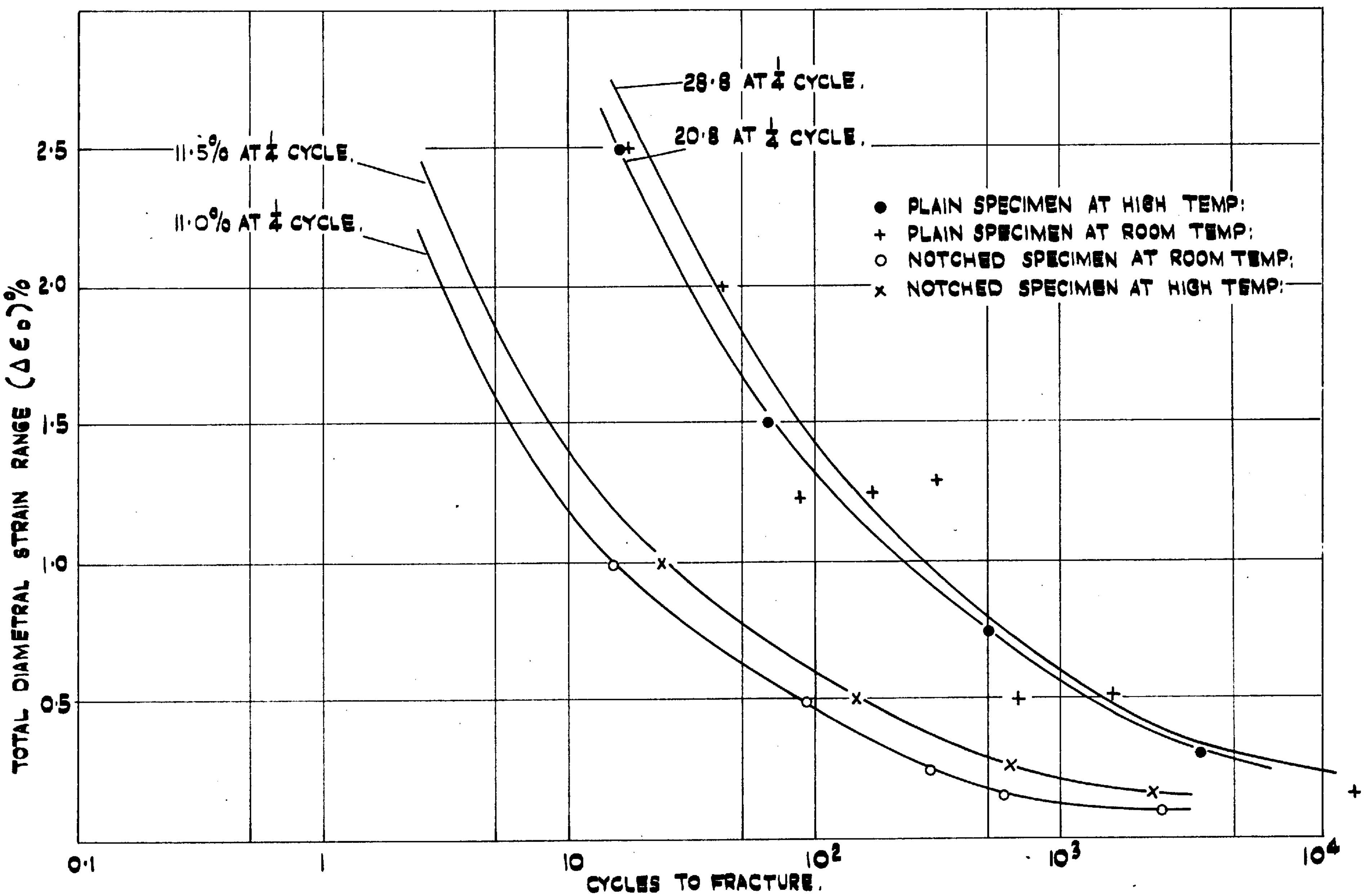

FIG. 51. STRAIN CYCLING OF "S" CAST MILD STEEL.

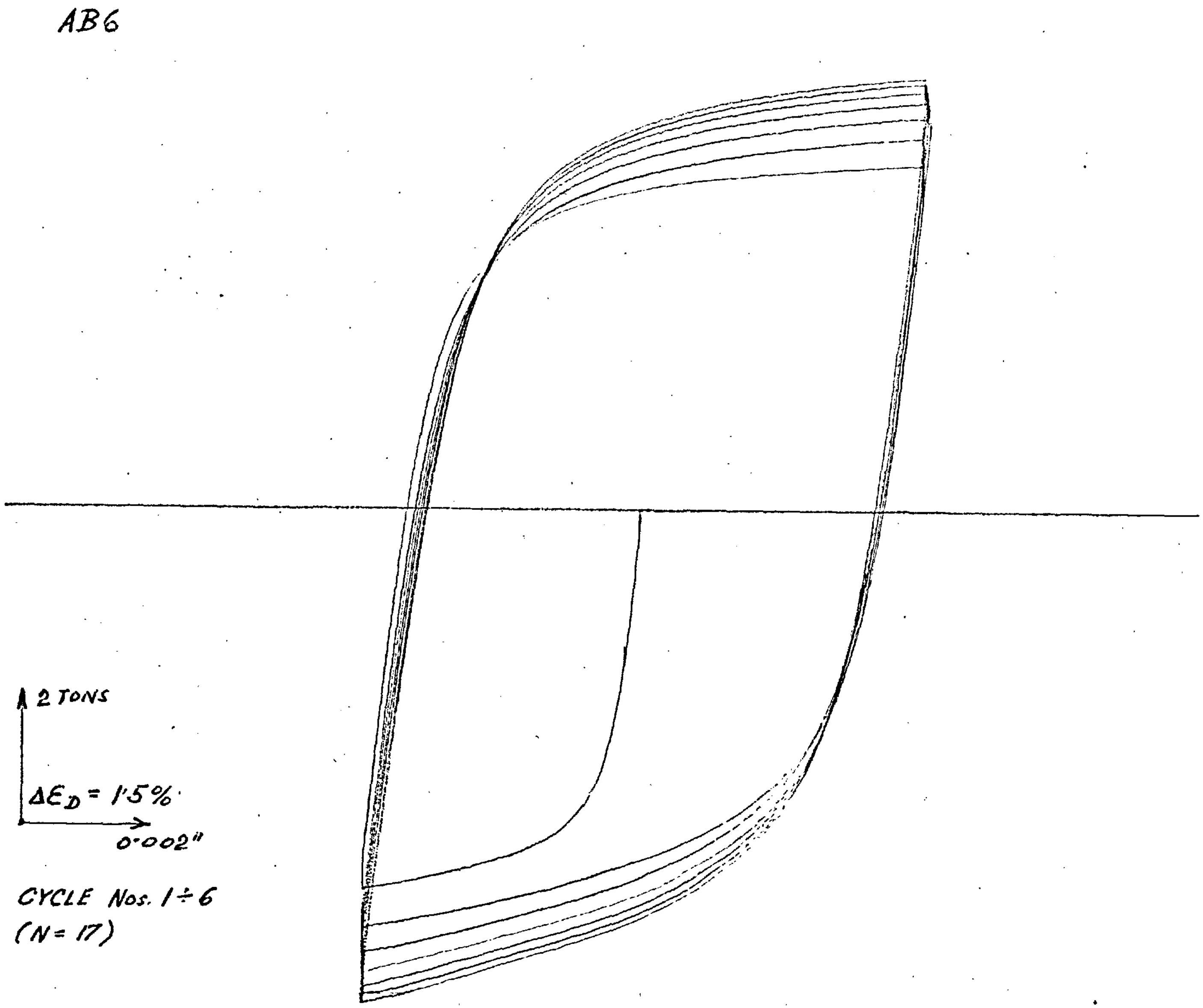

Fig. 52 . Strain hardening of cast iron A.

3BB8-L-VN

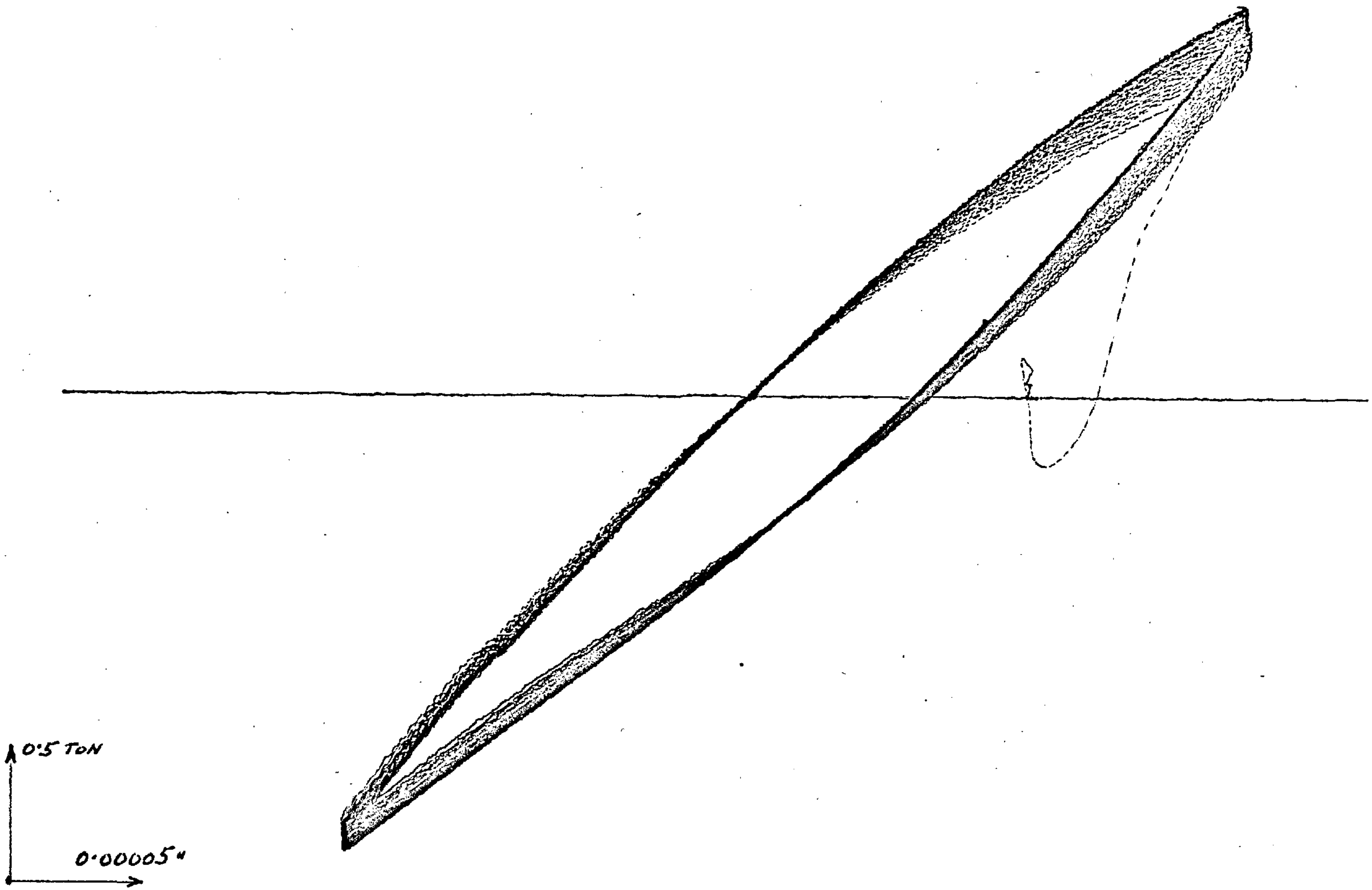

919 – 955
$\Delta\epsilon_D$ = 0·06%
Cycle nos. 30÷66

Fig. 53 . Cast iron B. Strain cycling and fracture.

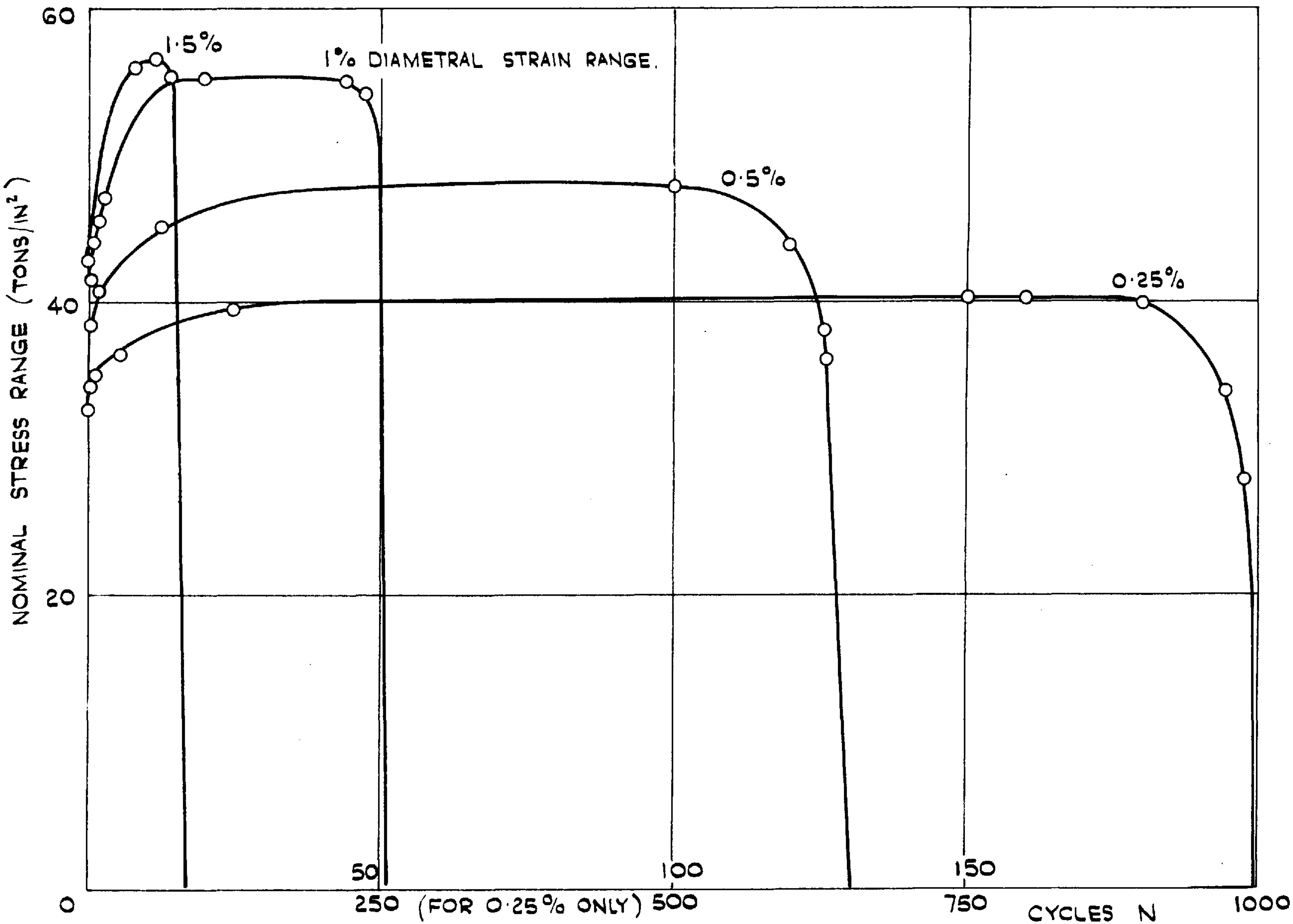

FIG. 4. Variation of stress range during strain cycling at room temperature of cast iron A

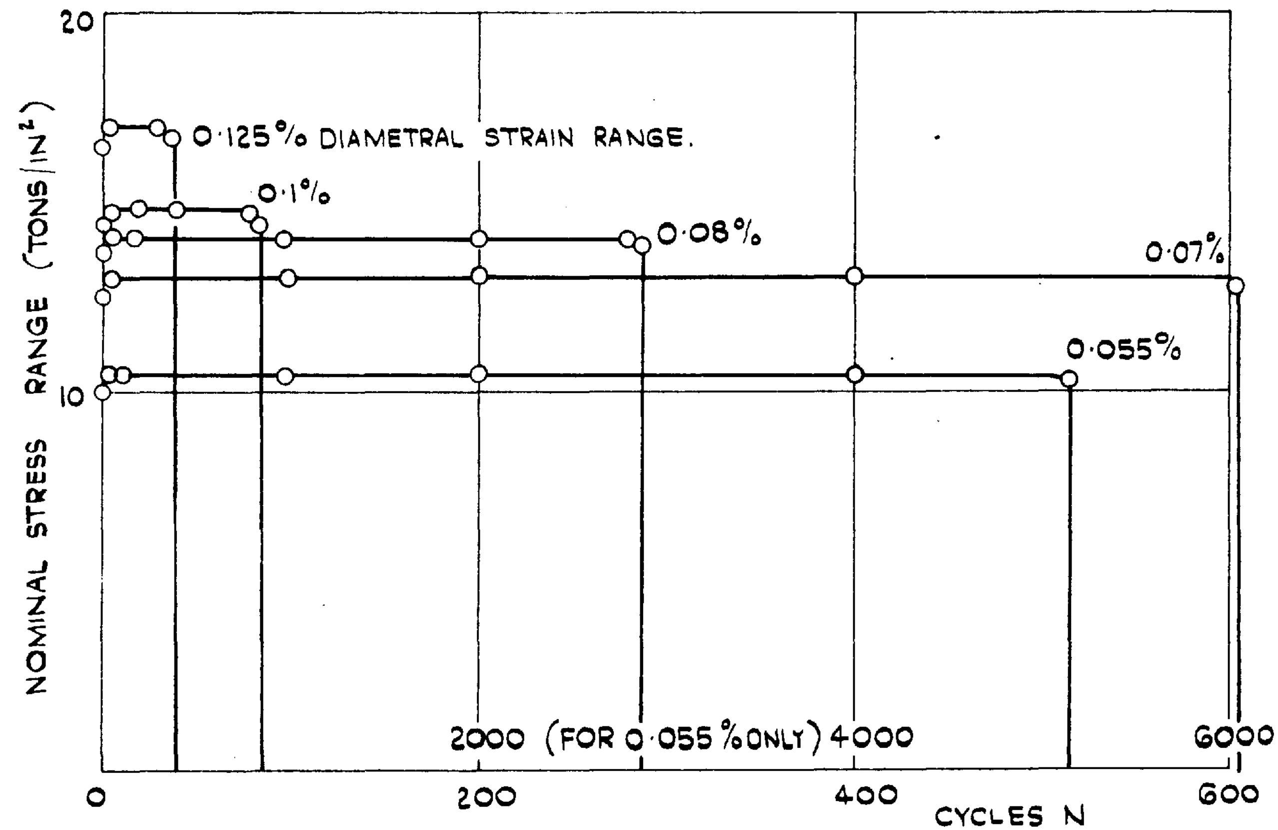

FIG.55. Variation of stress range during strain cycling at room temperature of cast iron B

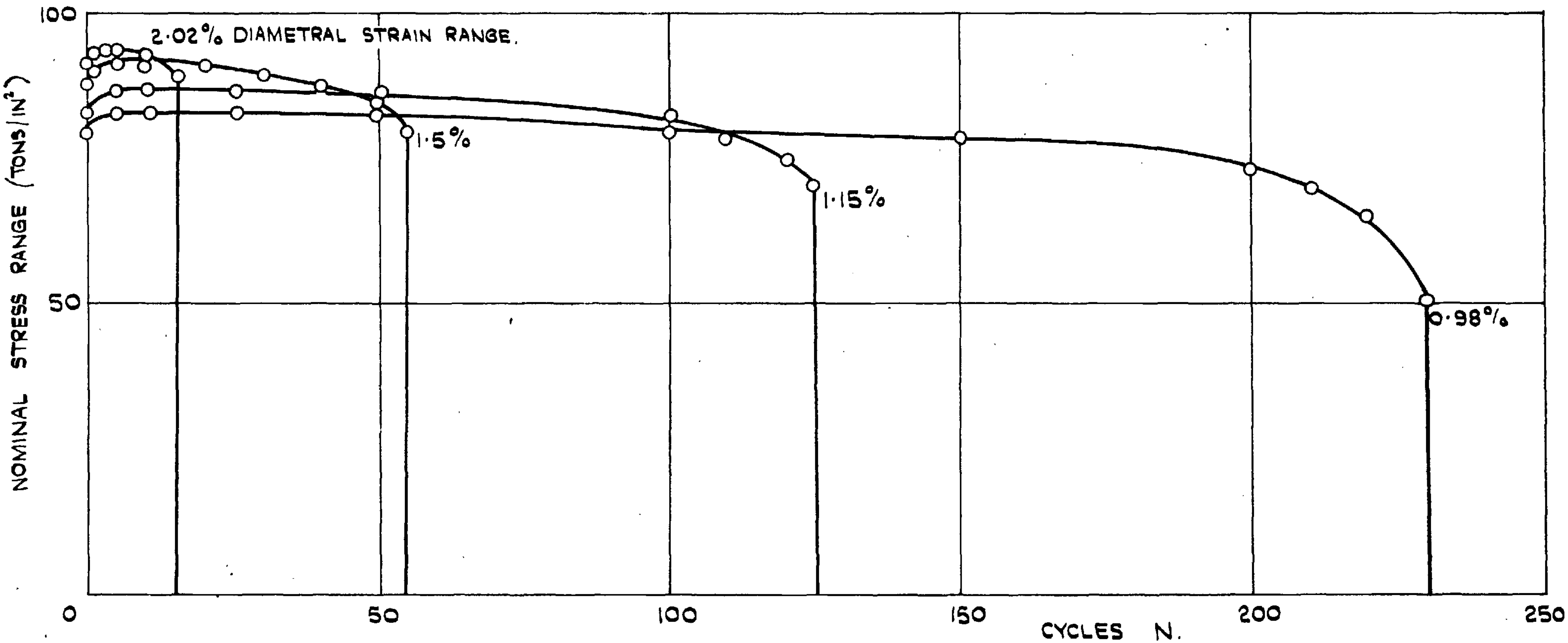

FIG. 56. Variation of stress range during strain cycling at room temperature of cast steel C

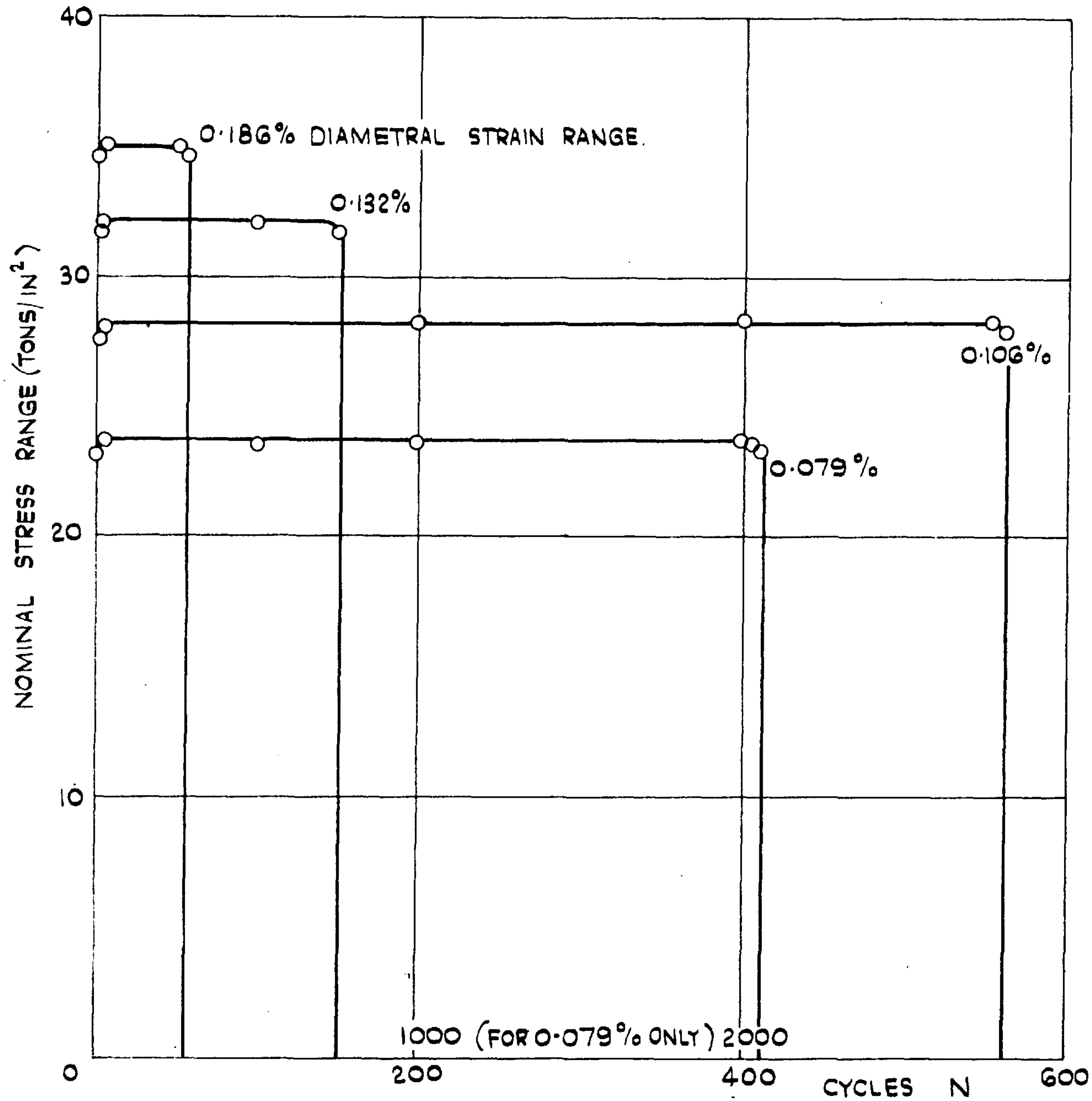

FI^.57. Variation of stress range during strain cycling at room temperature of cast iron E

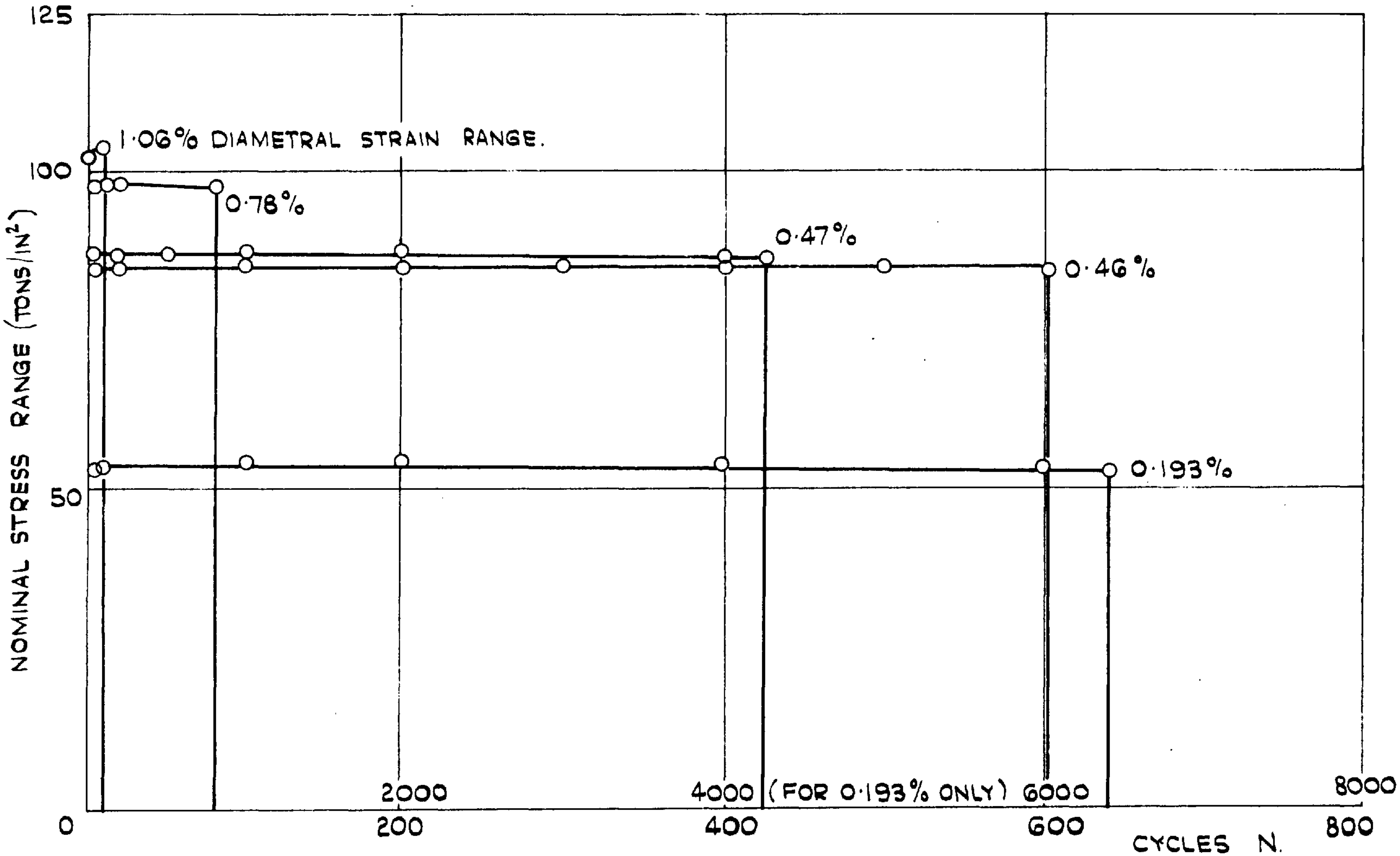

FI .5°. Variation of stress range during strain cycling at room temperature of cast iron F

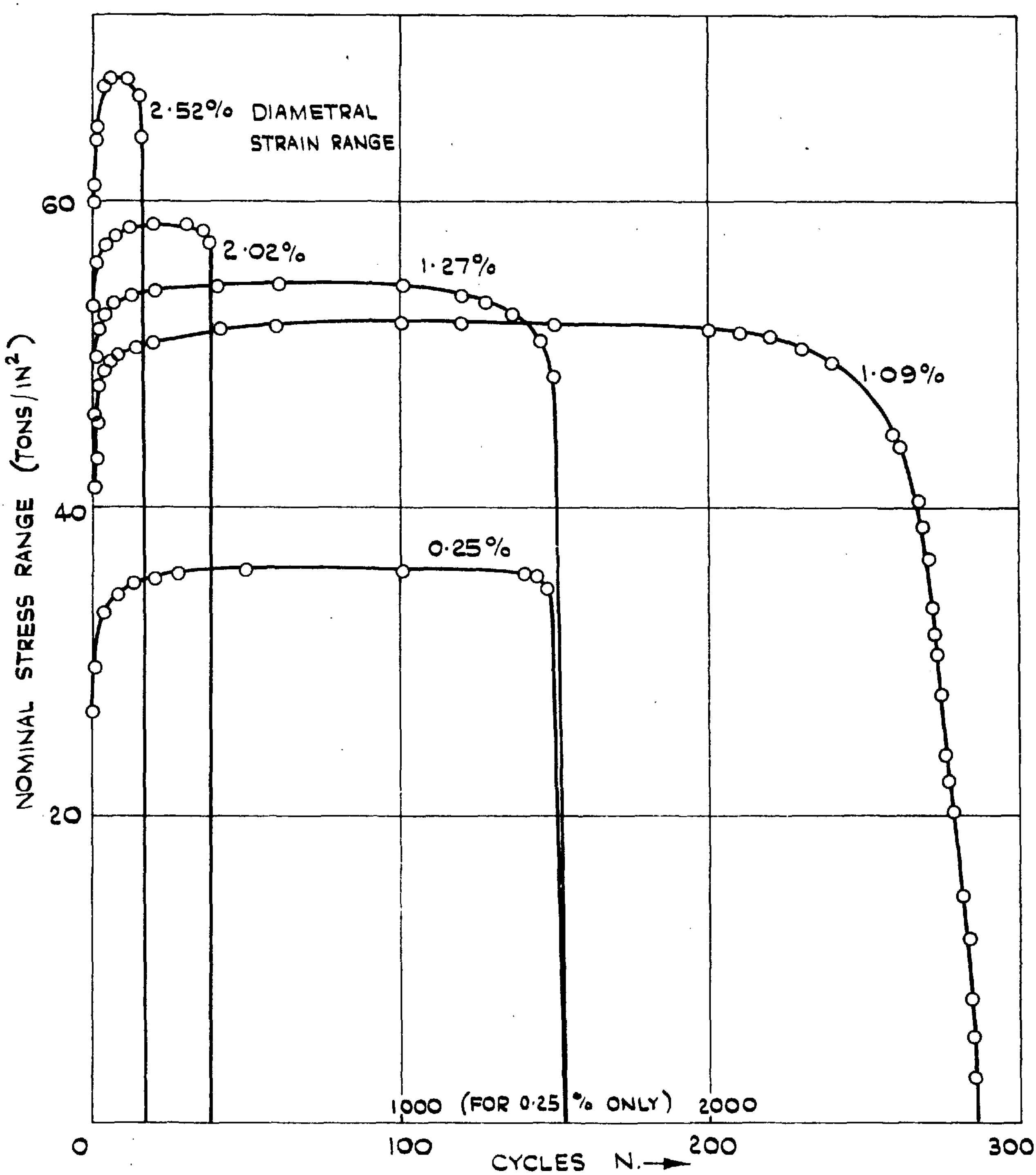

FIG. 59. VARIATION OF NOMINAL STRESS RANGE DURING STRAIN CYCLING OF CAST MILD STEEL S AT ROOM TEMP.

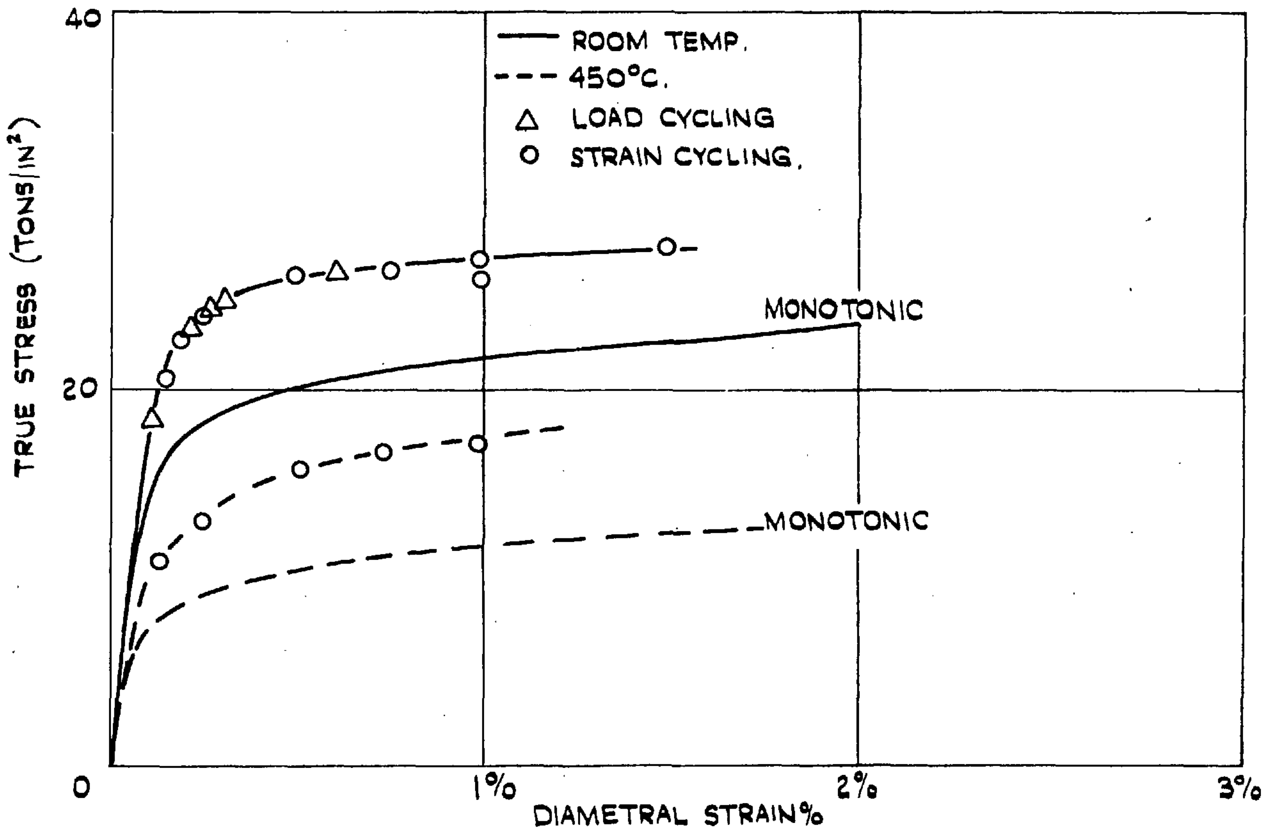

FIG.60. Basic stress-strain curves for cast iron A

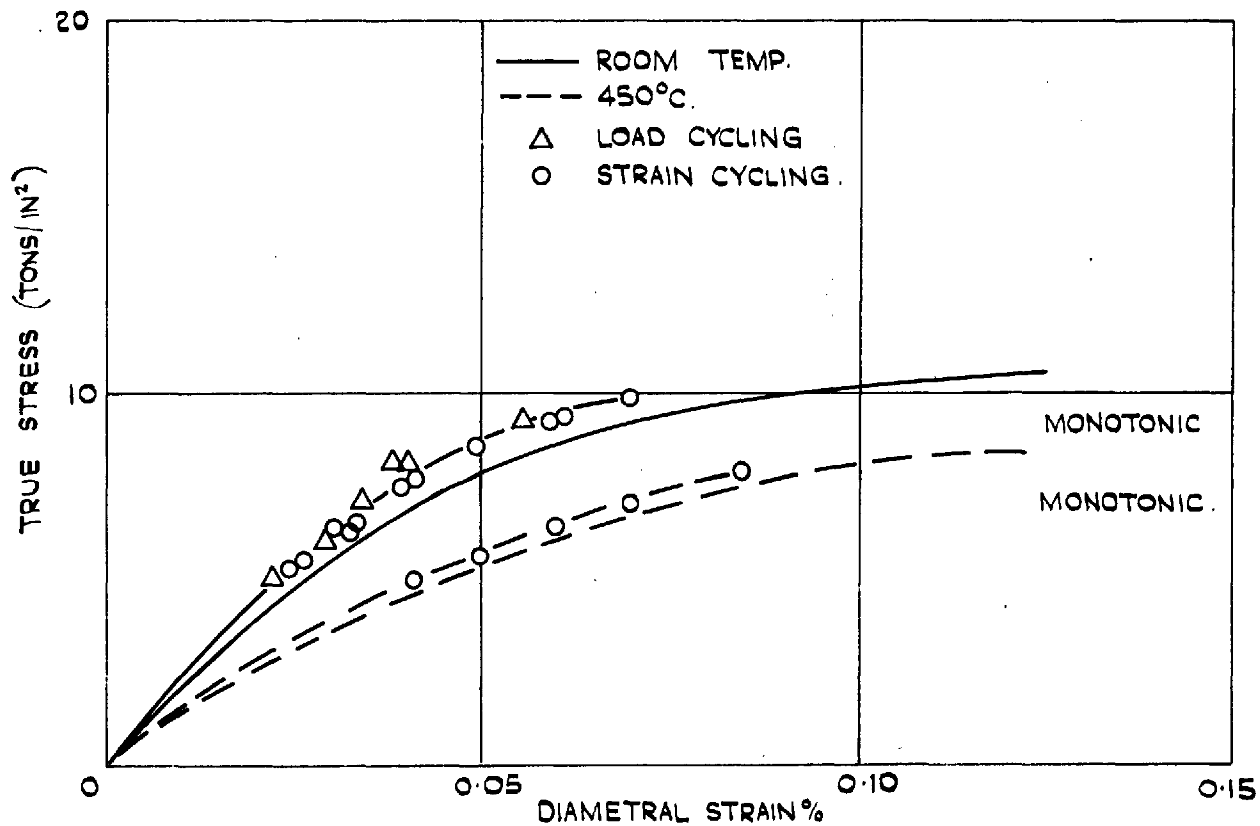

FIG.61. Basic stress-strain curves for cast iron B

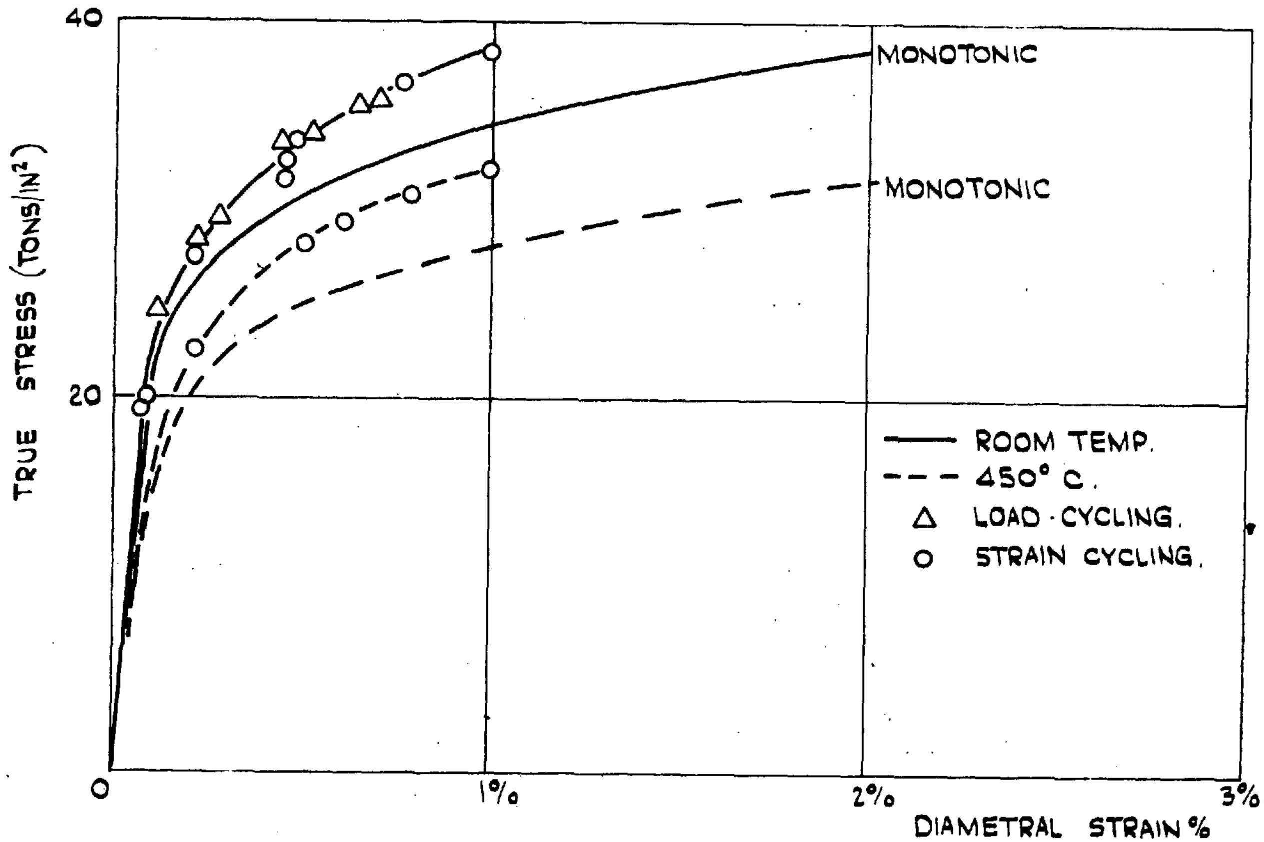

FIG.62. Basic stress-strain curves for cast steel C

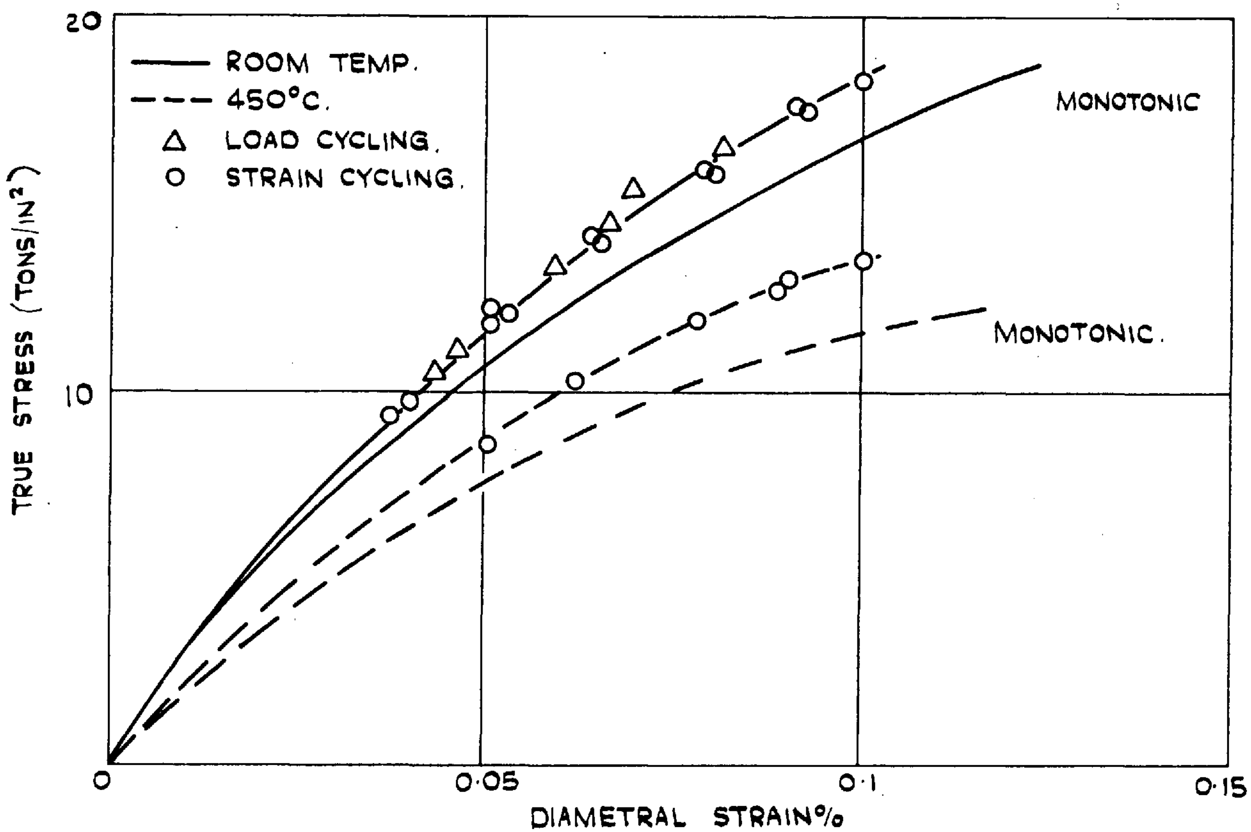

FIG.43. Basic stress-strain curves for cast iron E

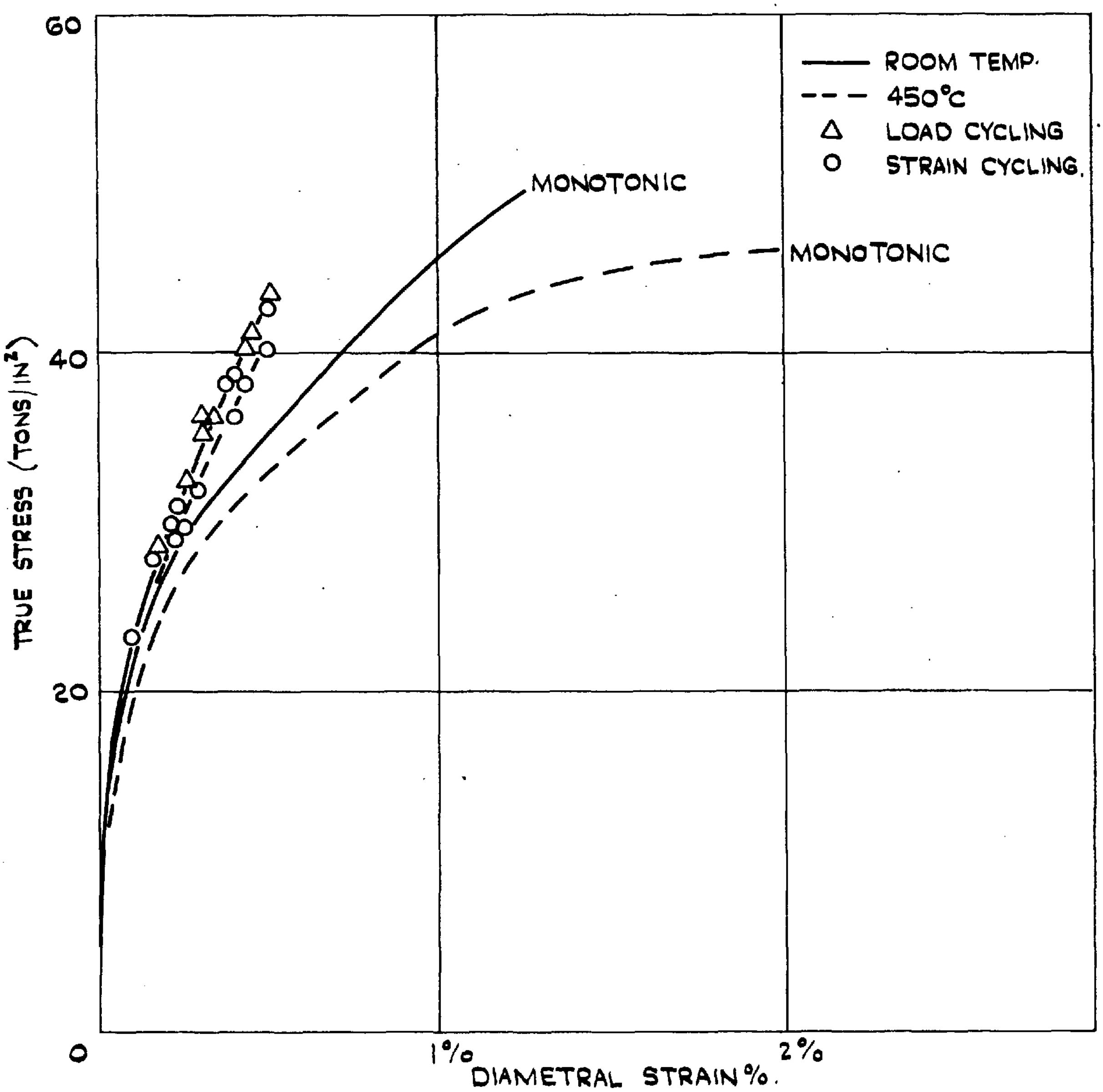

FIG.64. Basic stress-strain curves for cast iron F

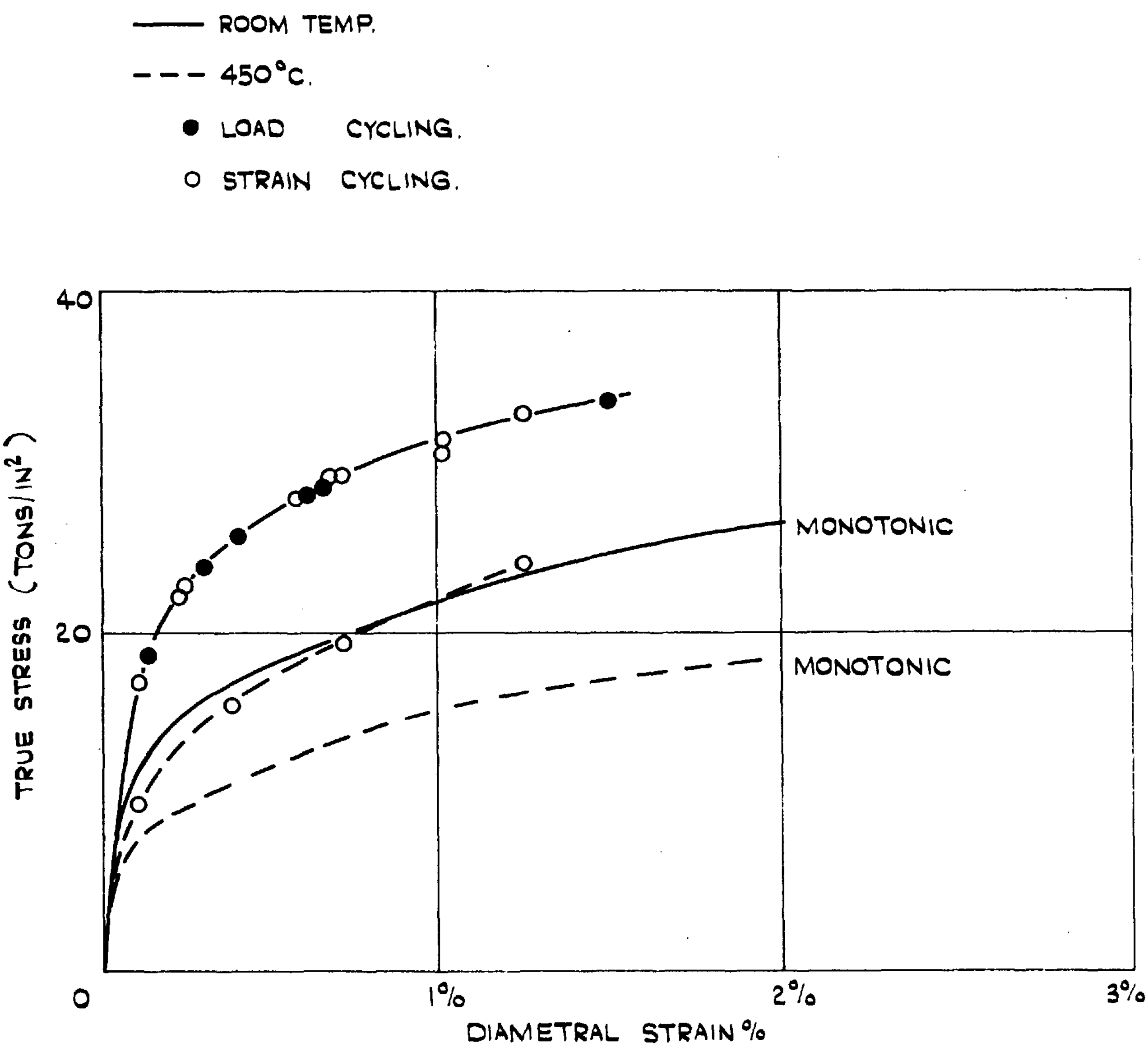

FIG.65. BASIC STRESS-STRAIN CURVES FOR CAST MILD STEEL. S

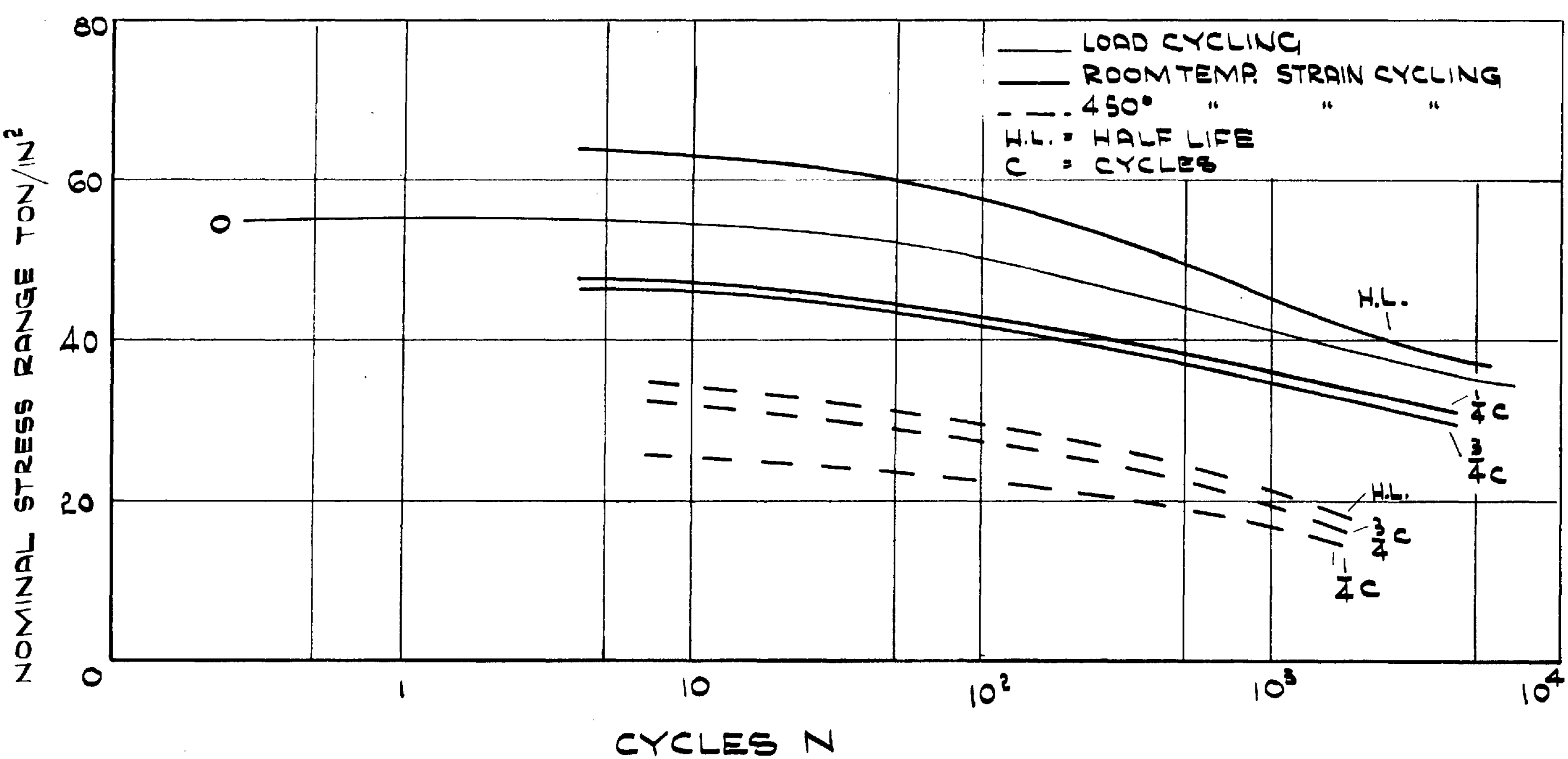

FIG.44. Load cycling with superimposed curves from strain cycling of Cast iron A

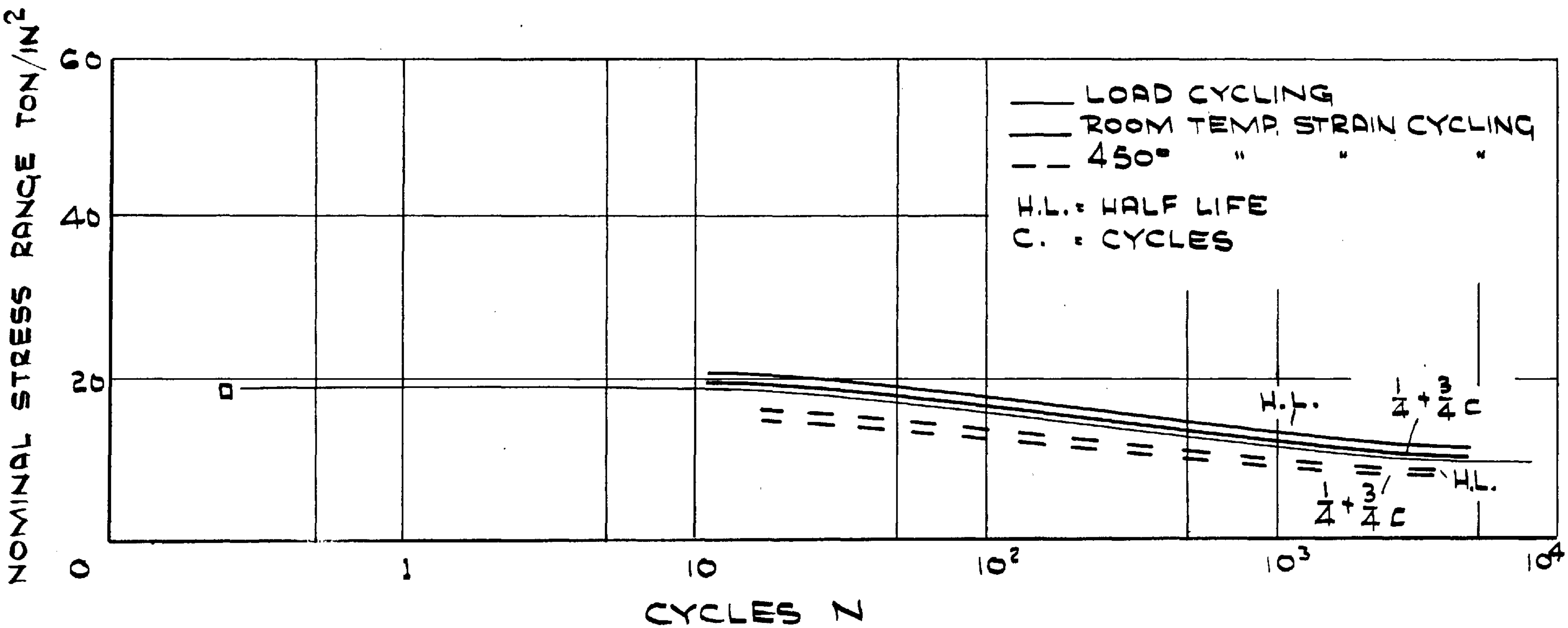

FI .47. Load cycling with superimposed curves from strain cycling of cast iron B

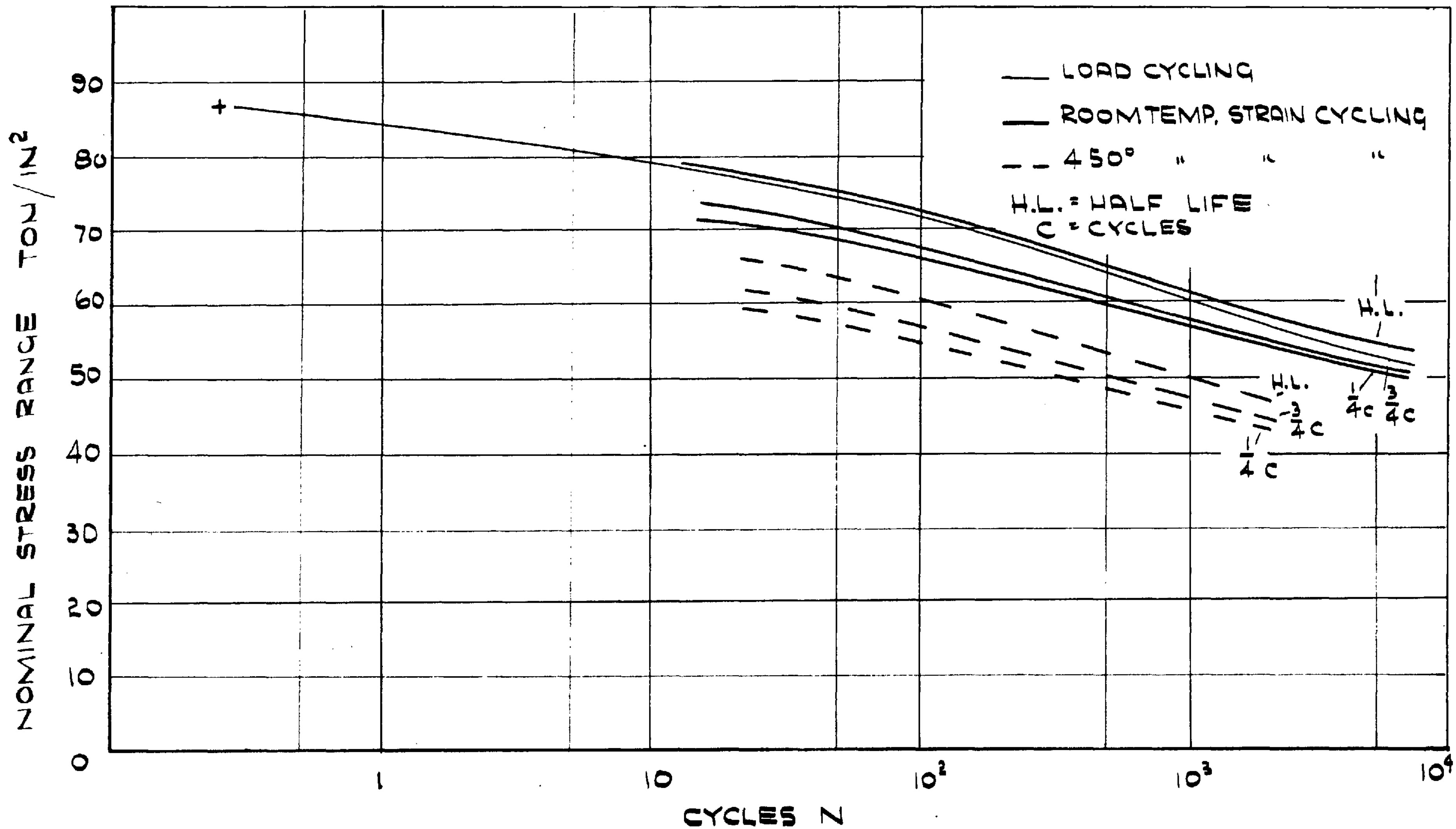

?.?. Load cycling with superimposed curves from strain cycling of cast steel C

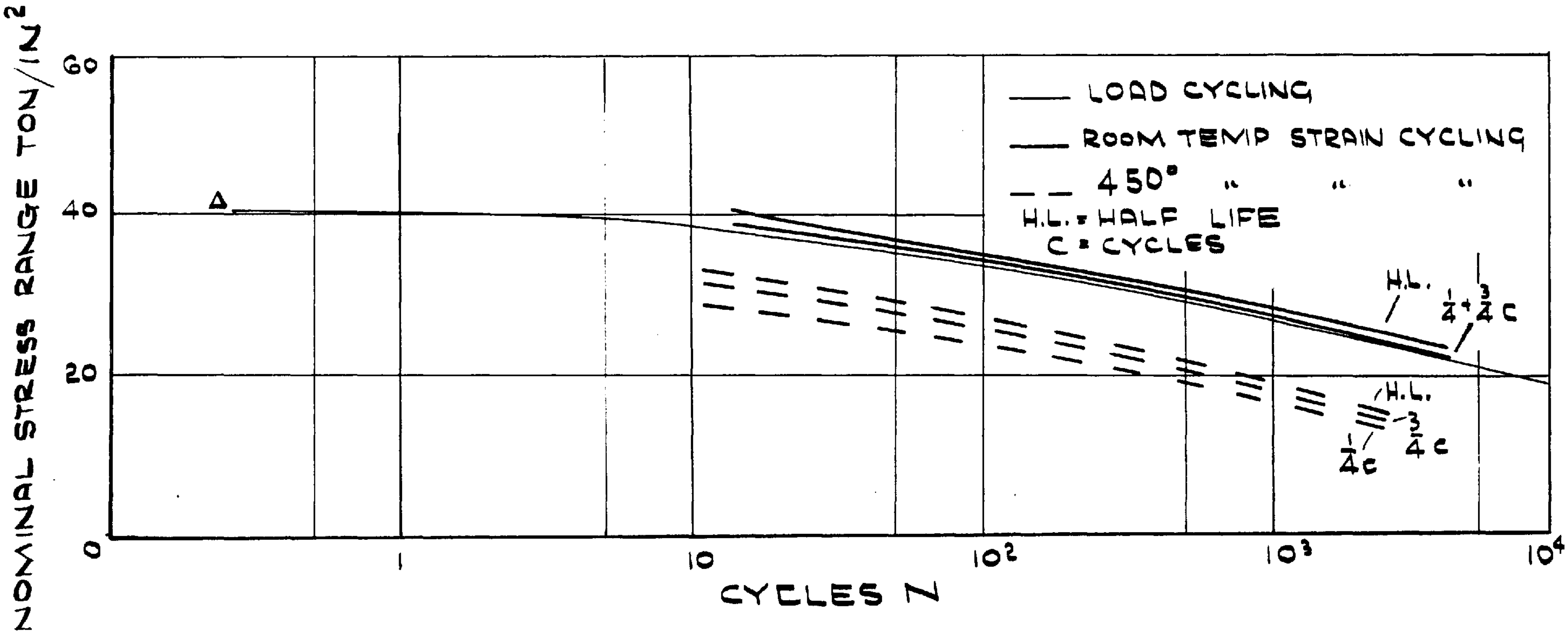

FIG.69.Load cycling with superimposed curves from strain cycling of cast iron E

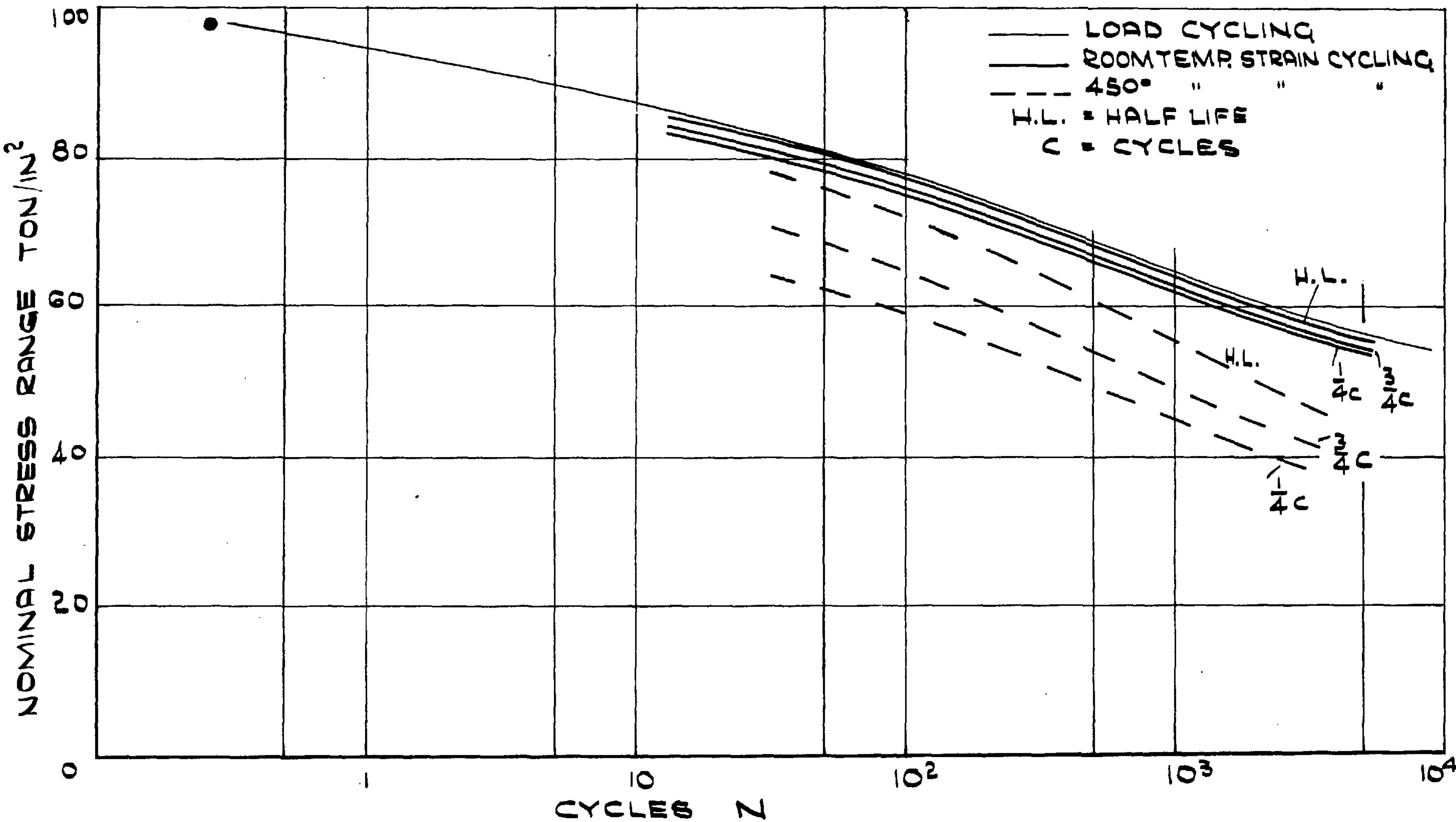

FIG.70. Load cycling with superimposed curves from strain cycling of cast iron F

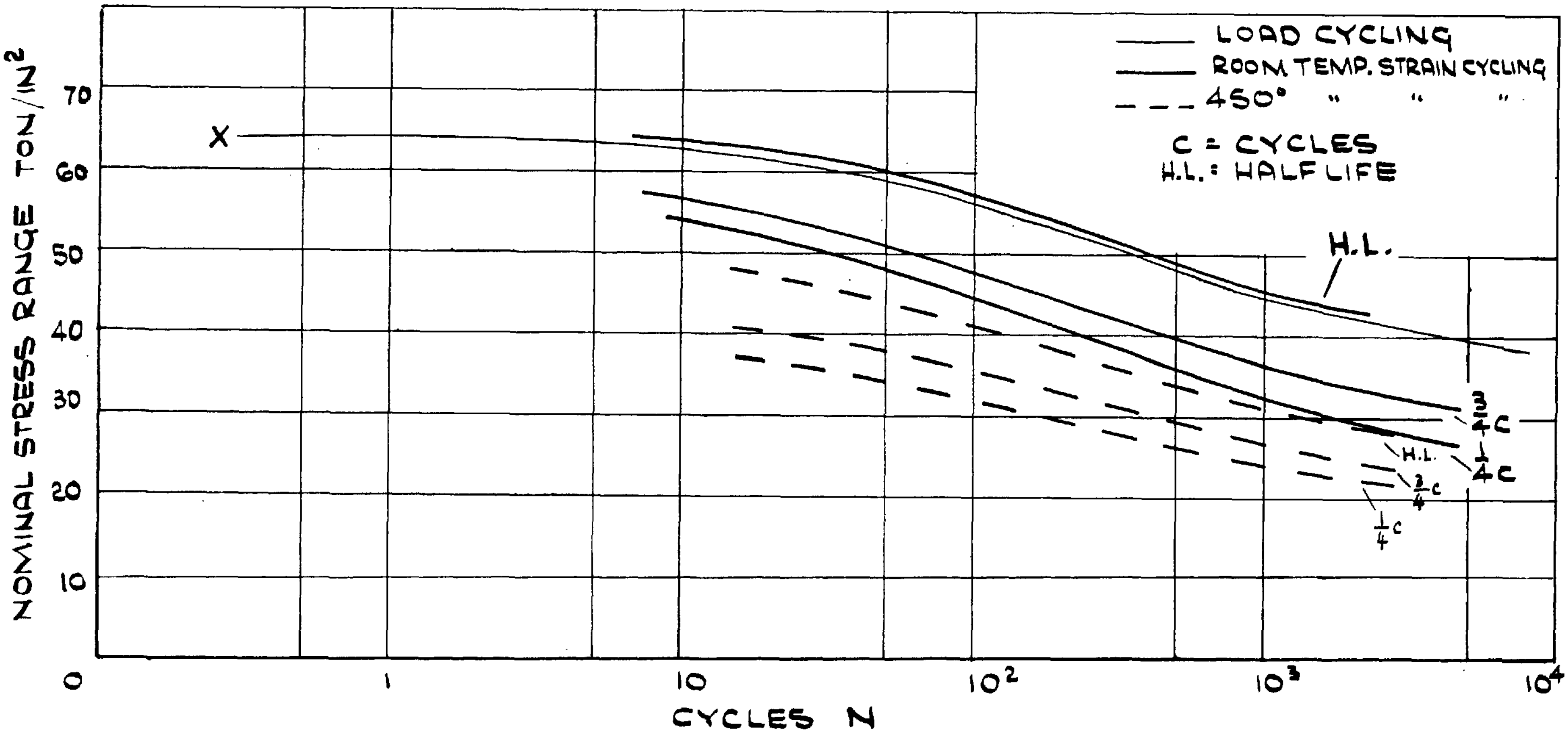

.71. Load cycling with superimposed curves from strain cycling of cast steel S

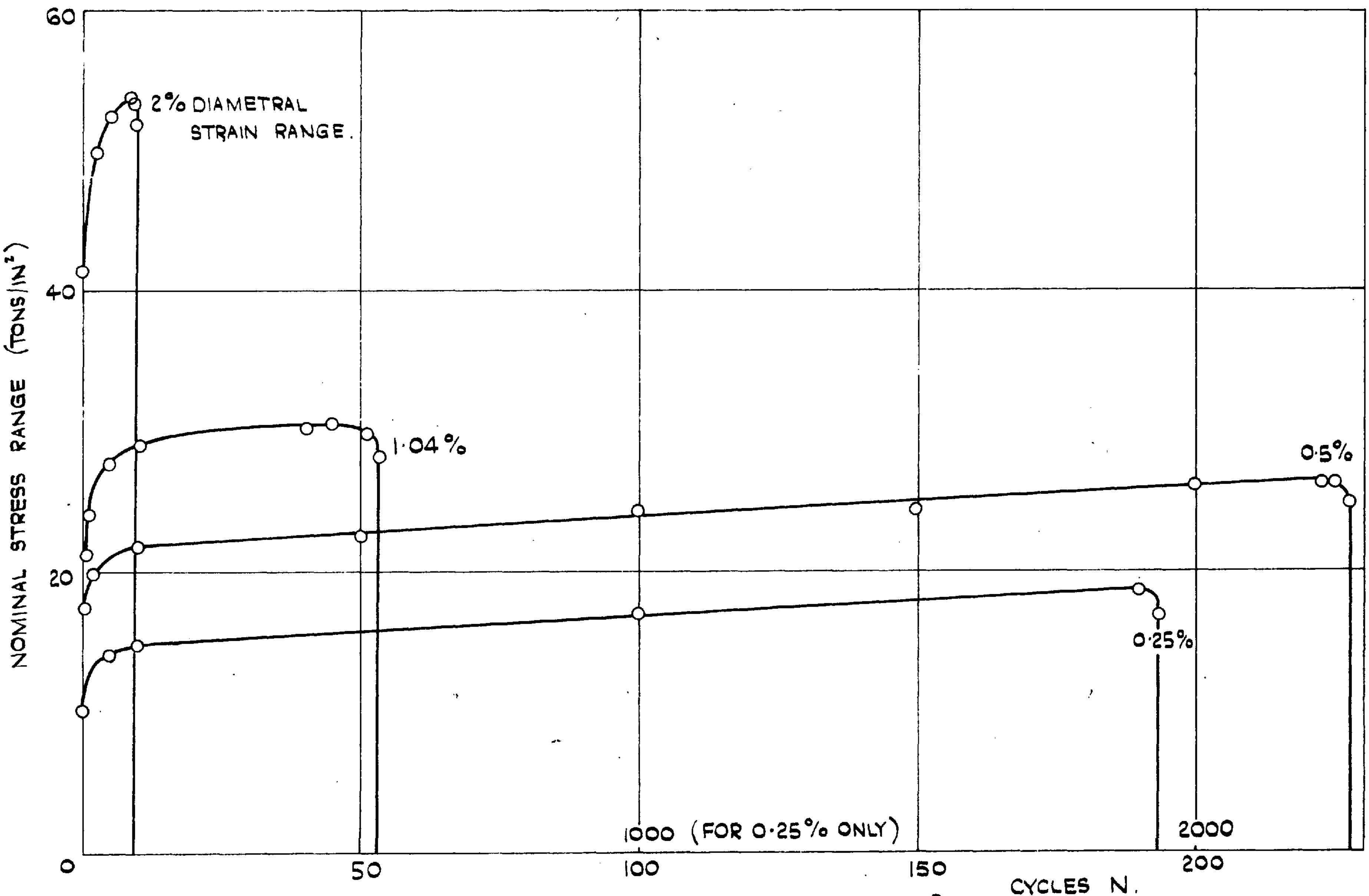

FIG.72. Variation of stress range during strain cycling at 450°C of cast iron A

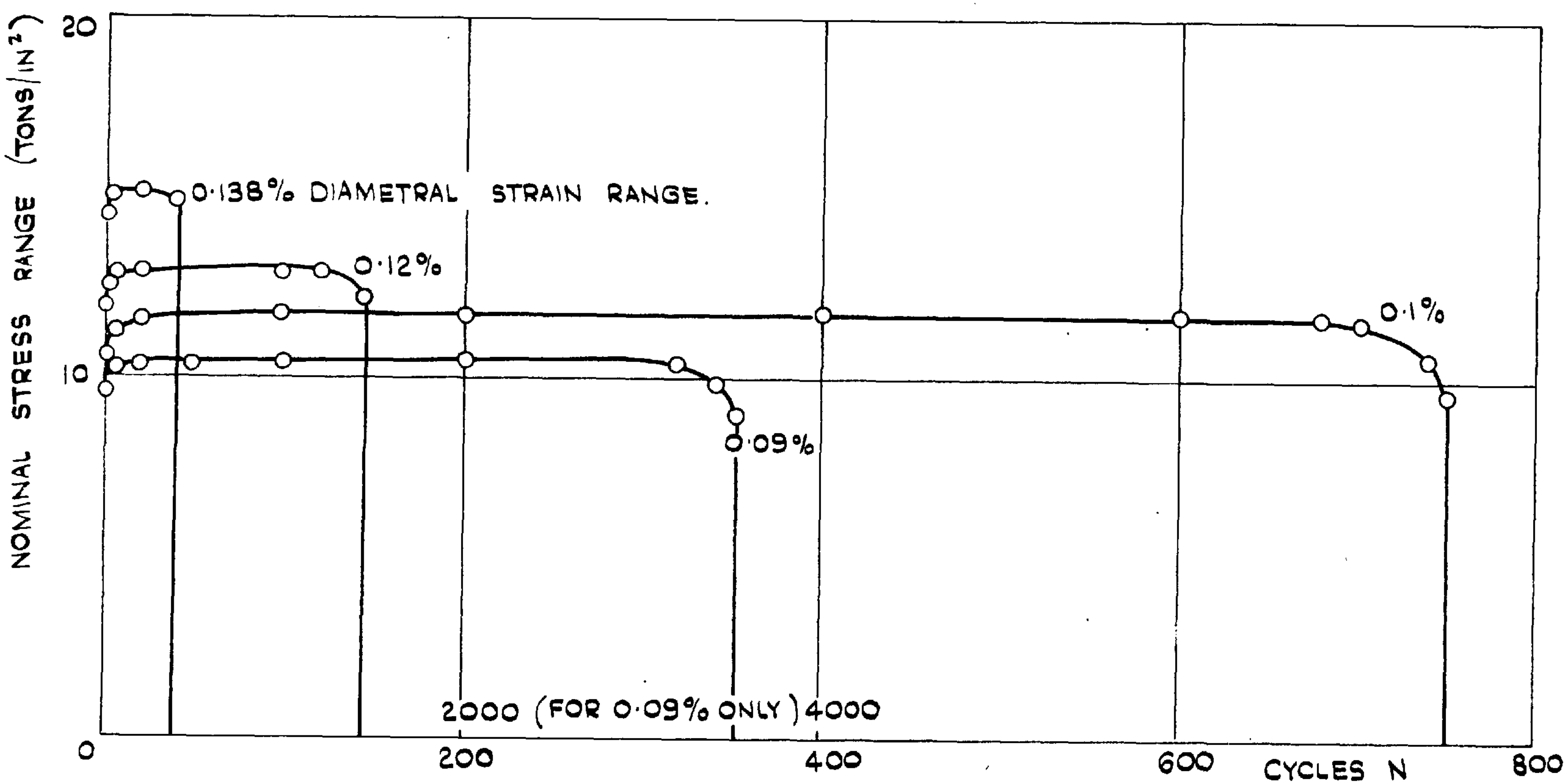

FIG.73. Variation of stress range during strain cycling at 450°C of cast iron B

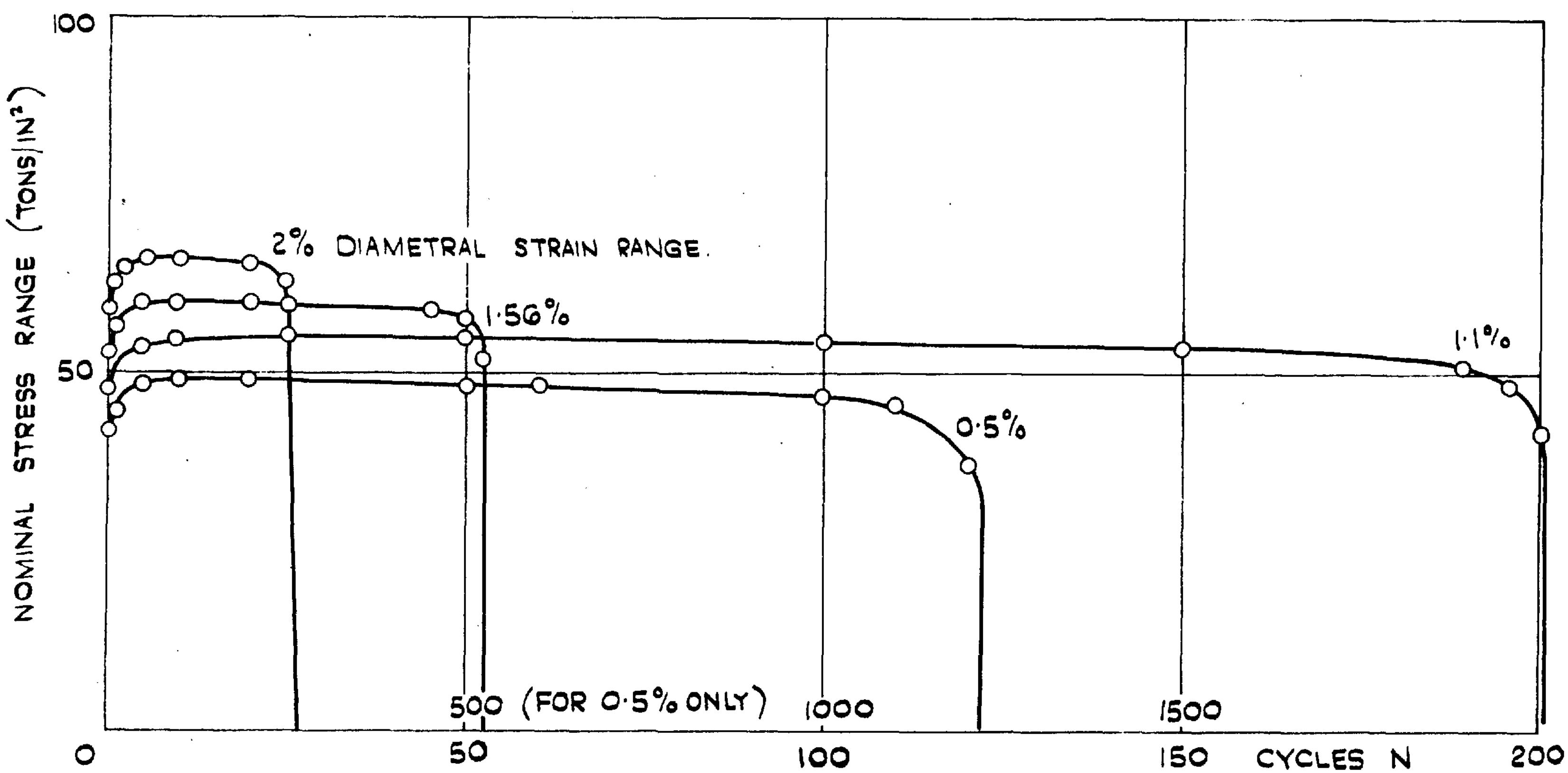

FIG.74. Variation of stress range during strain cycling at 450°C of cast steel C

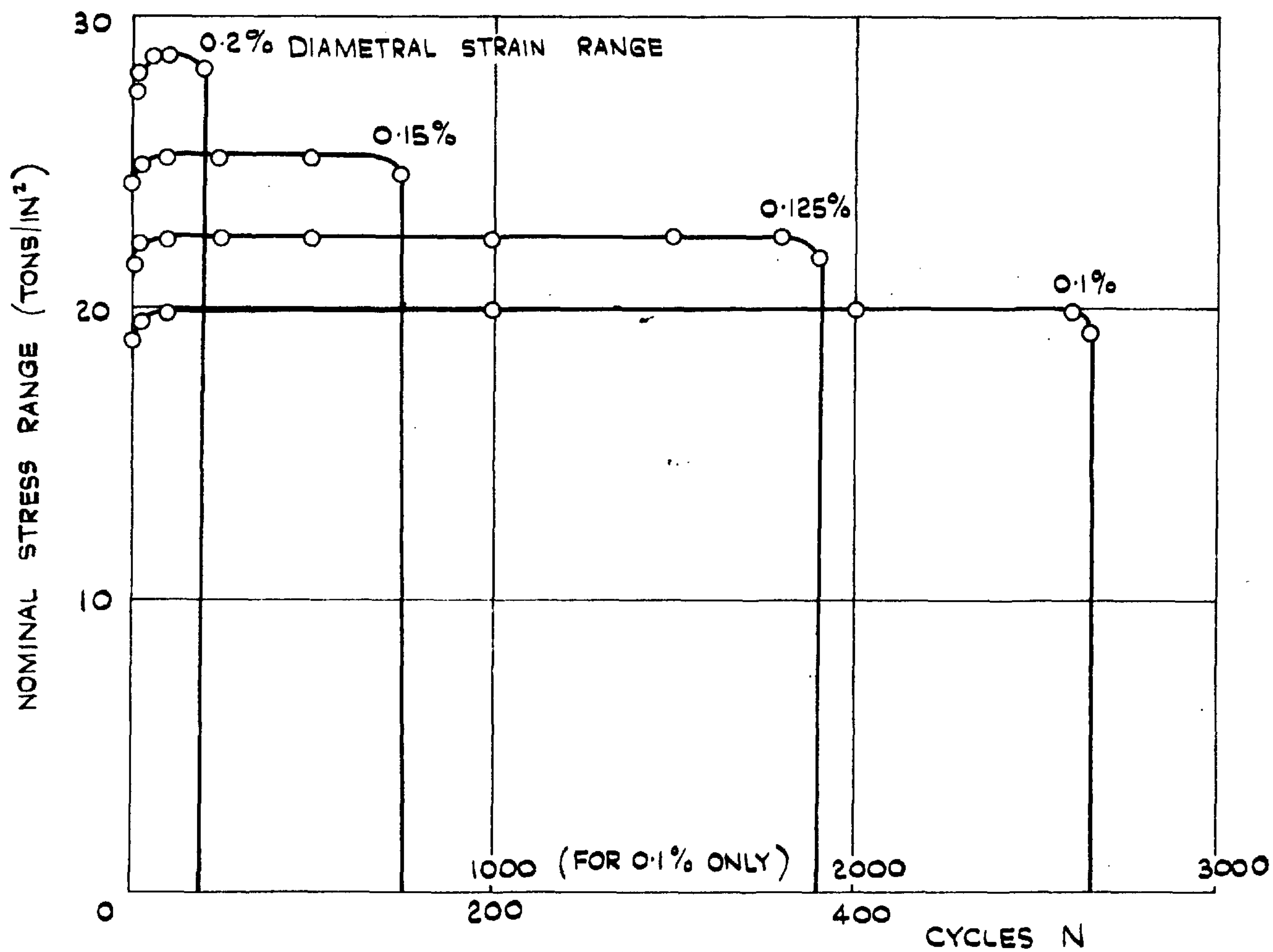

FIG.75. Variation of stress range during strain cycling at 450°C of cast iron E

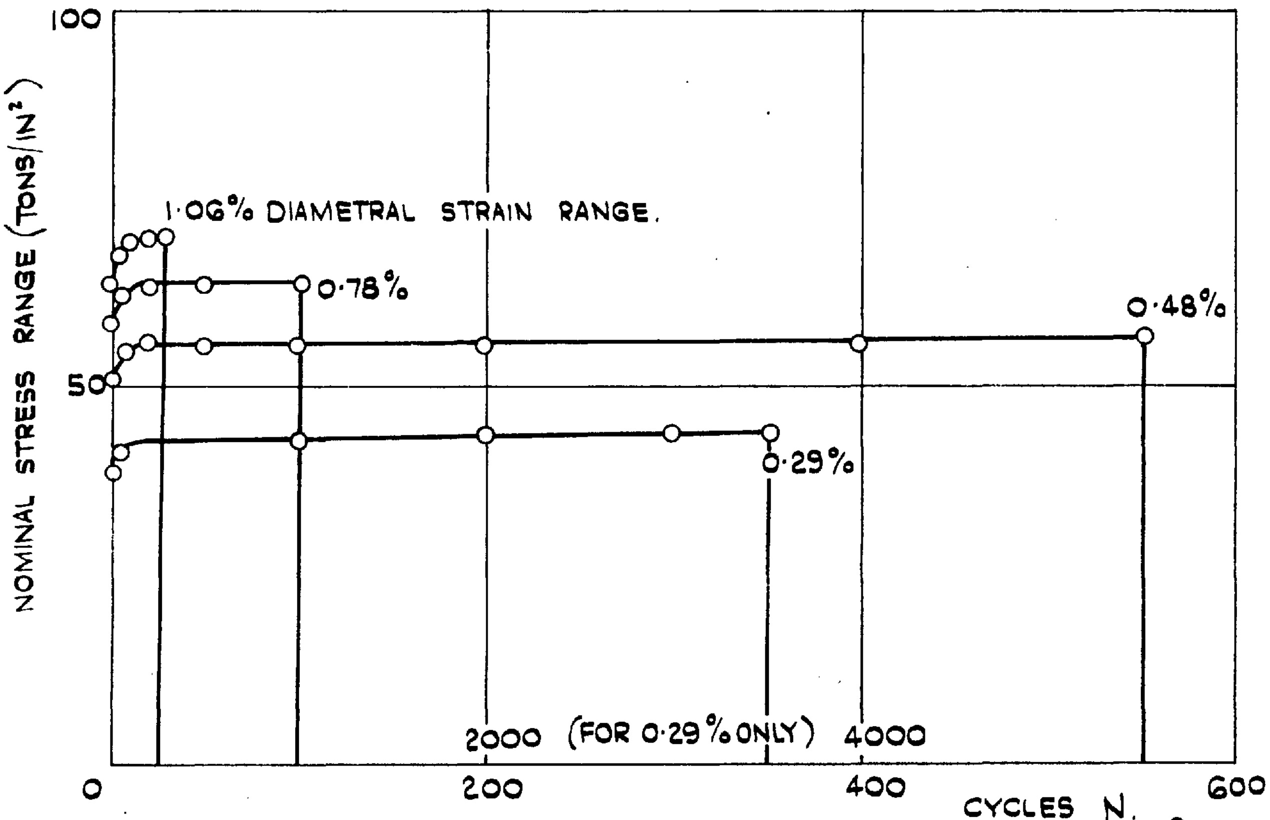

FIG.76. Variation of stress range during strain cycling at 450°C of cast iron F

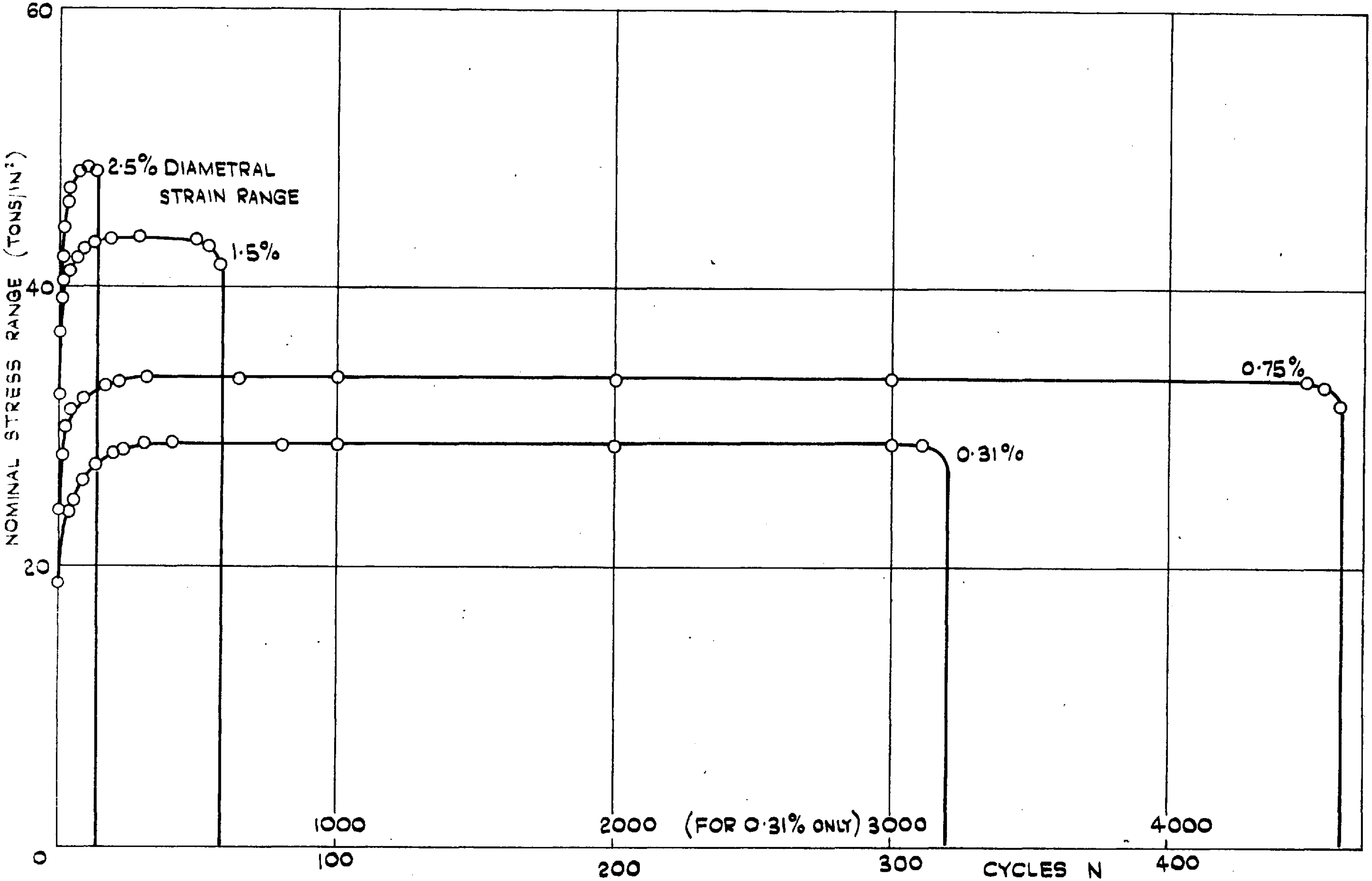

FIG.77. Variation of stress range during strain cycling at 450°C of cast steel S

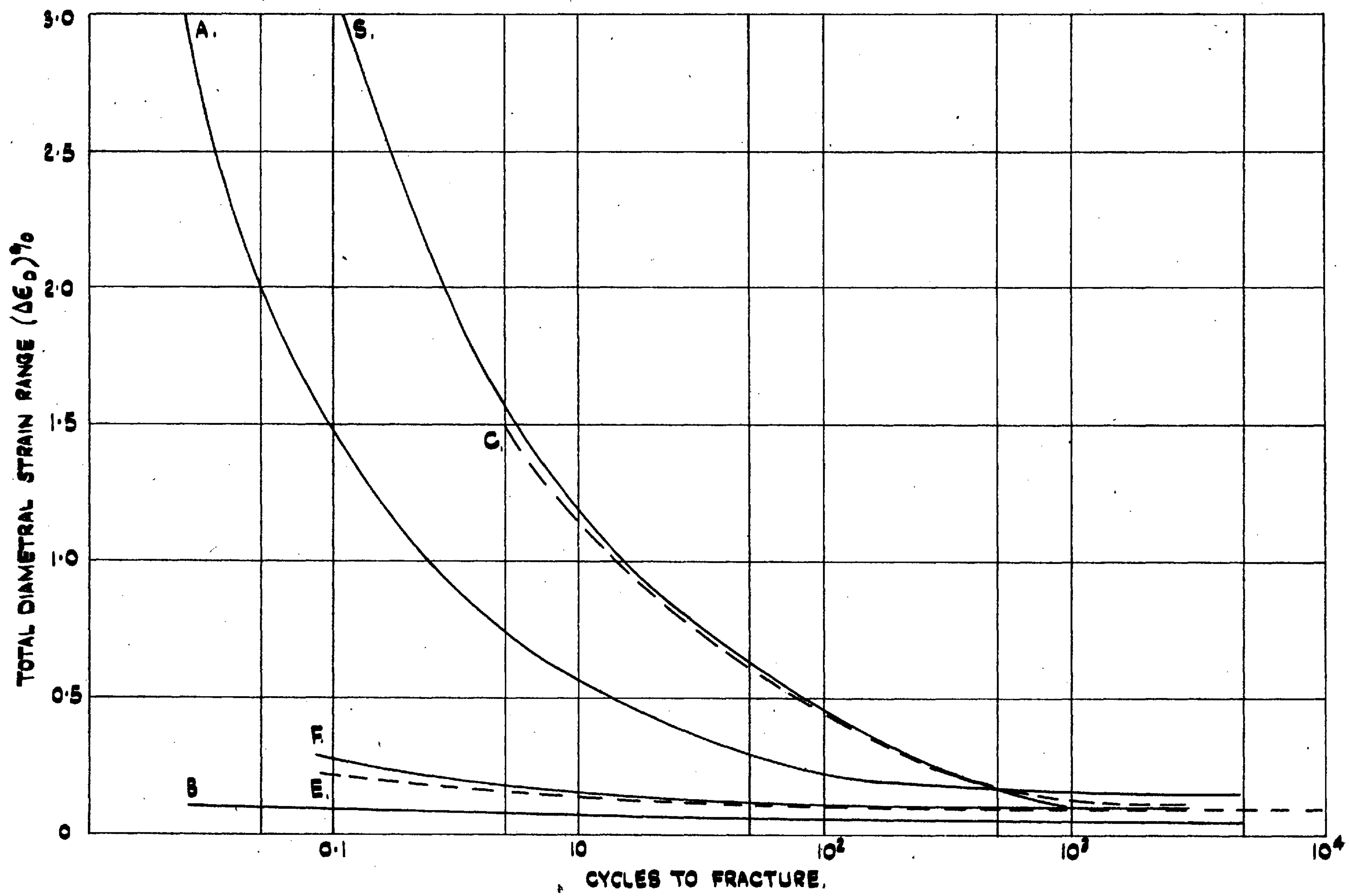

FIG.78. STRAIN CYCLING AT ROOM TEMPERATURE OF NOTCHED SPECIMENS.

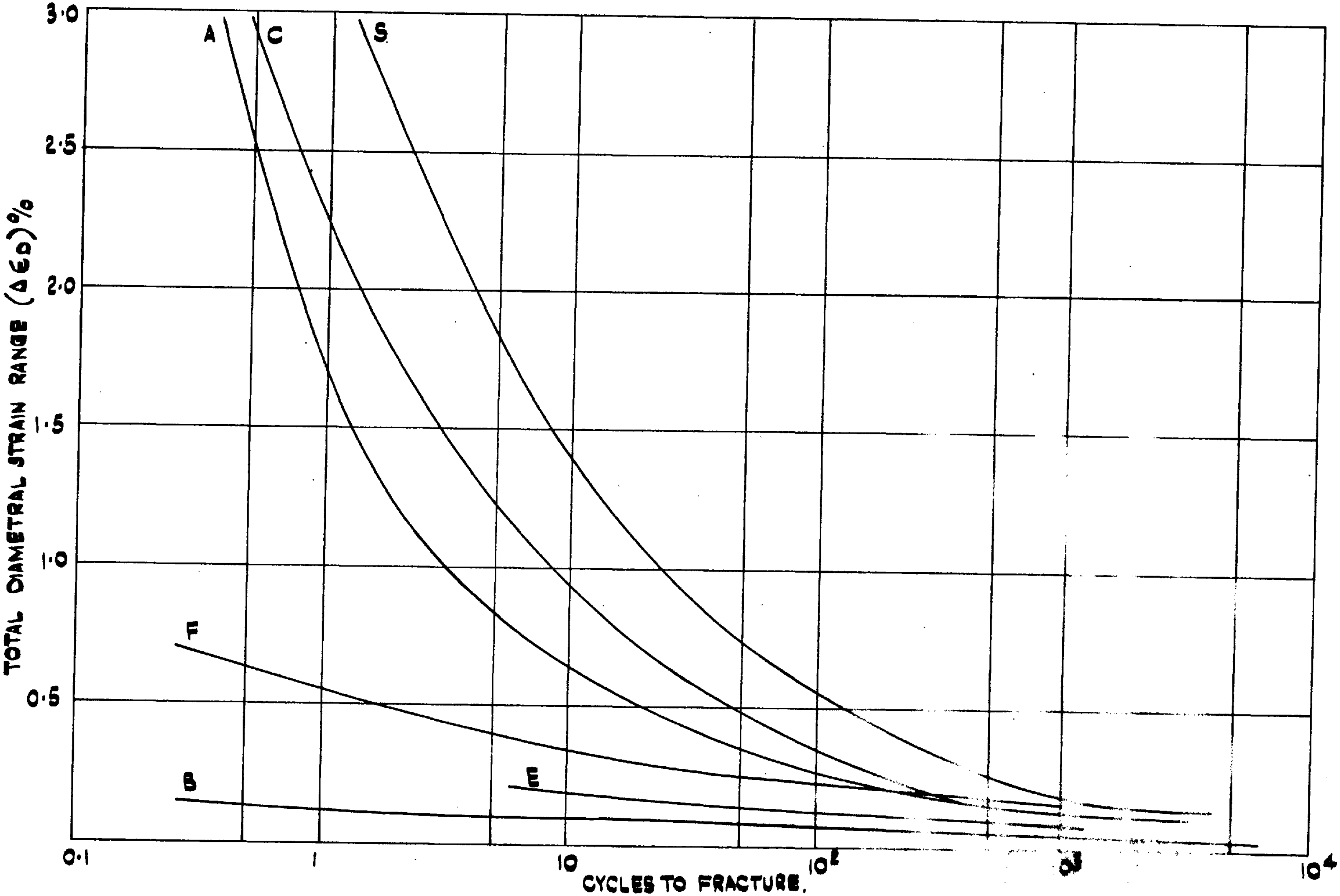

FIG. 79. STRAIN CYCLING AT HIGH TEMPERATURE OF NOTCHED SPECIMENS (450°C.)

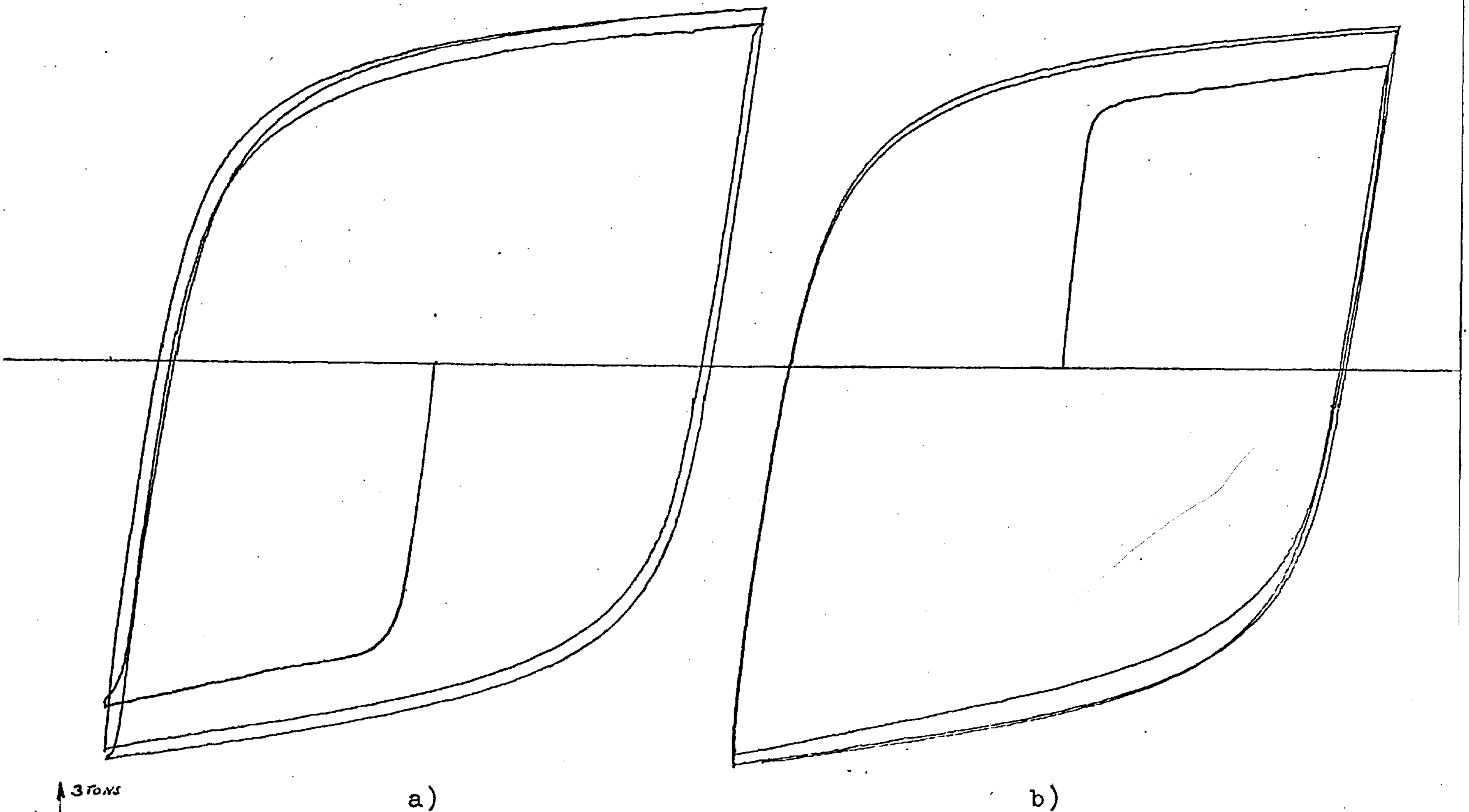

Fig.80 .Cast steel C. Strain cycling.
a)start in compression - b)start in tension.

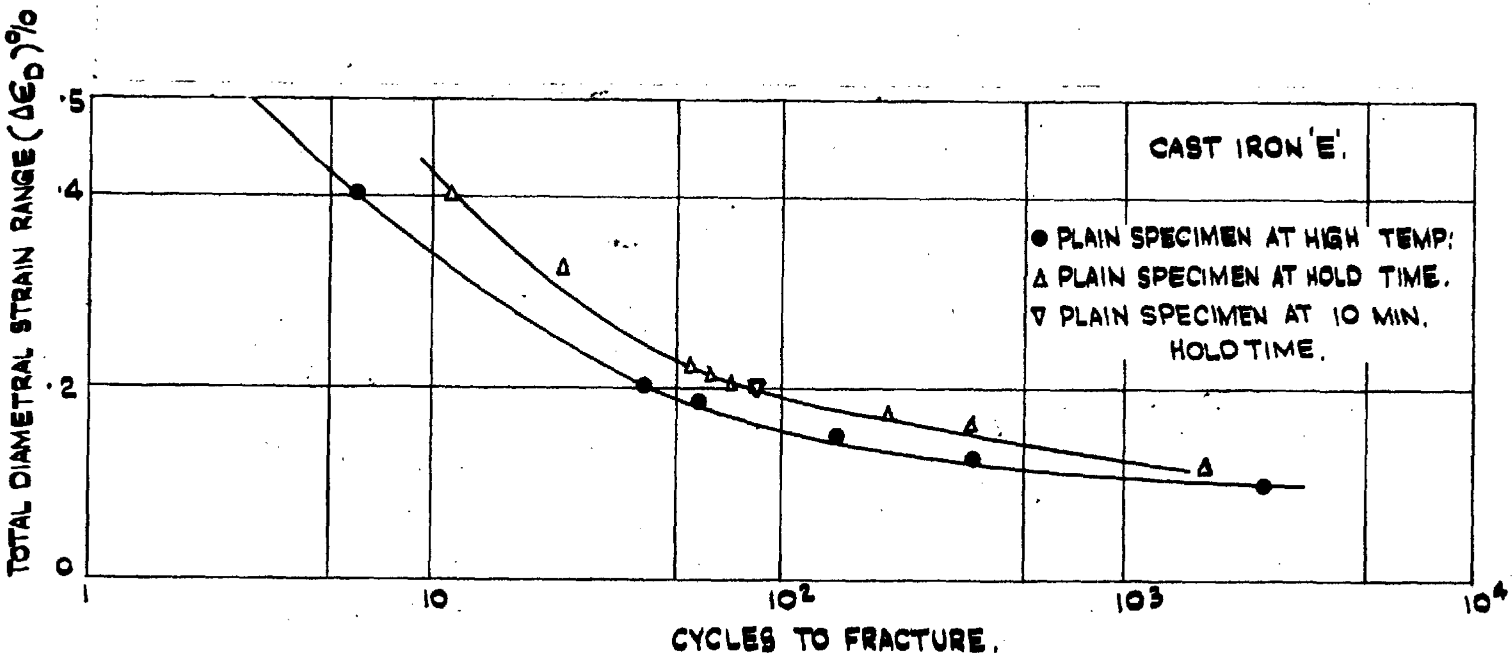

FIG. 81. 5 MIN: HOLD TIME (TENSION AND COMPRESSION) TESTS AT 450°C FOR 'E'

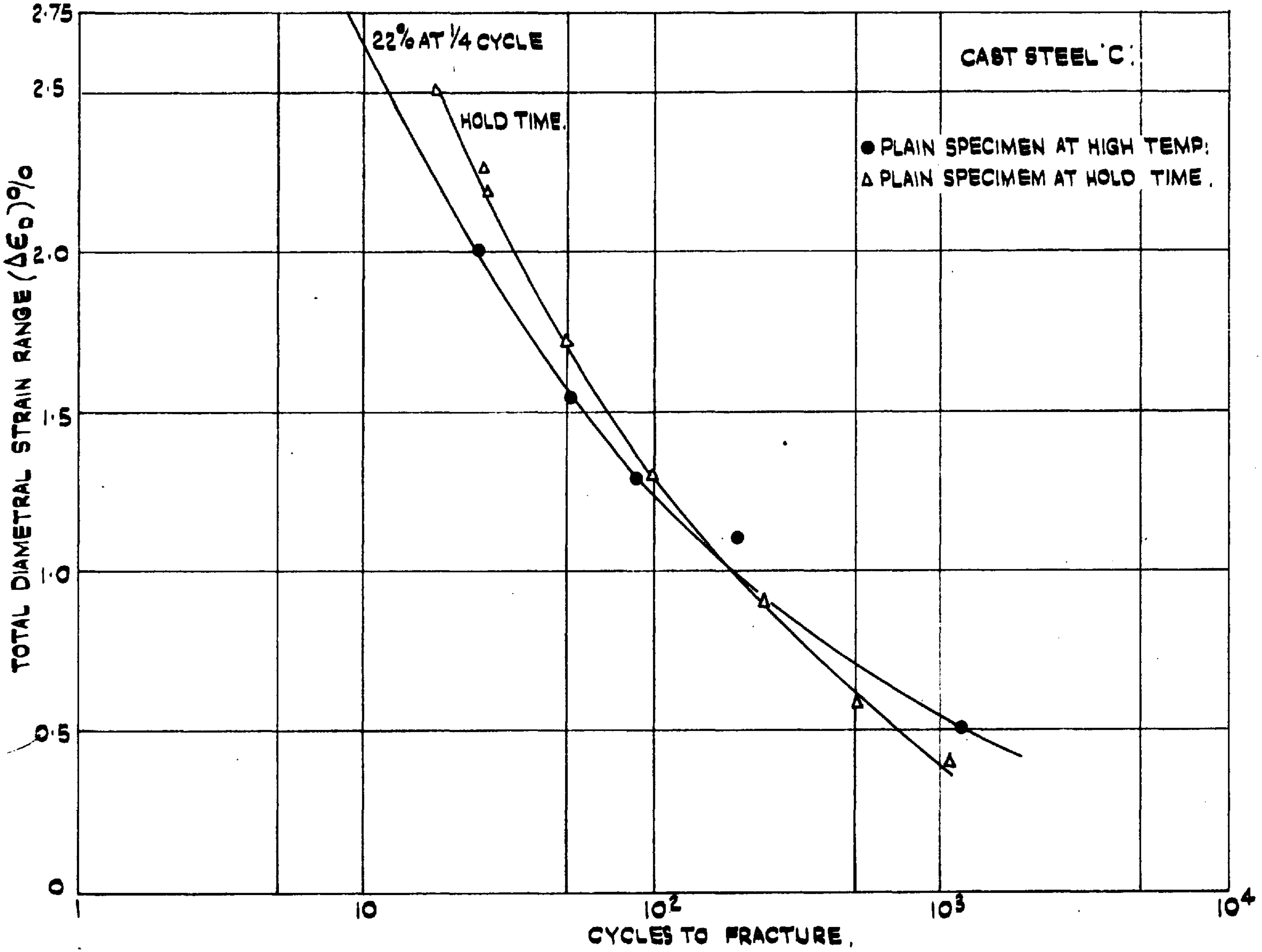

FIG.82. 5 min. Hold time (tension & compression) tests at 450°C for steel C.

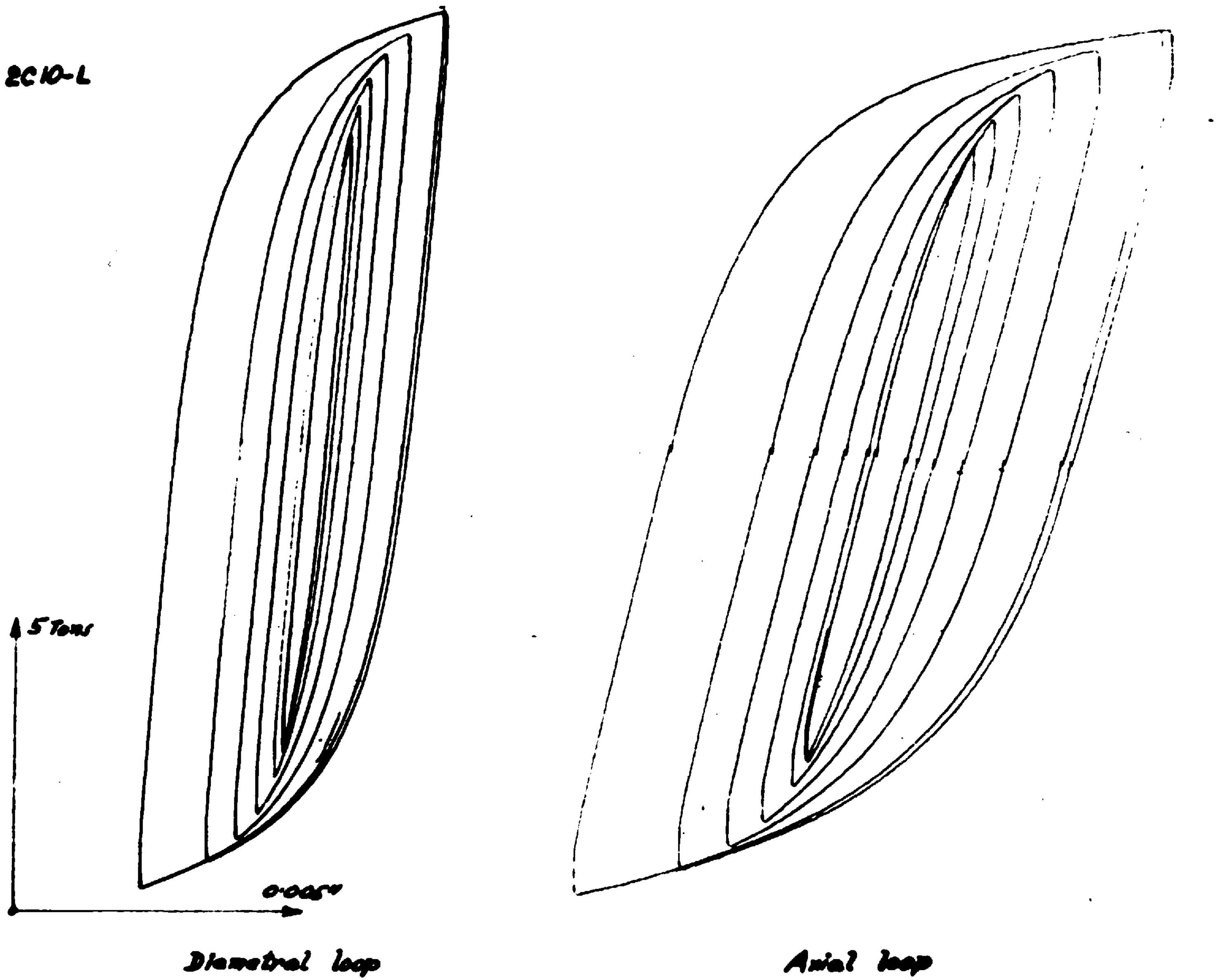

Fig. 83. Diametral and axial loops for incrementally decreasing load. Cast steel C.

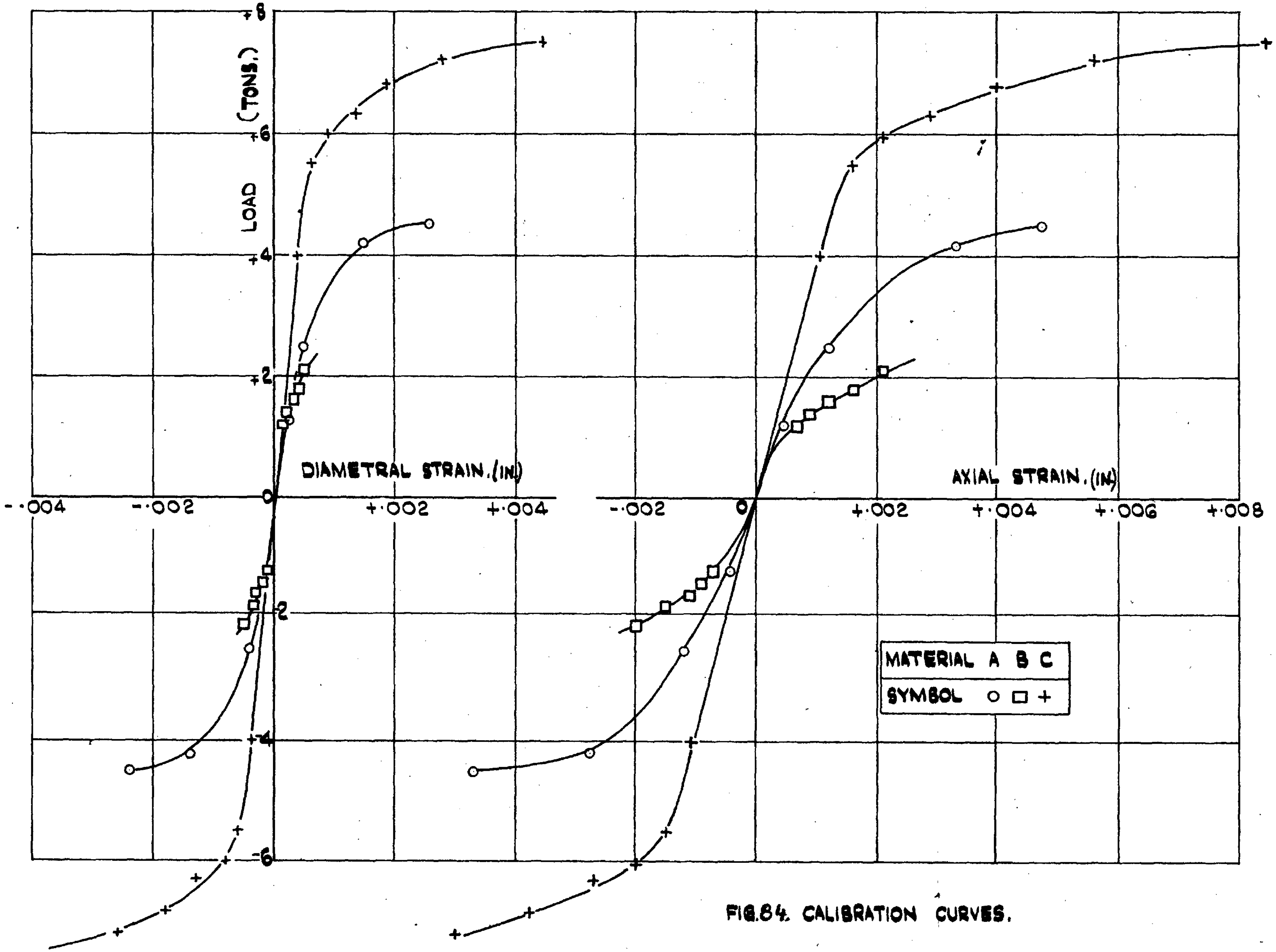

FIG. 84. CALIBRATION CURVES.

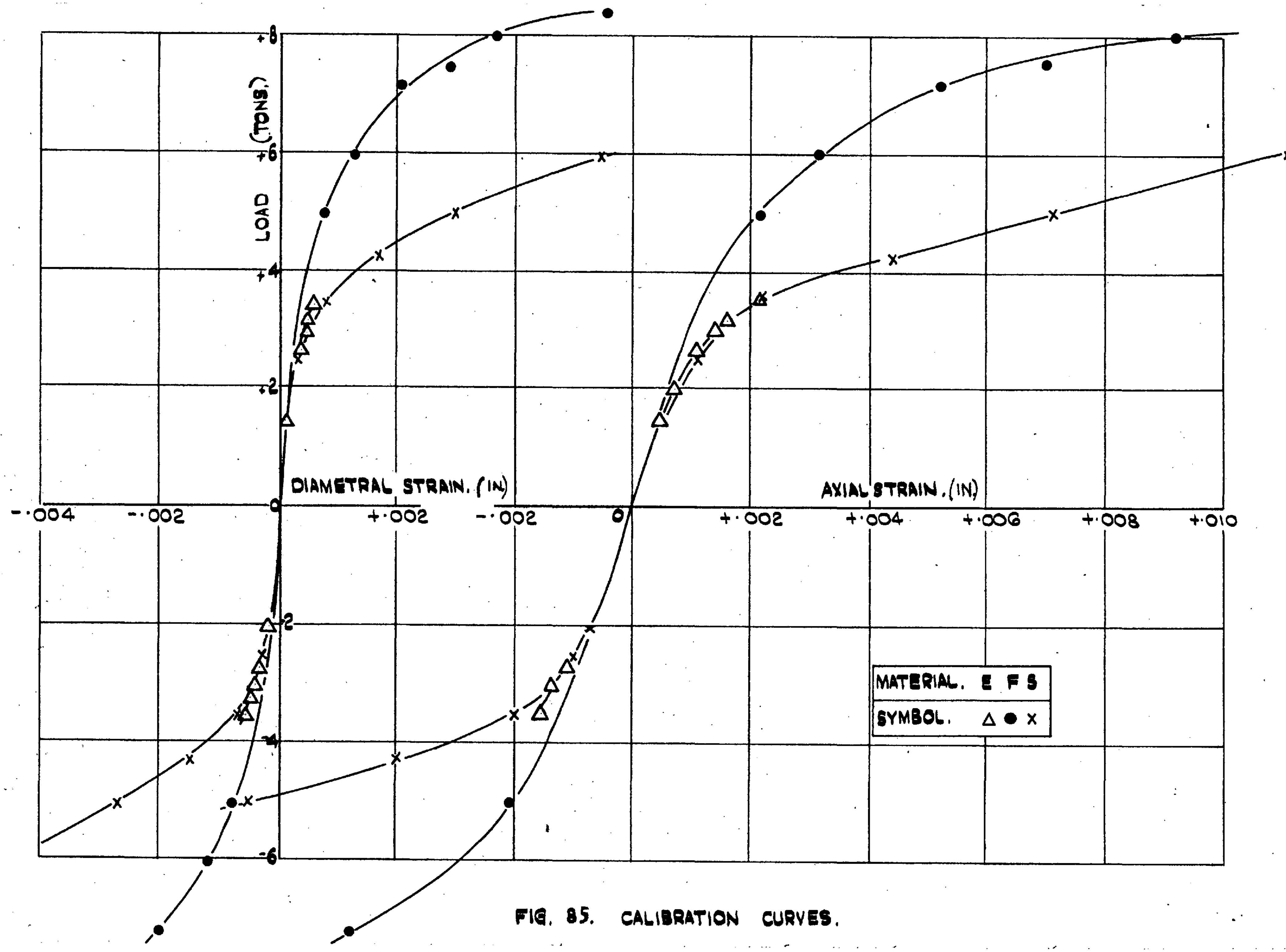

FIG. 85. CALIBRATION CURVES.

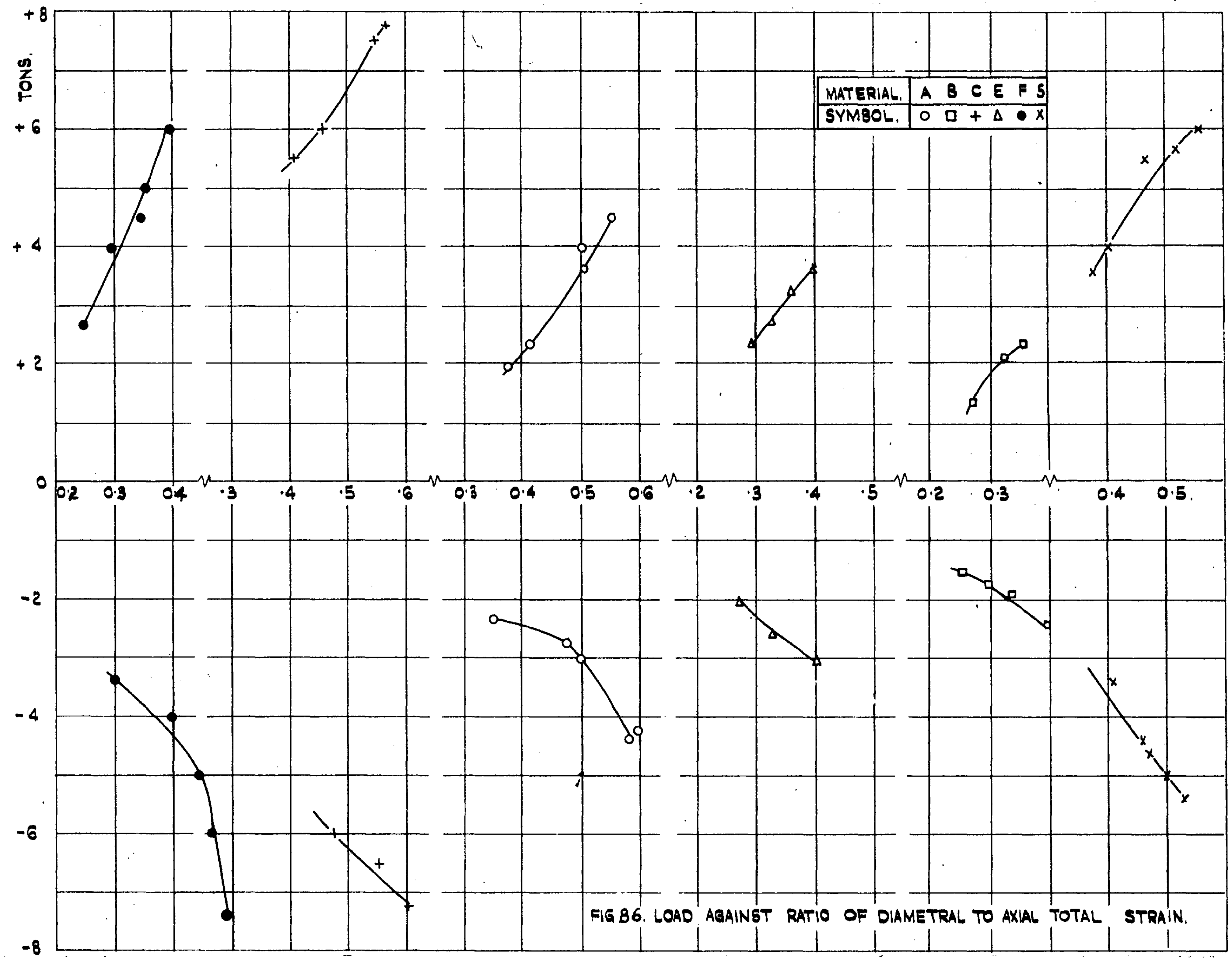

FIG.B6. LOAD AGAINST RATIO OF DIAMETRAL TO AXIAL TOTAL STRAIN.

MATERIAL	A	B	C	E	F	S	En25
SYMBOL	○	□	+	△	●	x	■

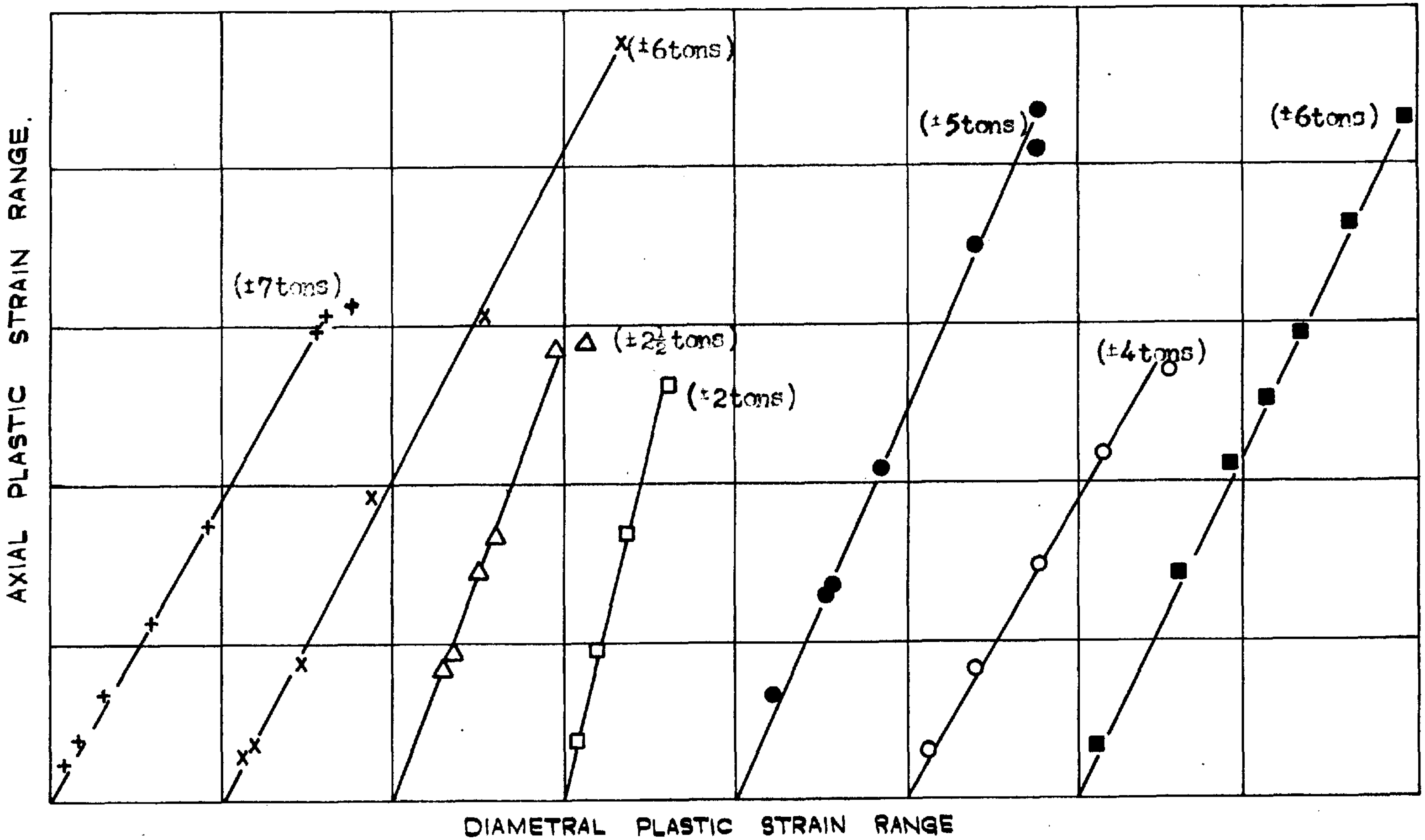

FIG. 87. CALIBRATION CURVES.

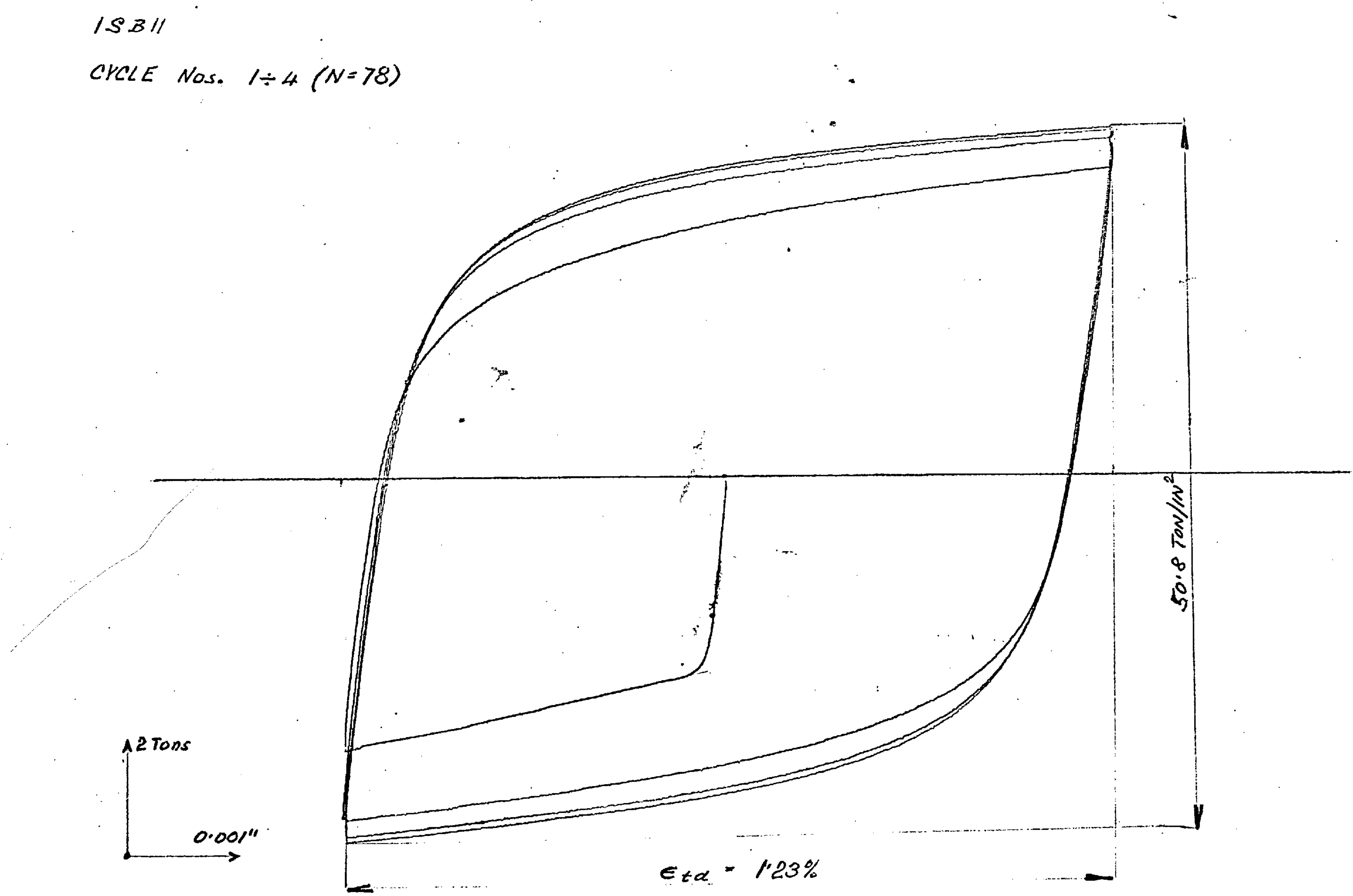

Fig. 88 . CAST MILD STEEL S Strain cycling. Strain hardening in the first 4 cycles.

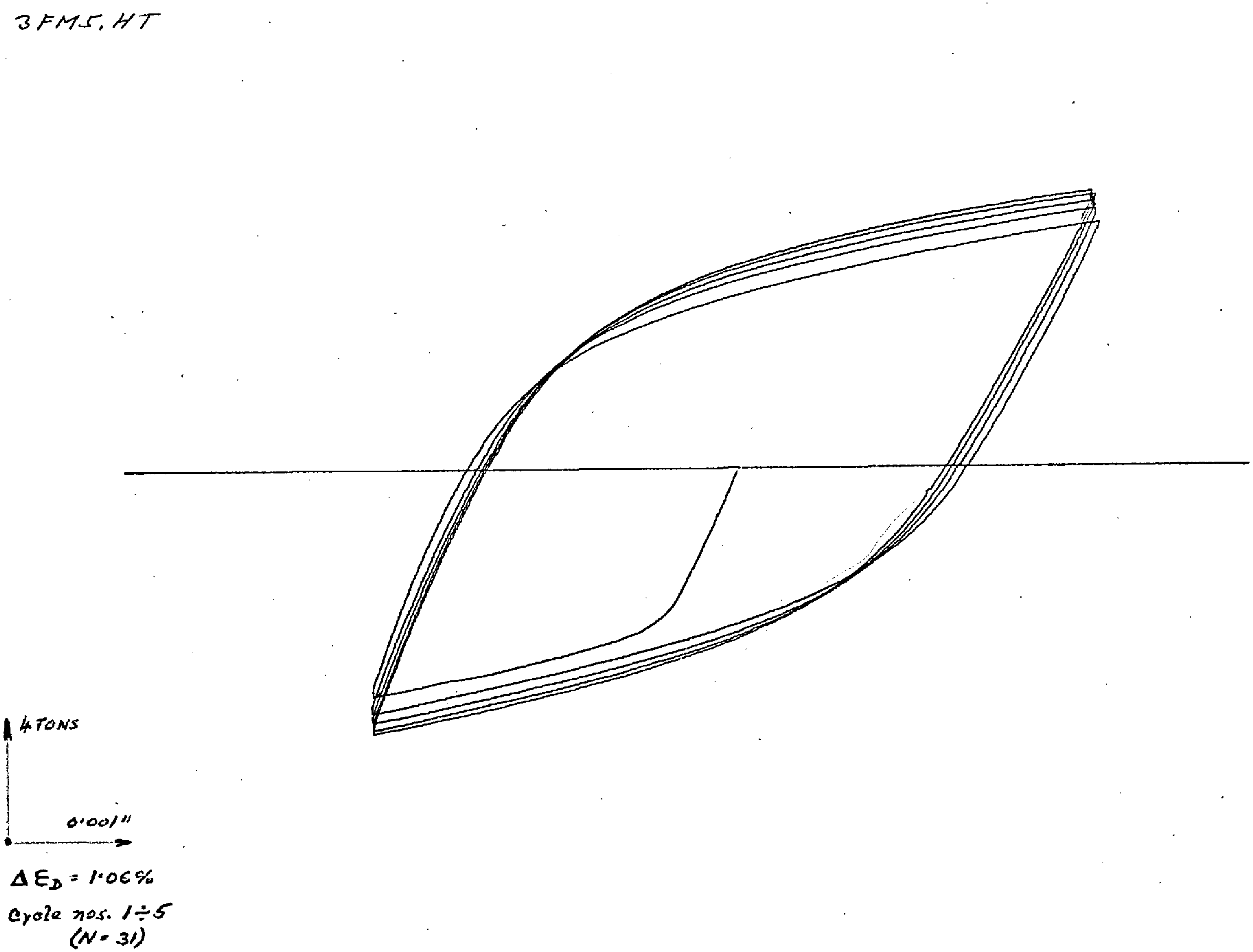

Fig. 89 . Cast iron F. Strain cycling at 450°C. Strain hardening.

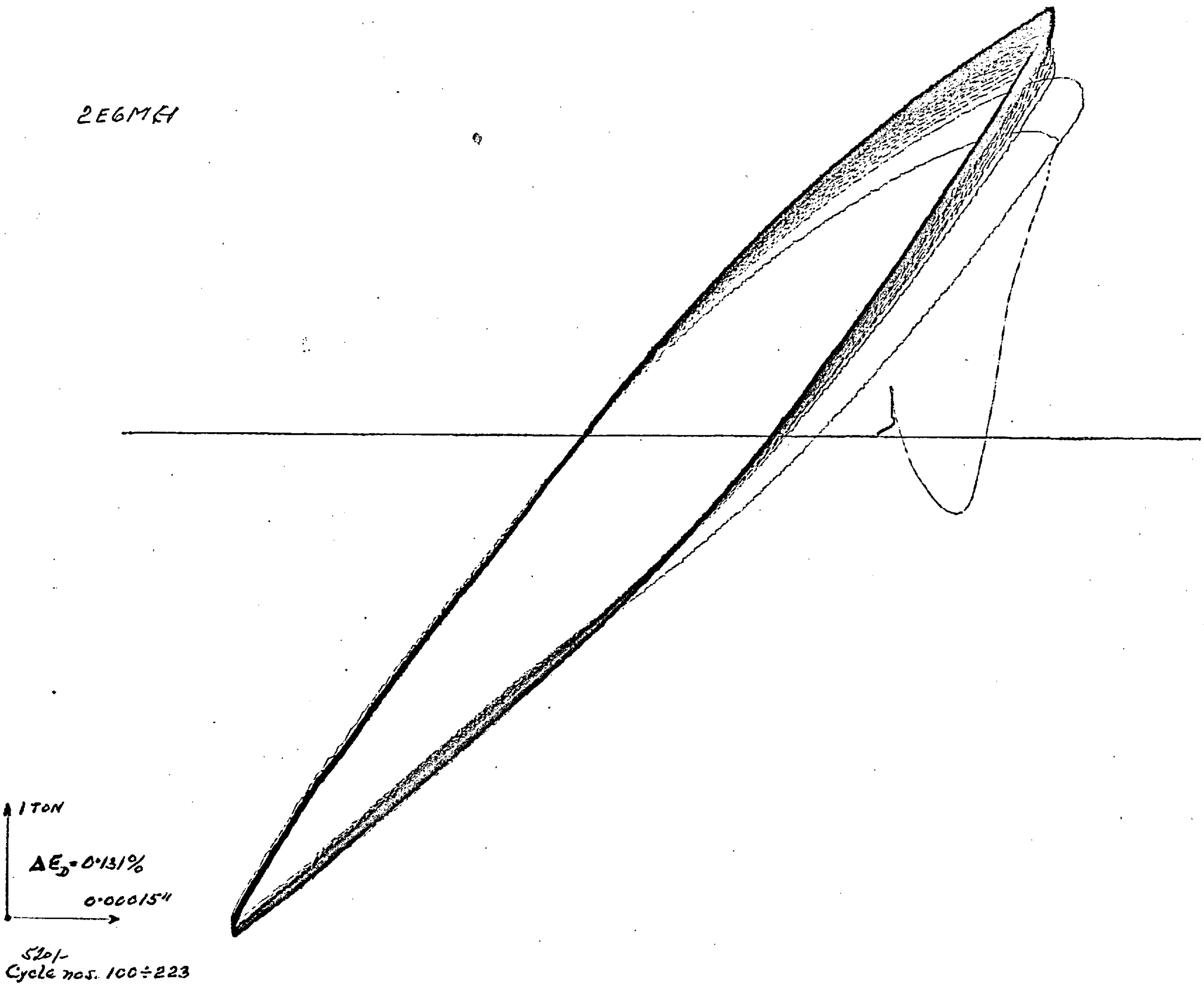

Fig. 90 .Cast iron E. Strain cycling and fracture.

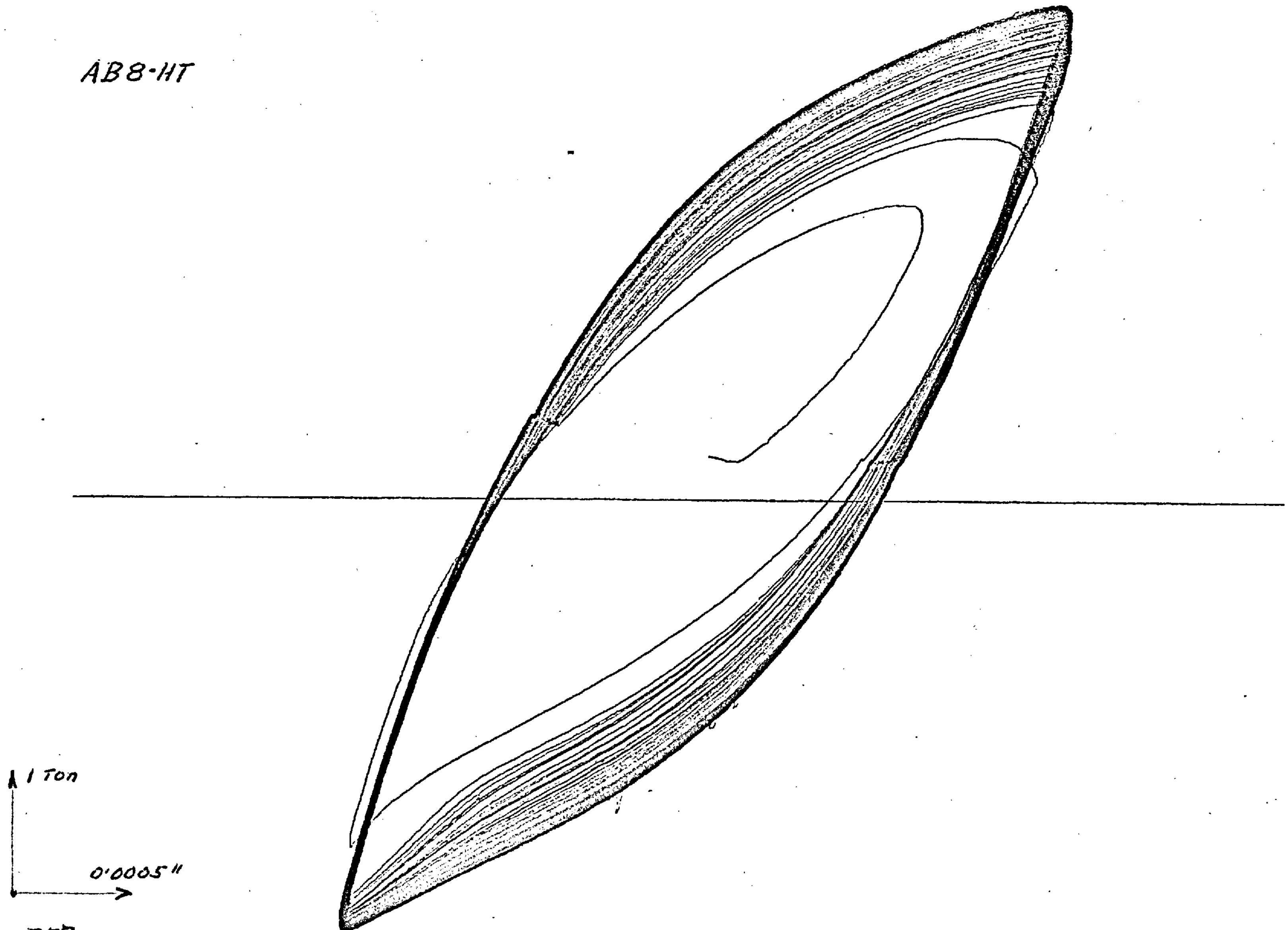

3757

$\Delta\varepsilon_D = 0{\cdot}3\%$

Cycle nos. 552÷649

Fig. 91 . Cast iron A. Strain cycling and fracture at 450°C.

1SB16

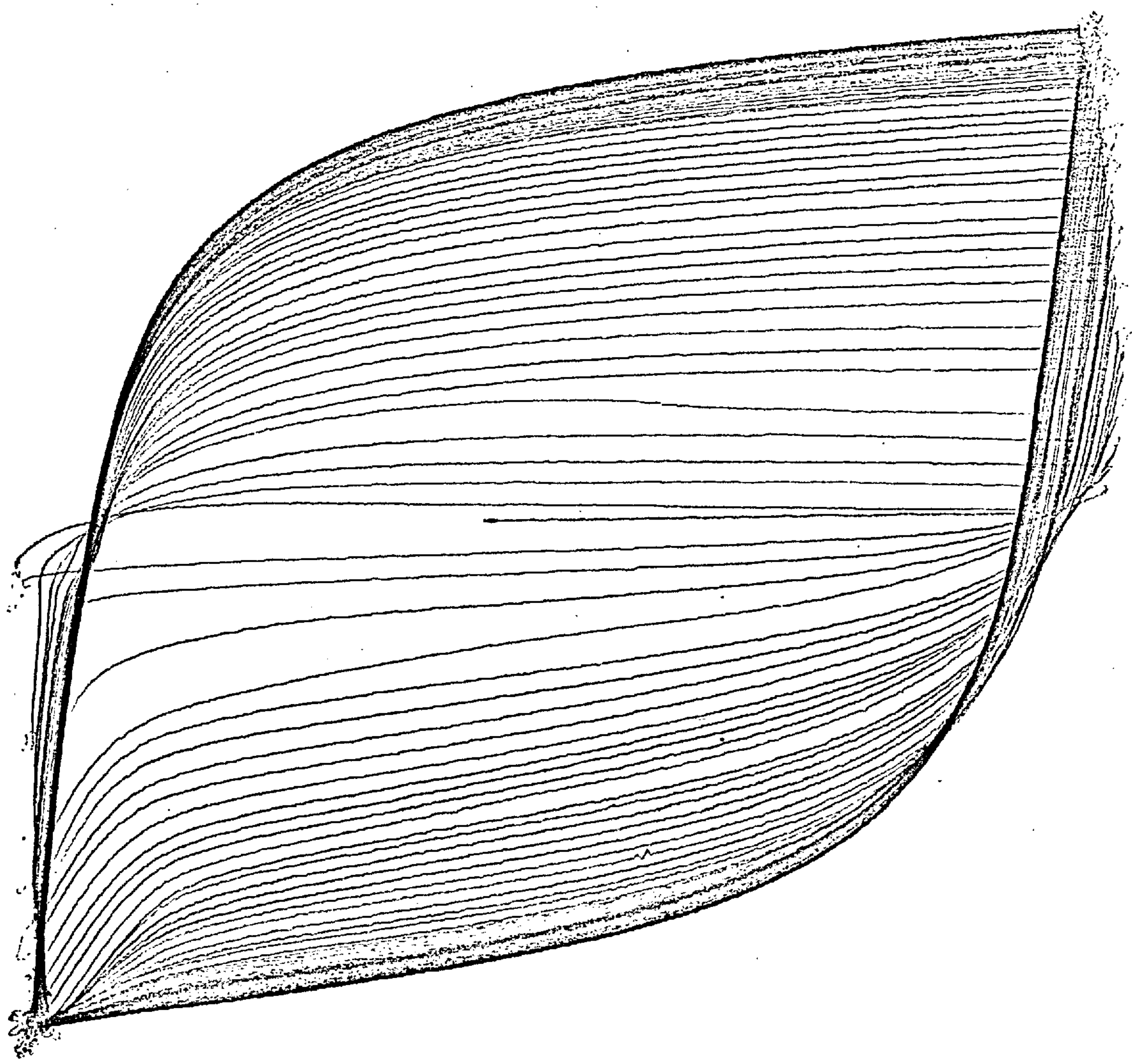

5345
5411 fracture
CYCLE Nos: 220÷286

1 Ton $\Delta\varepsilon_D = 1{\cdot}09\ \%$
0·0005"

Fig. 92 .Cast mild steel S. Strain cycling and fracture.

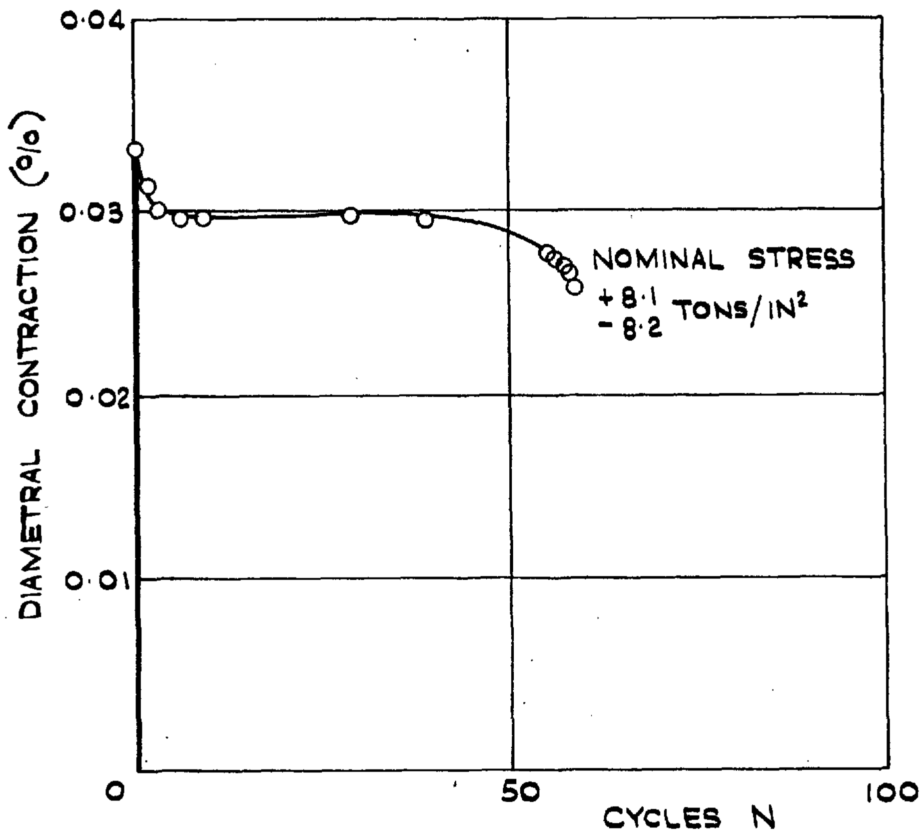

FIG.93. Cyclic creep of cast iron B

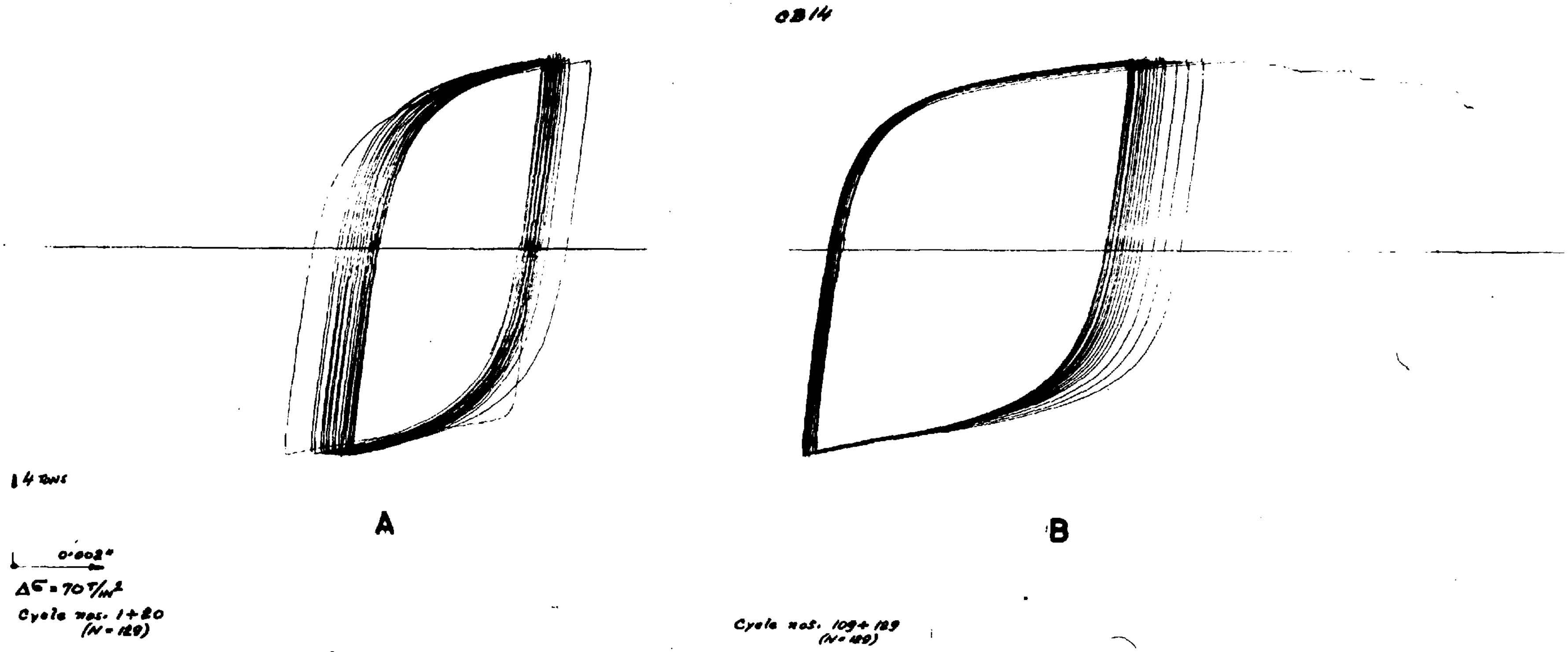

Fig. 94. Cast steel C. Cyclic creep in compression.

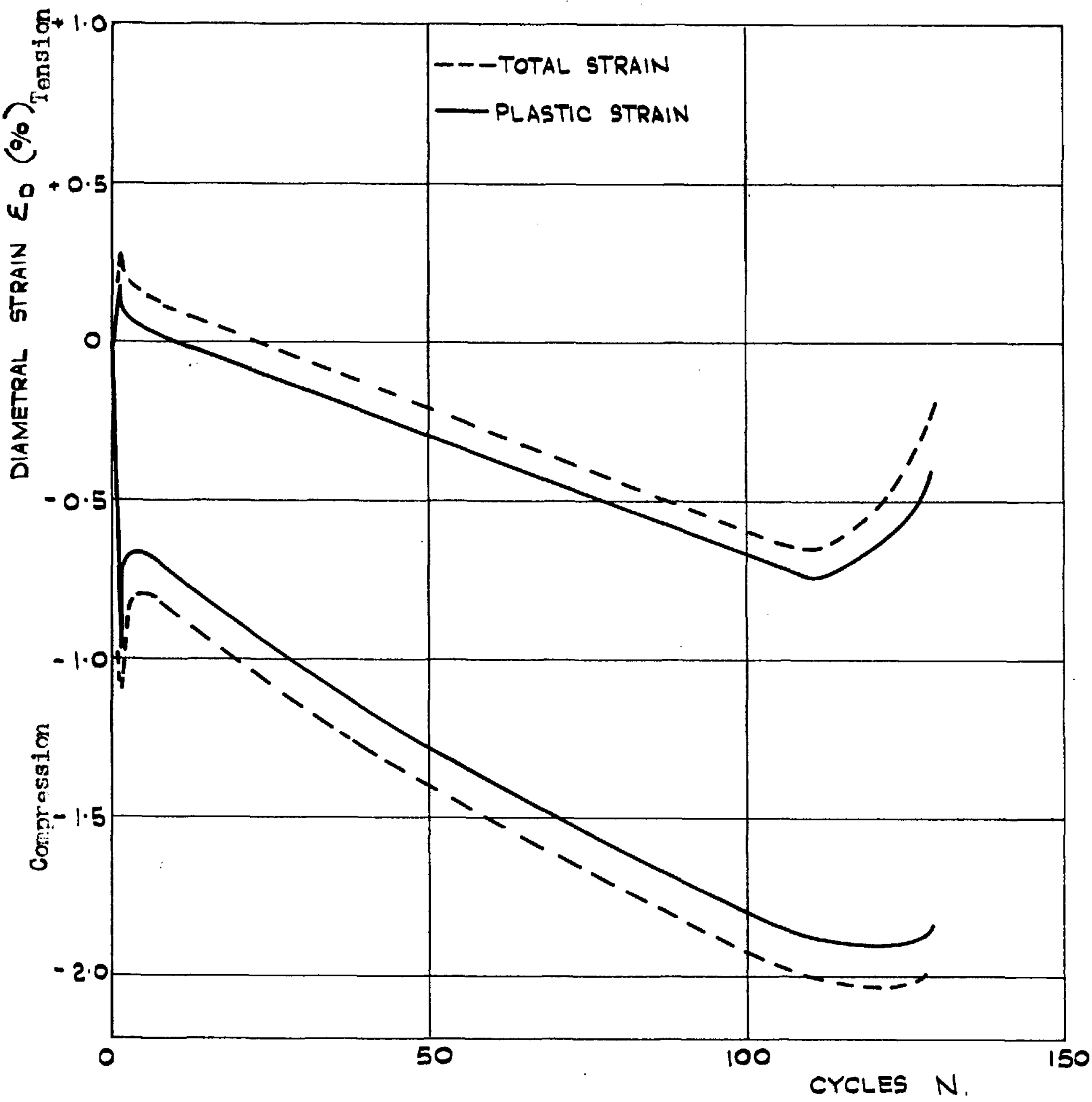

FIG.95. Cyclic creep of cast steel C in compression.

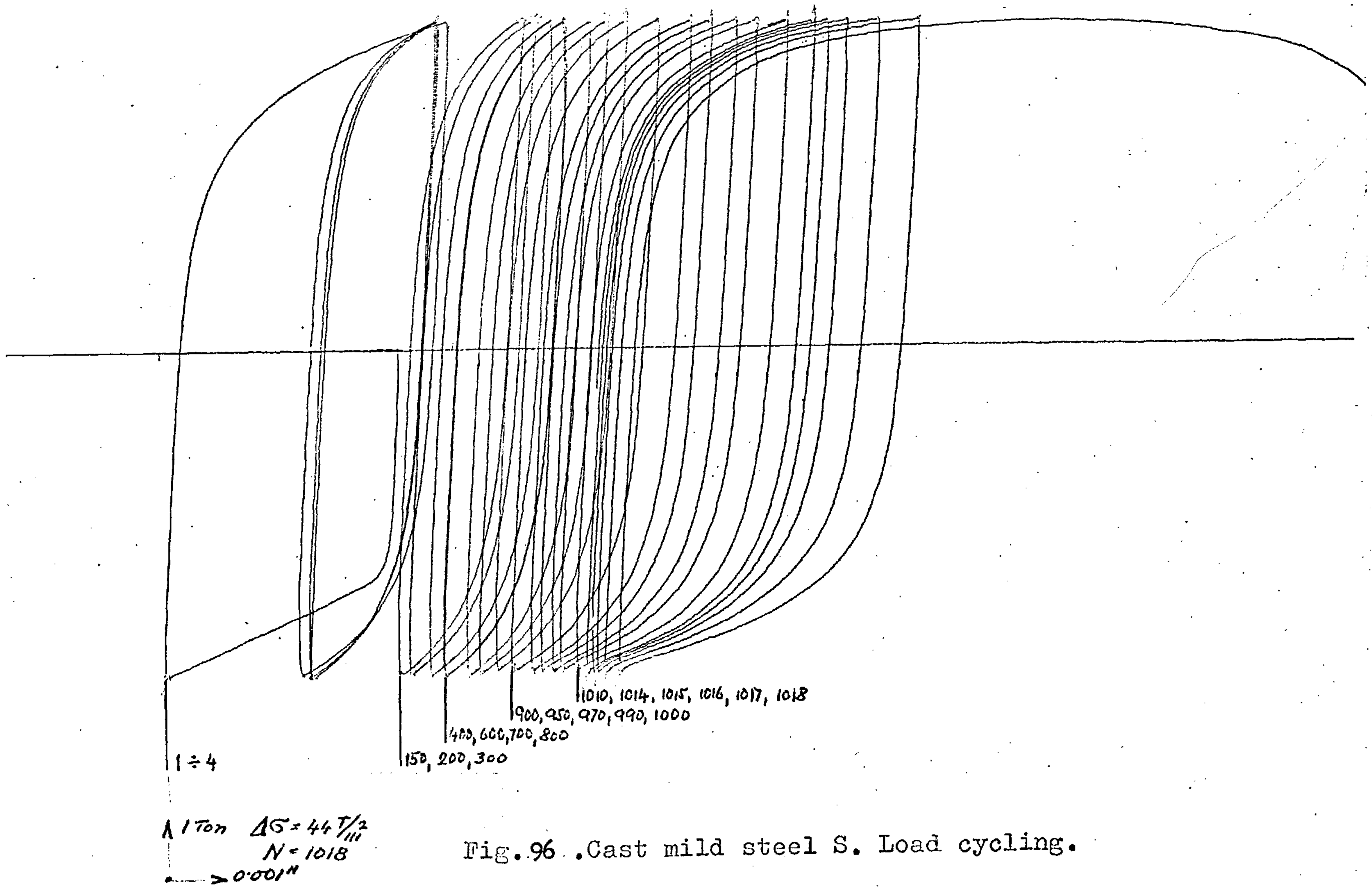

Fig. 96 .Cast mild steel S. Load cycling.

IF M6

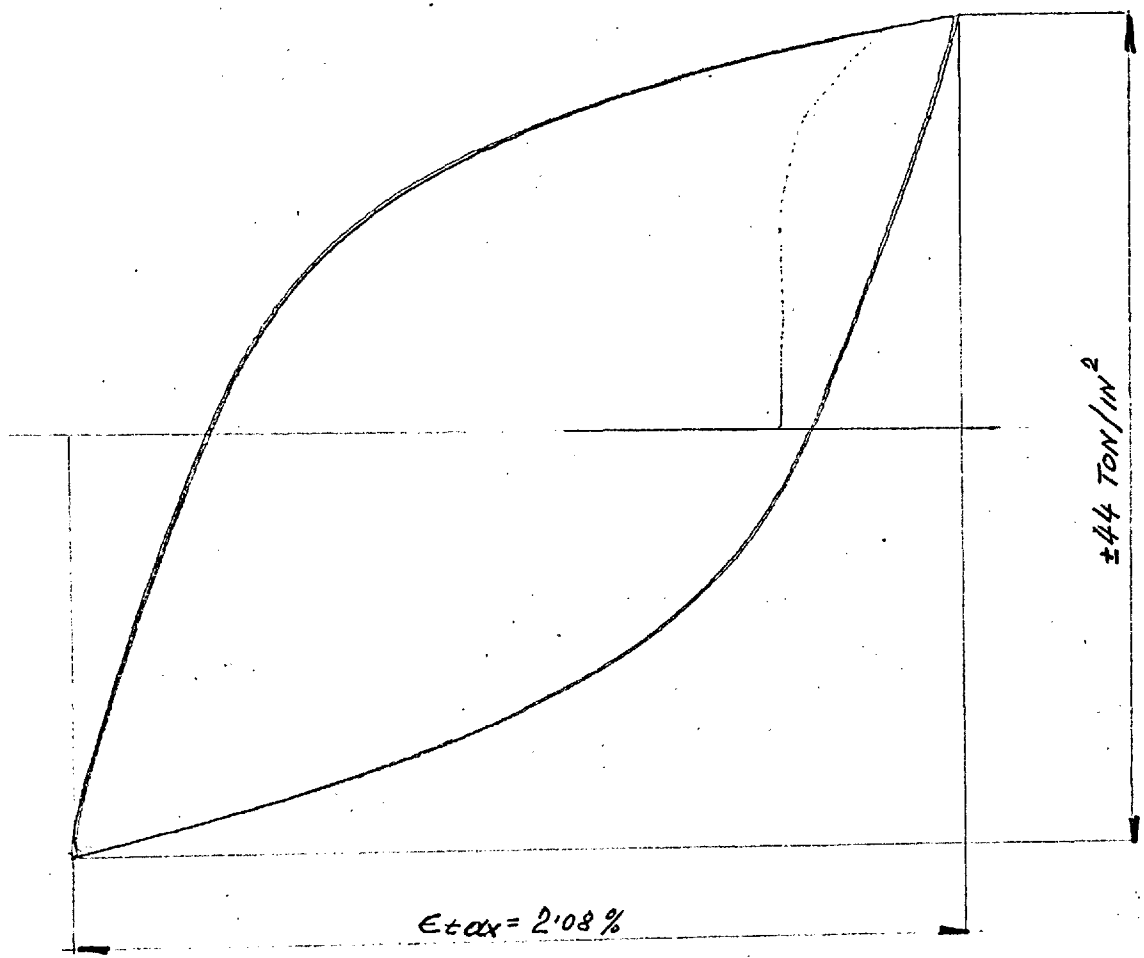

4 TONS

0·002"

Δσ = 88 T/in²

5551
52
53
54
55 Broken

Cycle nos. 3÷7 (N=7)

CAST IRON F

Fig. 97. Cast iron F. Load cycling.

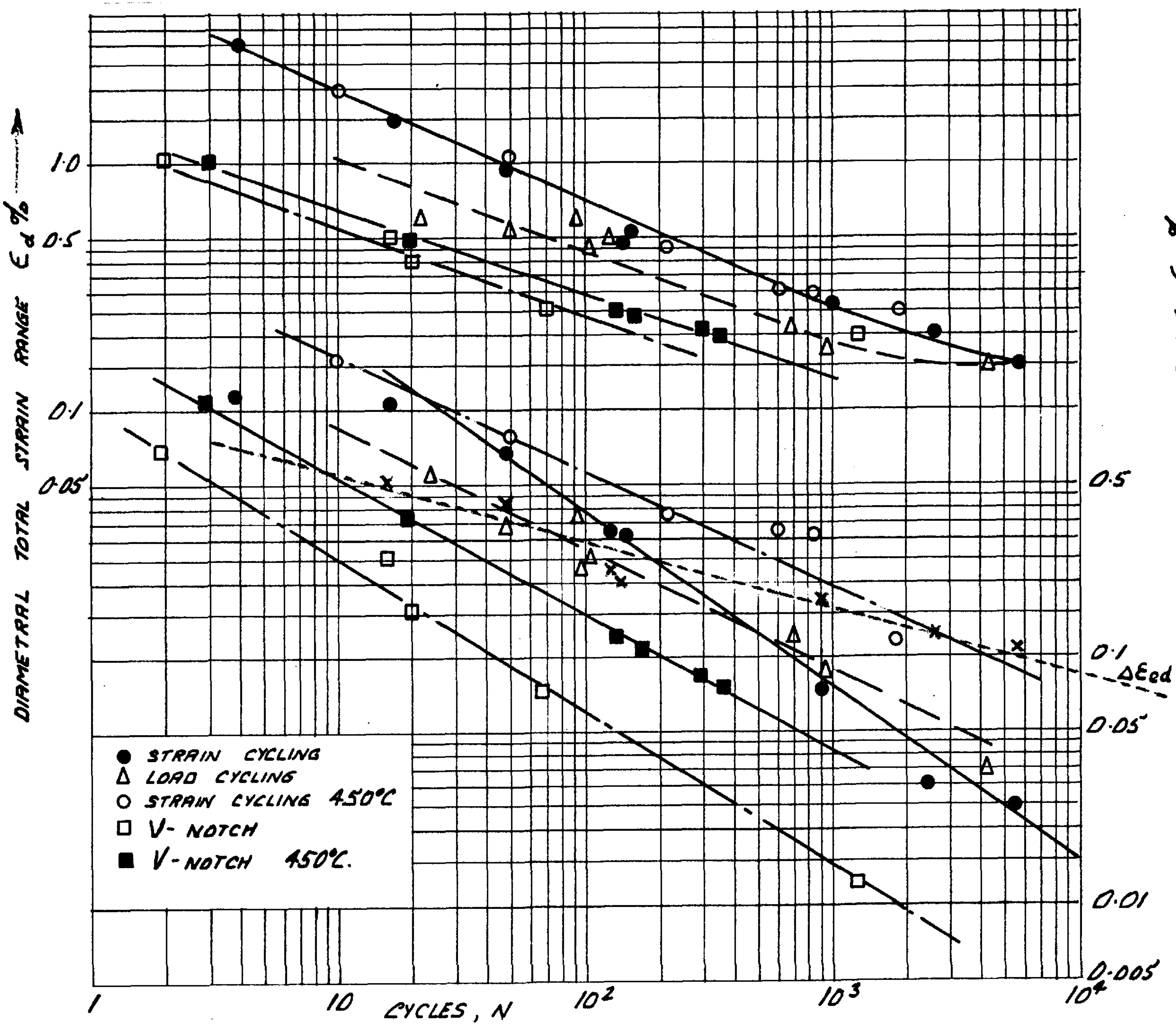

FIG. 98. STRAIN RANGE - CYCLE CURVES FOR CAST IRON A.

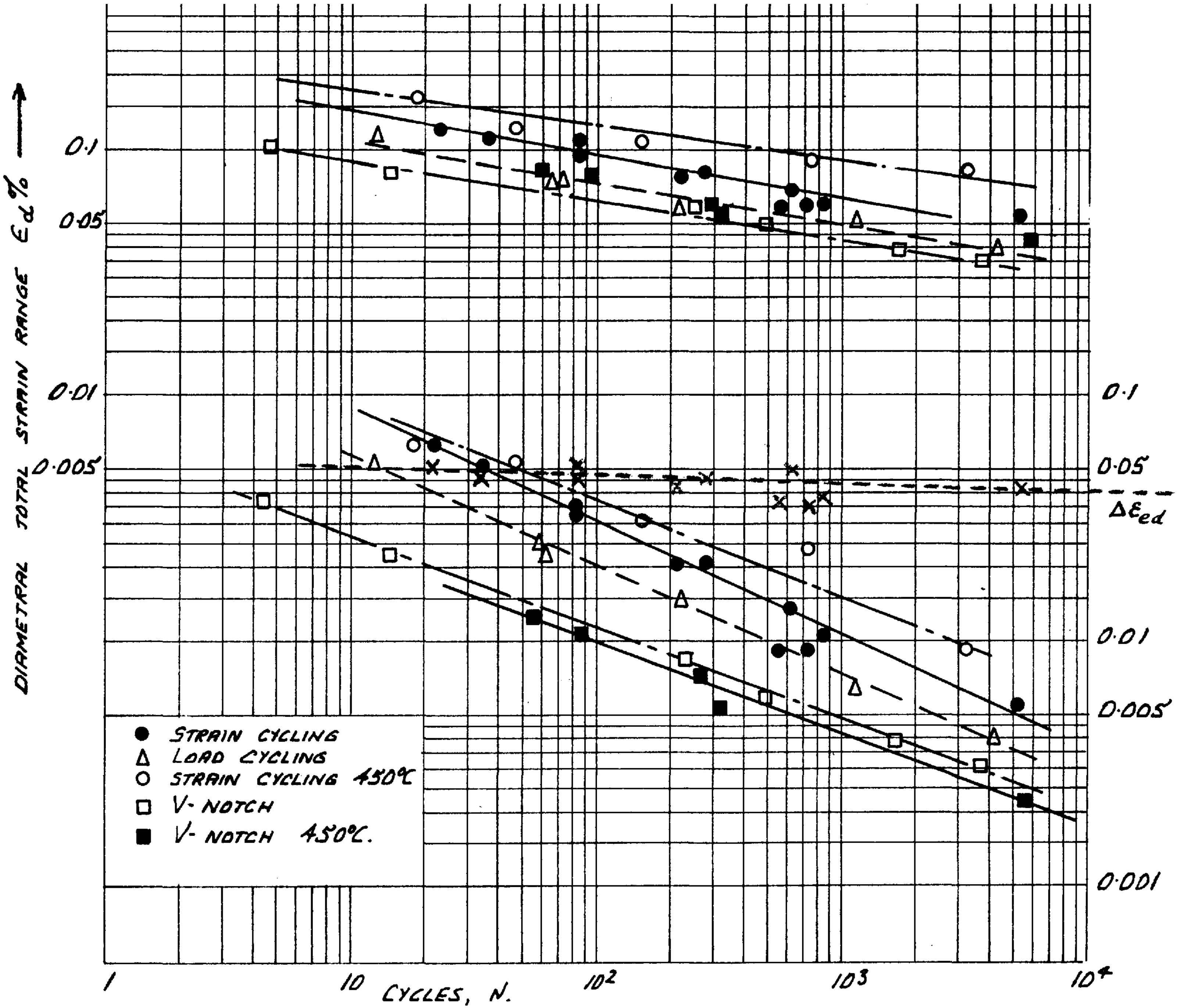

FIG. 99. STRAIN RANGE - CYCLE CURVES FOR CAST IRON B

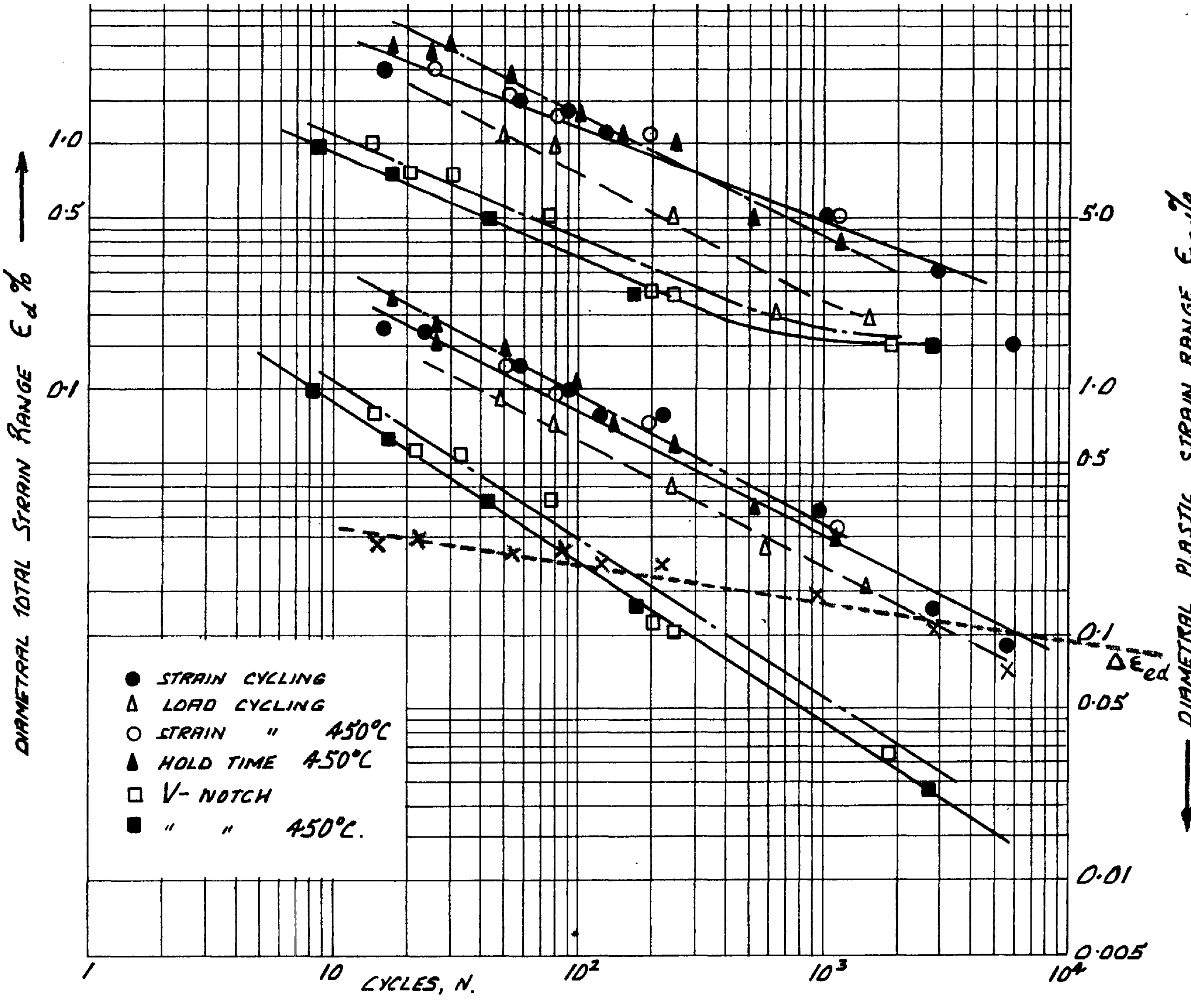

FIG. 100 STRAIN RANGE - CYCLE CURVES FOR CAST STEEL "C"

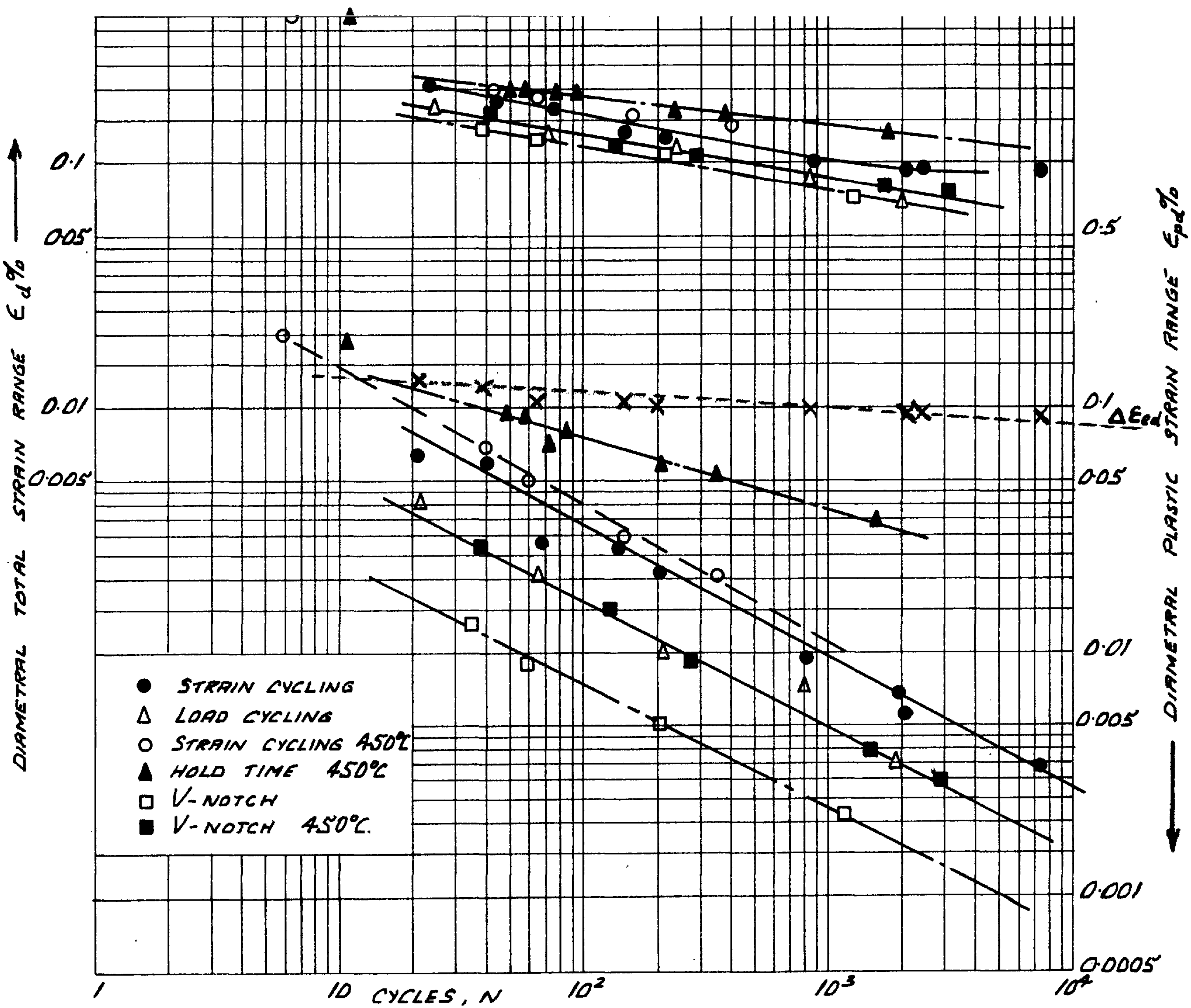

FIG. 101 STRAIN RANGE - CYCLE CURVES FOR CAST IRON E

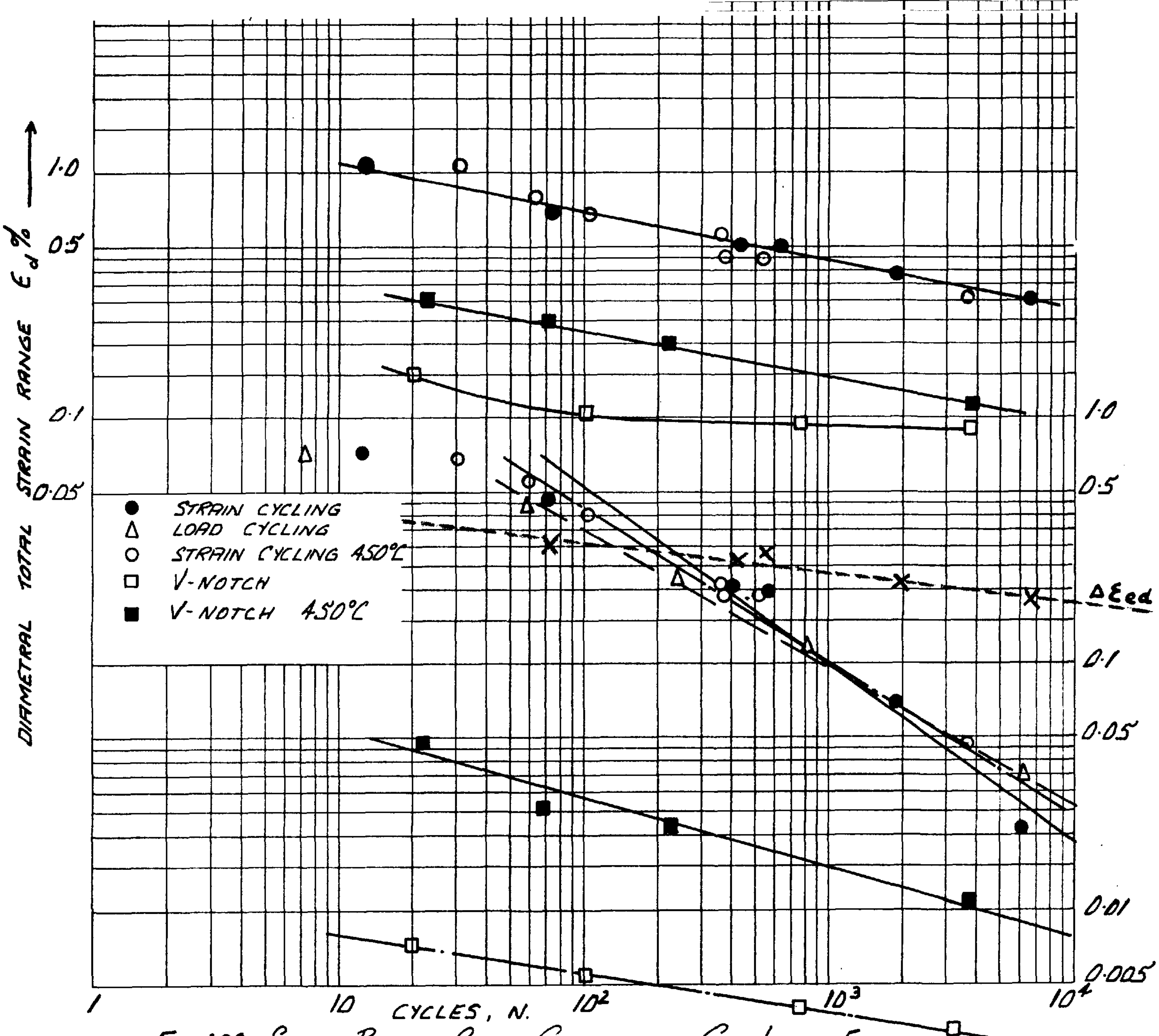

FIG. 102 STRAIN RANGE-CYCLE CURVES FOR CAST IRON F

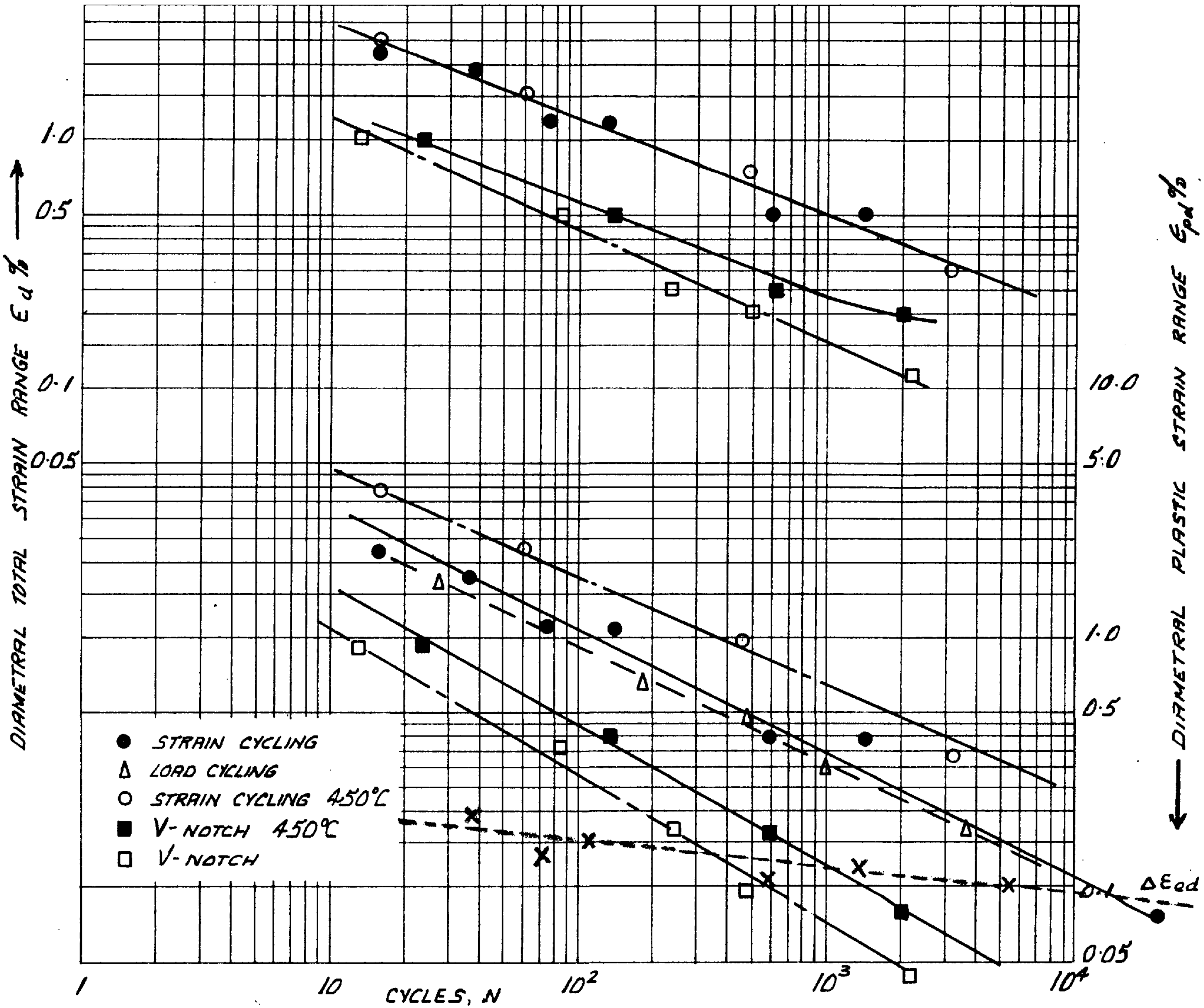

FIG. 103 STRAIN RANGE- CYCLE CURVES FOR CAST STEEL S.

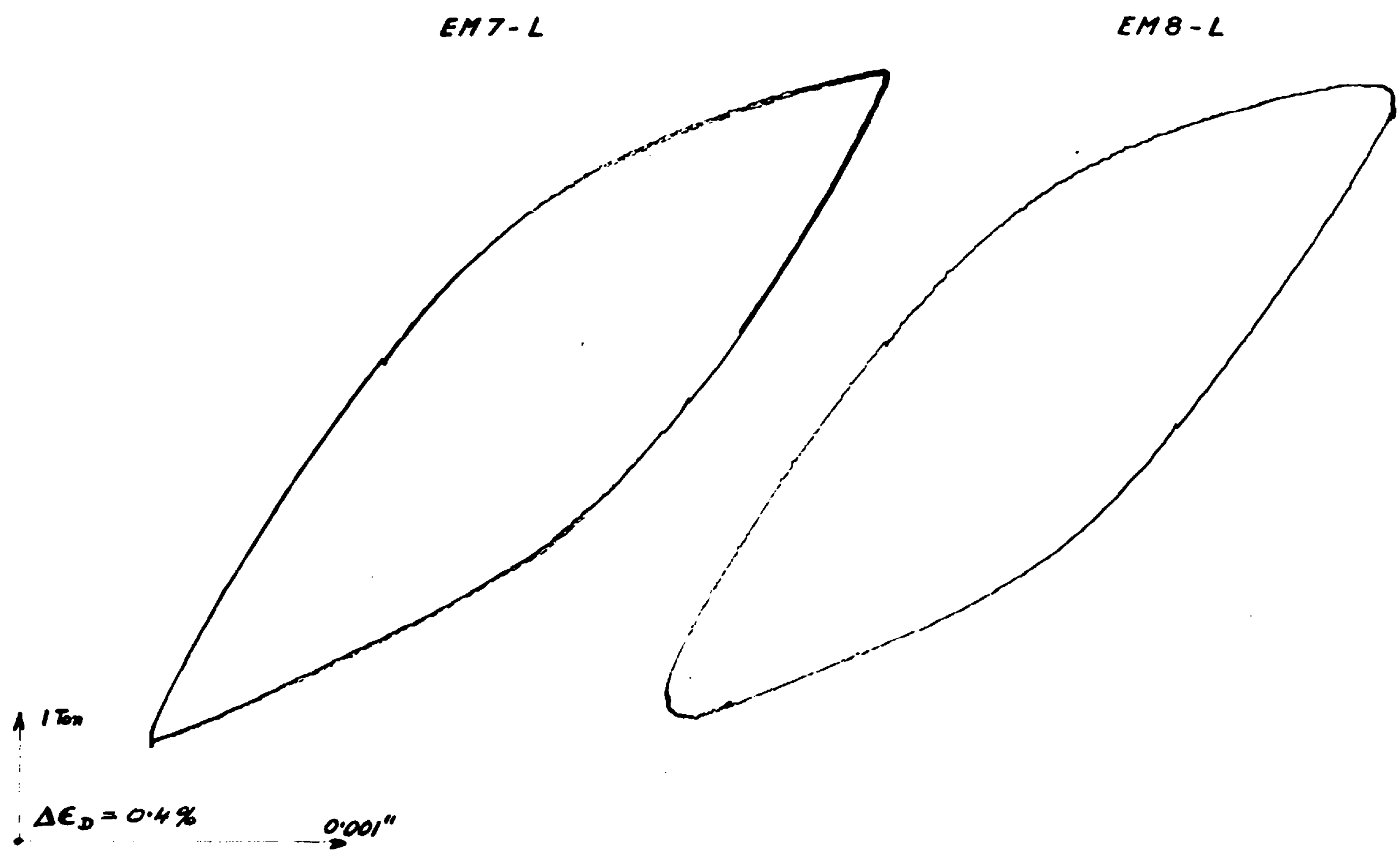

a)
7042
CYCLE No. 3. (N=6)

b)
7028
CYCLE No.3. (N = 11)

Fig. 104. Strain cycling at 450°C of cast iron E. a) without hold time
b) with 5 min. hold time.

2C14-L

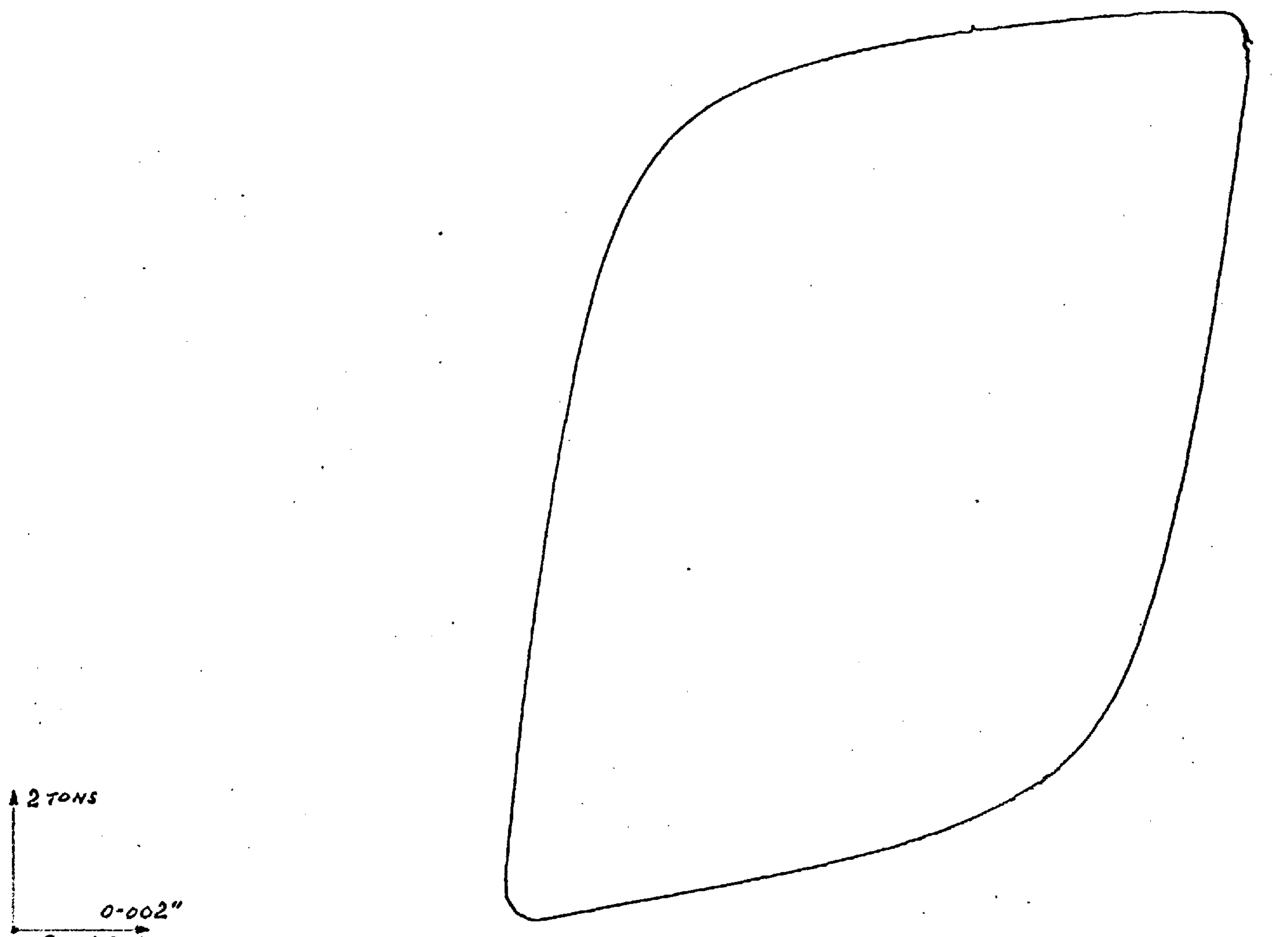

$\Delta\varepsilon_D = 1{\cdot}8\,\%$

658

Cycle no. 43 (N=51)

Fig. 105. Cast steel C. Strain cycling at 450°C with 5 min. hold time.

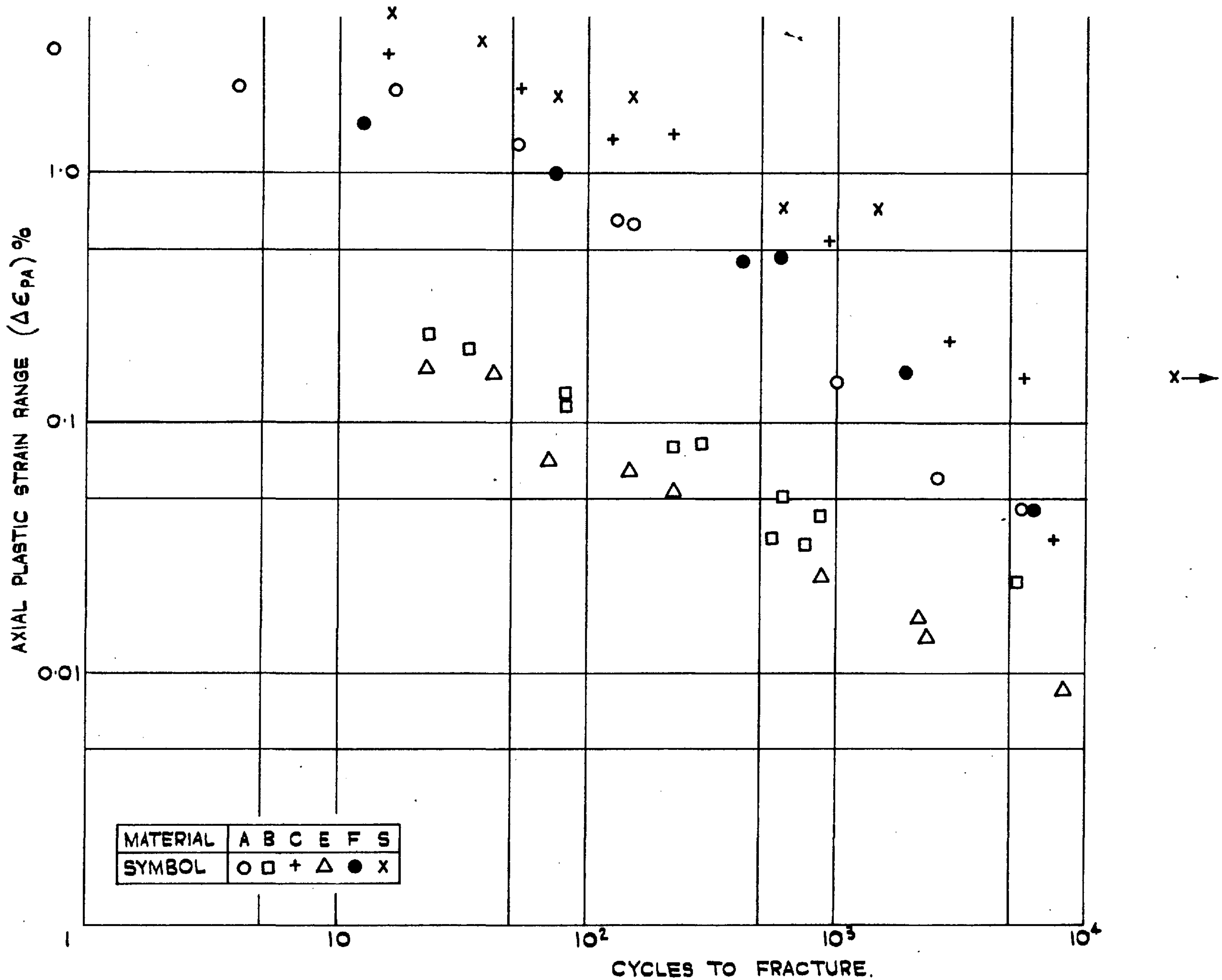

Fig. 106 Strain cycling of plain specimens at room temperature.

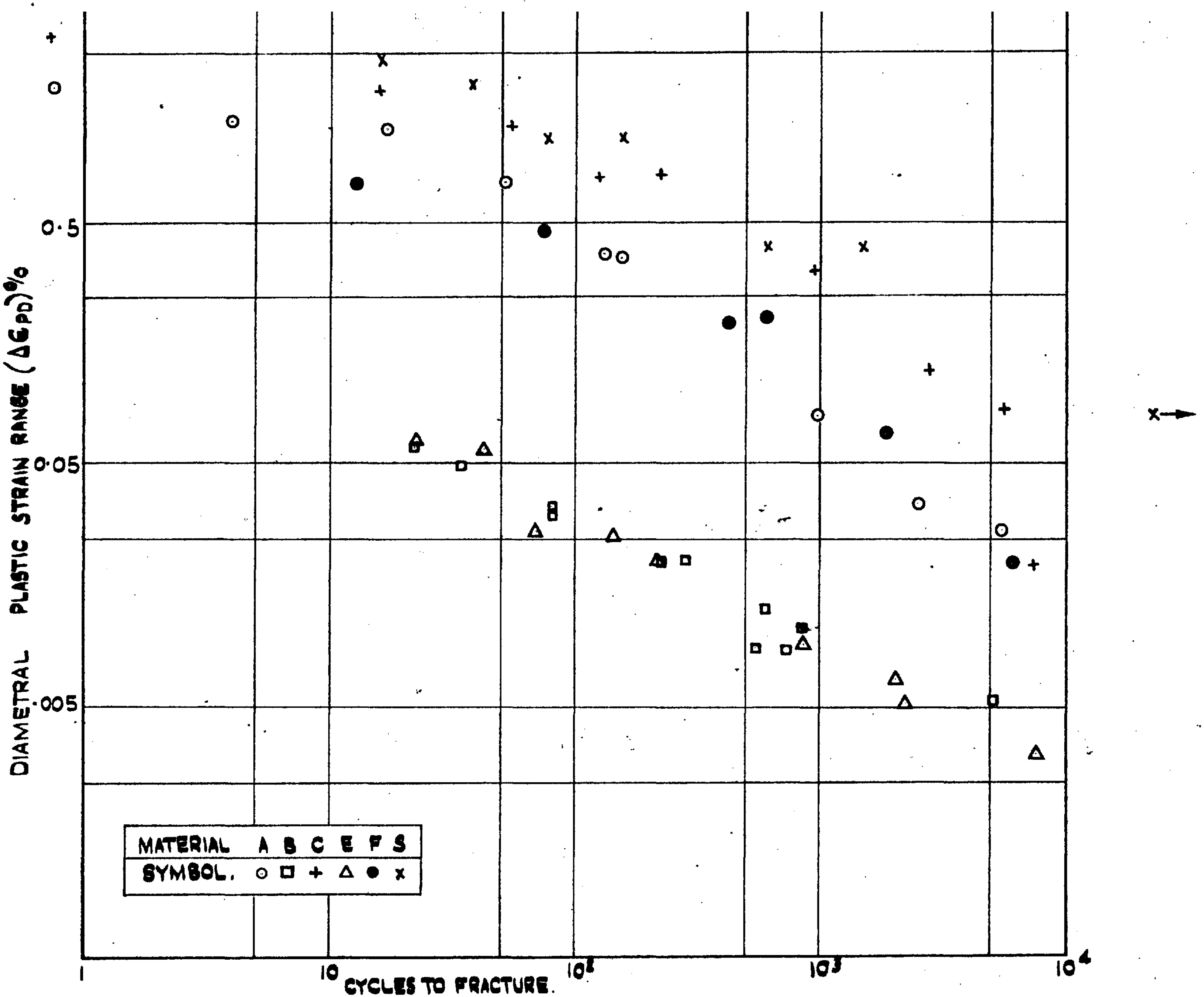

FIG.107 STRAIN CYCLING OF PLAIN SPECIMENS AT ROOM TEMPERATURE.

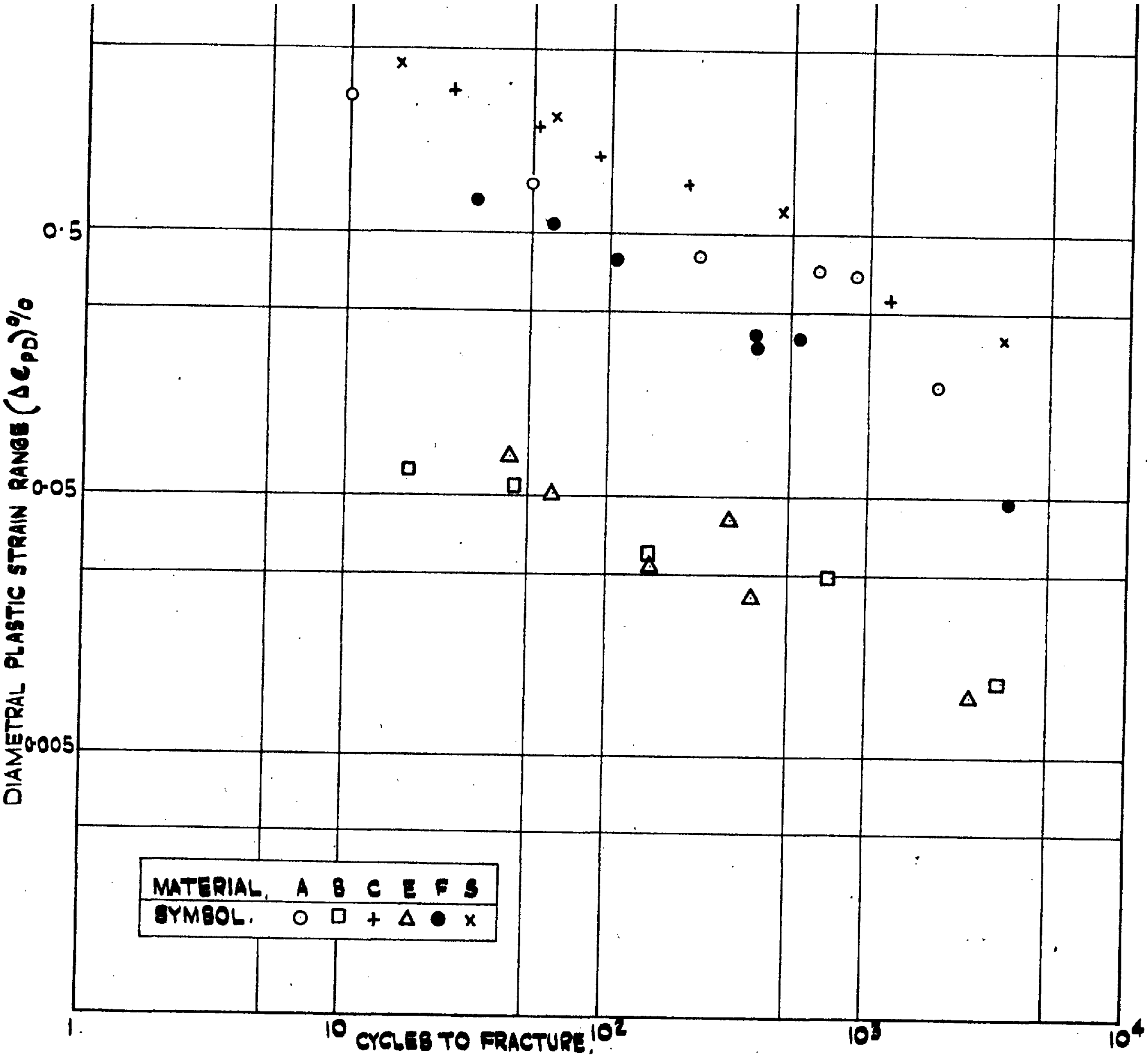

FIG. 108. STRAIN CYCLING OF PLAIN SPECIMENS AT HIGH TEMPERATURE.

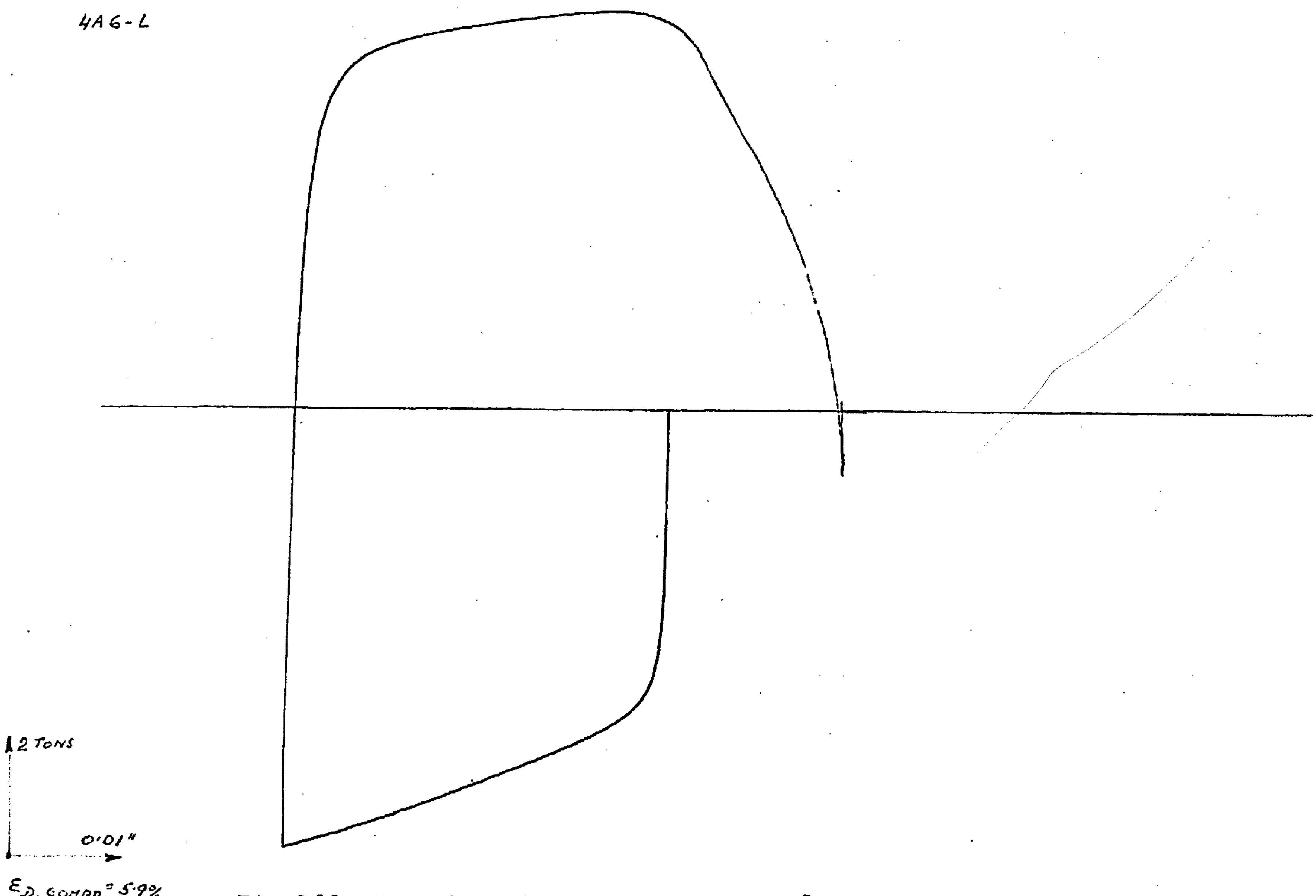

Fig.109. Cast iron A. Strain cycling, $\frac{3}{4}$-cycle test.

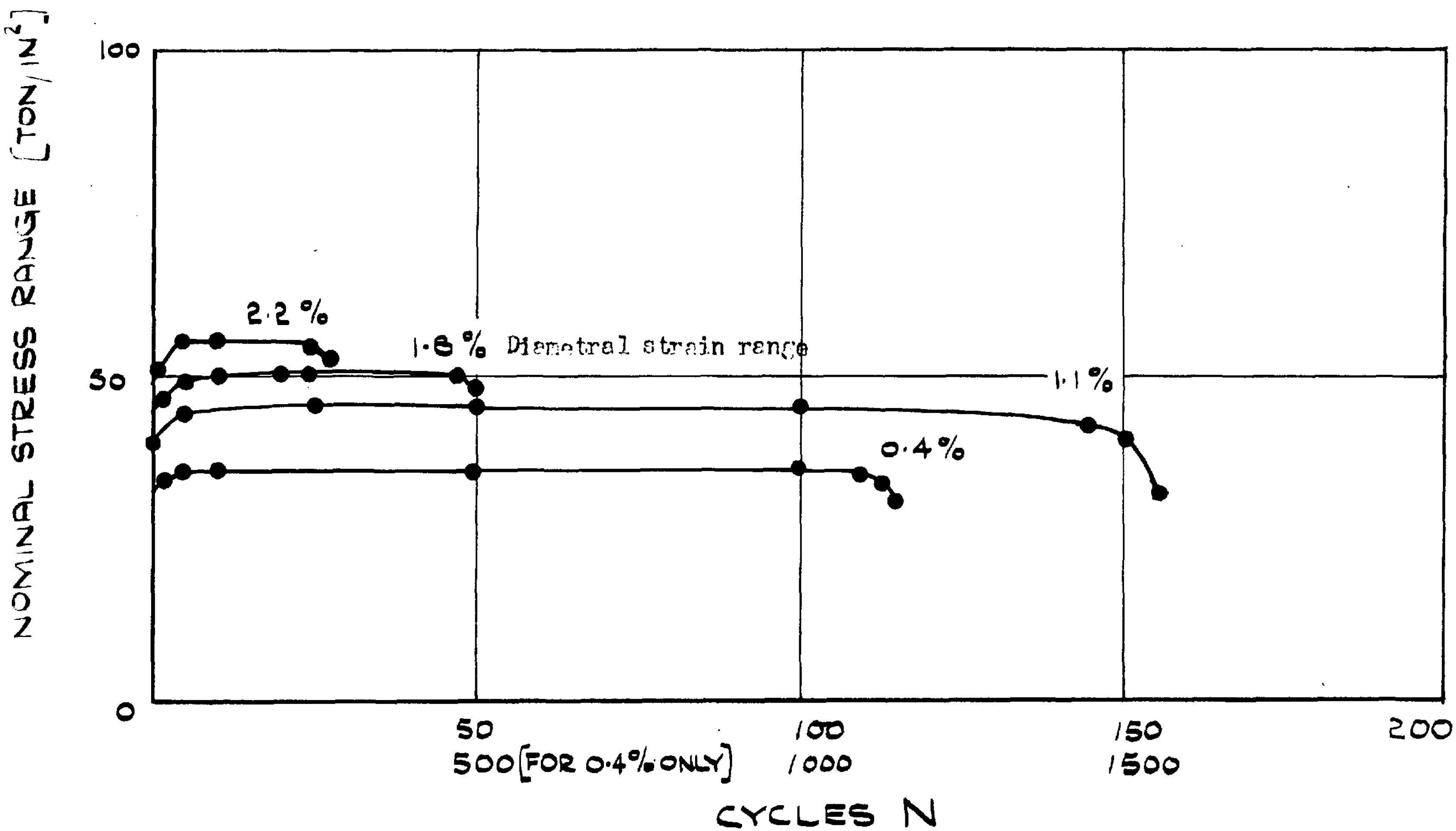

FIG.110. Variation of stress range at hold time of cast steel C

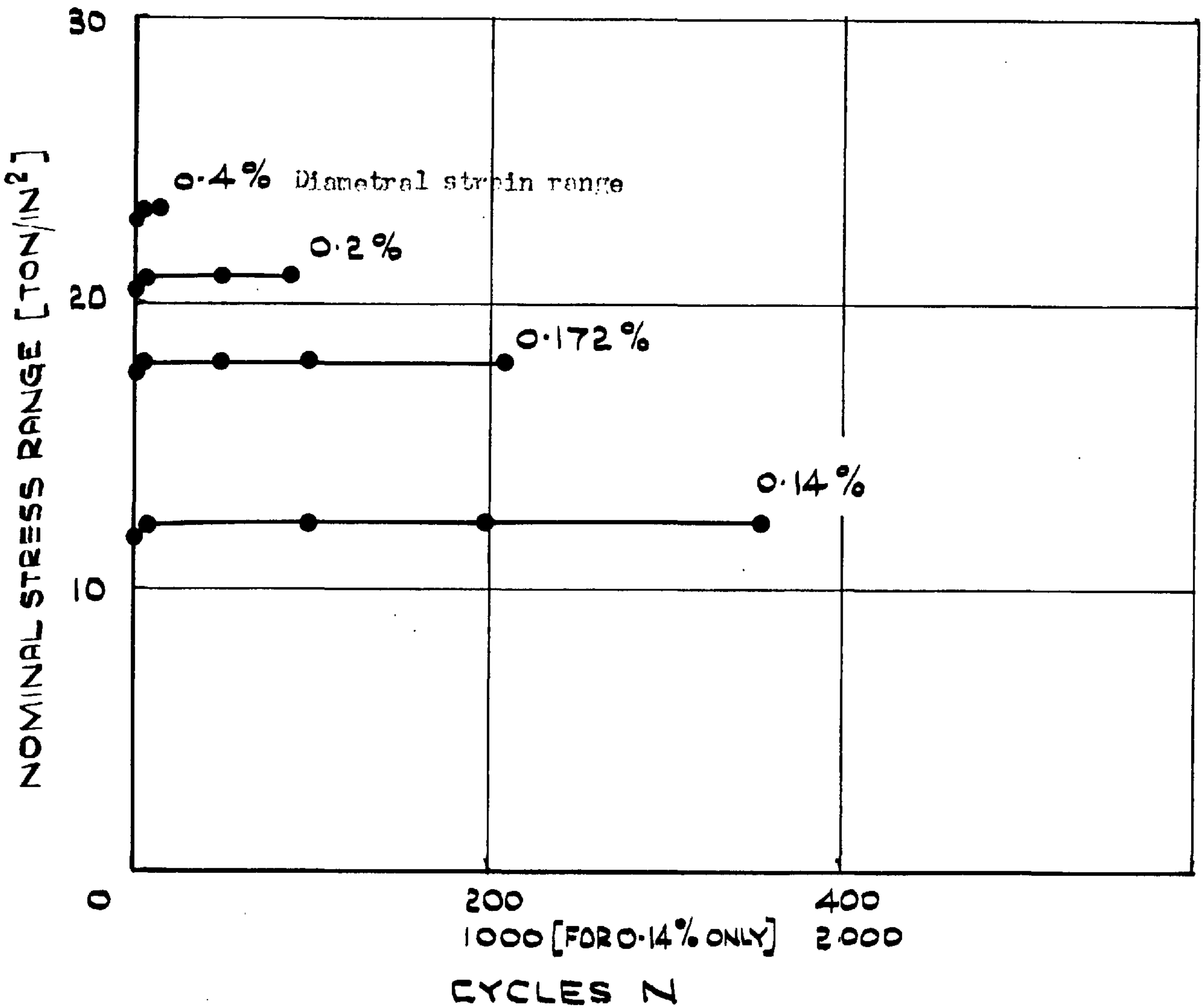

FIG.111. Variation of stress range at hold time of cast iron E

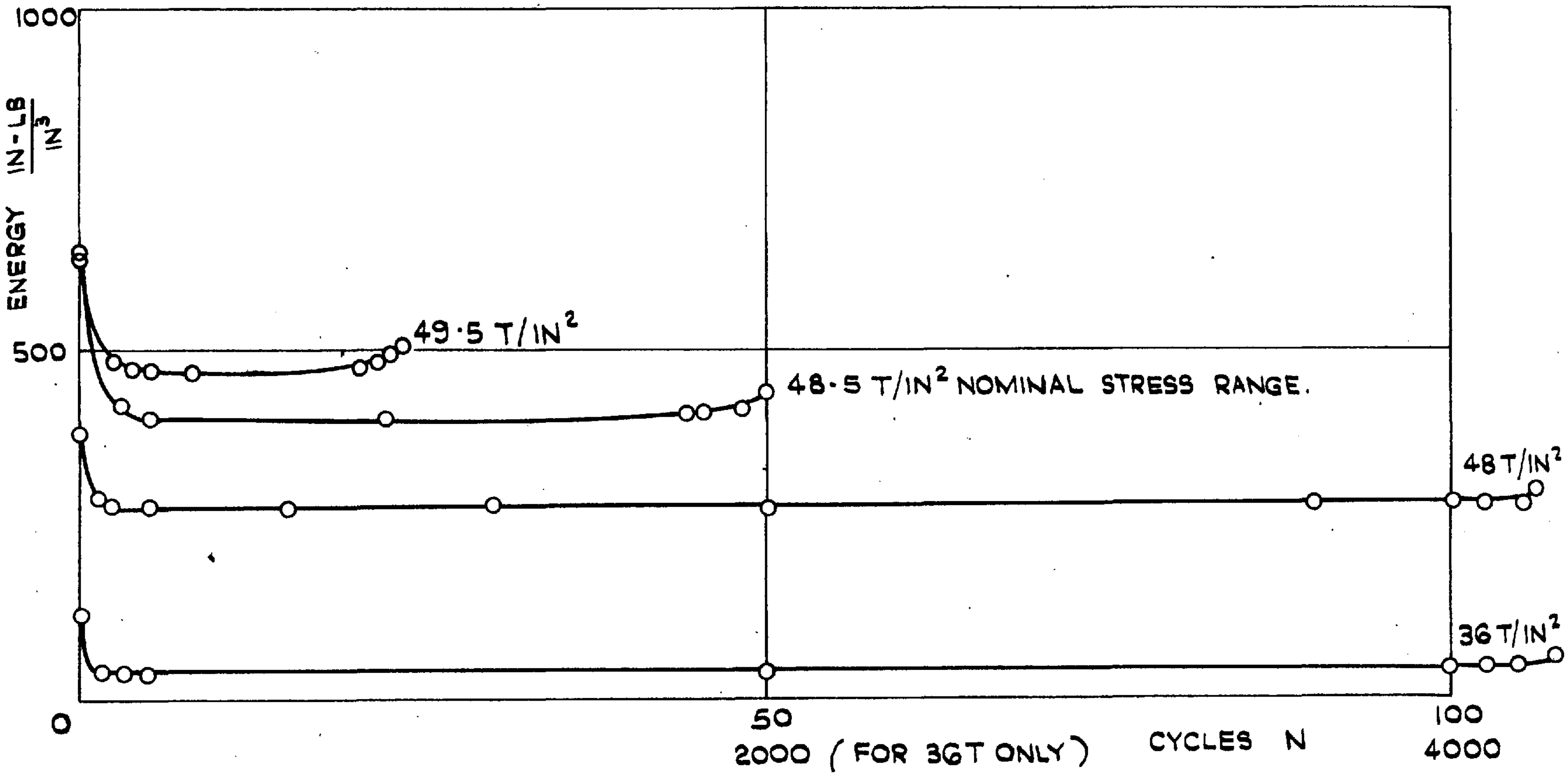

FIG.112. Variation of energy during load cycling of cast iron A

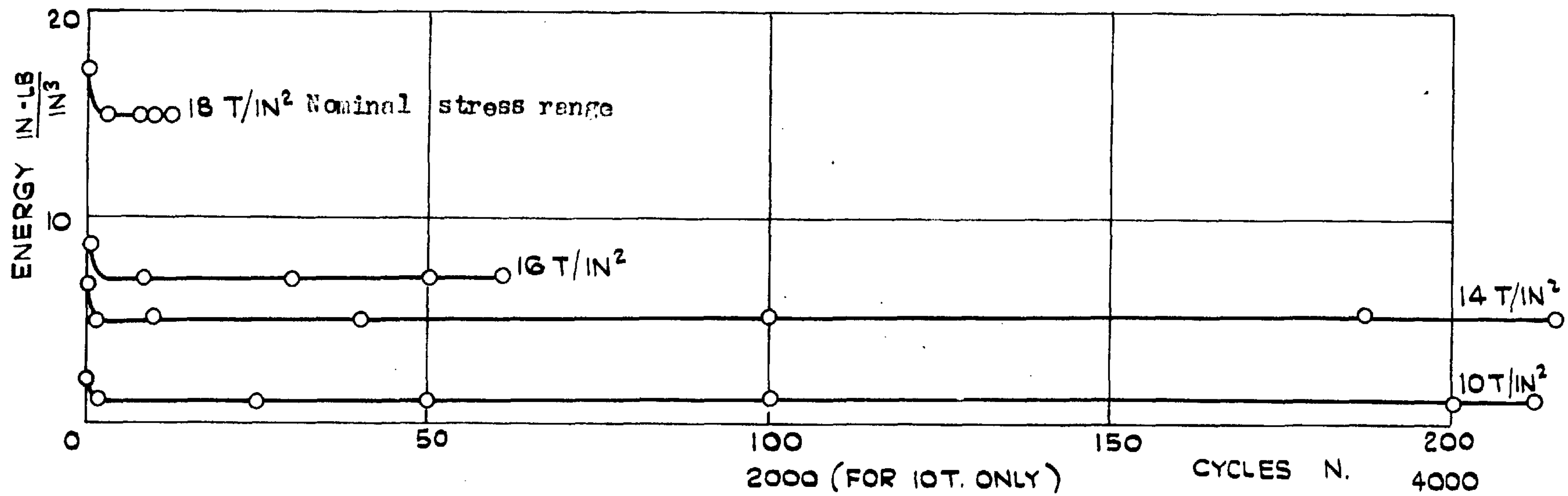

FIG.113. Variation of energy during load cycling of cast iron B

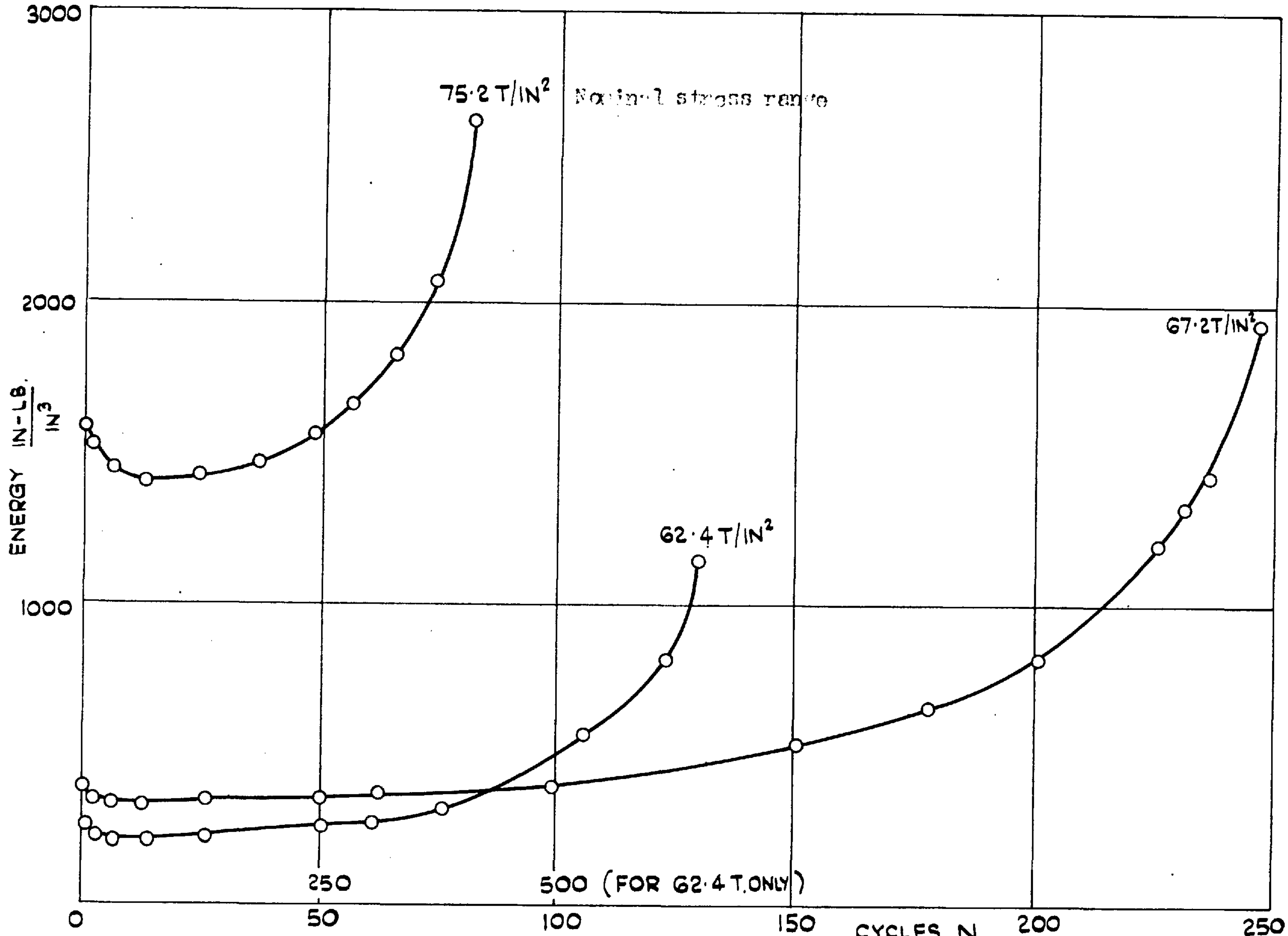

FIG. 114. Variation of energy during load cycling of cast steel C

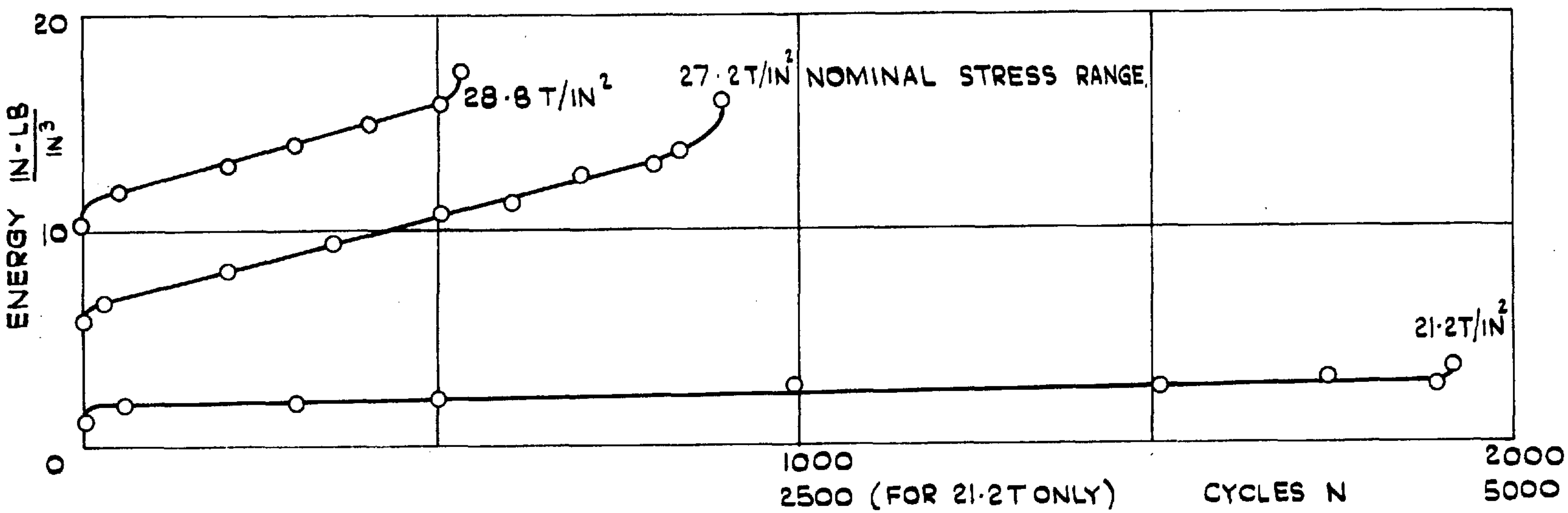

FIG.115. Variation of energy during load cycling of cast iron E

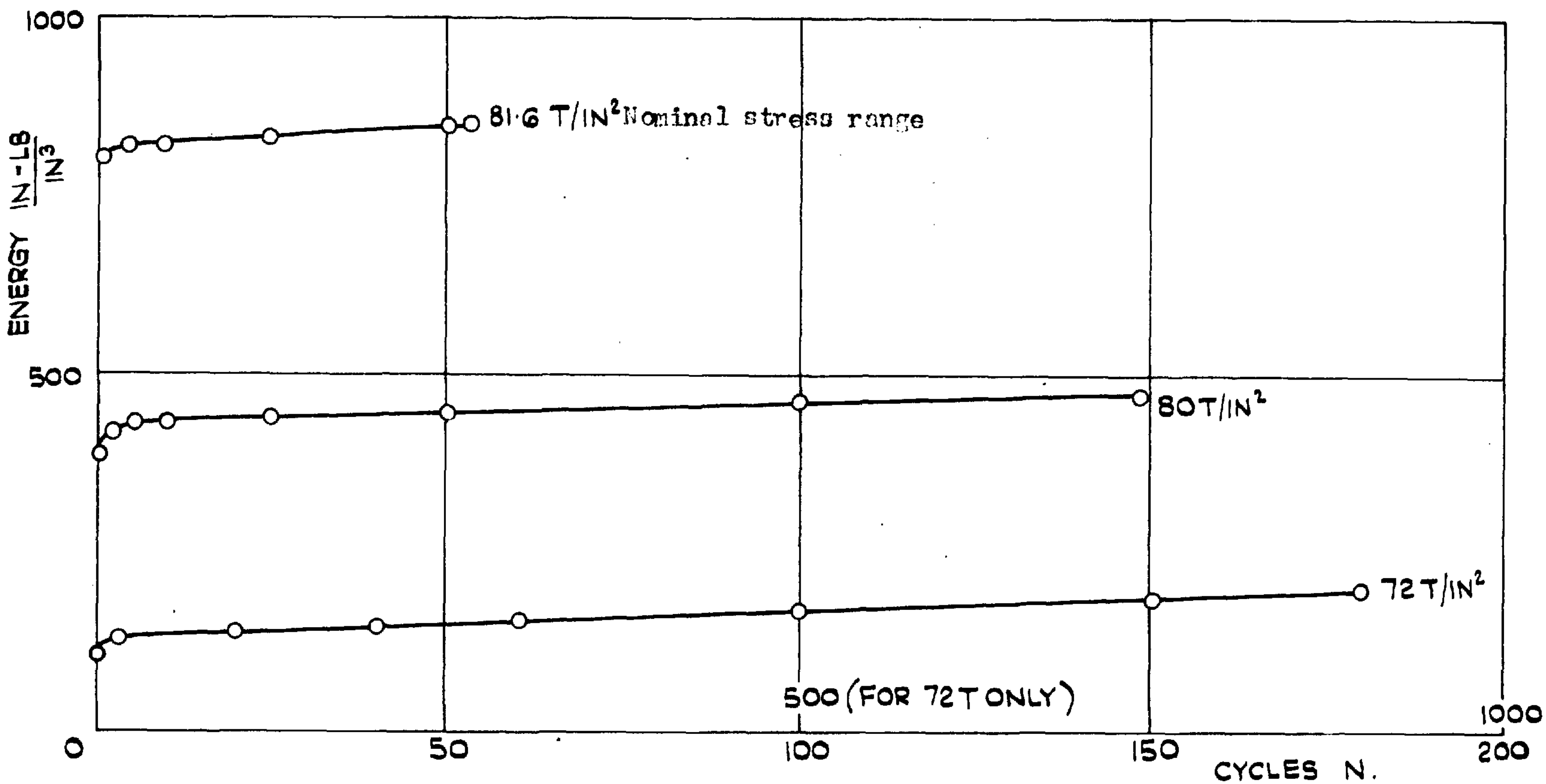

FIG.116. Variation of energy during load cycling of cast iron F

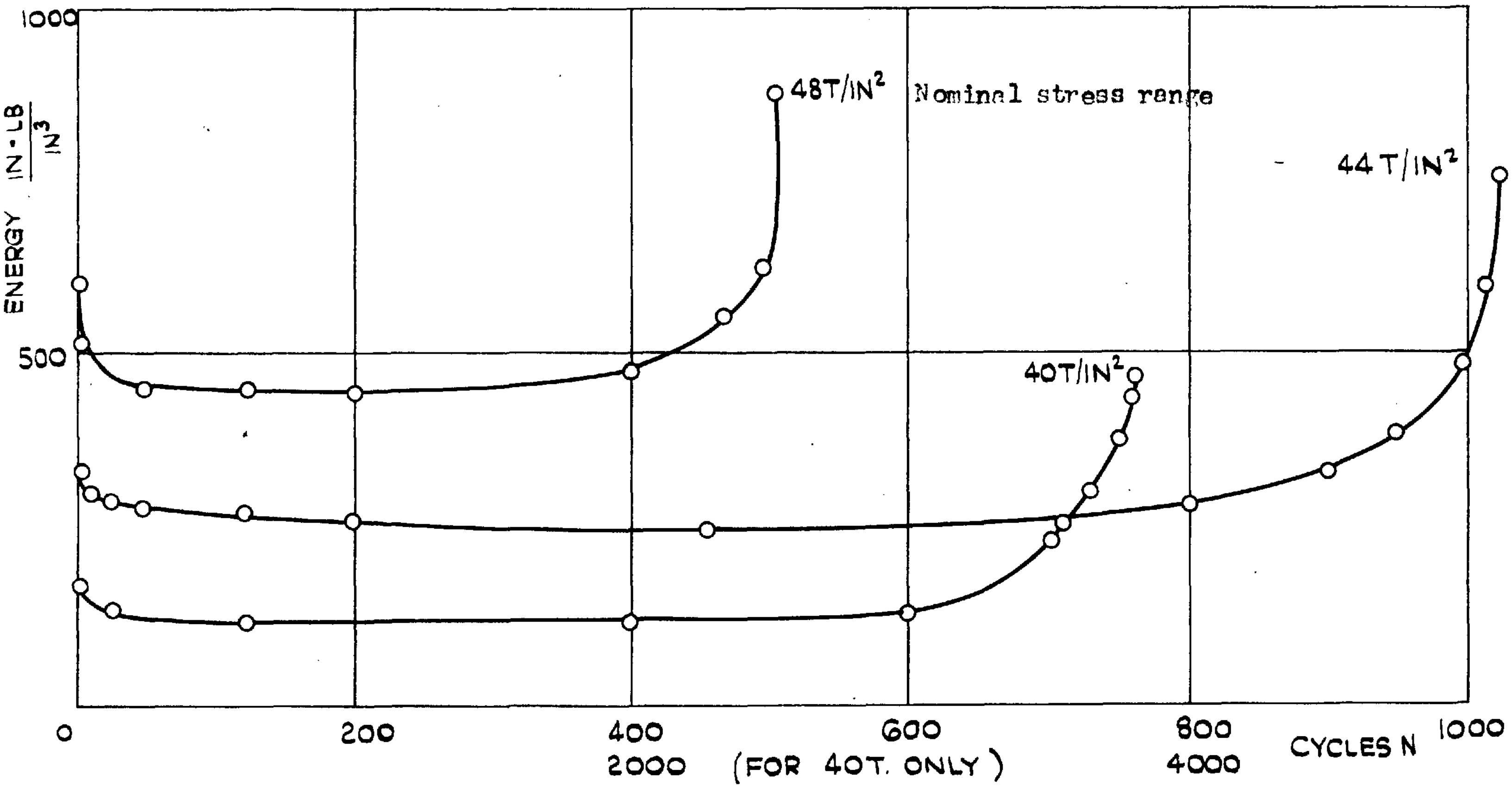

FIG.117. Variation of energy during load cycling of cast steel S

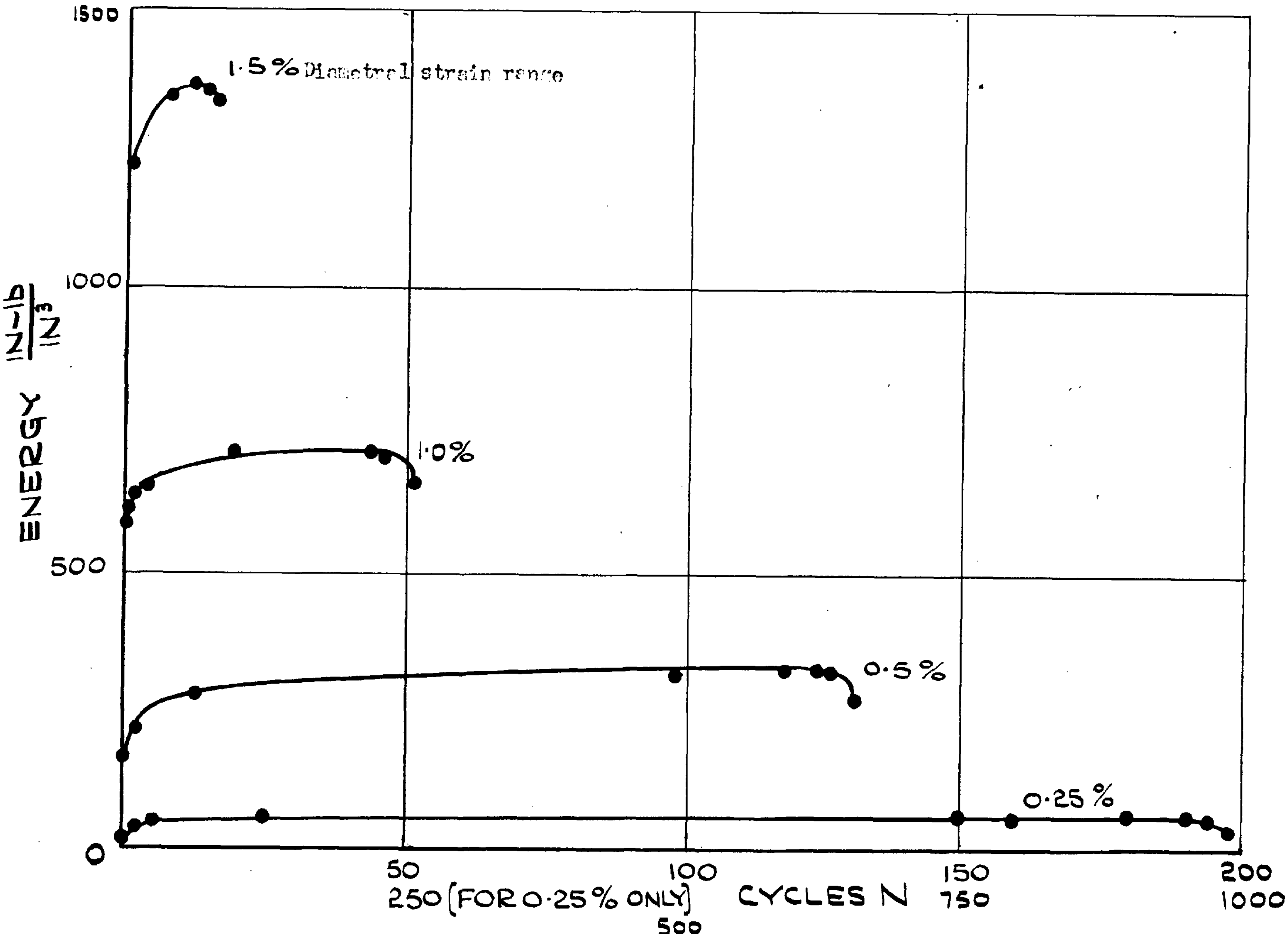

FIG.118. Variation of energy during strain cycling at room temperature of cast iron A

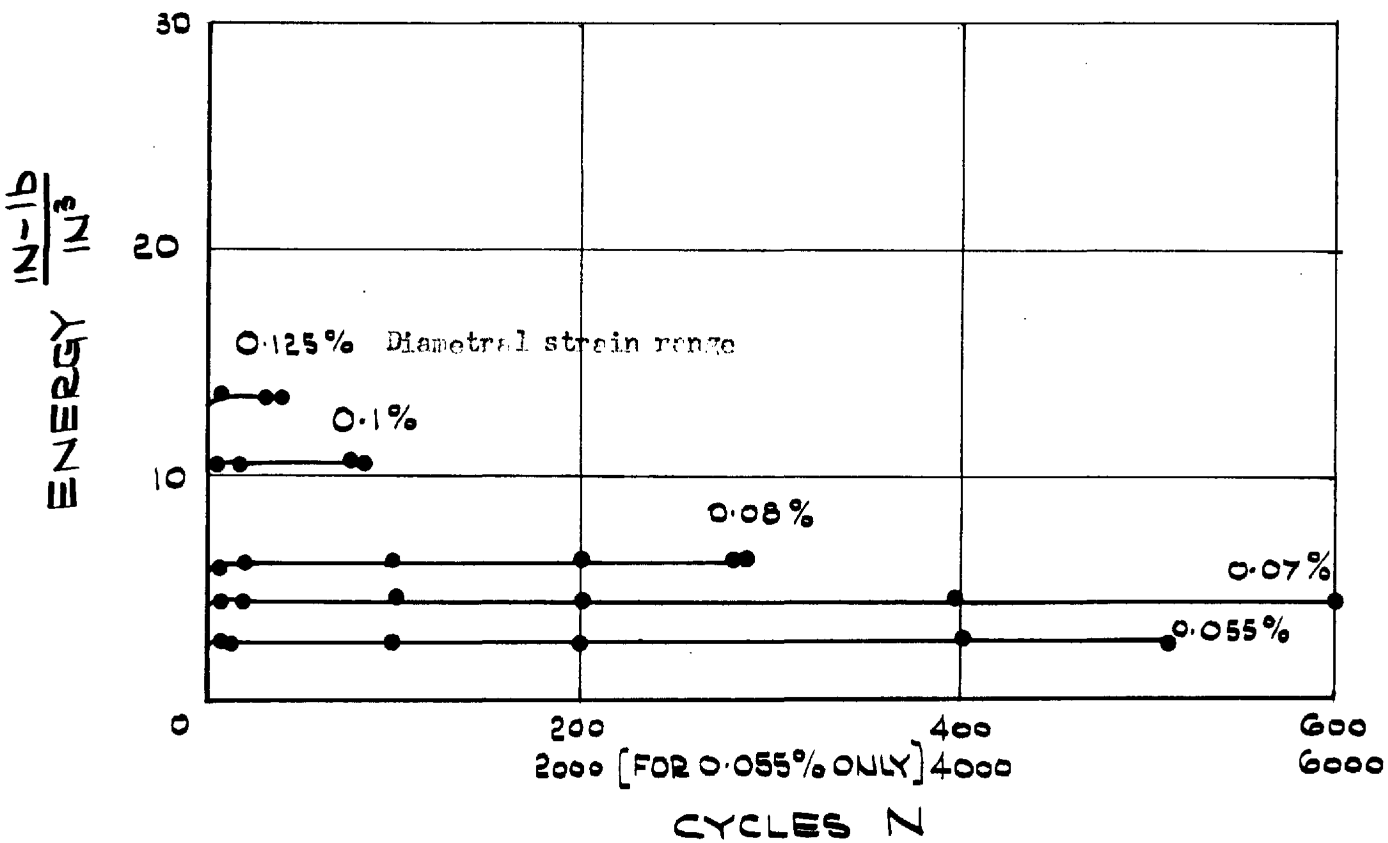

FIG.119. Variation of energy during strain cycling at room temperature of cast iron B

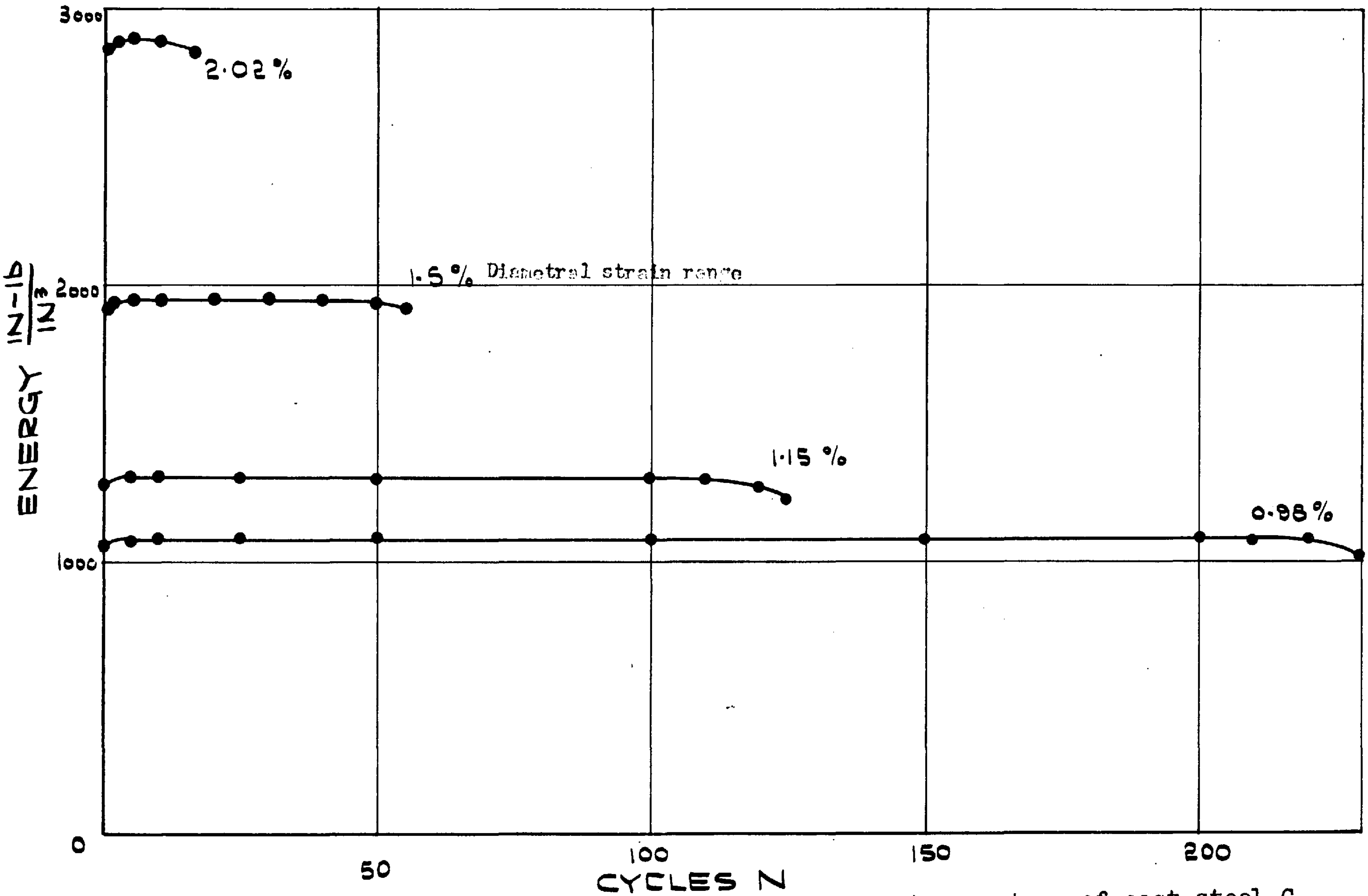

FIG. 120. Variation of energy during strain cycling at room temperature of cast steel C

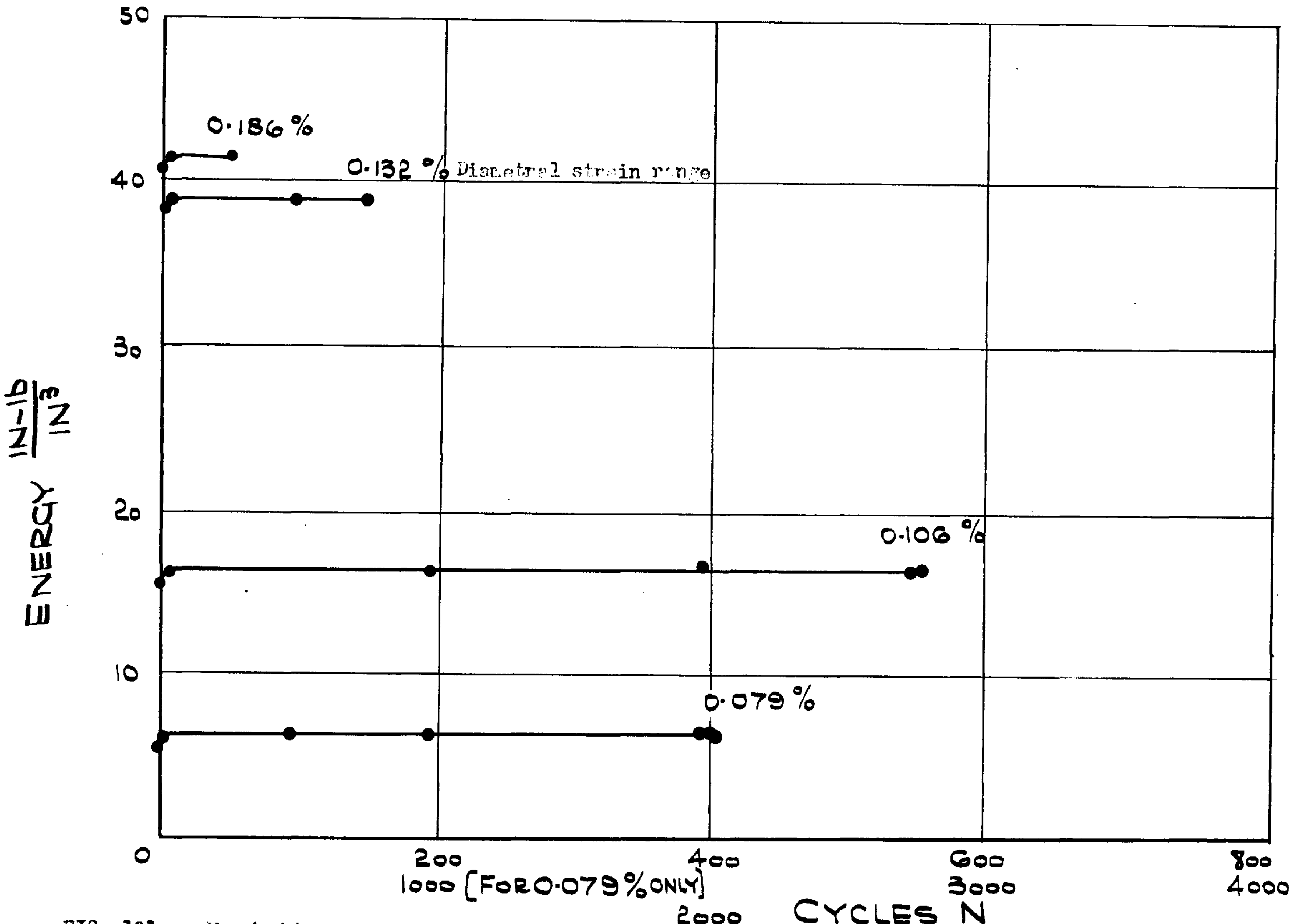

FIG. 121. Variation of energy during strain cycling at room temperature of cast iron E

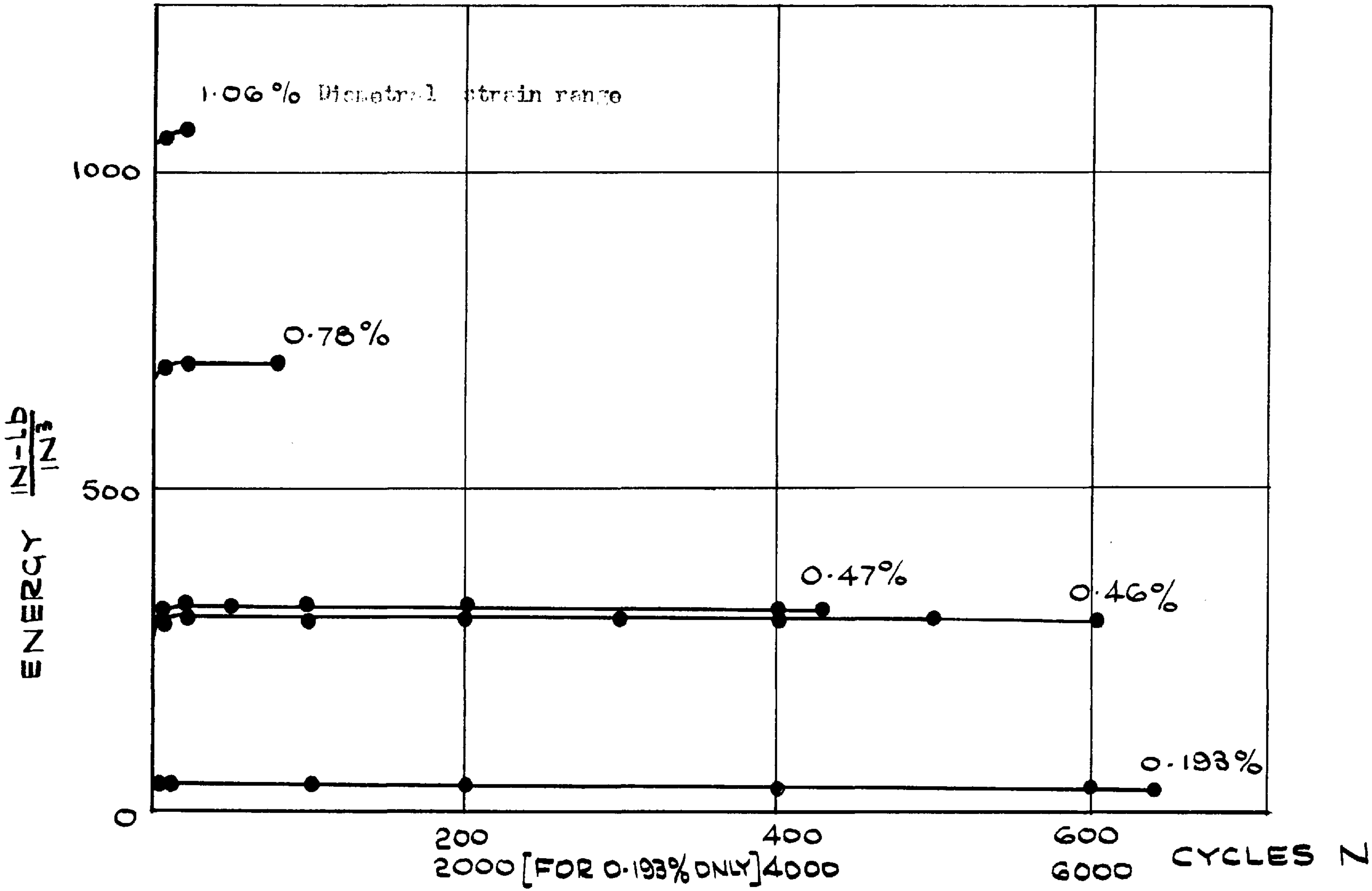

FIG. 122. Variation of energy during strain cycling at room temperature of cast iron F

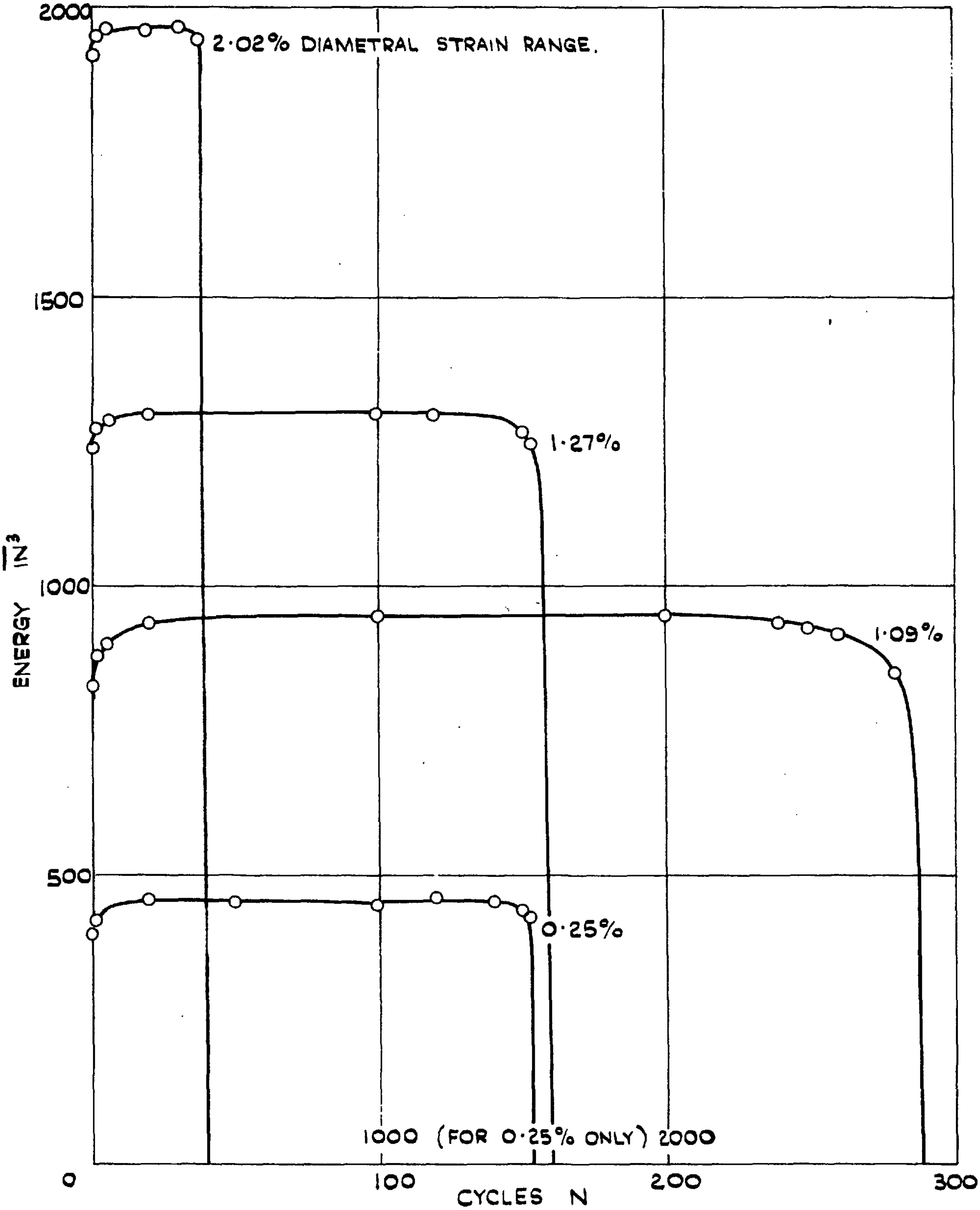

FIG.123. VARIATION OF ENERGY DURING STRAIN CYCLING OF CAST MILD STEEL S AT ROOM TEMP.

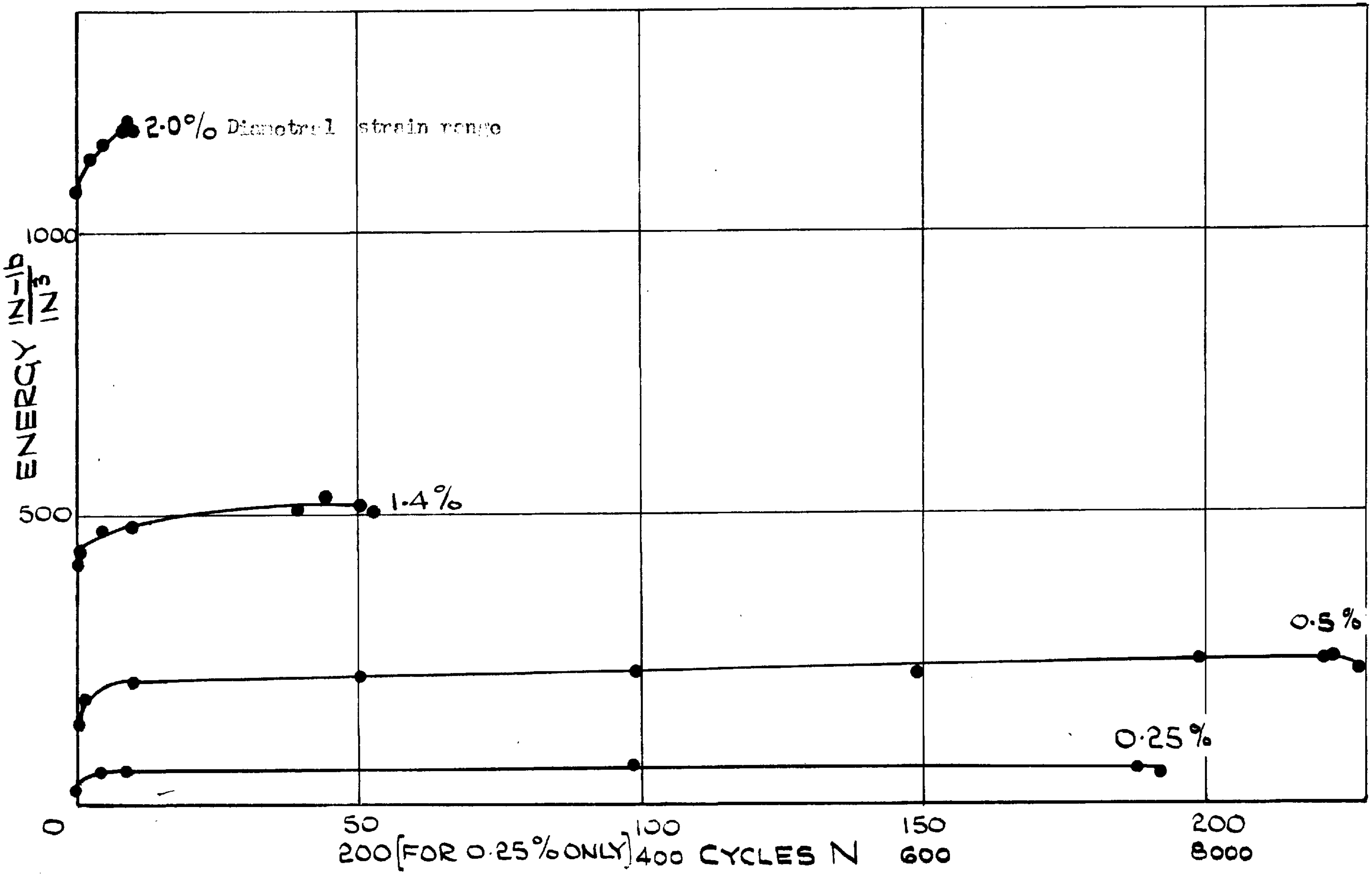

FIG.124. Variation of energy during strain cycling at 450° of cast iron A

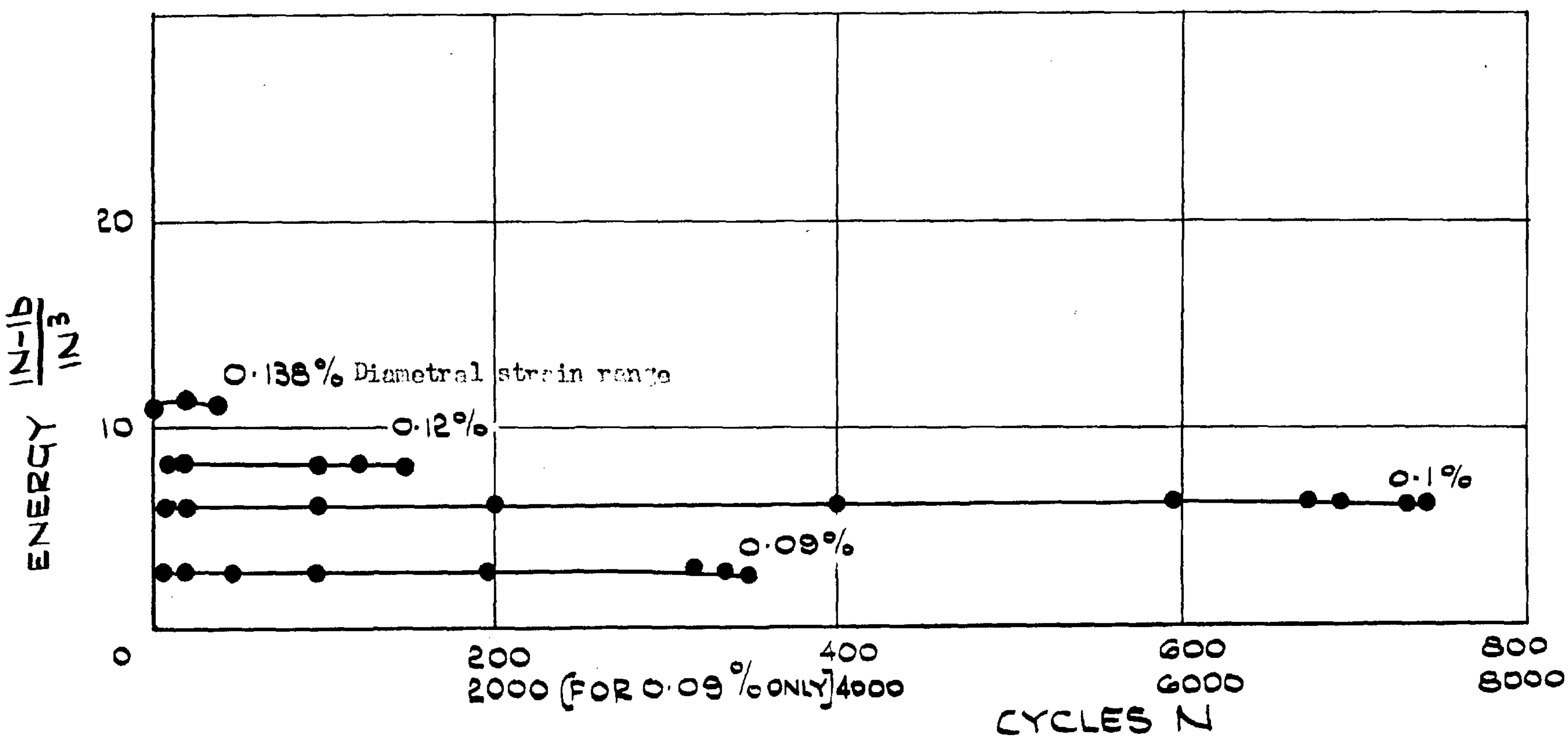

FIG.125. Variation of energy during strain cycling at 450° of cast iron B

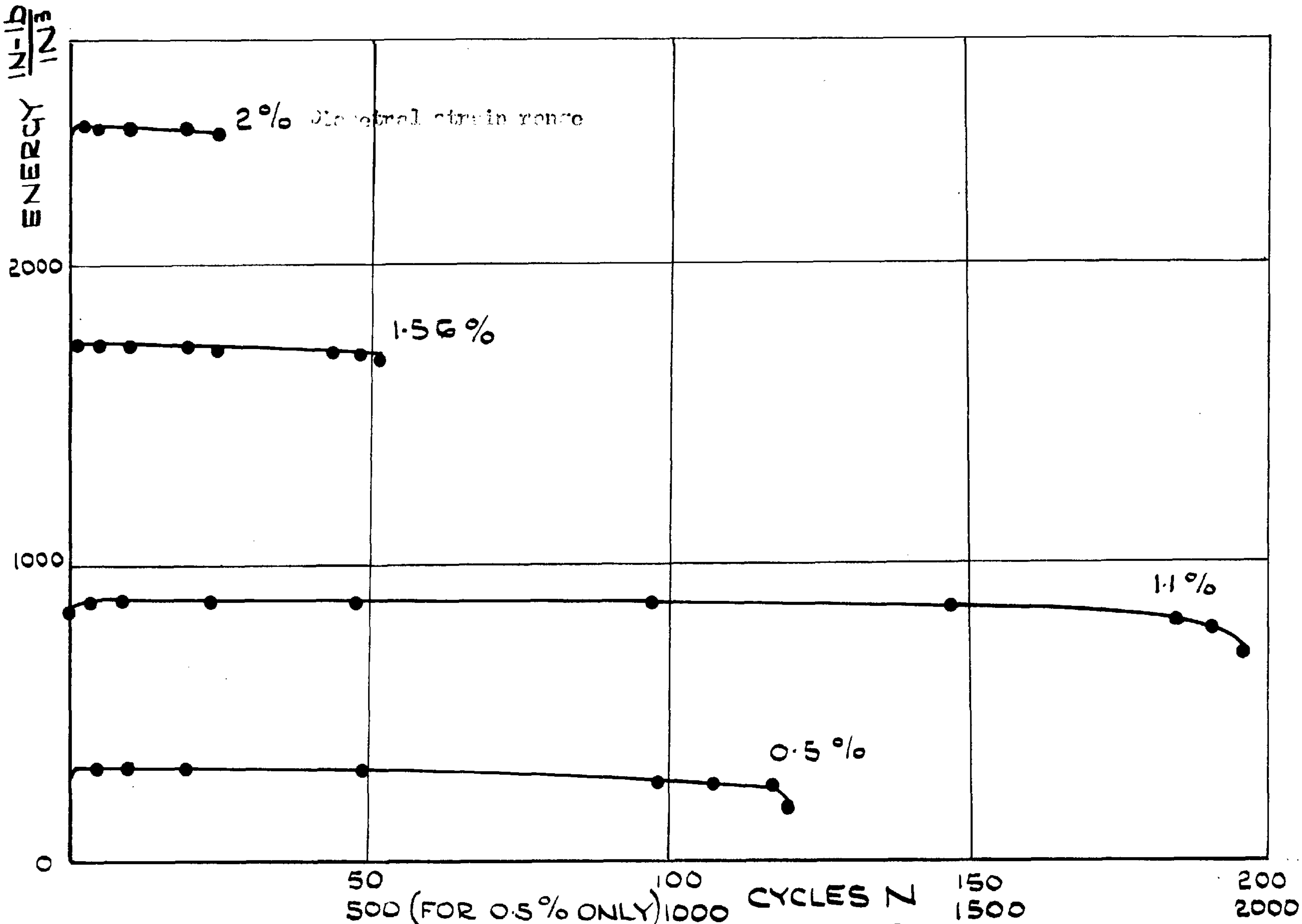

FIG.126. Variation of energy during strain cycling at 450° of cast steel C

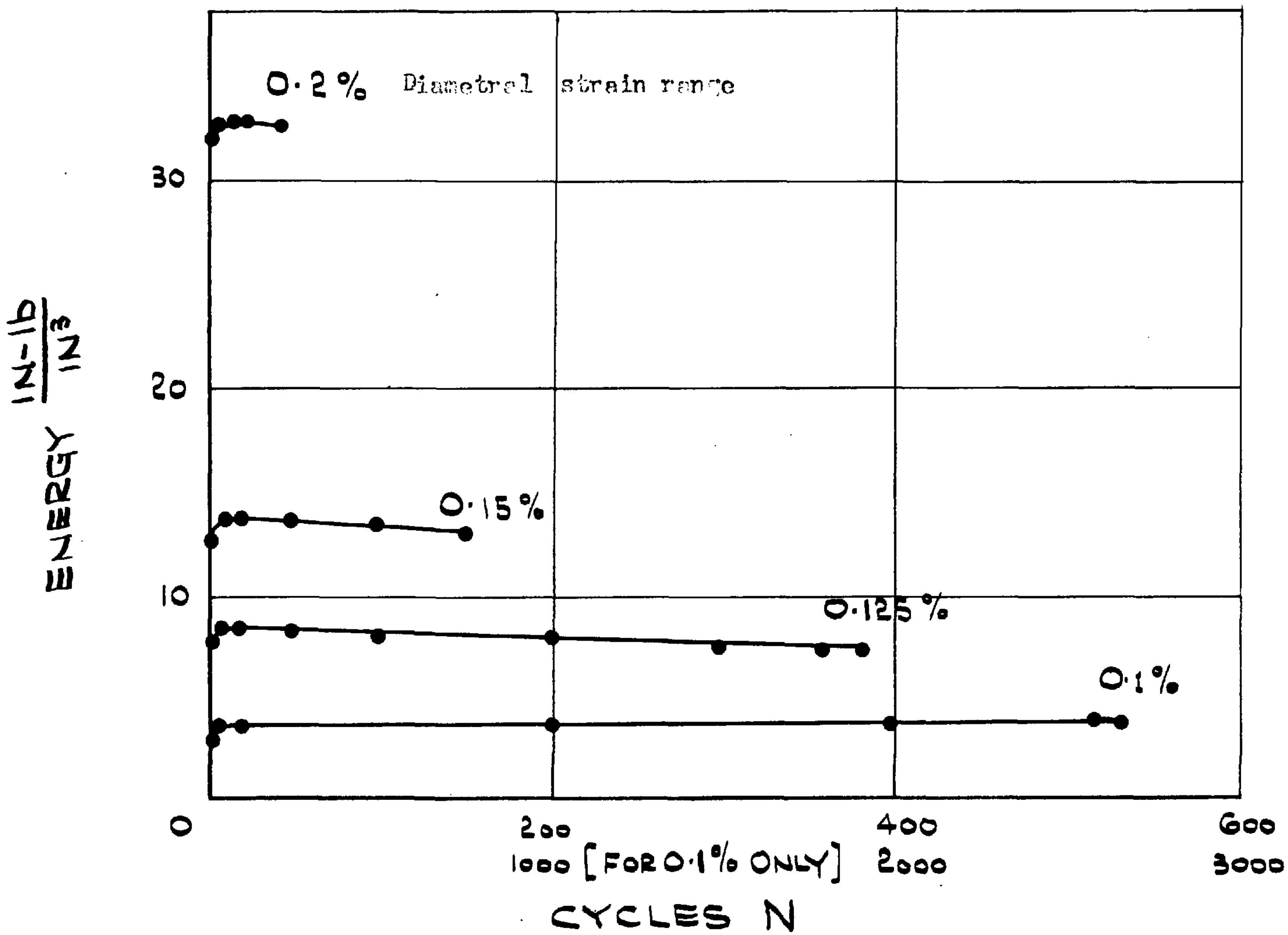

FIG.127. Variation of energy during strain cycling at 450° of cast iron E

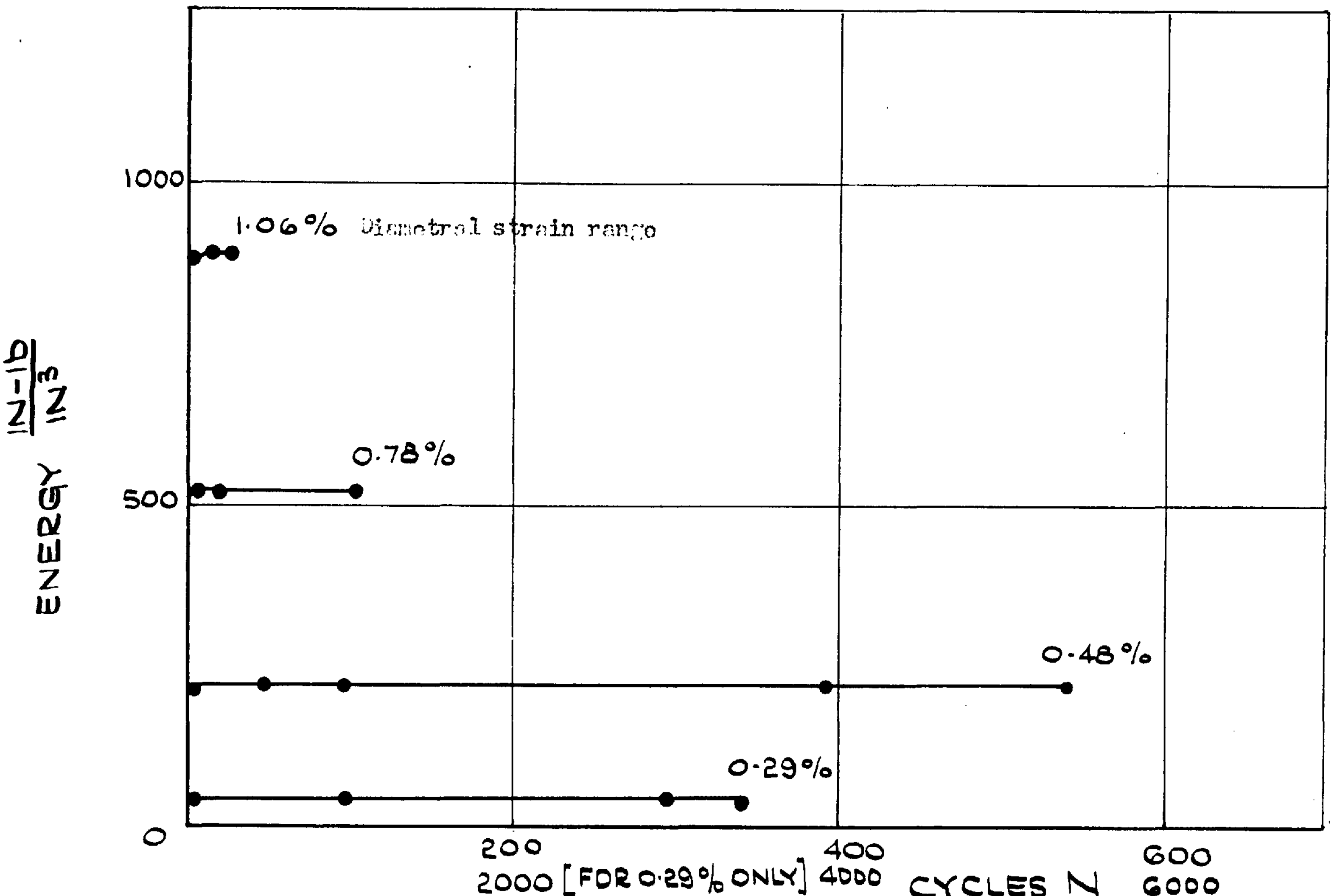

FIG.128. Variation of energy during strain cycling at 450° of cast iron F

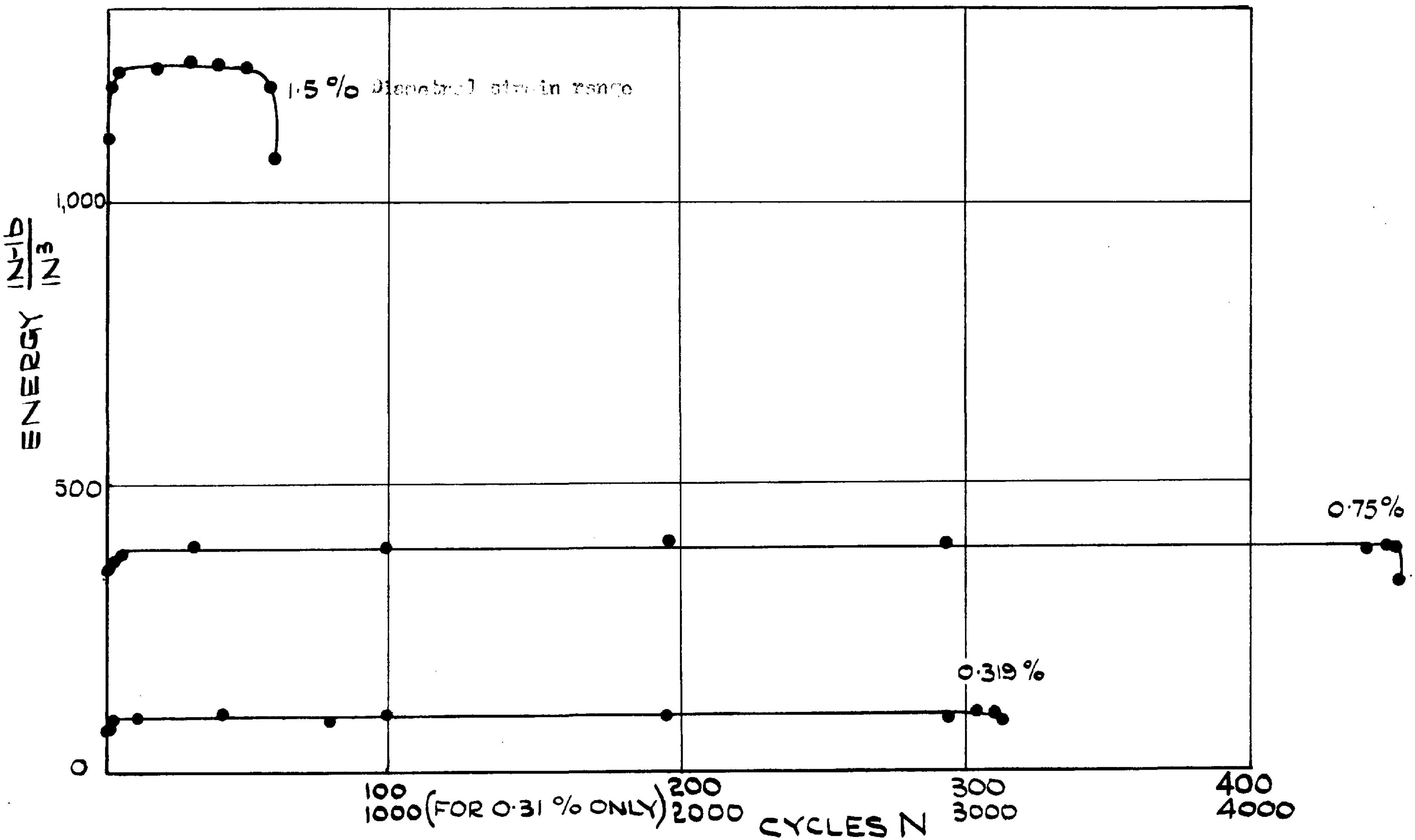

FIG.129. Variation of energy during strain cycling at 450°of cast steel S

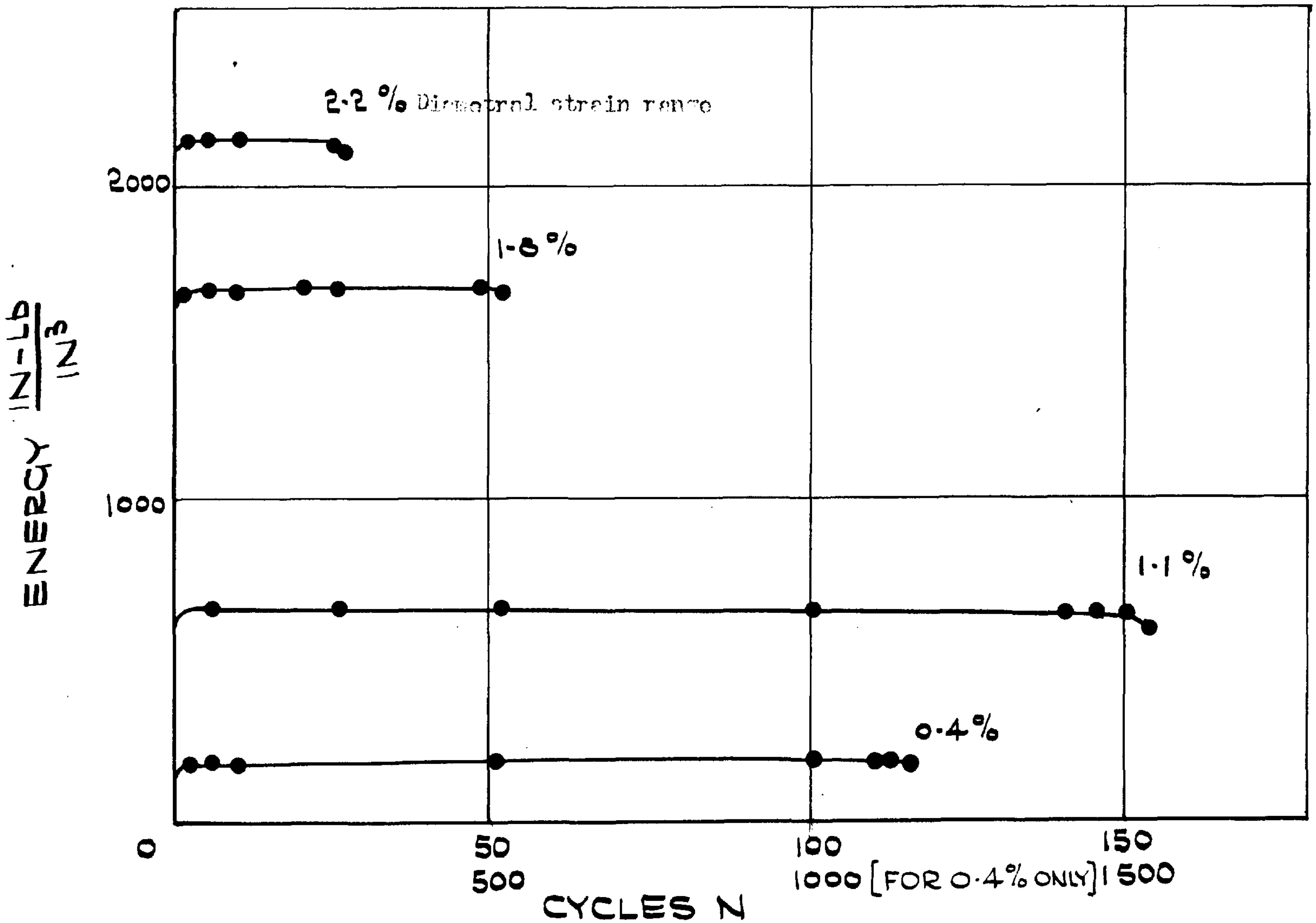

FIG.130. Variation of energy during hold time of cast steel C

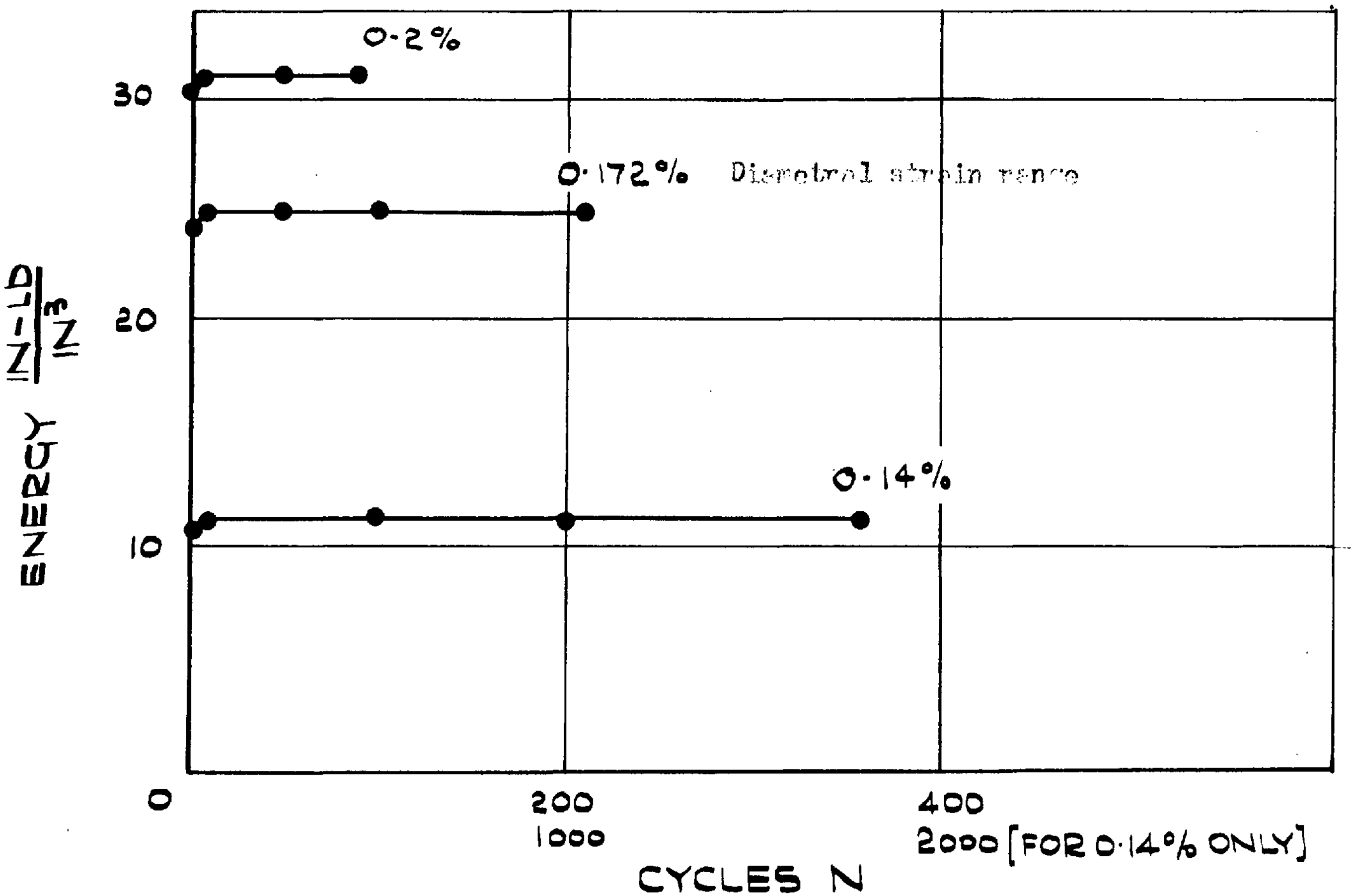

FIG.131. Variation of energy during hold time of cast iron E

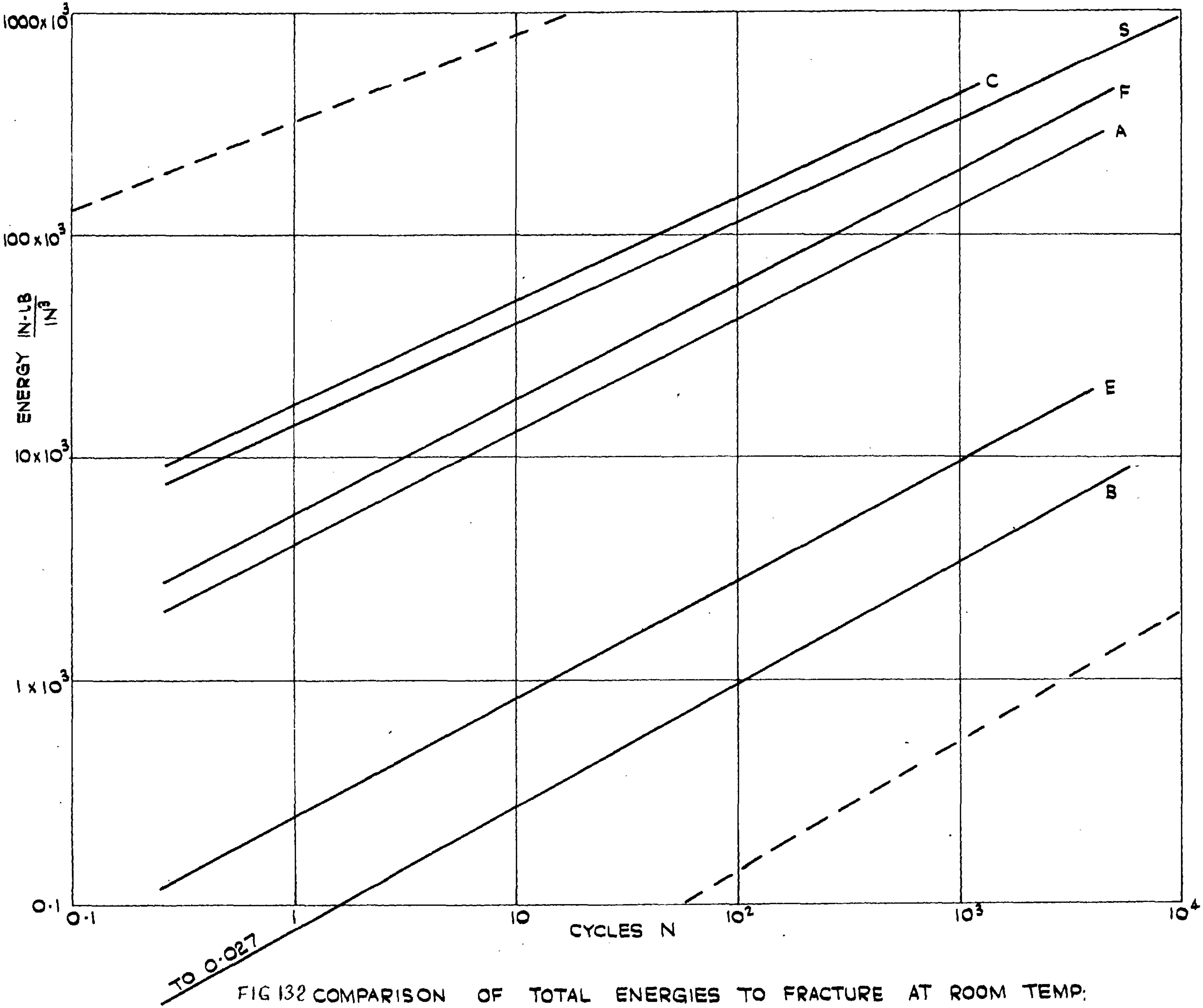

FIG 132 COMPARISON OF TOTAL ENERGIES TO FRACTURE AT ROOM TEMP.

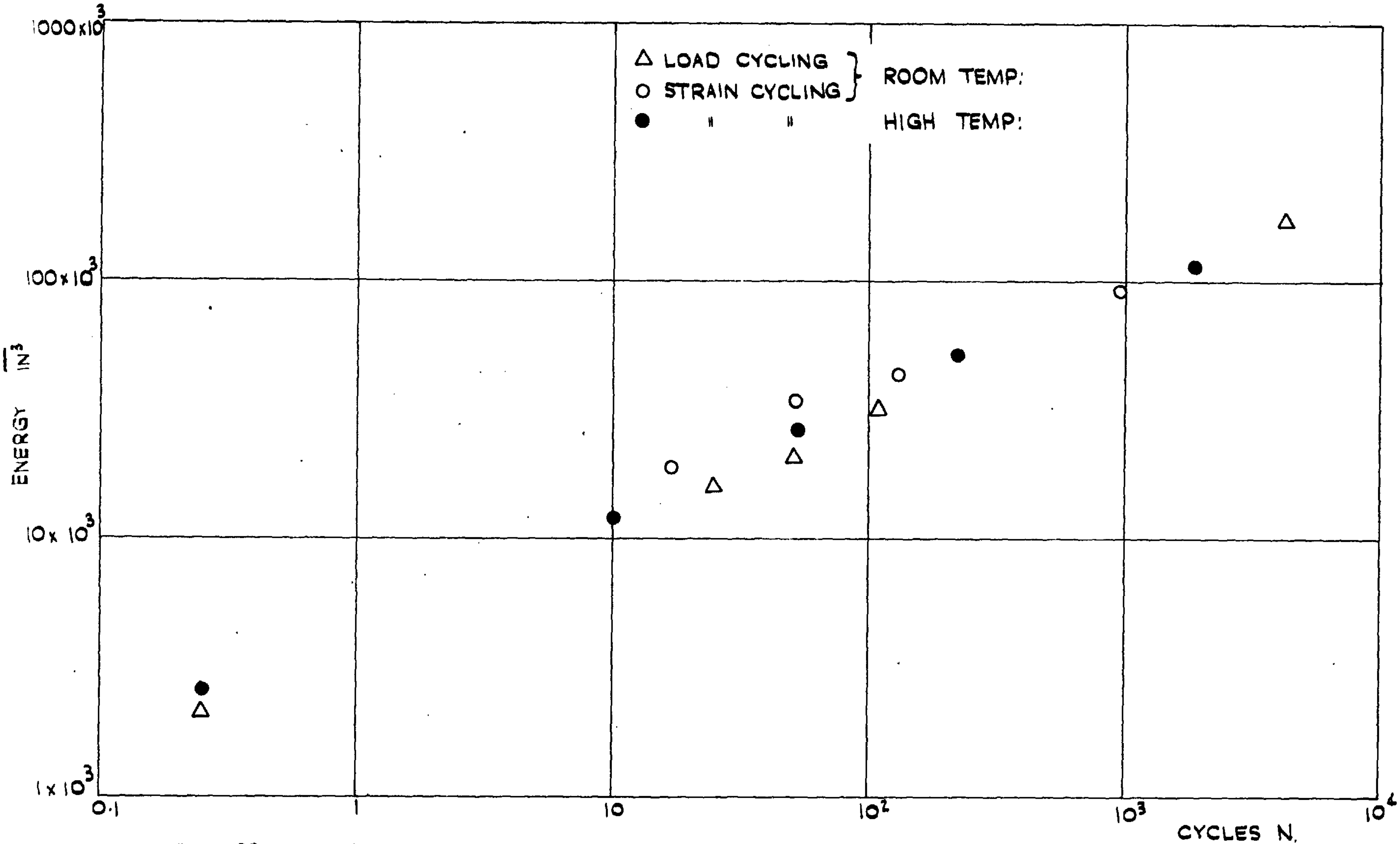

FIG.133. Total energy to fracture of cast iron A

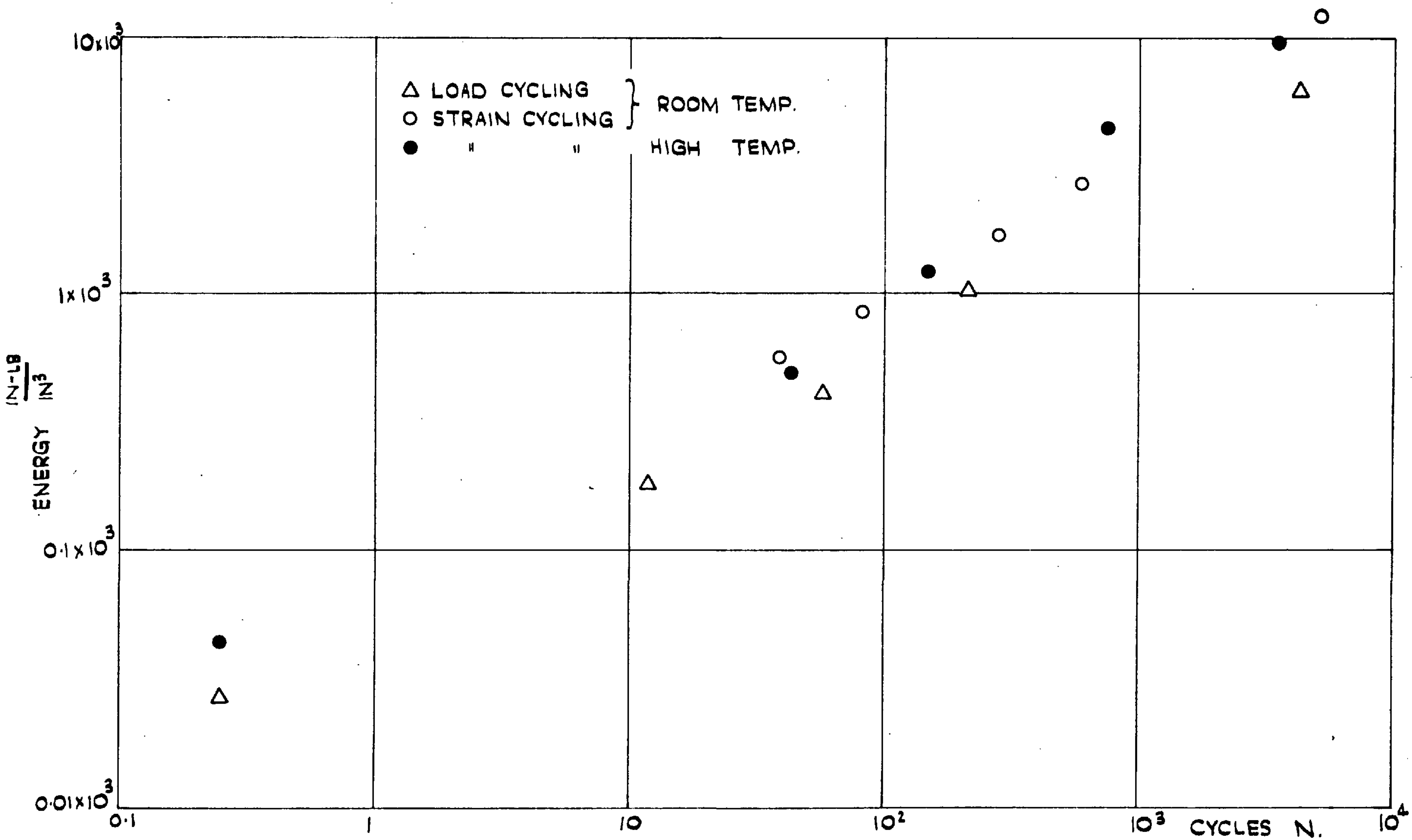

FIG.134. Total energy to fracture of cast iron B

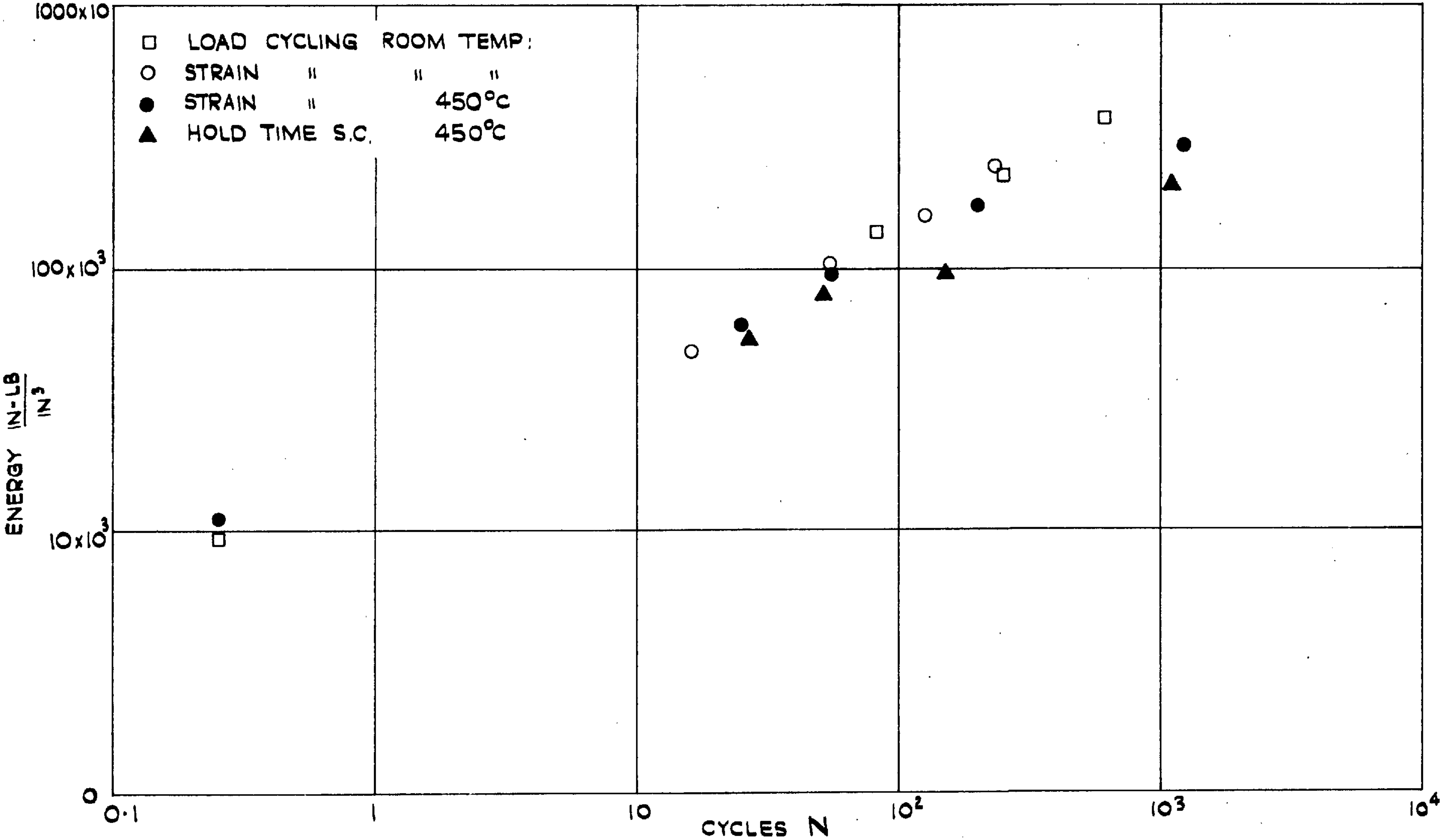

FIG.135. TOTAL ENERGY TO FRACTURE FOR CAST STEEL C.

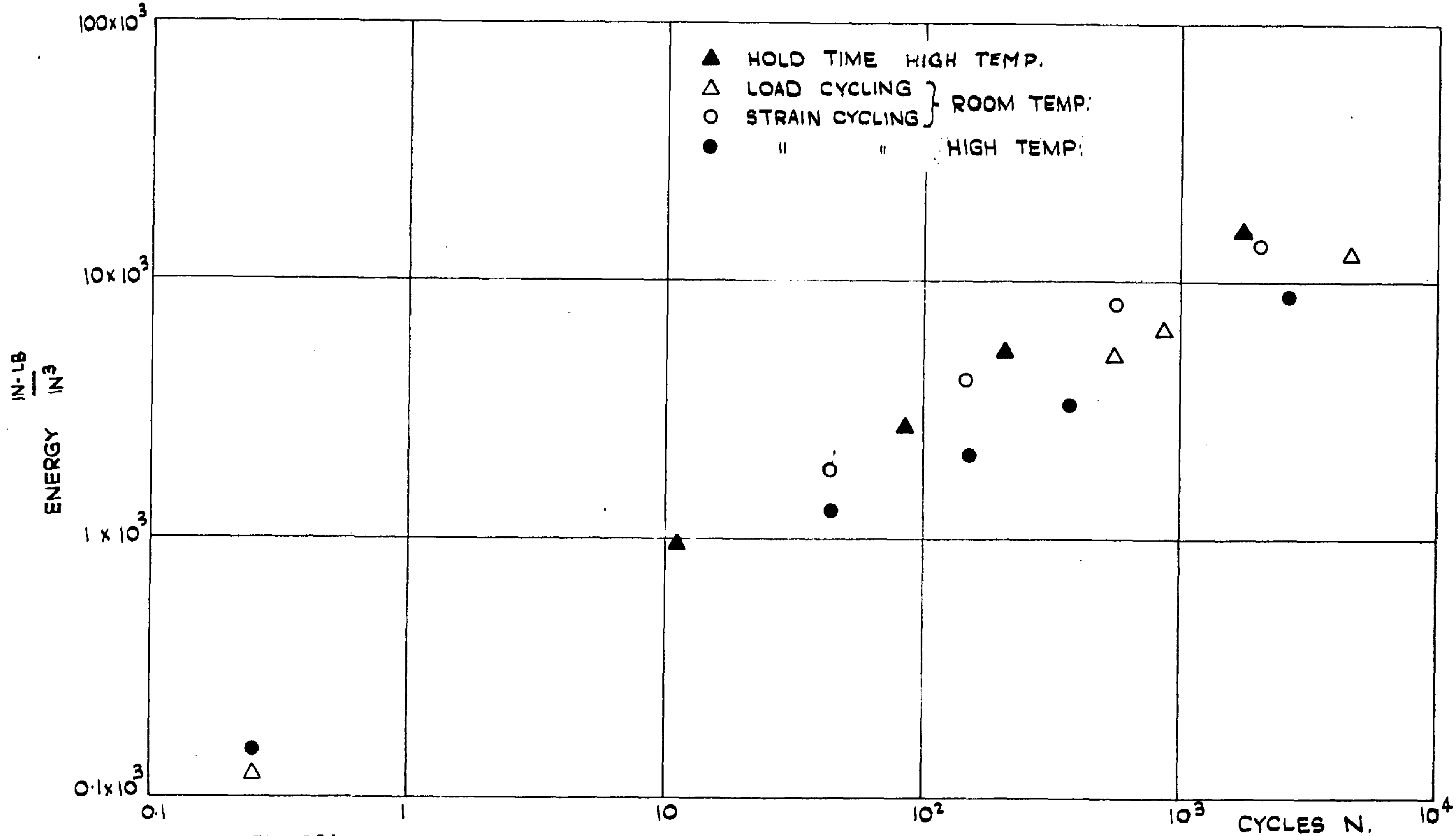

FIG.136. Total energy to fracture of cast iron E

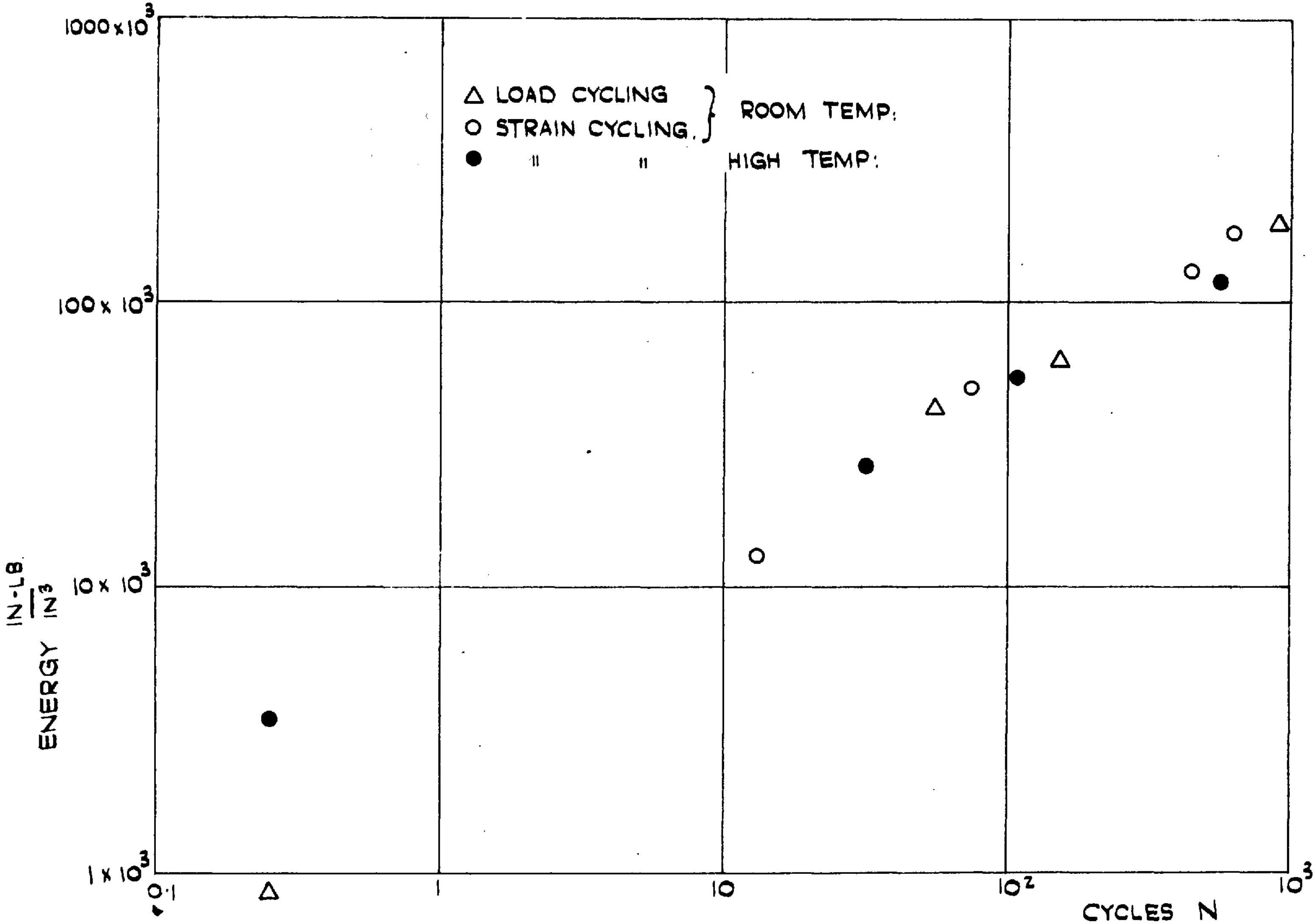

FIG.137. Total energy to fracture of cast iron F

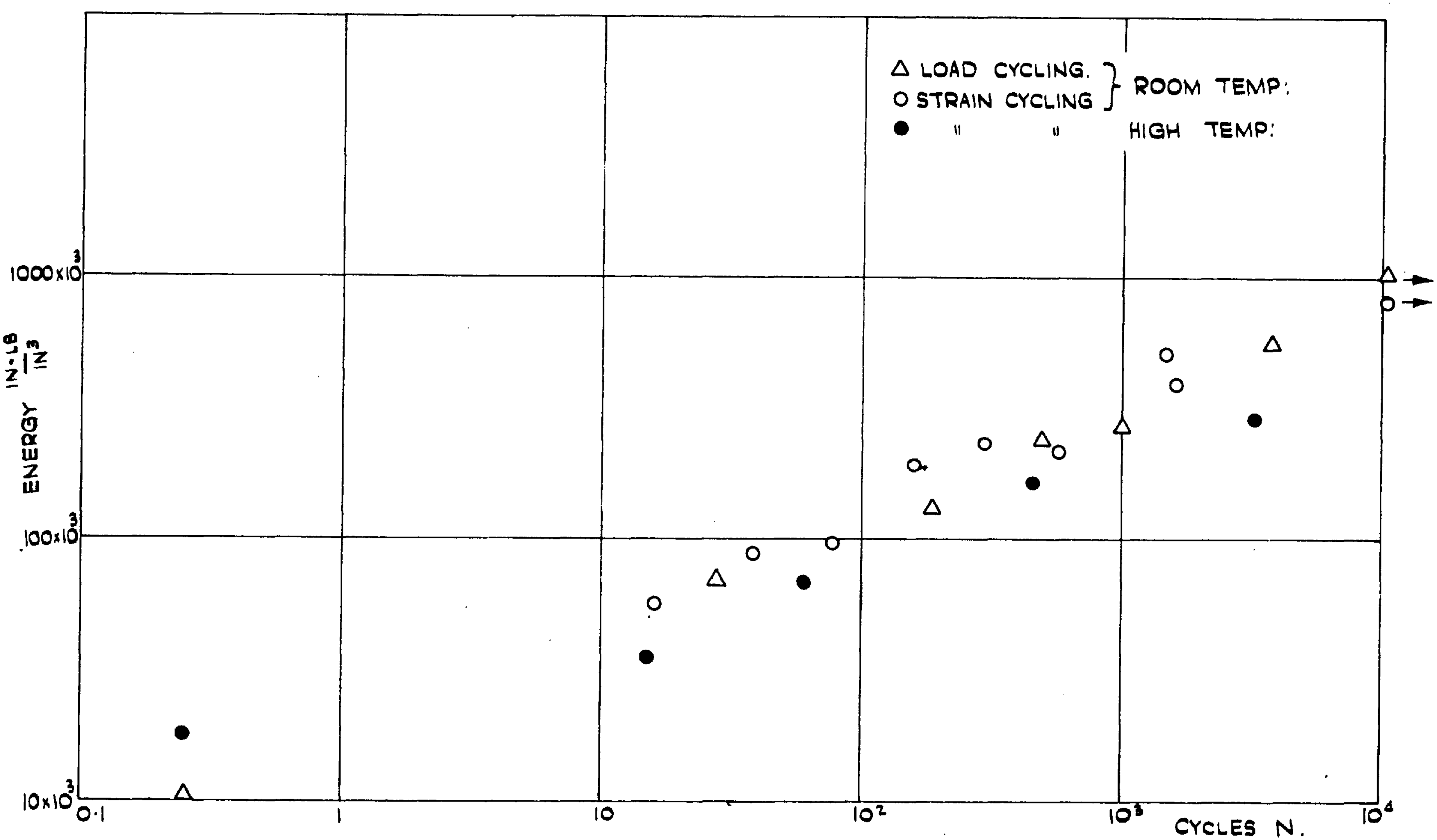

FIG.13F. Total energy to fracture of cast steel S

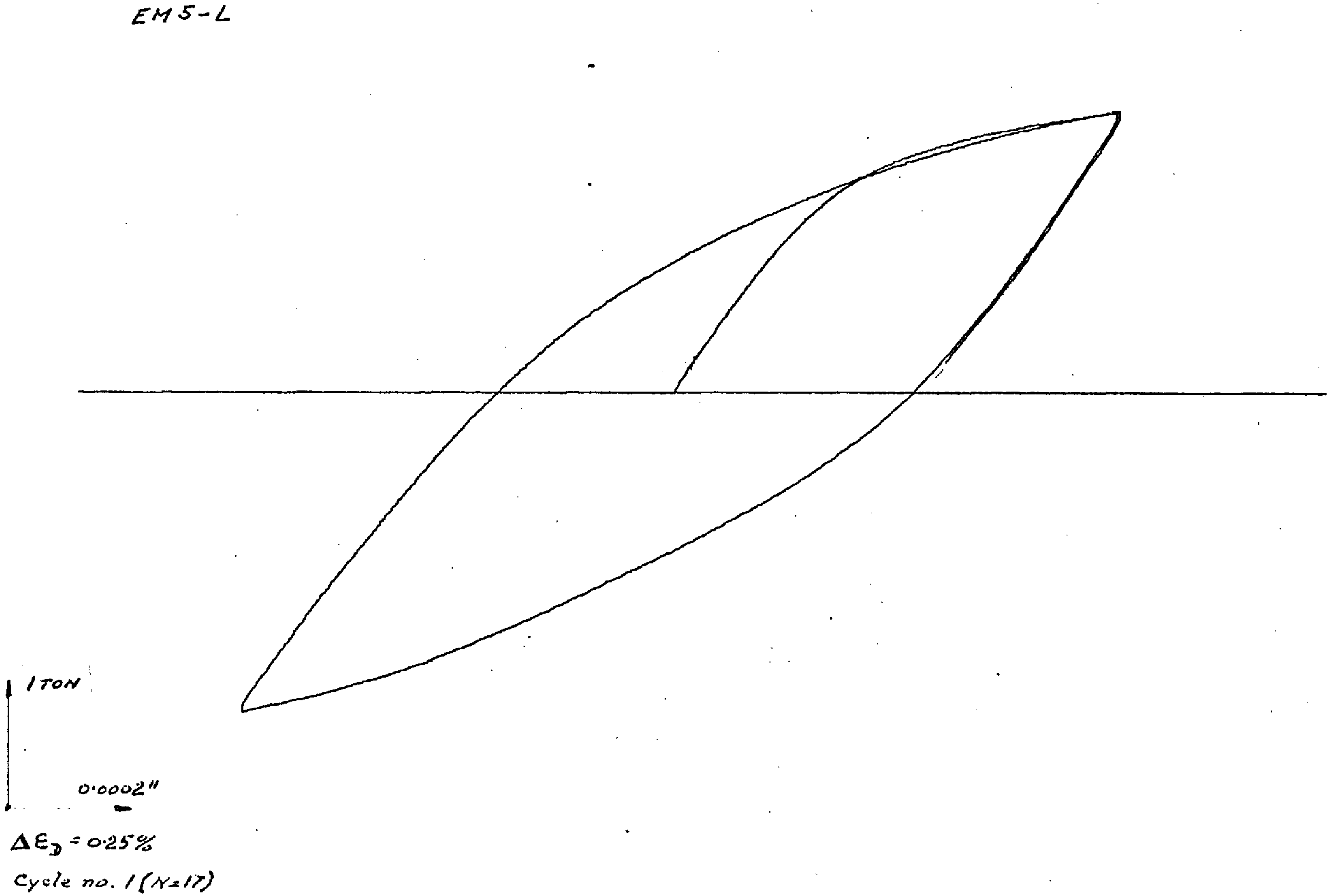

Fig.139. Cast iron E. Strain cycling, start in tension.

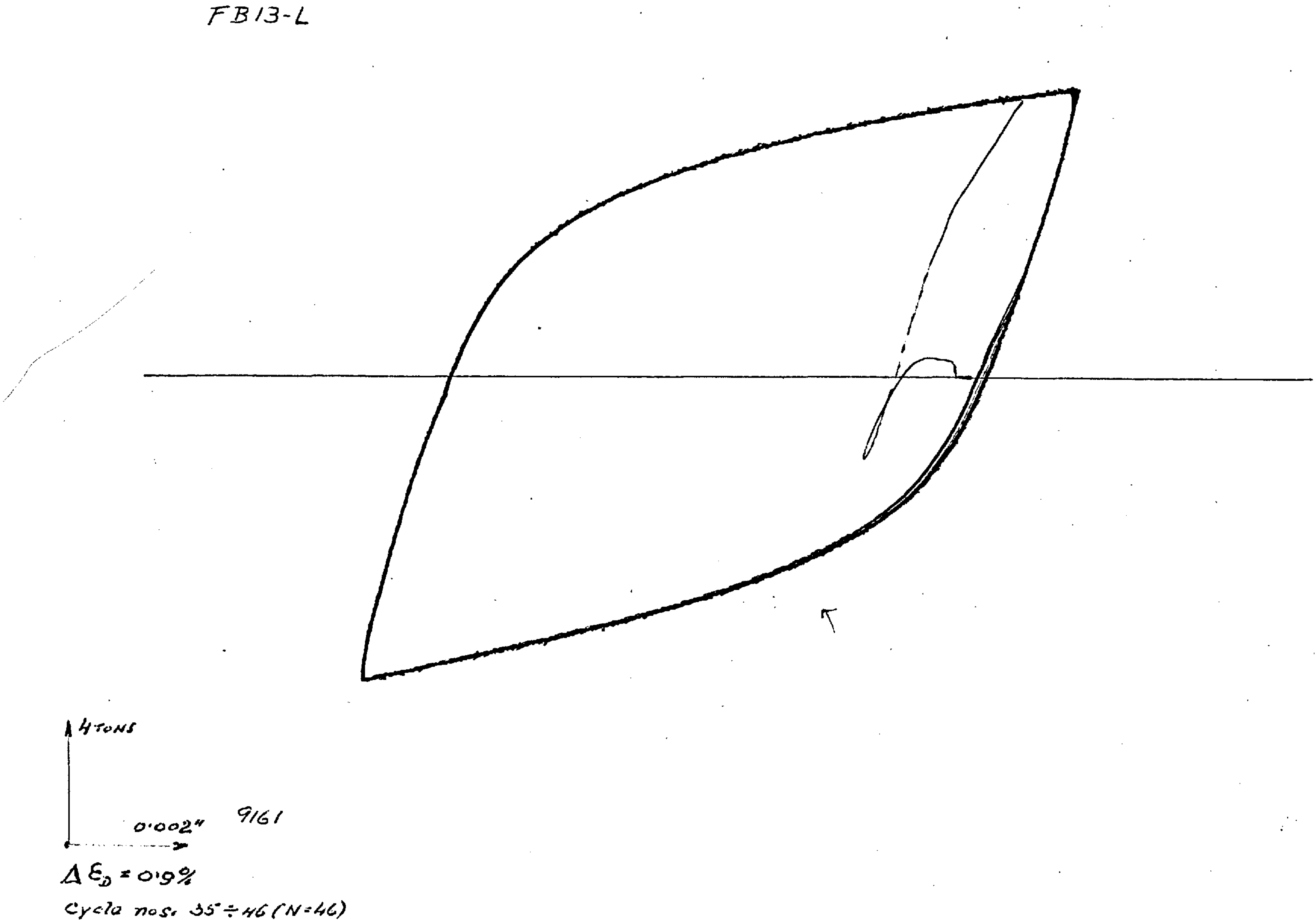

Fig. 140 .Cast iron F.Strain cycling (start in tension) Last 11 cycles.

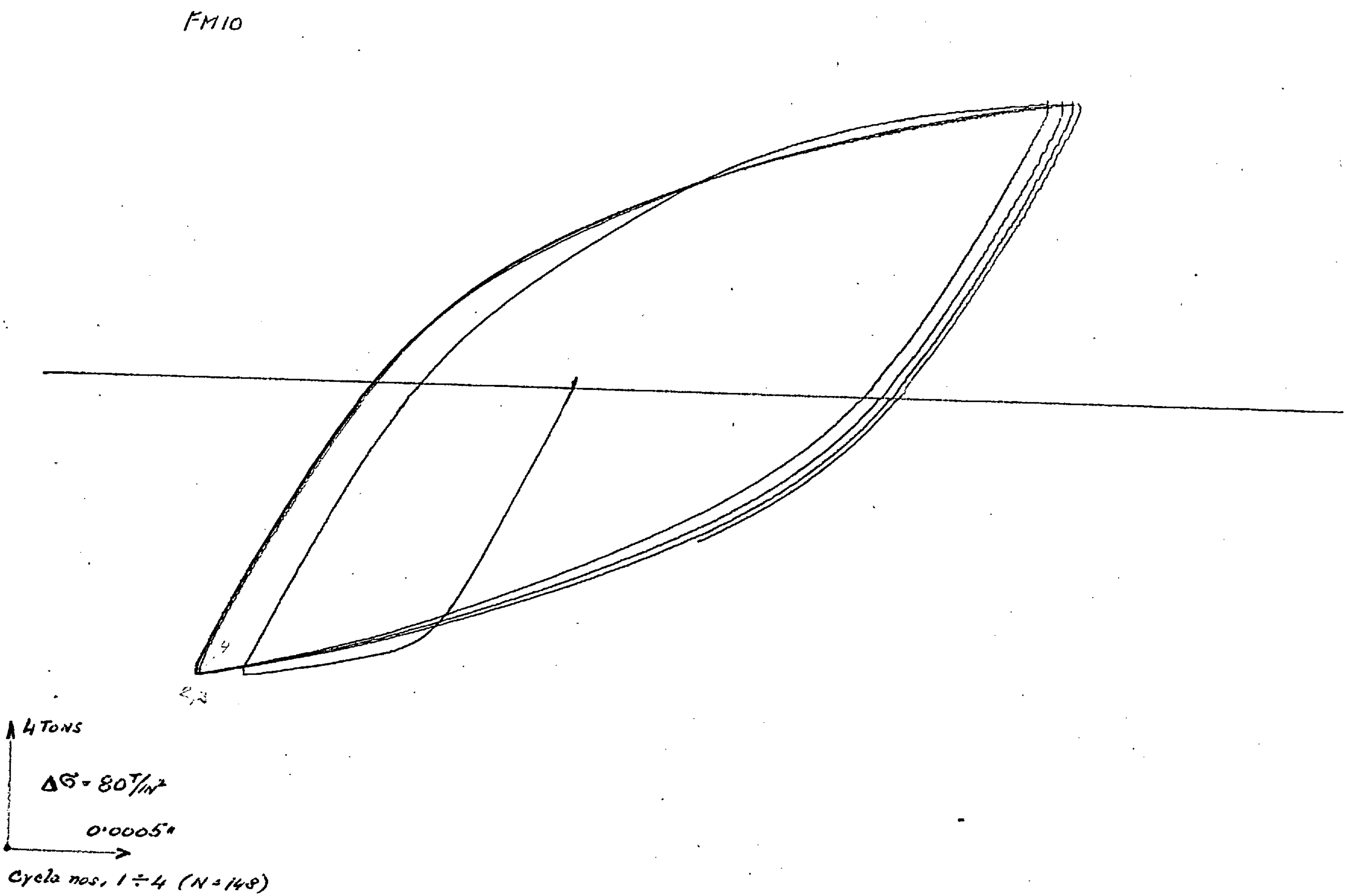

Fig.141.Cast iron F.Load cycling, first 4 cycles.

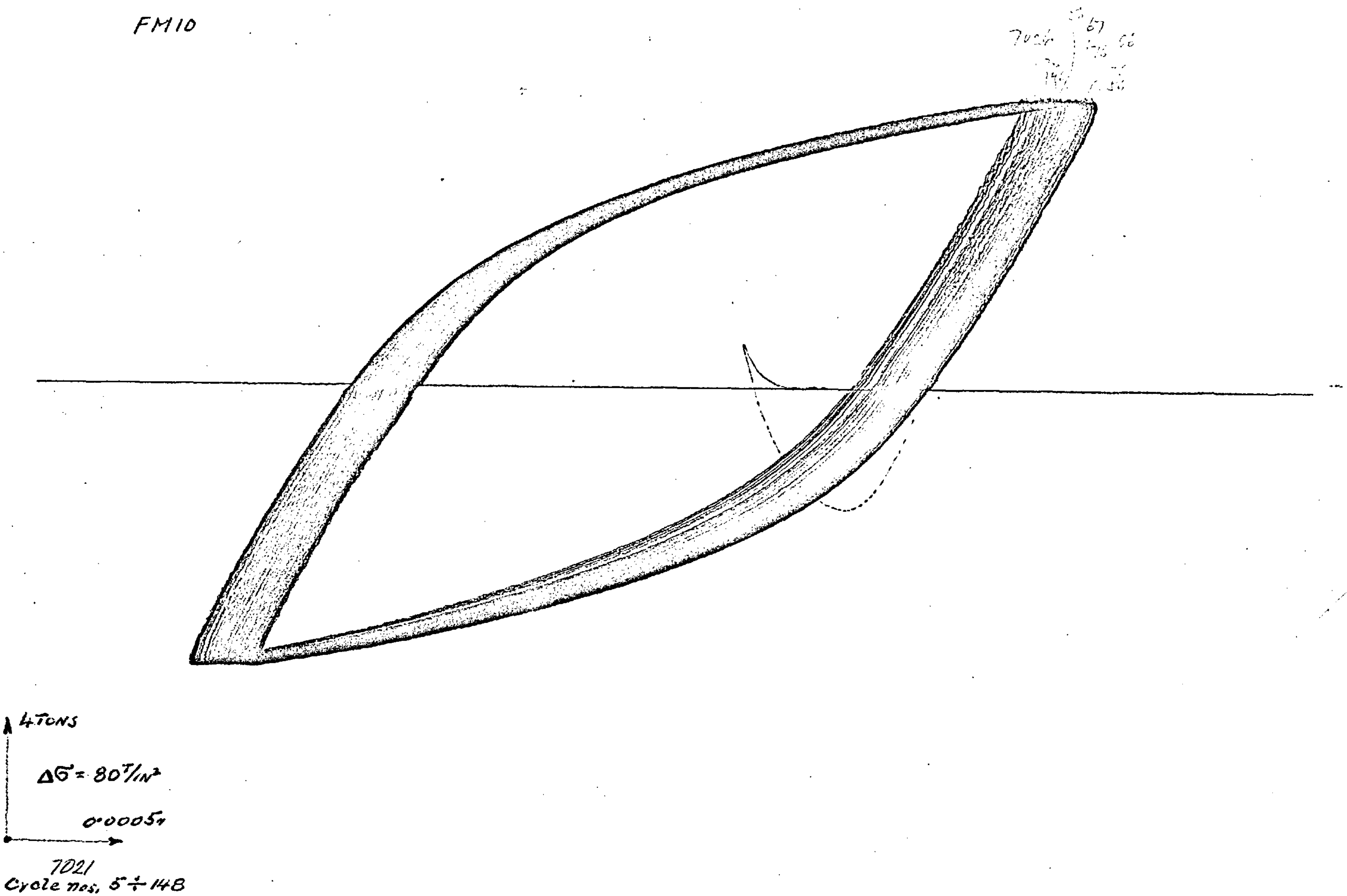

Fig. 142 .Cast iron F.Load cycling and fracture.

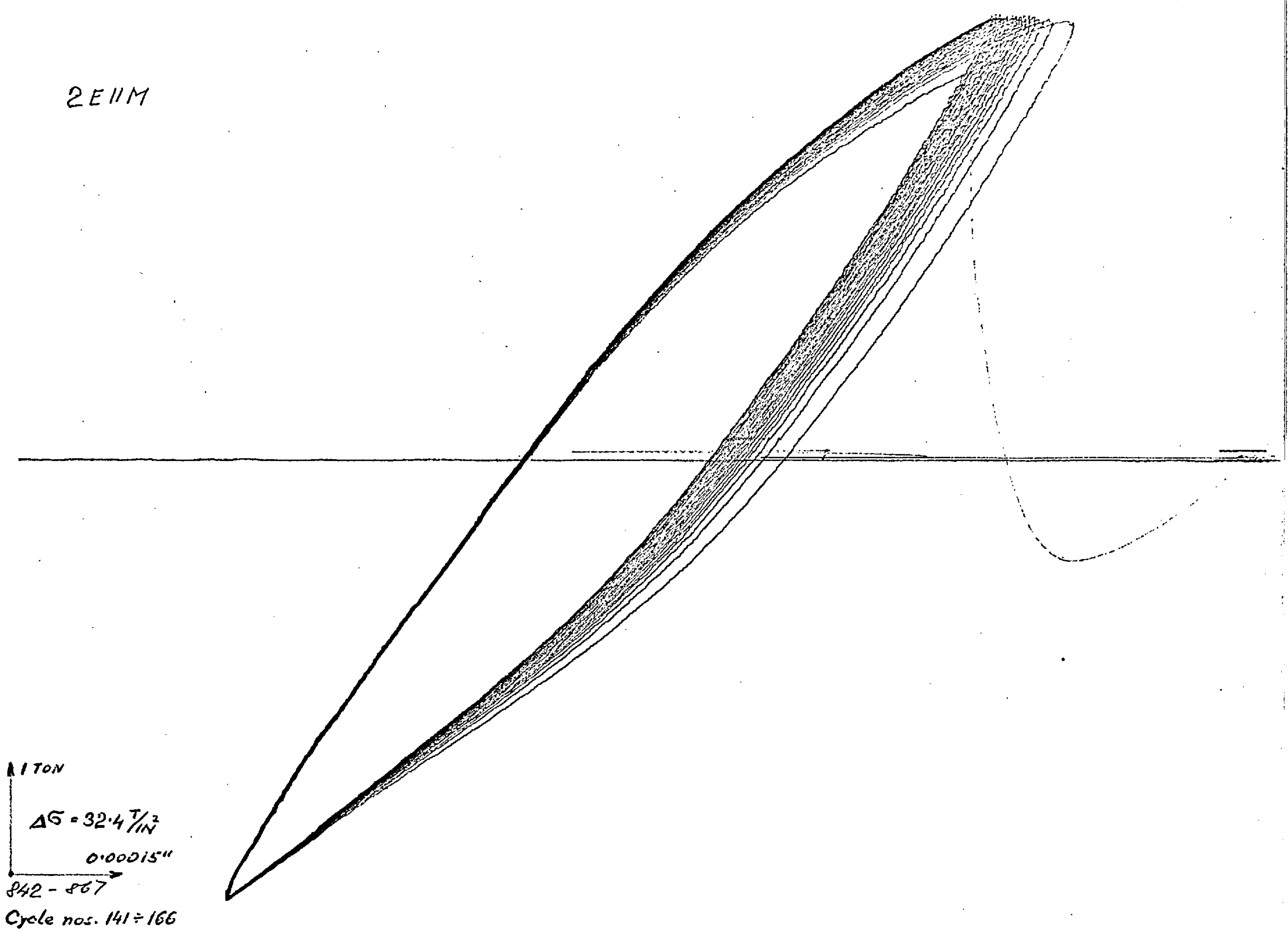

Fig. 143. Cast iron E. Load cycling and fracture.

1C M10

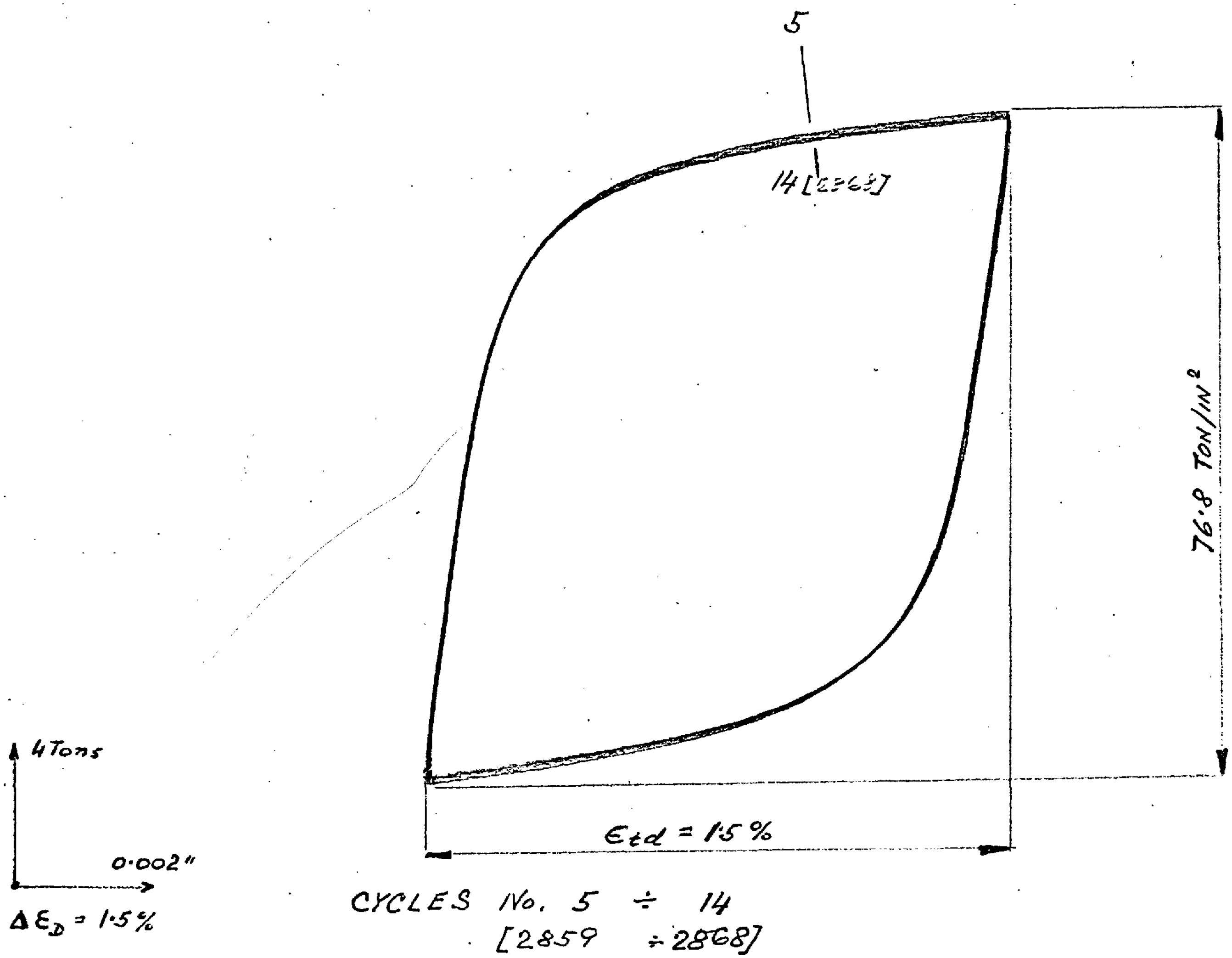

Fig. 144. CAST Cr - Mo STEEL C. Strain cycling.

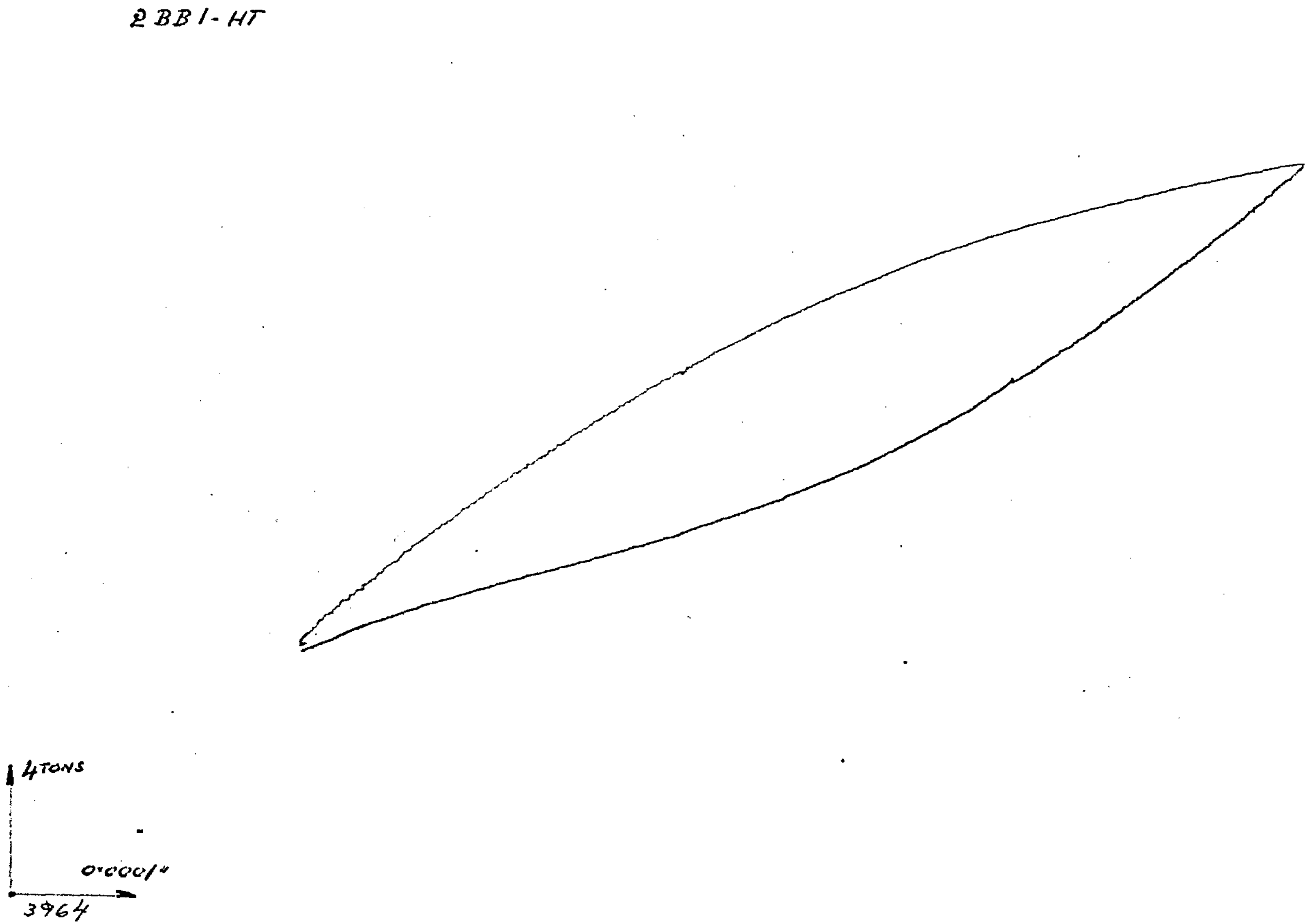

$\Delta\varepsilon_D$ = 0·138%
Cycle nos. 20 (N=44)

Fig. 145. Cast iron B. Strain cycling at 450°C.

2C2-HT

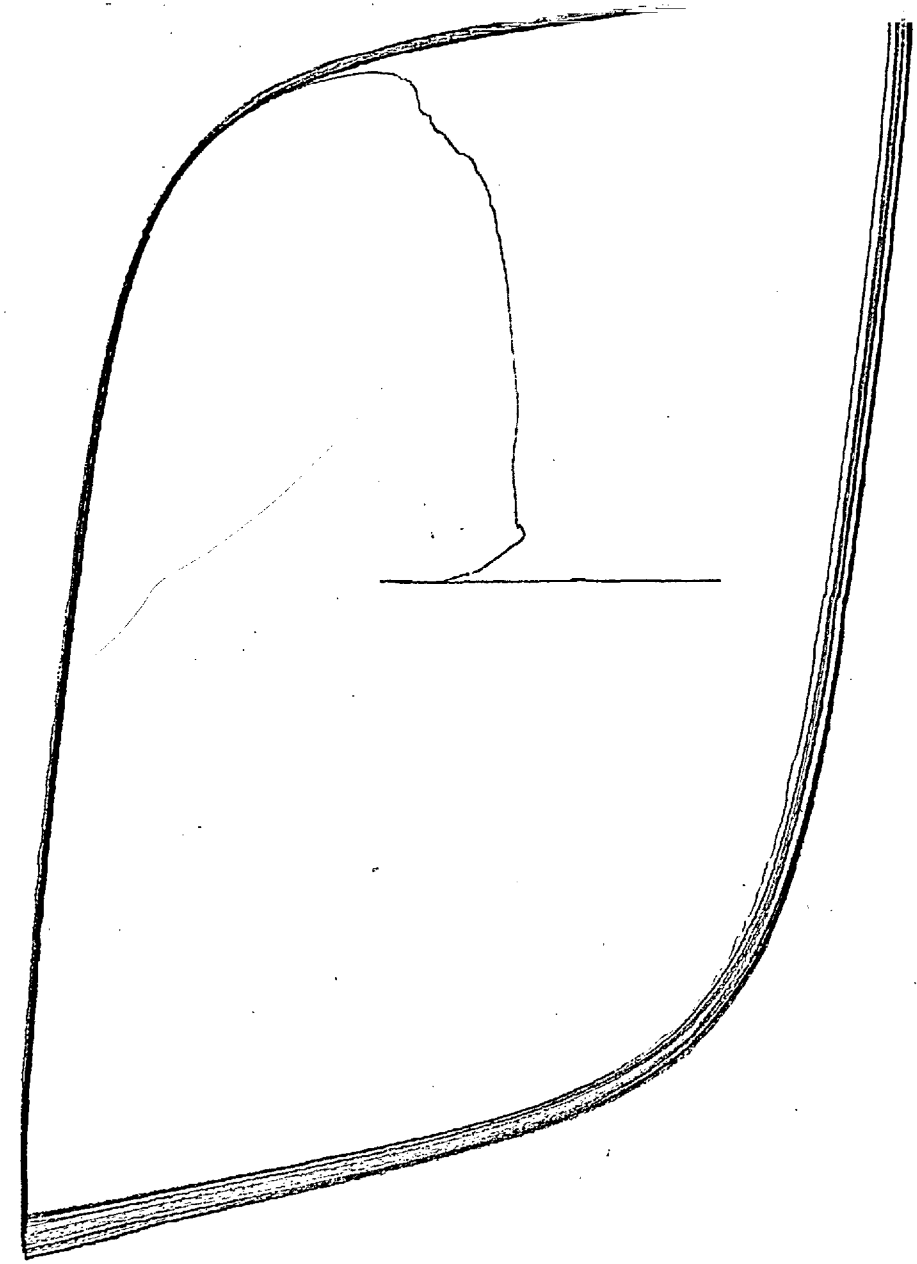

2 TONS

0·002"

$\Delta\epsilon_D = 2\%$

9639 - 9660

Cycle nos. 4 ÷ 25

Fig.146. Cast steel C. Strain cycling at 450°C.Fracture.

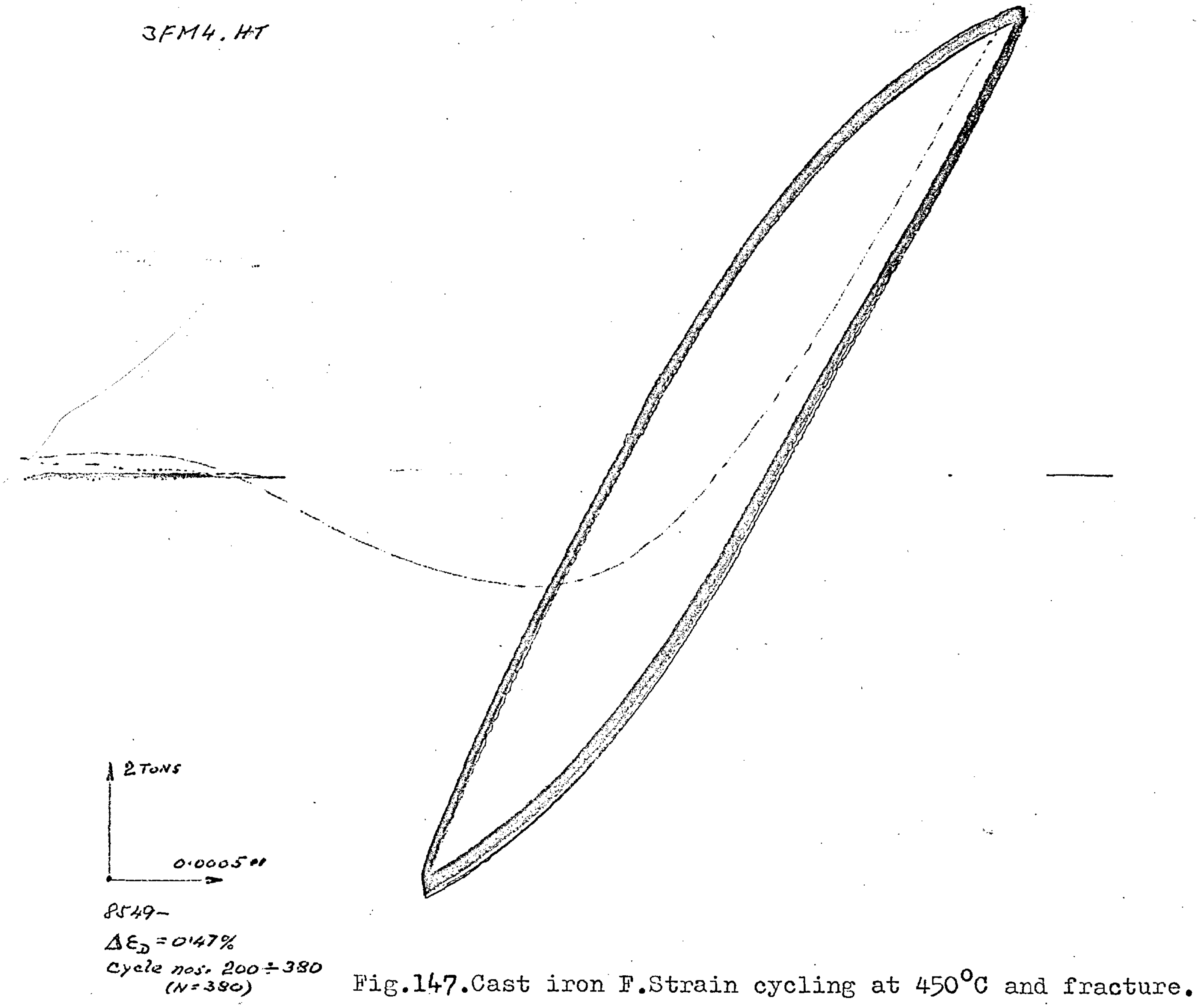

Fig.147.Cast iron F.Strain cycling at 450°C and fracture.

2SB4-HT

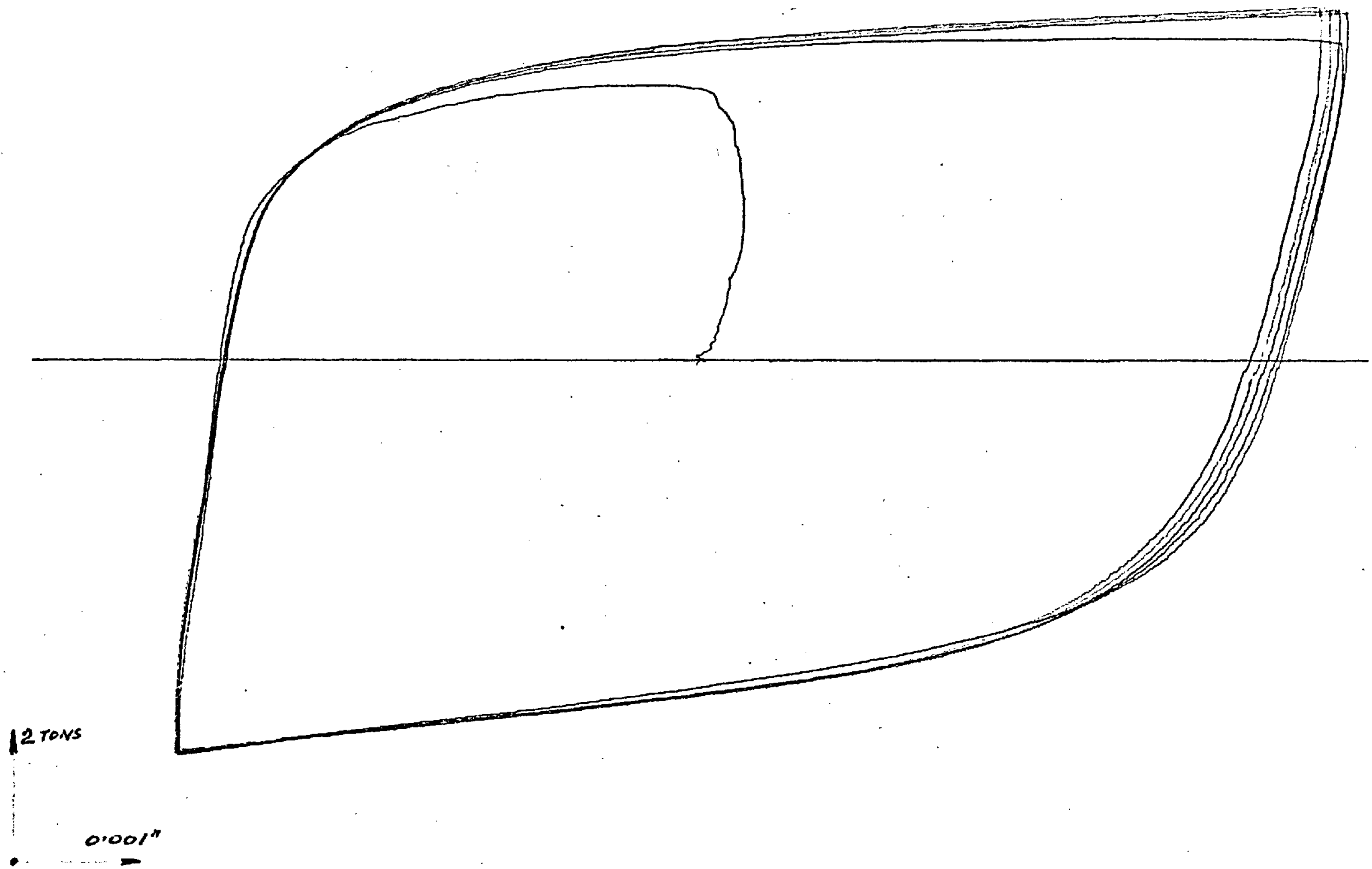

7523-

$\Delta\varepsilon_D = 1{\cdot}5\%$

Cycle nos. 50 ÷ 59
(N = 59)

Fig.148. Cast mild steel S. Strain cycling and fracture at 450°C.

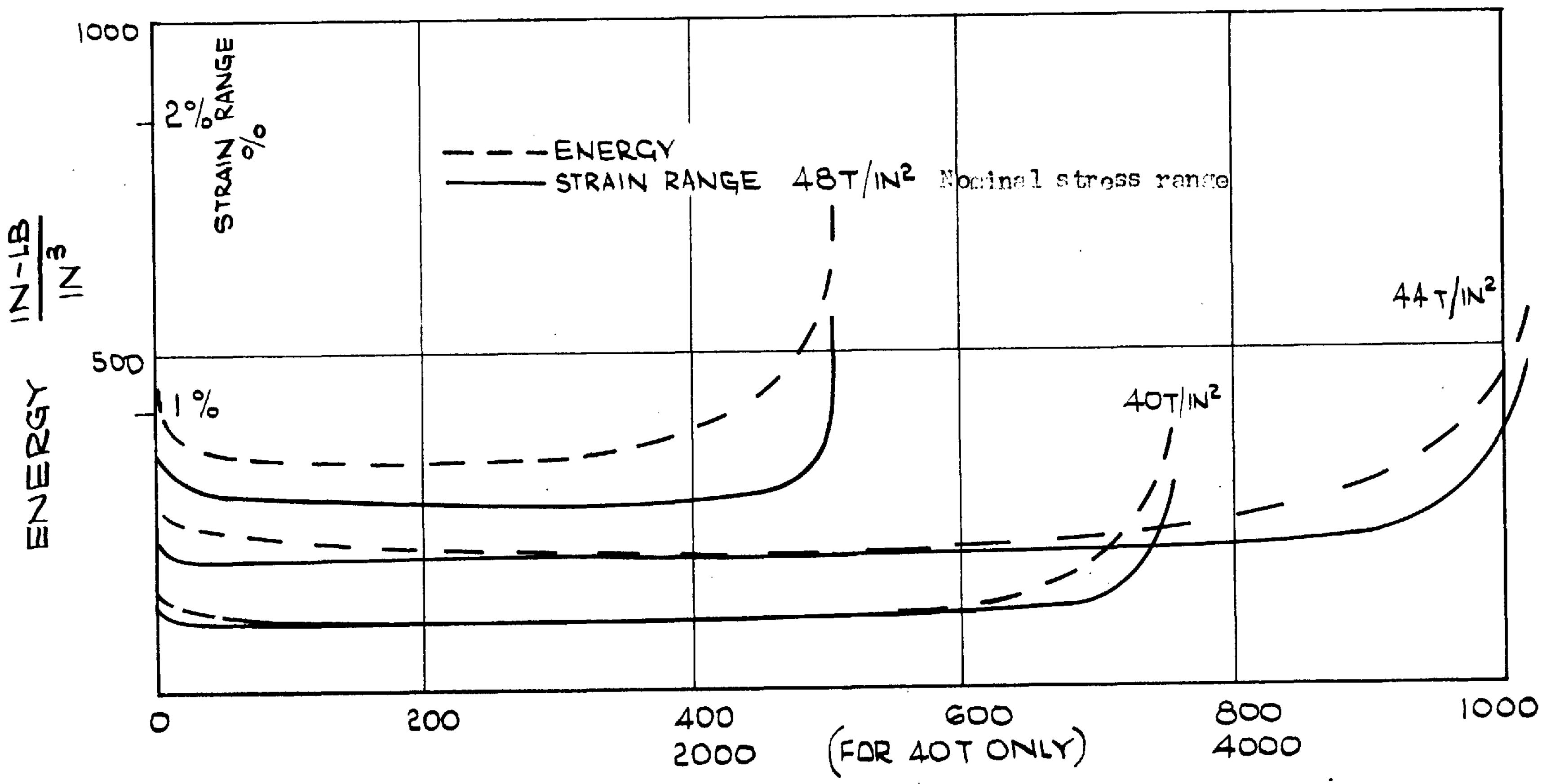

FIG.149. Comparison of energy with strain range during load cycling of cast mild steel S.

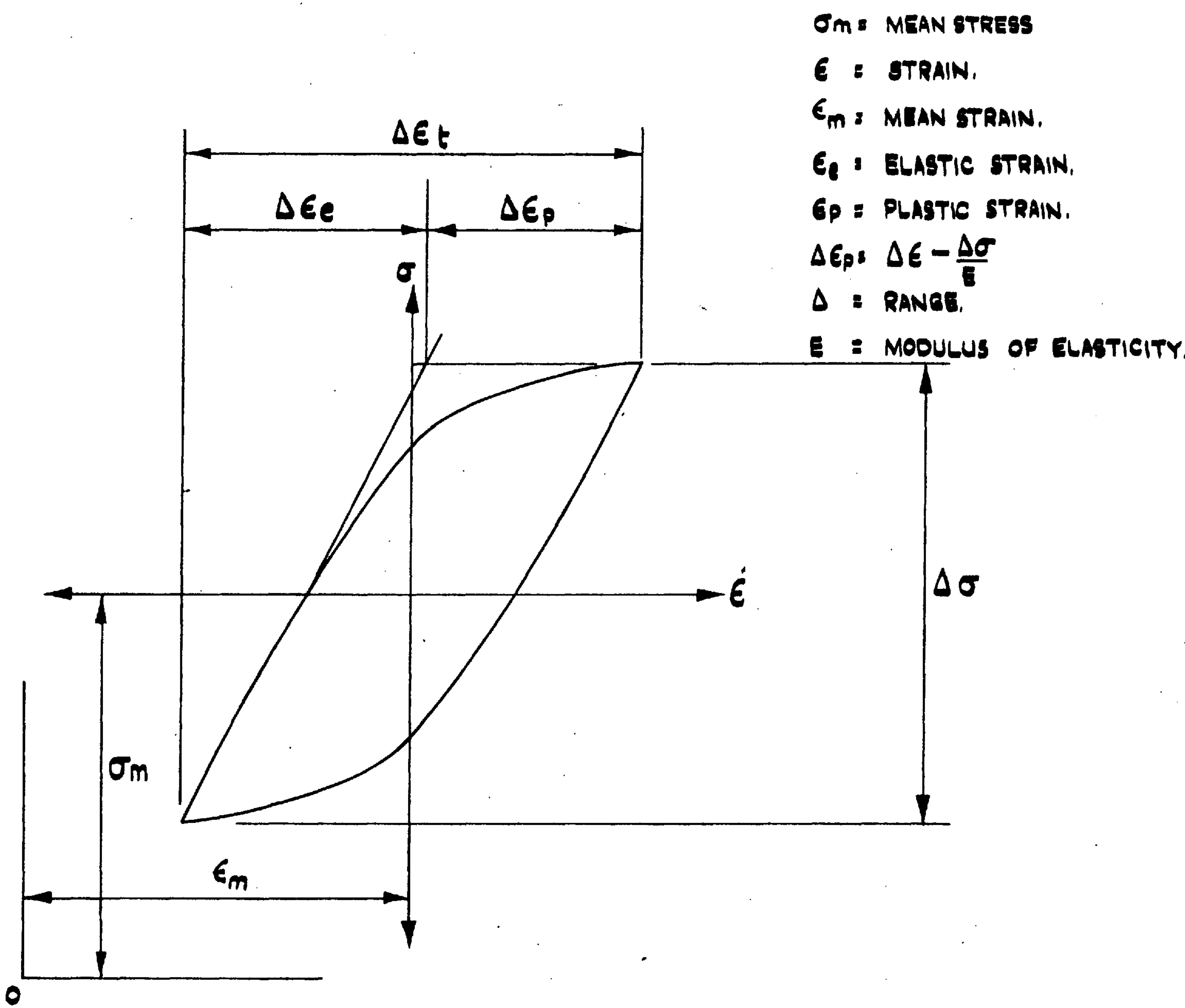

FIG. 150. HYSTERESIS LOOP OF A STRAIN CYCLED, FATIGUE SPECIMEN.

NFIDENTIAL

B.S.R.A. Report NS. 106

Marine Engineering Report No. 67

B·S·R·A

THE BRITISH SHIP RESEARCH ASSOCIATION

The Low-Cycle Fatigue Behaviour of Diesel-Engine Combustion-Chamber Materials

J. C. RADON, Dipl.Ing., D. J. BURNS, B.Sc.(Eng)., Ph.D., P. P. BENHAM, M.Sc.(Eng)., Ph.D.

1966

PRINCE CONSORT HOUSE

27–29 ALBERT EMBANKMENT, LONDON, S.E.1

Confidential Classification

It is the policy of B.S.R.A. that its member firms should receive the first benefits of the results of its researches. For this reason the research reports are in the first instance issued only to member firms and are marked 'Confidential'.

This restriction is not intended to limit in any way the use that member firms make of the reports within their establishments or in any discussions with their customers and sub-contractors. The Research Council are most anxious that member firms should derive the maximum of benefit from the research results and for this reason have placed no limit on the number of copies supplied to the members. The restriction does mean that no information contained in the report should be included in any published material without the consent of the Association and that copies should not be supplied to firms outside the British shipbuilding, ship-repairing, marine-engineering, and shipping industries.

Firms will be advised in each instance when the confidential restriction is removed.

If it is considered that it would be helpful to have a discussion on the contents of this report, B.S.R.A. would be pleased to arrange for a senior member of its research staff or the author or authors to visit the member firm concerned.

B.S.R.A. REPORT NS. 106

MARINE ENGINEERING REPORT NO. 67

B·S·R·A

THE BRITISH SHIP RESEARCH ASSOCIATION

The Low-Cycle Fatigue Behaviour of Diesel-Engine Combustion-Chamber Materials

(Research Item M.4)

J. C. RADON, Dipl.Ing., D. J. BURNS, B.Sc.(Eng)., Ph.D.,

(Imperial College of Science and Technology, London)

P. P. BENHAM, M.Sc.(Eng)., Ph.D.

(Queen's University of Belfast)

1965

PRINCE CONSORT HOUSE

27–29 ALBERT EMBANKMENT, LONDON, S.E.1

PRODUCED BY UNEOPRINT
set on electric keyboards
photo-reproduced and printed offset
at The Gresham Press
UNWIN BROTHERS LIMITED
Old Woking Surrey England

(U 916)

THE LOW-CYCLE FATIGUE BEHAVIOUR OF DIESEL-ENGINE COMBUSTION-CHAMBER MATERIALS

J. C. RADON, Dipl.Ing., D. J. BURNS, B.Sc.(Eng)., Ph.D.,
P. P. BENHAM, M.Sc.(Eng)., Ph.D.

SUMMARY

Cyclic thermal stresses produced in combustion-chamber components by starting and stopping or running a Diesel engine on part load may lead to fatigue cracking.

There is evidence that the resistance materials offer to cycles of mechanical strain, total and plastic, has an important bearing on their thermal fatigue strength. The object of the present work is to show the influence of strain range, ambient temperature, strain concentration (notch), and short hold-times at maximum and minimum strains on the mechanical strain-cycling fatigue behaviour of a selection of combustion-chamber materials.

The present results suggest that cast steels and nodular cast irons will have better thermal fatigue properties than flake graphite cast irons. However, this conclusion may have to be modified when tests with longer hold-times at maximum and minimum strains have been completed.

THE LOW-CYCLE FATIGUE BEHAVIOUR OF DIESEL-ENGINE COMBUSTION-CHAMBER MATERIALS

J. C. RADON, Dipl.Ing., D. J. BURNS, B.Sc.(Eng)., Ph.D.,
P. P. BENHAM, M.Sc.(Eng)., Ph.D.

§ 1. INTRODUCTION

1 Thermal stresses usually result from one or more of the following conditions:-

(1) Two interconnected components having different coefficients of expansion undergo a rise in temperature.

(2) Two interconnected components undergo different rises in temperature.

(3) The temperature distribution in a component is such that it cannot take up a freely expanded shape.

At least two of these conditions are always present in Diesel-engine combustion chambers,and cyclic thermal stresses (produced by starting and stopping or running the engine on part load) may lead to fatigue cracking.[1-4*]

2 Dearden[5] and others have suggested that such failures are less likely to occur if component materials have the following properties:-

(a) High thermal conductivity to avoid steep temperature gradients.

(b) Low thermal-expansion coefficient to avoid steep strain gradients.

(c) Low creep rate in compression.

(d) High thermal fatigue strength under conditions of cyclic plastic strain which lead to failure in less that 5,000 cycles.

(e) High ductility little affected by cyclic plastic strain.

3 The physical and static mechanical properties of combustion-chamber materials have been fairly well investigated,[5,6] whereas few attemps have been made to assess their low-cycle (less than 5,000) thermal fatigue properties.[6,7]

4 The execution and interpretation of true thermal-cycling tests on constrained laboratory-size specimens in extremely difficult. Fortunately there is evidence[8] that mechanical strain cycling at a constant temperature, T_c, somewhere between T_1 and T_2, is equivalent to thermal cycling between these limits provided that significant metallurgical changes do not occur. The object of the present work is therefore to show the influence of strain range, strain concentrations (notch), ambient temperature, and hold-times at maximum and minimum strains on the mechanical strain-cycling fatigue behaviour of a selection of materials which are or might be used for combustion-chamber parts.

---

* *References are given on p. 12.*

§ 2. TEST MATERIALS

5 Tables 1 and 2 give the code letters, compositions, heat treatments, and metallographical reports for four cast irons and two cast steels. The microstructures of the materials are shown in Plate 4.* Only two of the eight cast irons previously tested by Pope *et al*[2,6] have been included in the present test programme: type E as it was the most promising flake iron and the nodular graphite iron F since it appeared to have high thermal fatigue strength which might compensate for its low thermal conductivity. The composition of irons E and F has been kept essentially the same as in Baker and Pope's work except that the nickel content of iron F has been reduced from 2 to 1 per cent to improve its ductility.

6 The high-carbon, large-flake iron B which can withstand high surface temperatures, and the spheroidal austenitic iron A, were included after discussions with B.C.I.R.A. who were carrying out engine-running tests on these materials.

7 After some consideration it was decided to test a cast chrome–molybdenum steel, C, which is used for centre sections of tripartite assemblies, and a cast mild steel, S.

8 The cast irons B, E, and F were supplied in the form of hollow octagonal castings which were broken up into slabs 18 × 12 × 2 in. The cast steels C and S were supplied as slabs 14 × 9 × 2 in., and cast-iron A as slabs 12 × 8 × 1¼ in. The cutting-up diagram for these slabs is shown on Fig. 1; only one specimen could be obtained from each thickness of material A.

§ 3. APPARATUS AND SPECIMENS

9 As the present work was concerned with plastic deformation, it was necessary to measure both stress and strain while controlling one or the other, and to cycle at low speeds (less than 20 cycles per min) to avoid large increases in specimen temperature.

10 Fig. 2 shows the general arrangement of the straining unit of one of two hydraulic tension–compression (± 15 tons) fatigue machines designed for the present research. A vertical double-acting hydraulic cylinder with a 6-in. stroke is bolted to the underside of a flat steel table, 8, which is mounted at a convenient height on a steel framework. Two vertical steel columns, 6, are rigidly mounted on this table and carry a crosshead, 9, of the same dimensions as the table.

11 The upper end of the hydraulic ram carries a steel plate, 12, which is only used during strain-cycling tests with hold-times at maximum and minimum strains. This steel plate is held firmly in position by the holder, 3, of the bottom specimen grip.

12 The crosshead, 9, carries a centering plate, 7, for a strain-gauge load cell, 1, which in turn carries the holder, 2, of the top specimen grip.

13 The solid cylindrical specimens, Fig. 3 (a) and (b), have conical ends. When the grip nuts, 5, are tightened, the collets, 4, which are screwed on the specimen ensure that the specimen sits axially in the holder cones, 3. Both types of specimen have a 1-in. parallel gauge length; it was necessary to use the longer specimen, Fig. 3 (b), to accommodate a muffle furnace for high-temperature tests.

---

* *Figures and Plates will be found on pp. 14 to 36.*

TABLE 1

Material code letter	TC	Si	P	S	Mn	Ni	Cr	Mo	Al	Heat treatment
A	2·16 to 2·21	1·73 to 1·92	0·026 to 0·040	0·005 to 0·011	0·25 to 0·48	34·4 to 35·4	—	—	—	None
B	3·62	1·55	0·018	0·066	0·49	—	—	0·90	—	None
C	0·265	0·38	0·026	0·012	0·64	0·31	1·19	0·29	0·080	Anneal 925°C. Furnace cool. Normalise 880°C. Air cool. Temper 700°C. Air cool.
E	3·29	1·10	0·12	0·088	0·69	1·18	—	0·39	—	6 hours at 500°C.
F	3·50	2·64	—	0·019	0·36	1·26	—	—	—	4 hours at 950°C. Air cool. 2 hours at 625°C. Air cool.
S	0·215	0·37	0·024	0·013	0·70	0·16	0·14	0·06	0·052	Anneal 925°C. Furnace cool.

TABLE 2

Material code letter	Metallographical Report (see Plate 4 for microstructures)	Supplier
A	Predominantly nodular graphite in an austenitic matrix small amounts of carbide at the grain boundaries.	B.C.I.R.A.
B	Medium/coarse flake graphite in a matrix containing about equal amounts of ferrite and pearlite.	B.C.I.R.A.
C	Moderately coarse feathery bainite with segregation banding at the grain boundaries.	Clyde Alloy Steel Co. Ltd.
E	Medium flake graphite in a completely pearlitic matrix containing very small amounts of phosphide eutectic	Vickers-Armstrongs Ltd.
F	Well formed nodular graphite in a pearlitic matrix with small amounts of ferrite associated with the graphite	Sheepbridge Equipment Ltd.
S	Fine lamellar pearlite in a ferritic matrix	Clyde Alloy Steel Co..Ltd.

14 Cooling coils are fitted behind the specimen grips to protect the load cell and hydraulic ram during high-temperature tests. The split muffle furnace is controlled by a saturated core reactor to 1°C and the temperature variation along a specimen is no more than 1°C at 450°C.

15 Diametral extensometers (Plates 1 and 2) are used because of the short specimen gauge length, which is necessary to avoid buckling, and because of the difficulties of measuring axial strains at high temperatures. Changes in specimen diameter are detected by an inductance transducer, which is suspended perpendicular to the main axis of the specimen. It is necessary to fit an extension to the transducer probe for high-temperature tests, c.f. Plates 2 and 3. The axial extensometer shown on Plate 3 was only used to check the relationship between diametral and axial strain at room temperature.

16 Some specimens were tested with a circumferential Izod V notch 0·05-in. deep (see inset on Fig. 3 (a)), in such cases the diametral extensometer was positioned at a cross section well away from the notch.

17 Pressure is applied to the double-acting ram by a 2,000 lb per sq in. balanced vane pump through a four-way solenoid valve. Reversing of the ram is controlled through this solenoid valve by the amplified signal of the load cell or diametral extensometer. These load and strain signals are also continuously displayed on an X–Y recorder as hysteresis loops. The load and strain ranges can be controlled and/or measured to better than 0·75 per cent.

18 When cycling at high temperature between strain limits with a hold-time at each limit, it is necessary to provide mechanical limits for the movement of the hydraulic ram or a continuous electronic pressure control. The former method (see Fig. 2) is very simple and fairly effective. The steel plate, 12, travels between four sets of nuts which are adjusted and locked at the start of the test at maximum, or minimum, strain. When the nuts have been adjusted the ram pressure is increased slightly to ensure that these mechanical strain limits are always operative.

§ 4. RESULTS

19 The results of static tensile tests at room temperature and 450°C are summarised in Table 3. Typical stress–strain curves for these materials are shown in Figs. 4 and 5.

TABLE 3

Material code letter	At room temperature					At 450°C		
	U.T.S.	% RA	ϵ_f*	C	α	U.T.C.	%RA	ϵ_f*
A	27·2	13·7	14·5	25·0	0·60	15·6	17·3	17·6
B	9·7	0·31	0·3	1·7	0·45	8·7	0·52	0·46
C	43·6	23·5	26·1	31·0	0·52	34·8	35·0	44·2
E	20·8	0·45	0·7	1·2	0·48	17·0	0·59	0·92
F	49	1·58	2·5	17·5	0·50	44·8	5·36	5·66
S	32·6	32·0	38·8	44·0	0·50	20·0	41·3	53·0

* ϵ_f, the fracture ductility is defined as log A_o/A_f where A_o is the initial specimen area and A_f is the fracture area.

20 Since thermal fatigue is primarily a strain-cycling phenomenon[5,8] reversed-load (stress) cycling tests have only been carried out on plain specimens at room temperature, Fig.6, for comparison with strain-cycling data. The form of hysteresis loop recorded during these tests is shown as Fig. 7. The gradual movement of the hysteresis loop along the strain axis is called cyclic creep; it occurred in all load-cycling tests.

21 The following reversed-strain cycling tests have been carried out at approximately zero mean stress and 4 cycles per min:-

(a) Tests on plain specimens at room temperature (Fig. 8) and 450°C (Fig. 9).

(b) Tests on notched specimens at room temperature (Fig. 10) and 450°C (Fig. 11).

Figs. 8 to 11 only show mean curves; the experimental points are shown for materials A, B, C, E, F, and S on Figs. 12 to 17 respectively.

22 All tests, strain or load-cycling, started in compression; the nomenclature used to describe the hysteresis loops is explained on Fig. 18. The stress range, $\Delta\sigma$, and ratio of elastic to plastic strain $\Delta\epsilon_e/\Delta\epsilon_p$ changed significantly during the strain-cycling tests on materials A and S (Figs. 19 to 23). Reversed-strain cycling tests have also been carried out on materials E and C with five minute hold-times at maximum and minimum strains (Figs. 24 and 25). The forms of hysteresis loop recorded during these tests is shown as Fig. 26 (b); Fig 26 (a) shows the form of strain-cycling hysteresis loop obtained without hold-times.

§ 5. DISCUSSION OF RESULTS

23 The order of merit in which the strain-cycling tests on plain specimens at room temperature (Fig. 8) place the six materials is modified when the ambient temperature is increased to 450°C and/or a strain concentration (notch) is introduced (Figs. 9 to 11). However, it will be noticed that the large-flake cast-iron B is always at the bottom of this order of merit.

24 Of particular interest is the large drop in fatigue strength shown by the nodular cast-iron F when notched. This and the fact that iron F has a lower thermal conductivity than iron E helps to explain why engine-cycling tests[5] indicate that iron E is the better material for cylinder heads.

25 Thermal fatigue is primarily a strain-cycling phenomenon and the danger of using simple load against cycles to failure (S-N) curves when assessing thermal fatigue strength can be shown by comparing Figs. 6 and 8. Up to 10,000 cycles, load-cycling fatigue strength can be related to tensile strength, Fig. 6 and Table 3; whereas strain-cycling data (Fig. 8) give a different order of merit for the materials and shows no correlation with tensile strength.

26 However, if hysteresis loops are recorded during load-cycling tests it is possible to derive diametral strain-range against cycles-to-failure data for comparison with the results of strain-cycling tests (Fig. 8). The two types of test then give the same order of merit for the materials; the curves derived from load-cycling data are thought to be lower than strain-cycling curves because of the cyclic creep which occurs during load cycling. The magnitude and direction (tensile or compressive) of this cyclic creep is dependent on the small mean stress acting and the ability of the material to strain harden (Figs. 19 to 22) or strain soften,[9] during cyclic straining.

27 Figs. 8 to 17 are plots of total diametral strain range, $\Delta\epsilon_{td}$, against cycles to fracture, N. It is possible to convert total diametral to total axial strain range, $\Delta\epsilon_{ta}$, by using the equation derived in the following manner.

If $\Delta\epsilon_{ta}$ is the total axial strain range

$$\Delta\epsilon_{ta} = \Delta\epsilon_{pa} + \Delta\epsilon_{ea} = \Delta\epsilon_{pa} + \frac{\Delta\sigma}{E}, \tag{1}$$

where $\Delta\epsilon_{pa}$ = plastic axial strain range,

$\Delta\epsilon_{ea}$ = elastic axial strain range,

$\Delta\sigma$ = axial stress range,

E = Young's modulus.

If constant volume in the plastic range is assumed

$$\Delta\epsilon_{pa} = 2\Delta\epsilon_{pd}, \tag{2}$$

where $\Delta\epsilon_{pd}$ is the plastic diametral strain range, but

$$\Delta\epsilon_{pd} = \Delta\epsilon_{td} - \Delta\epsilon_{ed},$$

$$\Delta\epsilon_{pd} = \Delta\epsilon_{td} - \frac{\gamma\Delta\sigma}{E}, \tag{3}$$

where $\Delta\epsilon_{td}$ = total diametral strain range,

$\Delta\epsilon_{ed}$ = elastic diametral strain range,

γ = Poisson's ratio

Hence from Equations (1), (2), and (3)

$$\Delta\epsilon_{ta} = 2\Delta\epsilon_{td} + \frac{\Delta\sigma}{E}(1 - 2\gamma). \tag{4}$$

It should be noted that Equation (4) is based on the assumption of constant volume in the plastic range, constant values of E and γ, and no change in the axial stress range during a test. These assumptions are somewhat inaccurate for most of the materials tested, so experiments have been carried out, to date at room temperature only, to provide curves for converting total strains (Figs. 27 and 28).

28 Figs. 27 and 28 have been prepared from hysteresis loops of the form shown in Fig. 29. These loops were obtained by subjecting a specimen to incrementally increasing or decreasing load and by recording, simultaneously on two X–Y plotters, the outputs from diametral and axial extensometers (X axes) (see Plate 3) and the machine load cell (Y axes).

29 The form of calibration hysteresis loop shown as Fig. 29, can also be used to check the assumption of constant volume in the plastic range implied in Equation (4). If this were correct the ratio of axial to diametral plastic-strain range would be 2:1. Fig. 30 is a plot of these parameters for the six cast materials and a rolled 2½ Ni–Cr–Mo steel, EN 25, in the annealed condition. If an allowance is made for experimental error, say 2 per cent, then Fig. 30 shows that an assumption of constant volume in the plastic range is not justified for materials B, E, and F although it would only be seriously in error for the flake irons E and B. Gilbert[10] has also observed this behaviour in flake-graphite cast irons and explains it by assuming that tensile strain is partly deformation of the matrix and partly enlargement of the space occupied by the flake graphite. In view of this it may be necessary to obtain calibration curves similar to those in Fig. 27 at 450°C.

30 It has been established[11] that many materials subjected to strain cycling conform to the relationship

$$\Delta\epsilon_{pa} N^{\alpha} = C \qquad (5)$$

where $\Delta\epsilon_{pa}$ is the axial plastic-strain range, N is cycles to failure, and α and C are material constants. To see if this relationship holds for the present materials, curves of log $\Delta\epsilon_{pa}$ against log N have been plotted (Fig. 31) for the room-temperature tests on plain specimens. The values for ϵ_{pa} on Fig. 31 have been obtained by multiplying diametral plastic-strain ranges taken from hysteresis loops (c.f. Fig. 18) by the appropriate factor taken from Fig. 30.

31 Fig. 31 suggests that at room temperature in the endurance range 50—5, 000 cycles, there is a linear relationship between log $\Delta\epsilon_{pa}$ and log N for at least four of the test materials as required by Equation (5). According to Coffin[11] the constant C should correlate with the fracture ductility, ϵ_f, of the material and α should be about 0·5. Values for α and C have been taken from Fig. 31 and are listed with the fracture ductilities, calculated from simple tensile-test data, in Table 3. This table shows that there is no simple connection between fracture ductility and C for these materials although α is about 0·5 as suggested by Coffin. The use of Equation (5) in design calculations has been discussed at length by Coffin,[11] Langer,[12] and Manson.[13]

32 The hysteresis loops recorded during strain-cycling tests (see Fig. 26 (a) and (b)) have also been used to prepare graphs of diametral plastic-strain range against cycles to fracture for each test material, Figs. 32 to 37. The diametral plastic-strain ranges plotted for notched specimens were measured at a cross section well away from the notch and are therefore of doubtful value.

33 The agreement between room-temperature and 450°C fatigue data revealed by Figs. 12 to 17 and Figs. 32 to 37, suggests that the calibration curves in Fig. 30 can also be used for converting high-temperature diametral plastic-strain data provided that significant hold-times are not included in the tests.

34 The only significant changes that occurred when the ambient temperature was increased from room to 450°C were the increase in ductility shown by all materials (see Table 3), the increase in fatigue strength shown by notched specimens of material F, and the change in strain-cycling fatigue behaviour shown by material E when 5-minute hold-times were introduced at maximum and minimum strains (Figs. 25 and 35).

35 However, other investigations[11,14] have shown that it will be necessary to investigate the effect of longer hold-times, in compression only and at other ambient temperatures (up to 550°C), to ascertain the limits of temperature and cycling rate beyond which creep phenomena seriously influence the fatigue resistance of combustion-chamber materials.

36 Other factors which have not been examined in the present tests, and which may affect the resistance that cast materials offer to cycles of thermal strain are:-

(a) *Cumulative damage.* The cumulative effect of cyclic thermal strains and those produced by the fluctuating gas pressure.

(b) *Mean stress and strain.* Combustion-chamber components are subjected to strain cycling about compressive mean stress and strain and these may improve the low-cycle fatigue behaviour of cast materials.

§ 6. CONCLUSIONS

37 The present mechanical strain-cycling tests on plain specimens suggest that cast steels C and S and nodular cast irons A and F will have better thermal fatigue properties than flake-graphite cast irons E and B.

38 The superiority of the cast steels and nodular cast irons is not so marked when a strain concentration (notch) is present. This and the fact that nodular-iron F has a lower thermal conductivity than medium-flake iron E partly explains why engine-cycling tests[5] indicated that iron E was the better material for cylinder heads.

39 The mechanical strain-cycling behaviour of the test materials can be predicted by the Manson–Coffin law $\Delta\epsilon_p N^{\alpha} = C$ in the endurance range 50–5,000 cycles.

40 Significant errors can be introduced by using Equation (4) to convert diametral to axial strains for cast materials E, B, and F.

41 Increasing the ambient temperature from room temperature to 450°C has very little effect on the reversed-strain cycling behaviour of all materials, except nodular-iron F. However, preliminary tests on materials E and C at 450°C show that hold-times at maximum and minimum strains are likely to influence fatigue behaviour.

42 It will be necessary to investigate the effect of longer hold-times at maximum and minimum strains, hold-times in compression only and at other ambient temperatures (up to 550°C) to ascertain the limits of temperature and cycling rate beyond which creep phenomena seriously influence the fatigue resistance of combustion-chamber materials.

ACKNOWLEDGEMENTS

Thanks are due to Professor Hugh Ford of Imperial College for his valued advice and encouragement throughout the work, as well as to The British Cast Iron Research Association for their kind assistance in several aspects of the work and for providing the photographs of the microstructures of the materials.

REFERENCES

1. An Investigation of the Factors Contributing to the Failure of Diesel-Engine Pistons and Cylinder Covers. FITZGEORGE, D. and POPE, J. A. B.S.R.A. Report No. 123. 1953.

2. Investigation of the Mechanism of Failure of I.C. Engine Components Exposed to Combustion Conditions. The Thermal and Elastic Properties of Eight Cast Irons. BAKER, S. G. and POPE, J. A. B.S.R.A. Report No. 227. 1957.

3. The Thermal Loading of Cylinder Heads and Pistons on Medium-Speed Oil Engines. BROCK, E. K. and GLASSPOOLE, A. J. Symposium on Thermal Loading of Diesel Engines, Birmingham, 21–22. 10. 64. Institution of Mechanical Engineers. 1965, p. 1.

4. Piston Thermal Loading. WHITEHOUSE, N. D., STOTTER, A., and GRAY, C. Symposium on Thermal Loading of Diesel Engines, Birmingham, 21–22. 10. 64. Institution of Mechanical Engineers. 1965, p. 143.

5. Residual Thermal Stress in Compression Ignition Engines. DEARDEN, A. Trans. Inst. Mar. Engrs, **74** (1962), p. 181.

6. The Creep, Stress-Relaxation, and Thermal-Strain Properties of Several High-Grade Cast Irons. BAKER, S. G. and POPE, J. A. B.S.R.A. Report No. 363. 1961.

7. Service Records of Mitsubishi Nagasaki Diesel UE Type Engines and Improvements Made on the Engines. FUGITA, H. Trans. Inst. Mar. Engrs, **73** (1961), p. 37.

8. Thermal Fatigue and its Relation to Creep Rupture and Mechanical Fatigue. SHUJI TAIRA. Proceedings of 3rd Symposium on Naval Structural Mechanics. Pergamon Press Ltd. 1964, p. 187.

9. Cyclical Strain Softening of a Heat Treated Steel. MACKENZIE, C. T. and BENHAM, P. P. Engineer, Lond., **241** (Dec. 1962), p. 1104.

10. Stress/Strain Properties of Cast Iron and Poisson's Ratio in Tension and Compression. GILBERT, G. N. J. B.C.I.R.A. Journal, **9** (May 1961), p. 347.

11. Low Cycle Fatigue: A Review. COFFIN, L. F. Applied Materials Research, **1** (Oct. 1962), p. 129.

12. Design of Pressure Vessels for Low-Cycle Fatigue. LANGER, B. F. A.S.M.E. Paper 61-WA.-18. Dec. 1961 (abstracted in J. Mech. Engng, **83** (Dec. 1961), p. 96).

13. Thermal Stresses in Design:

    Part 18. Working Stresses for Ductile Materials. MANSON, S.S. Machine Design, **32** (23. 6. 60.), p. 153.

    Part 19. The Cyclic Life of Ductile Materials. MANSON, S.S. Machine Design, **32** (7. 7. 60.), p. 139.

14. Strain-Fatigue Properties of Some Steels at 950°F (510°C)—with a Hold in the Tension Part of the Cycle. WALKER, C.D. Joint International Conference on Creep, 30th Sept. – 4th Oct. 1963. Institution of Mechanical Engineers. Session 3, Book 2, p. 3-49.

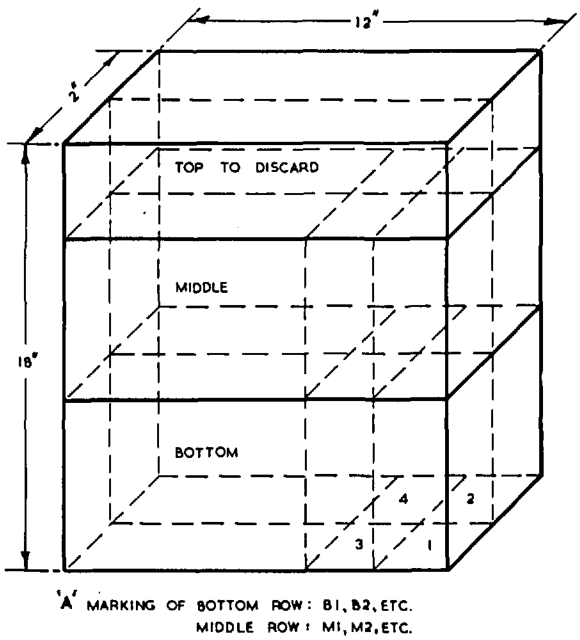
12"
2"
18"
TOP TO DISCARD
MIDDLE
BOTTOM
4
2
3
1
'A' MARKING OF BOTTOM ROW: B1, B2, ETC.
MIDDLE ROW: M1, M2, ETC.

Fig. 1

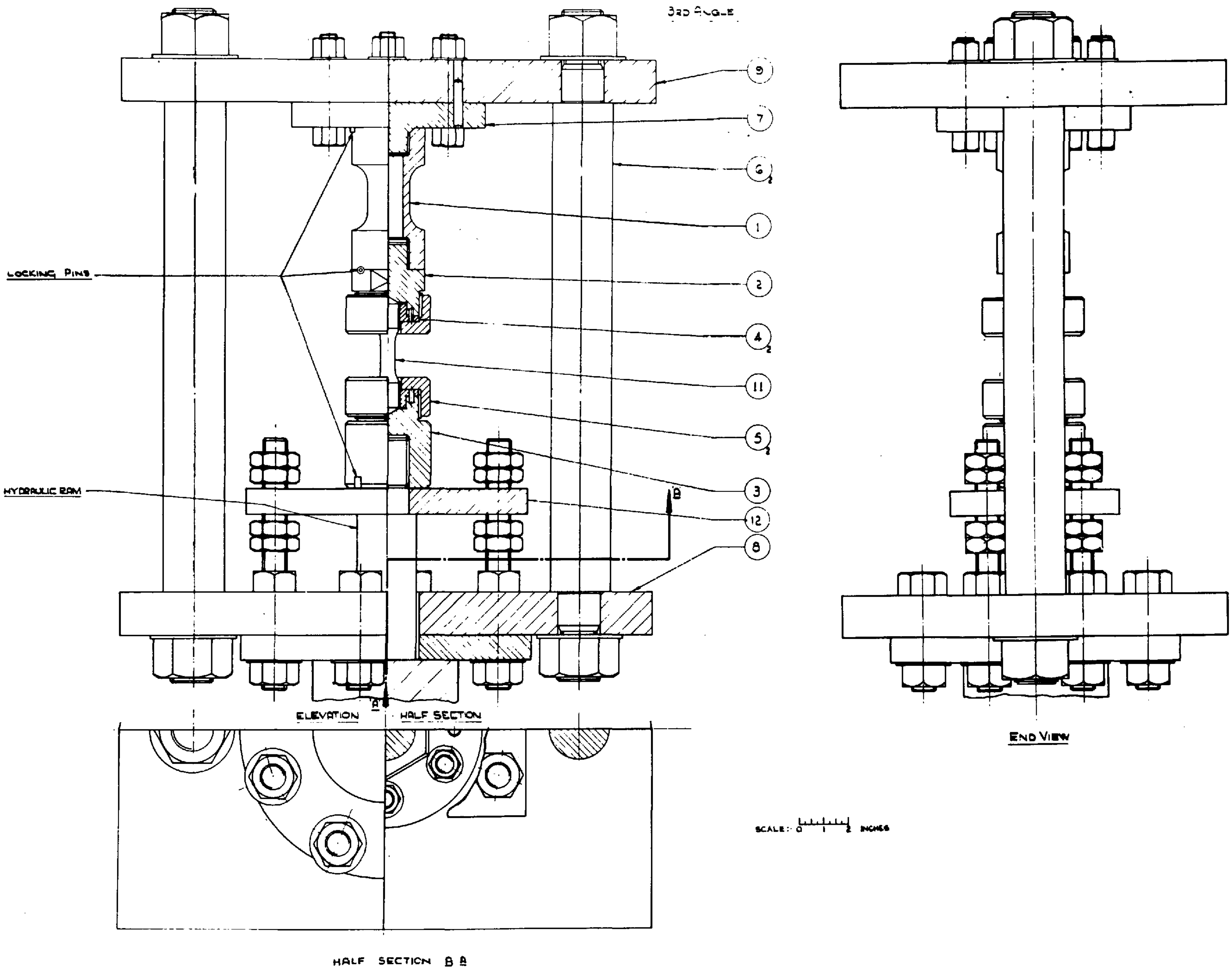

Fig. 2 — HIGH-STRAIN FATIGUE MACHINE ASSEMBLY.

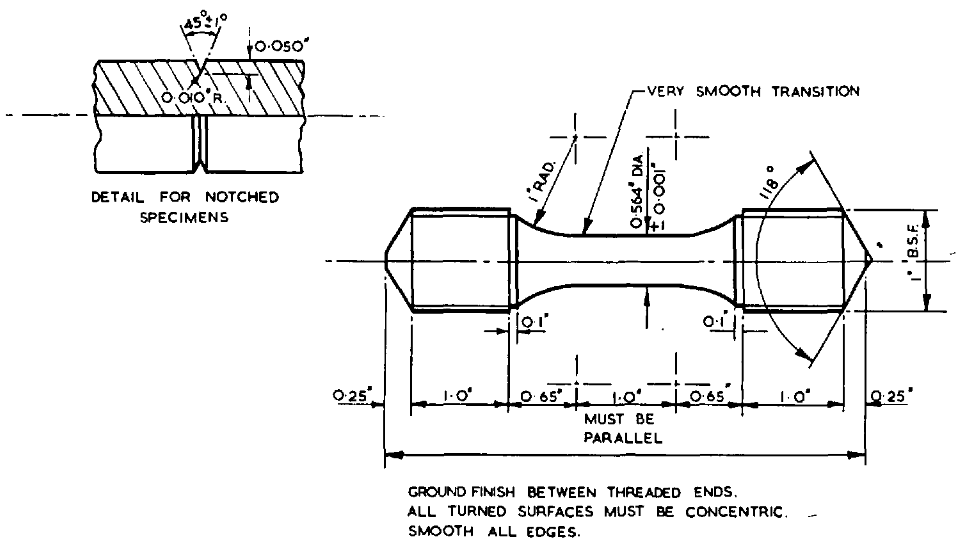

(a) Room-temperature specimen.

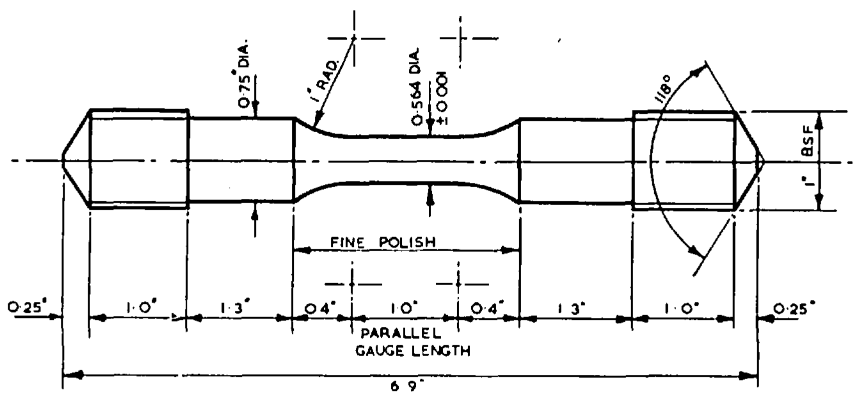

(b) High-temperature specimen.

Fig. 3—DETAILS OF SPECIMEN.

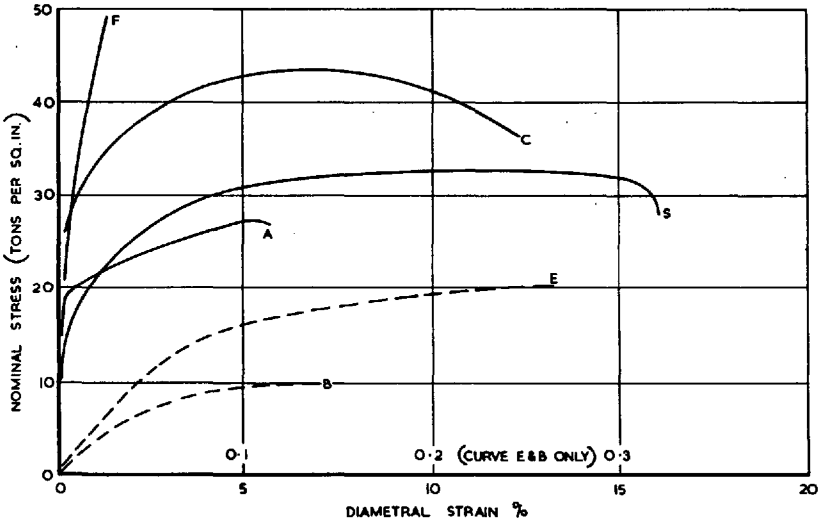

Fig. 4—STATIC STRESS-STRAIN CURVES AT ROOM TEMPERATURE.

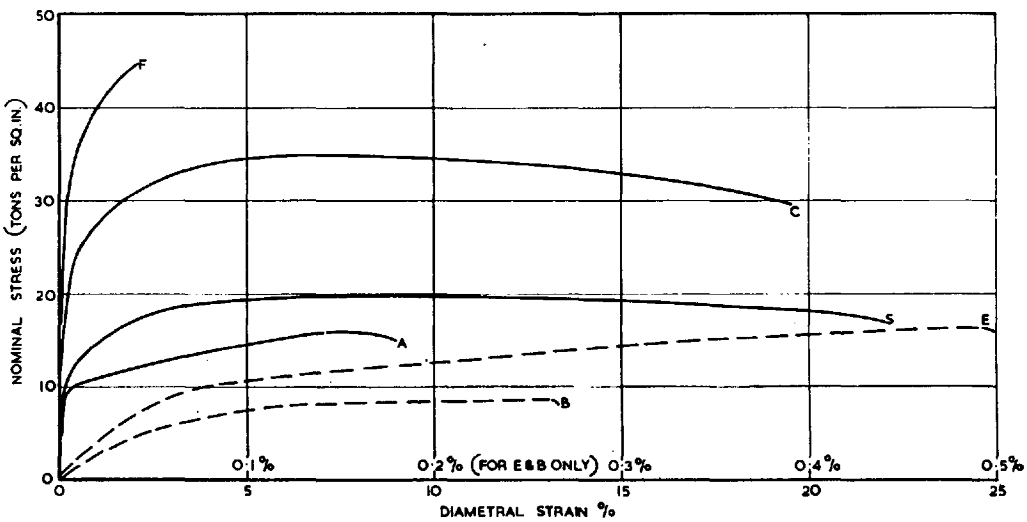

Fig. 5—STATIC STRESS-STRAIN CURVES AT 450°C.

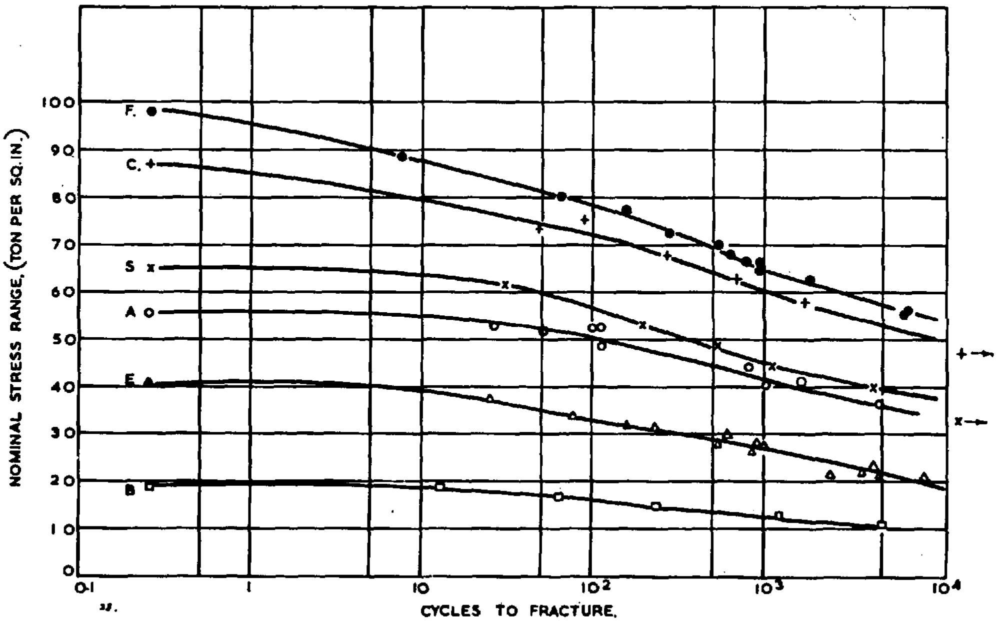

Fig. 6—LOAD CYCLING OF PLAIN SPECIMENS.

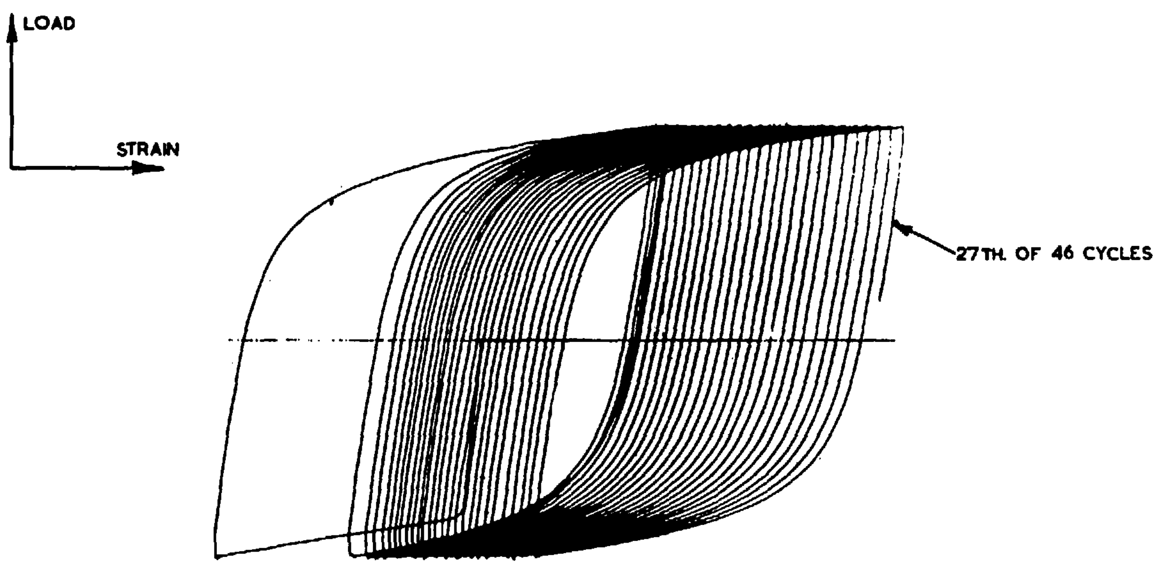

Fig. 7—CYCLIC CREEP OF CAST STEEL C DURING LOAD CYCLING.

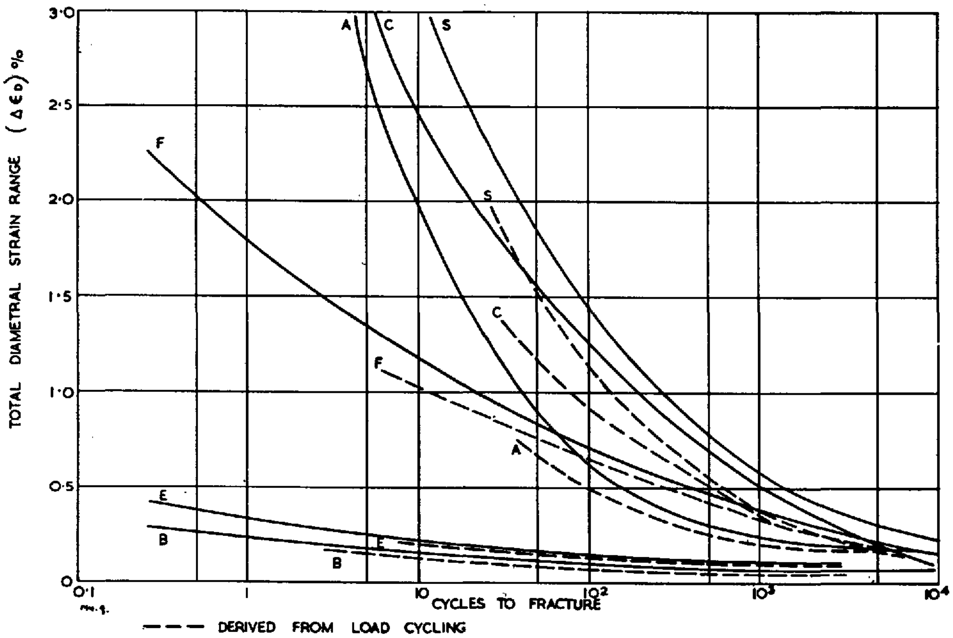

Fig. 8—STRAIN CYCLING AT ROOM TEMPERATURE OF PLAIN SPECIMENS.

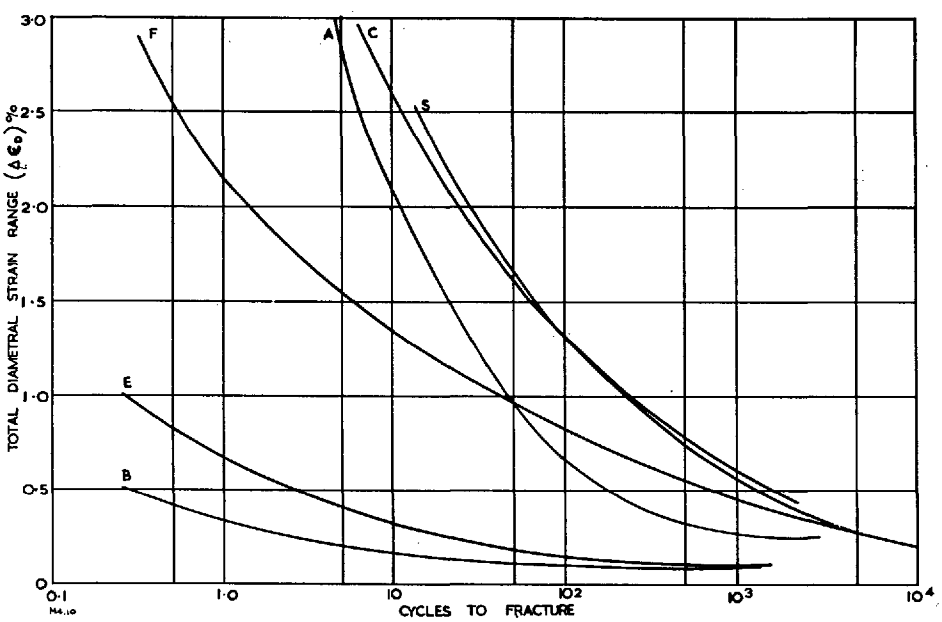

Fig. 9—STRAIN CYCLING AT HIGH TEMPERATURE OF PLAIN SPECIMENS (450°C).

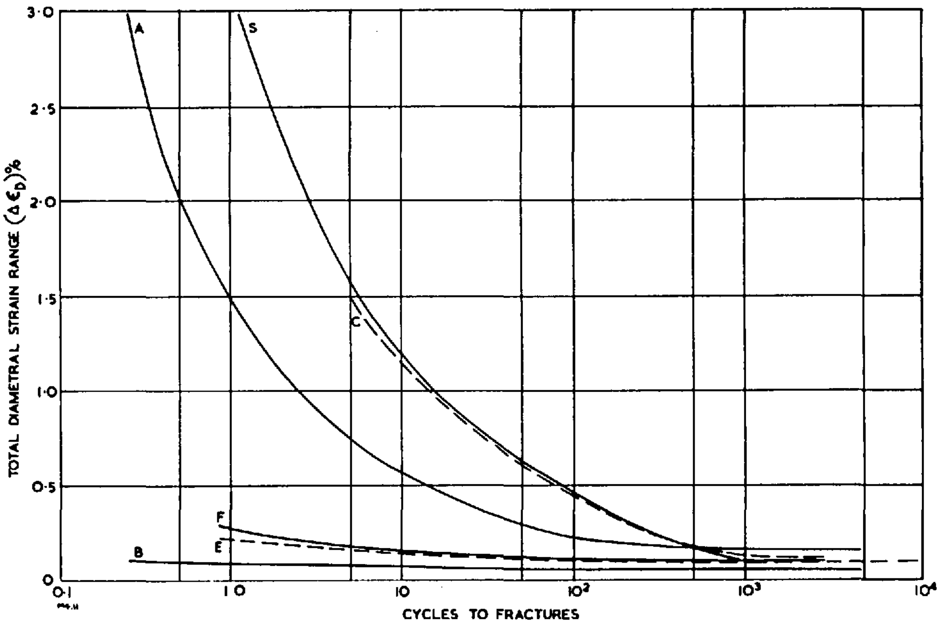

Fig. 10—STRAIN CYCLING AT ROOM TEMPERATURE OF NOTCHED SPECIMENS.

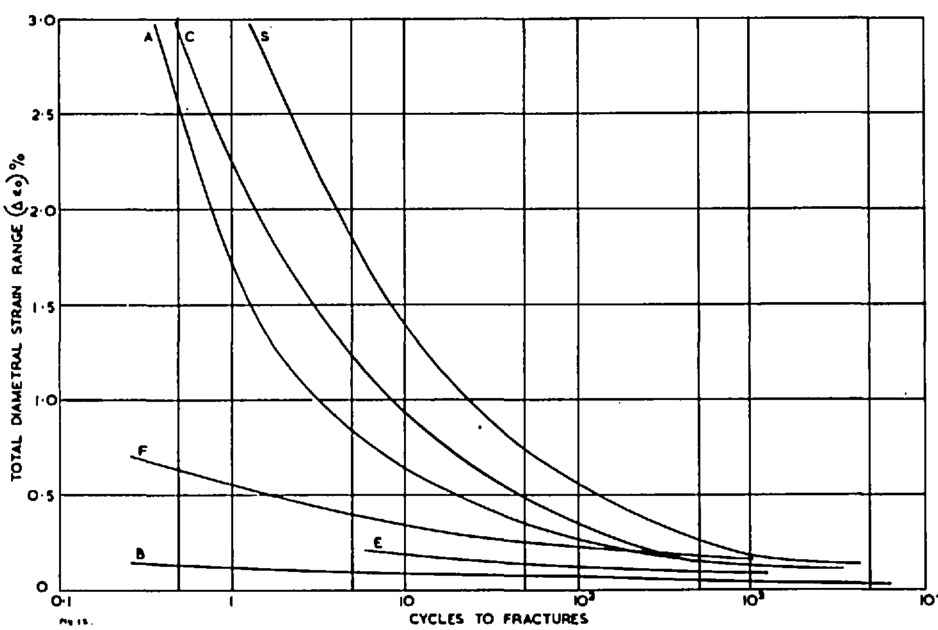

Fig. 11—STRAIN CYCLING AT HIGH TEMPERATURE OF NOTCHED SPECIMENS (450°C).

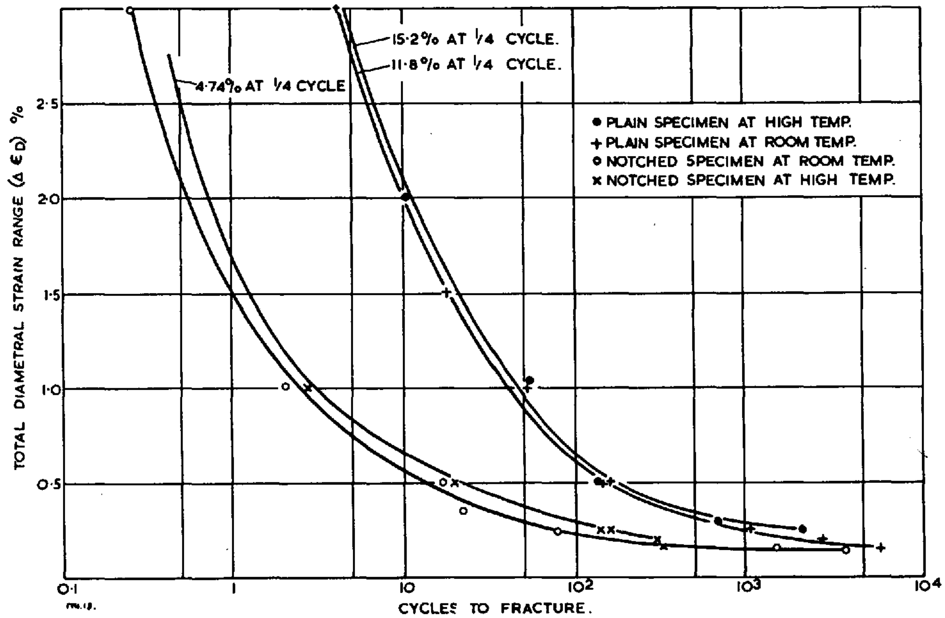

Fig. 12—STRAIN CYCLING OF CAST-IRON A.

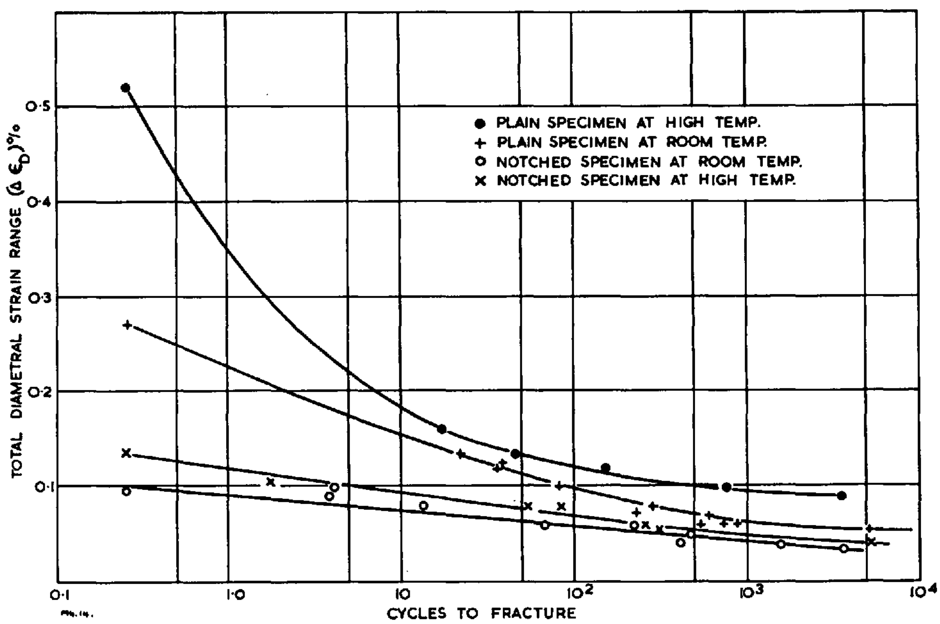

Fig. 13—STRAIN CYCLING OF CAST-IRON B.

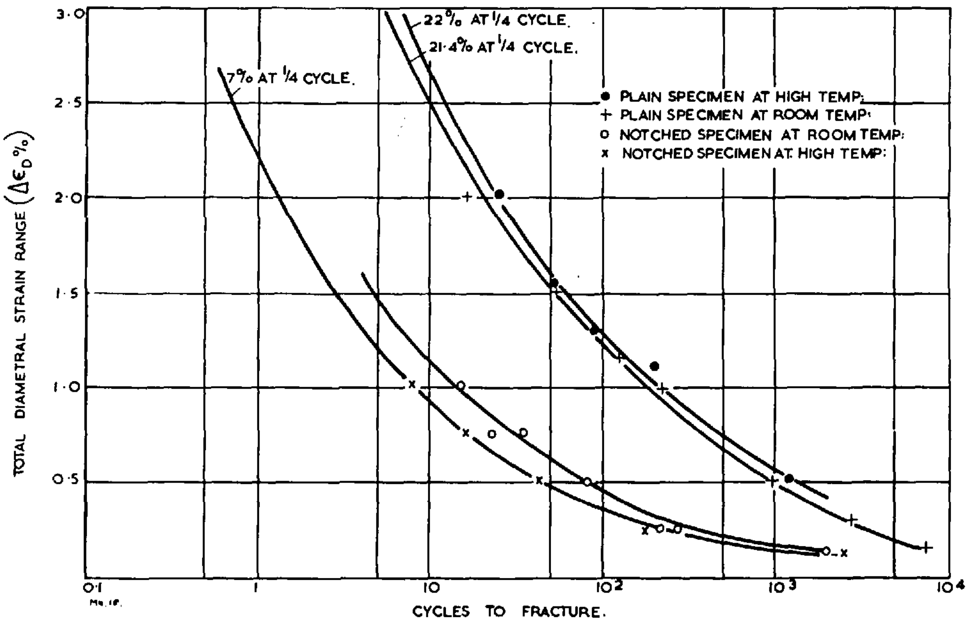

Fig. 14—STRAIN CYCLING OF CAST-STEEL C.

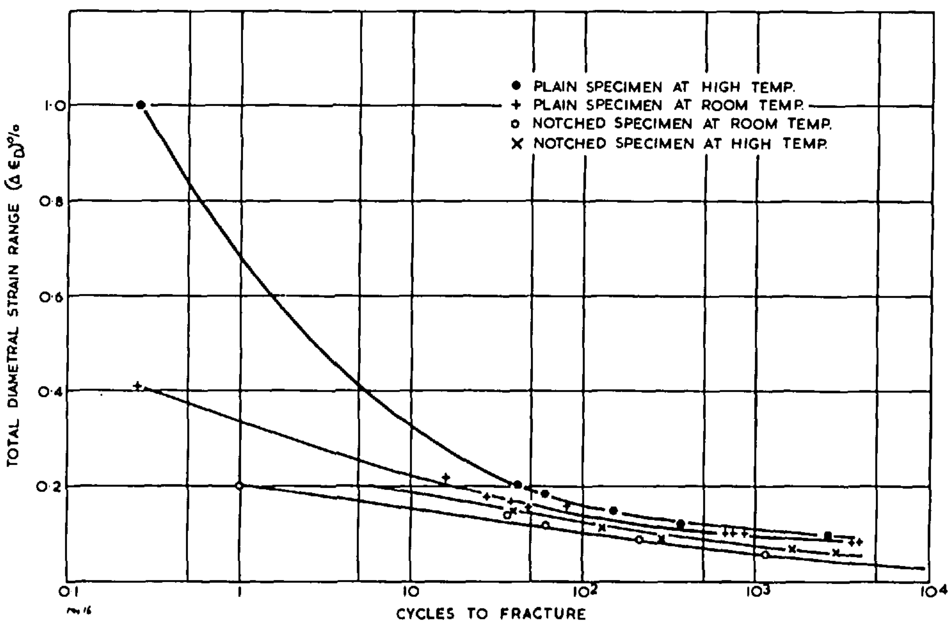

Fig. 15—STRAIN CYCLING OF CAST-IRON E.

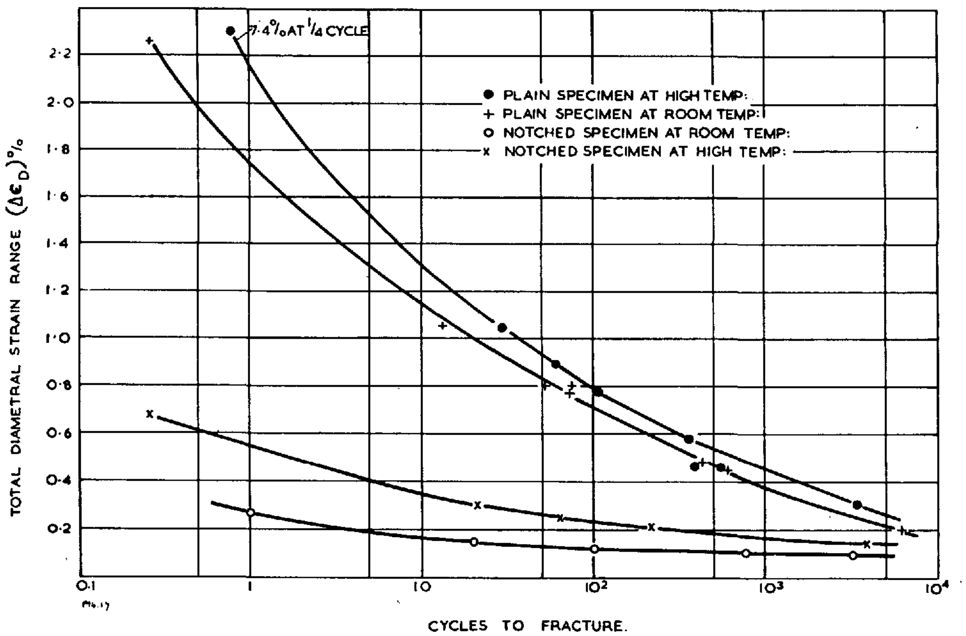

Fig. 16—STRAIN CYCLING OF CAST-IRON F.

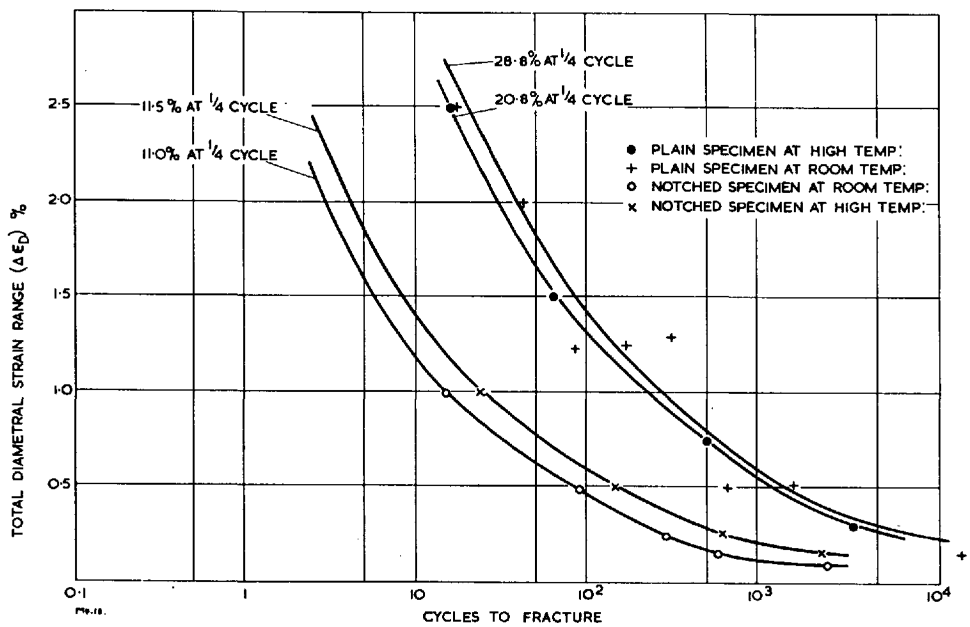

Fig. 17—STRAIN CYCLING OF CAST MILD-STEEL S.

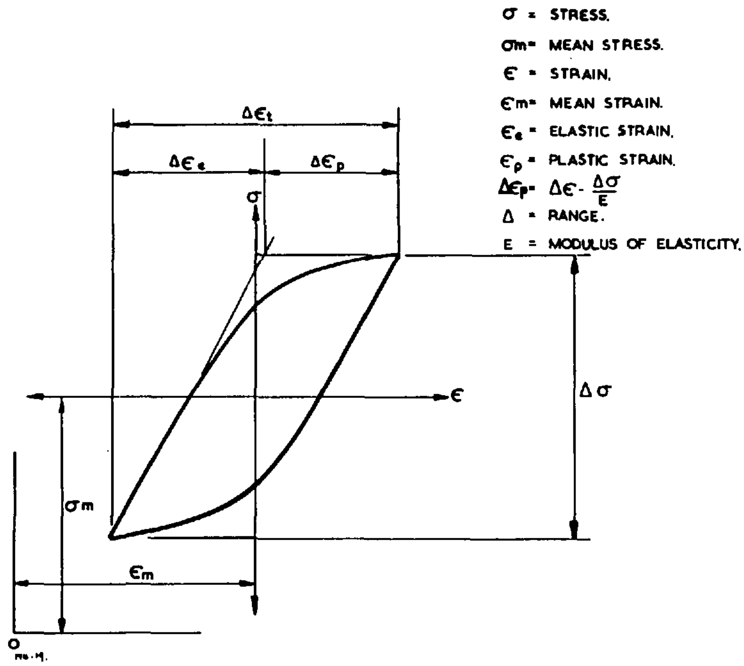

Fig. 18—HYSTERESIS LOOP OF A STRAIN-CYCLED FATIGUE SPECIMEN.

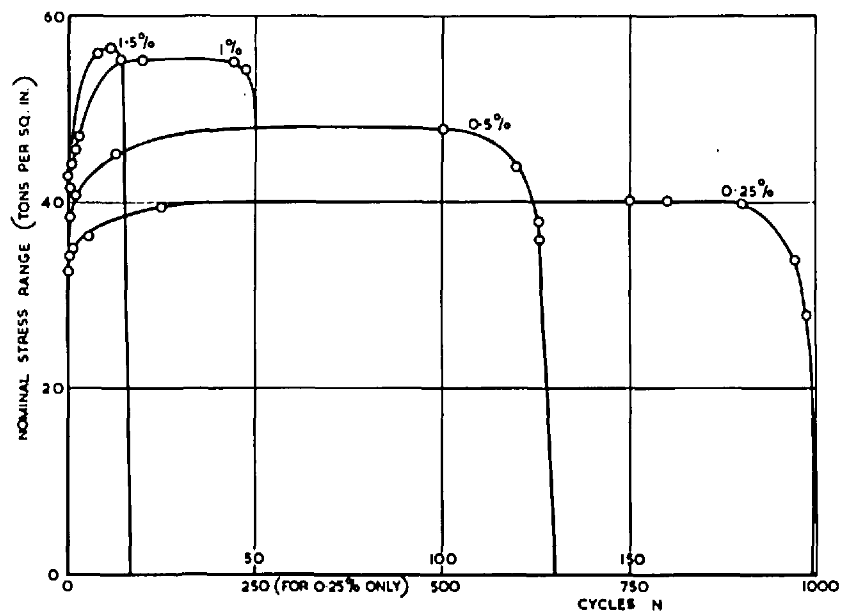

Fig. 19—VARIATION OF STRESS RANGE DURING STRAIN CYCLING AT ROOM TEMPERATURE OF CAST-IRON A.

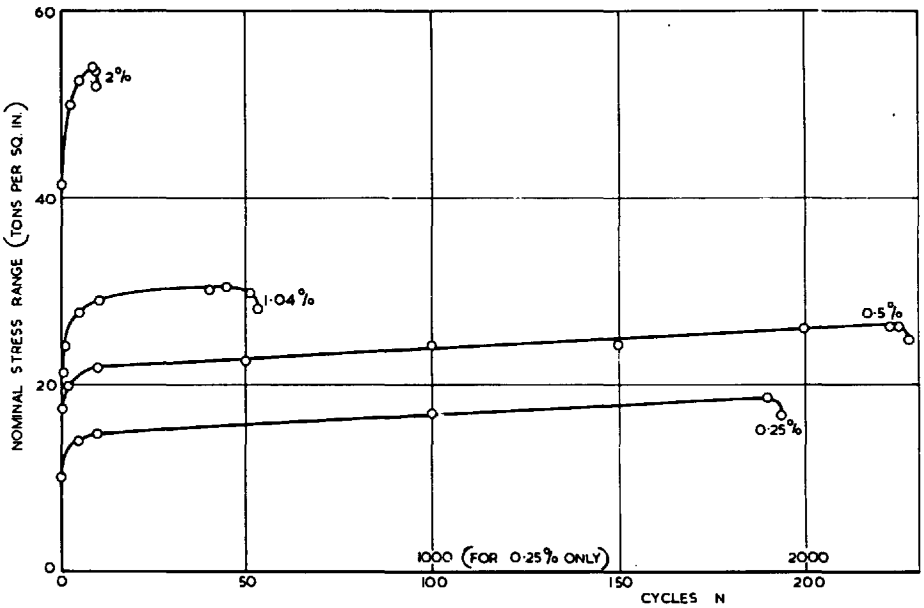

Fig. 20—VARIATION OF STRESS RANGE DURING STRAIN CYCLING AT 450°C OF CAST IRON A.

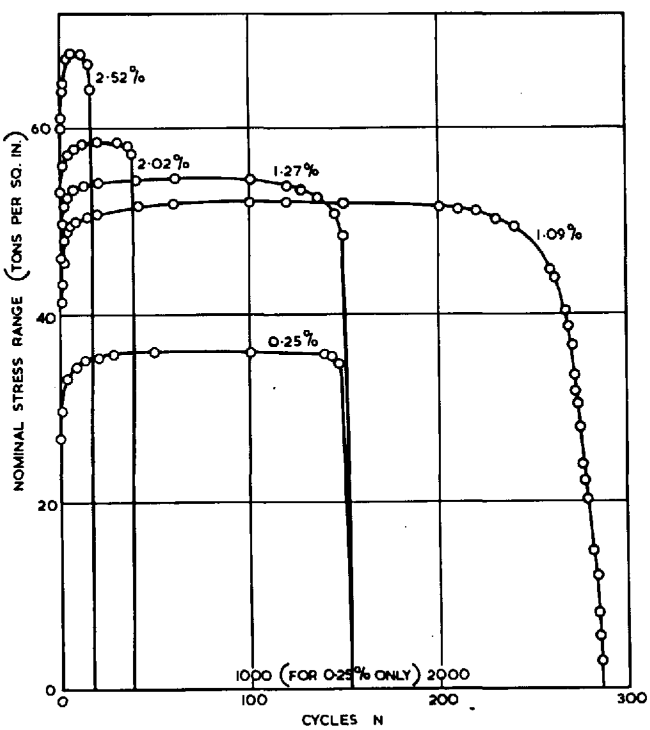

Fig. 21—VARIATION OF NOMINAL STRESS RANGE DURING STRAIN CYCLING OF CAST MILD-STEEL S AT ROOM TEMPERATURE.

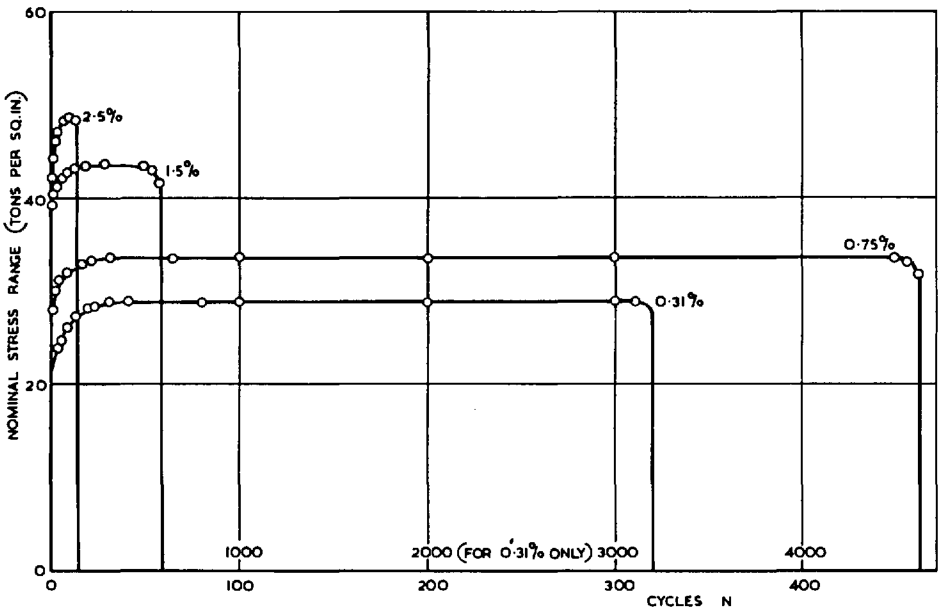

Fig. 22—VARIATION OF STRESS RANGE DURING STRAIN CYCLING AT 450°C OF CAST STEEL S.

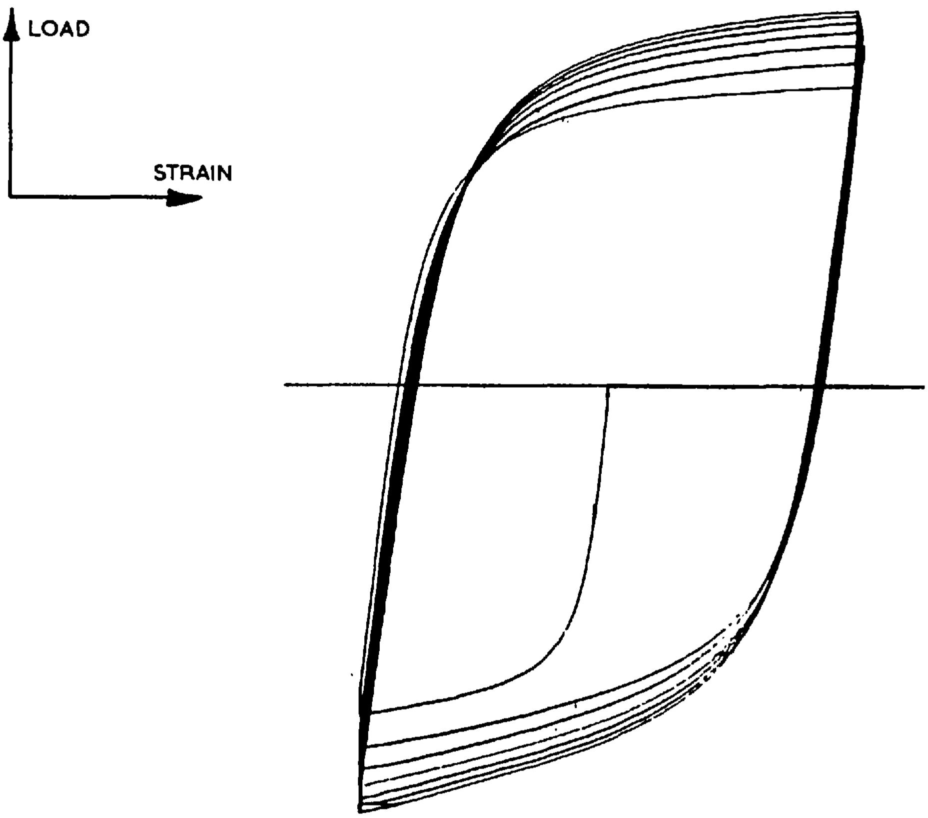

Fig. 23—TYPICAL HYSTERESIS LOOPS FOR STRAIN CYCLING.

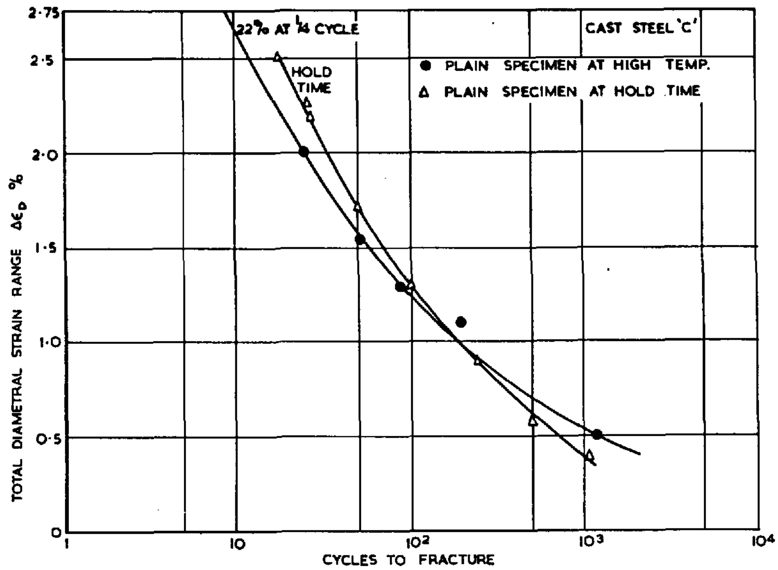

Fig. 24 — FIVE-MINUTE HOLD-TIME (TENSION AND COMPRESSION) TESTS AT 450°C FOR C.

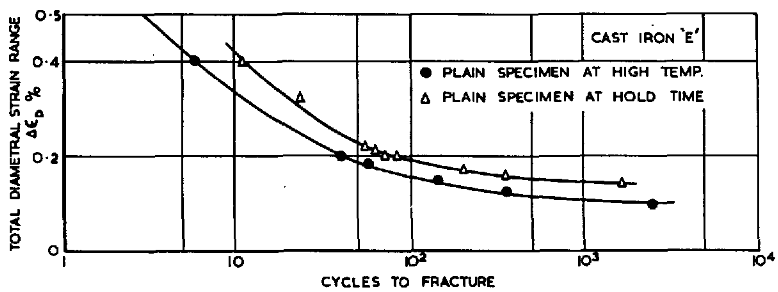

Fig. 25 — FIVE-MINUTE HOLD-TIME (TENSION AND COMPRESSION) TESTS AT 450°C FOR E.

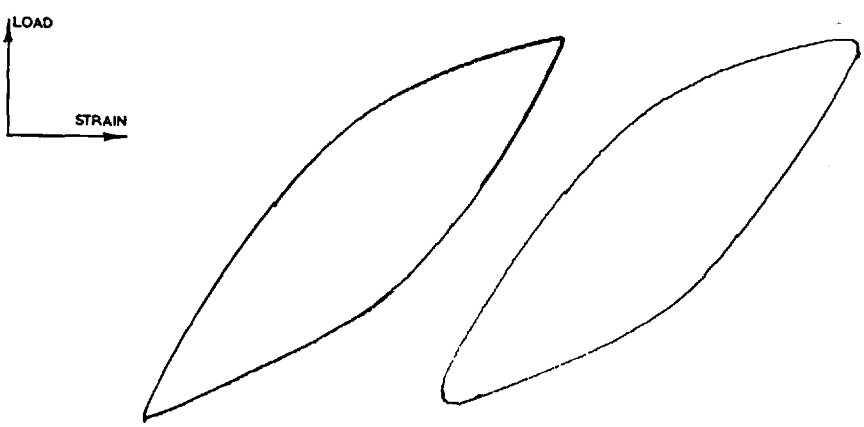

(a) Without hold-time (b) With hold-time

Fig. 26— TYPICAL HYSTERESIS LOOPS FOR MATERIAL C.

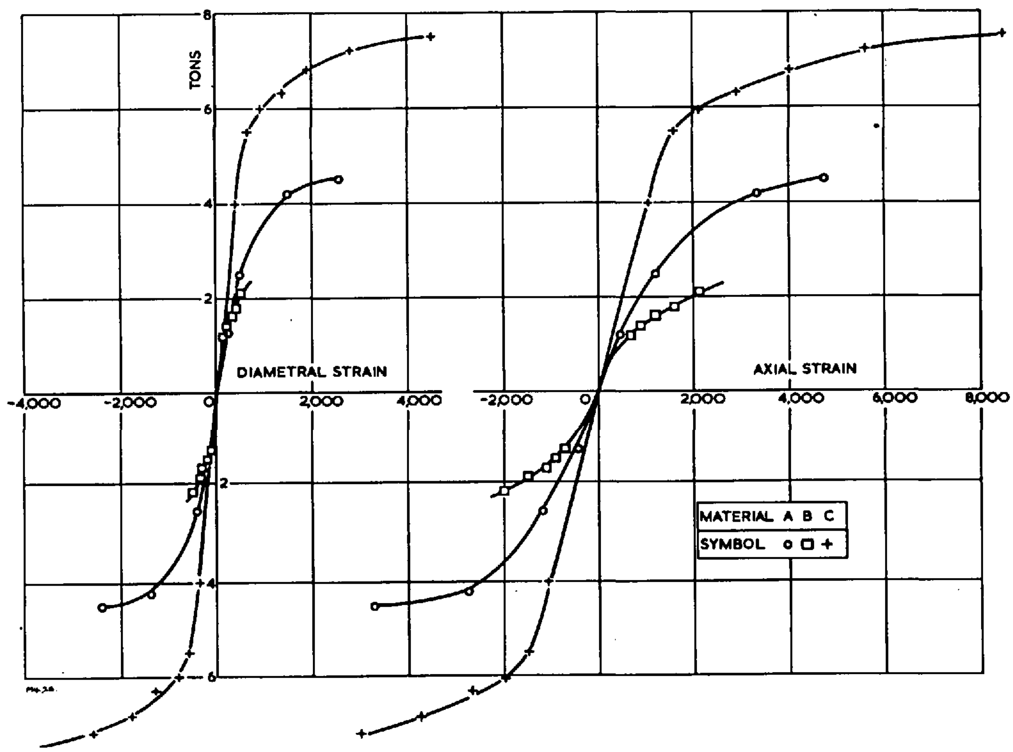

Fig. 27—CALIBRATION CURVES.

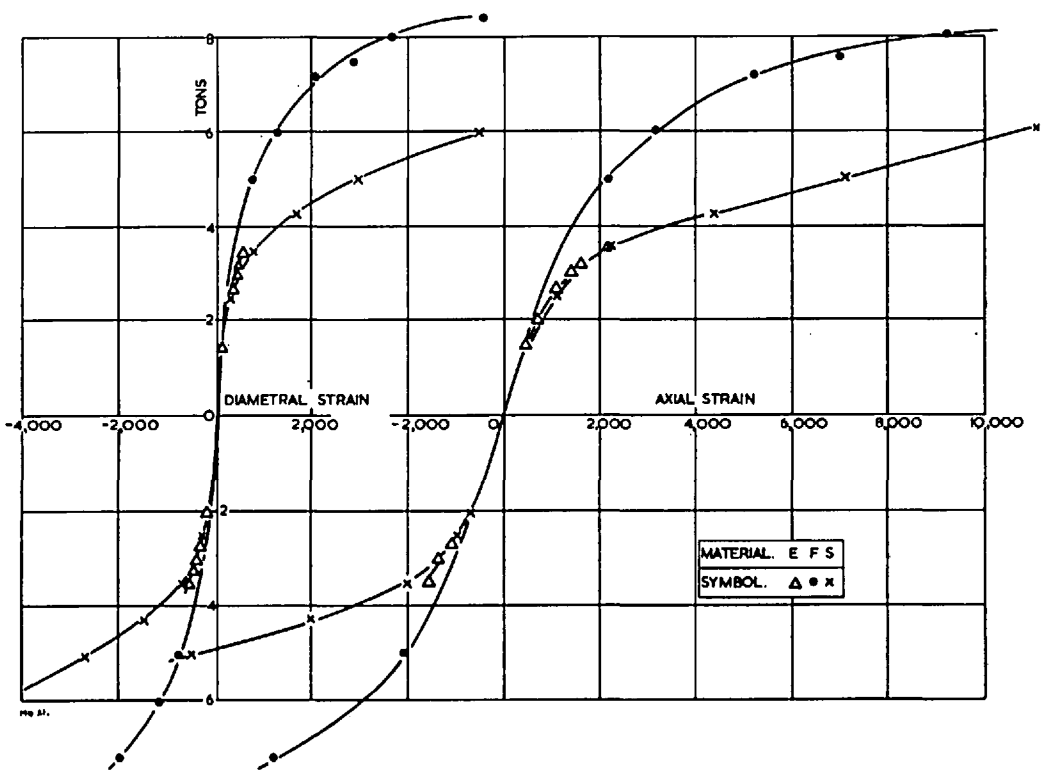

Fig. 28—CALIBRATION CURVES.

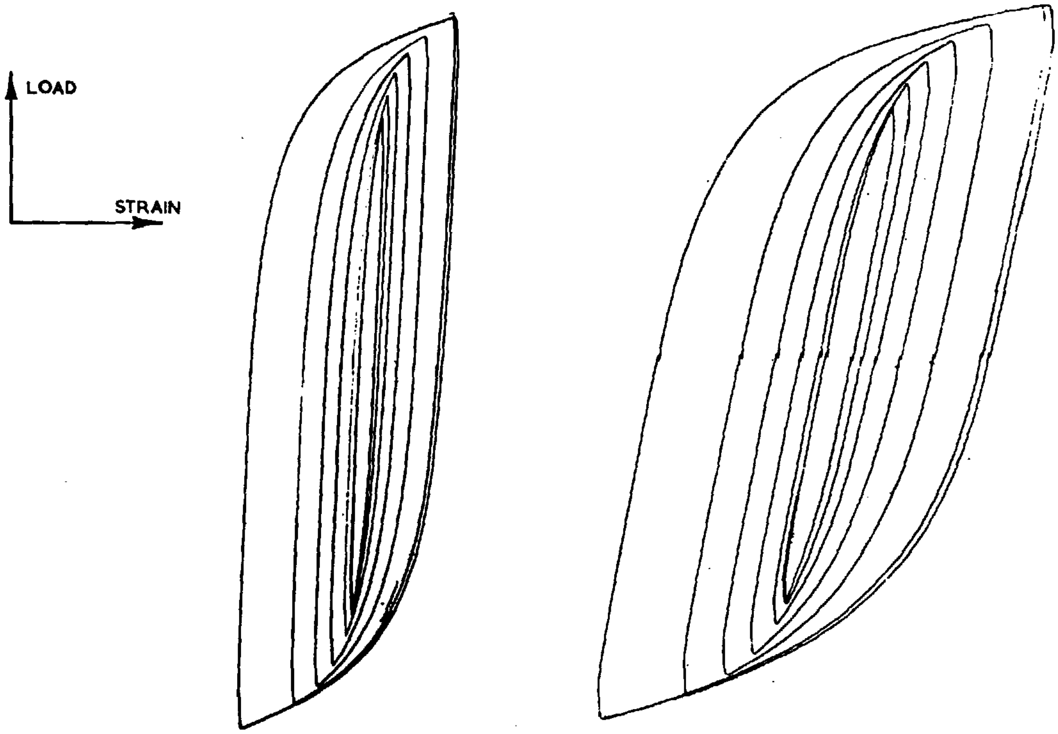

Diametral Axial

Fig. 29—TYPICAL HYSTERESIS LOOPS FOR INCREMENTALLY DECREASING LOAD.

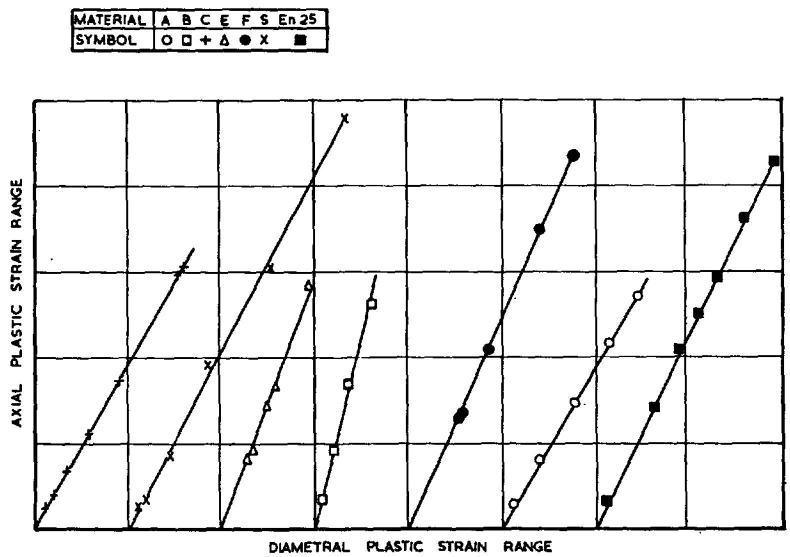

Fig. 30—CALIBRATION CURVES.

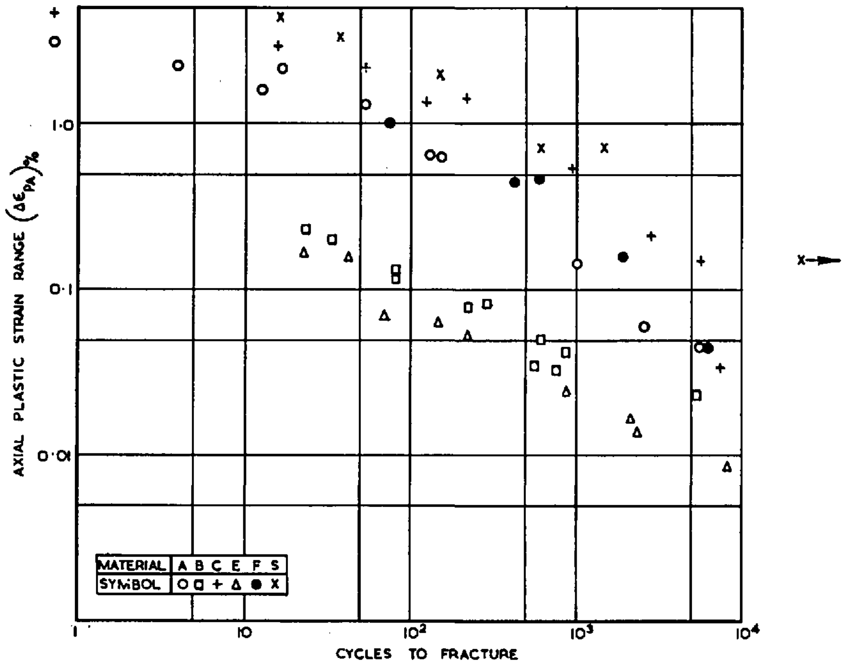

Fig. 31—STRAIN CYCLING OF PLAIN SPECIMENS AT ROOM TEMPERATURE.

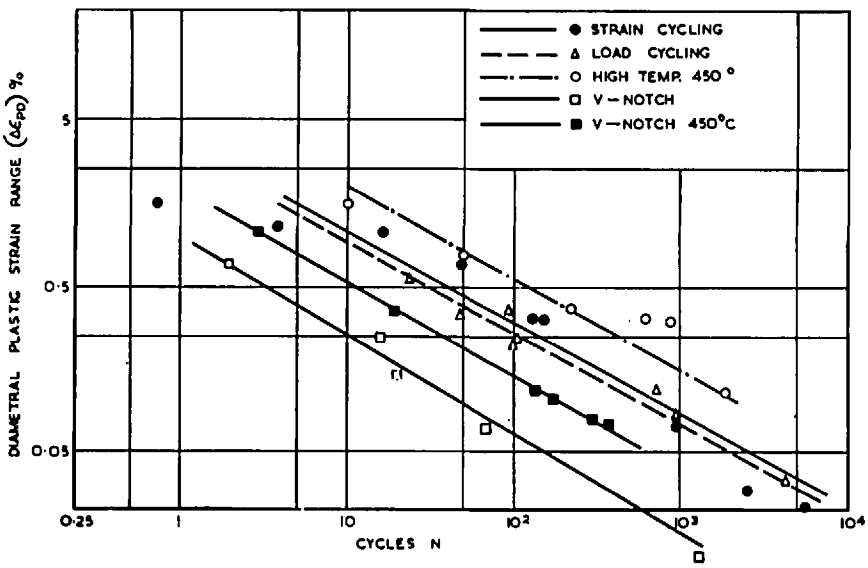

Fig. 32—PLASTIC-STRAIN RANGE VERSUS CYCLES. CAST-IRON A.

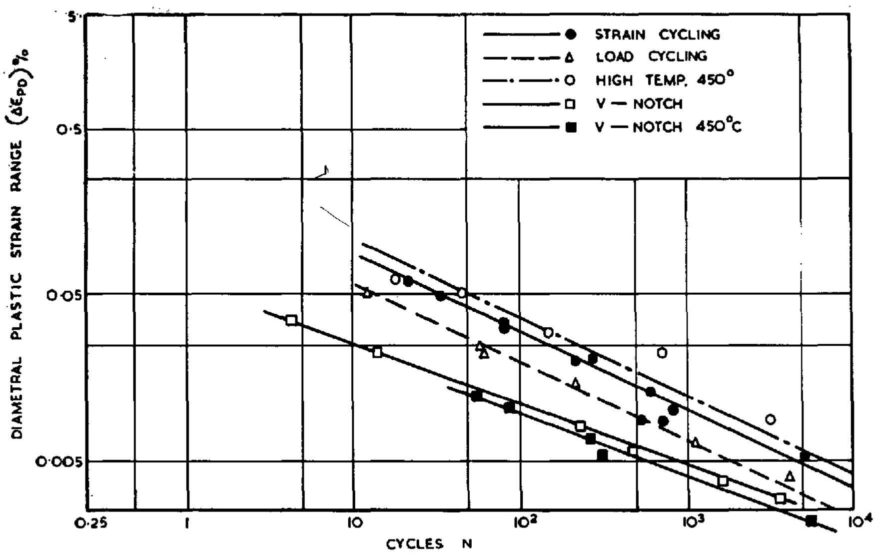

Fig. 33—PLASTIC-STRAIN RANGE VERSUS CYCLES. CAST-IRON B.

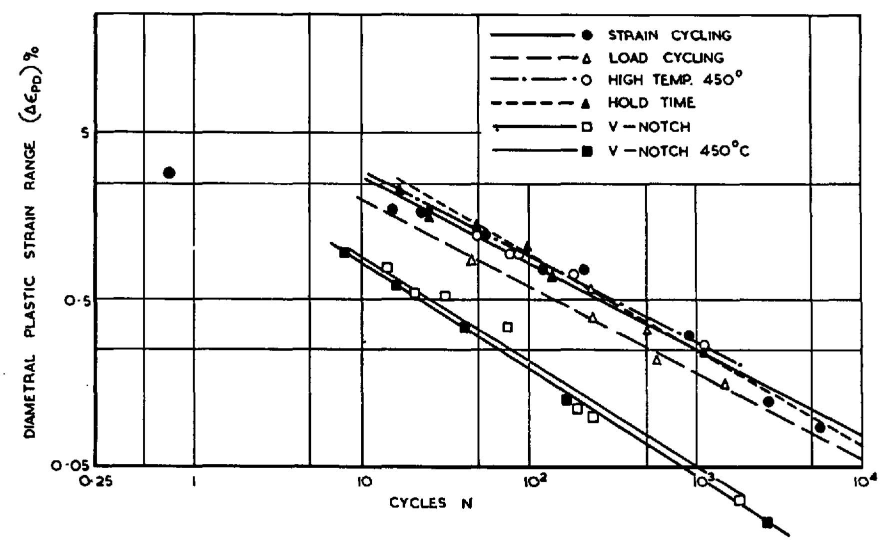

Fig. 34—PLASTIC-STRAIN RANGE VERSUS CYCLES. CAST-STEEL C.

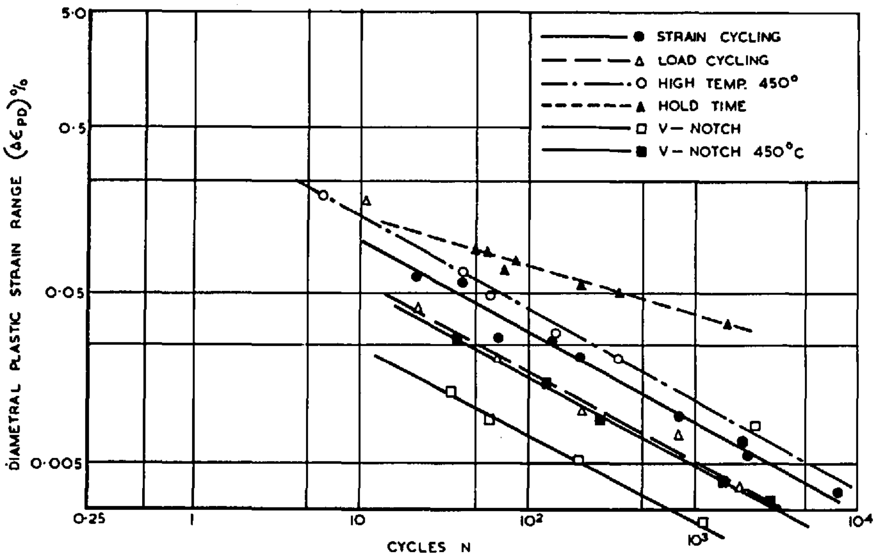

Fig. 35 — PLASTIC-STRAIN RANGE VERSUS CYCLES. CAST-IRON E.

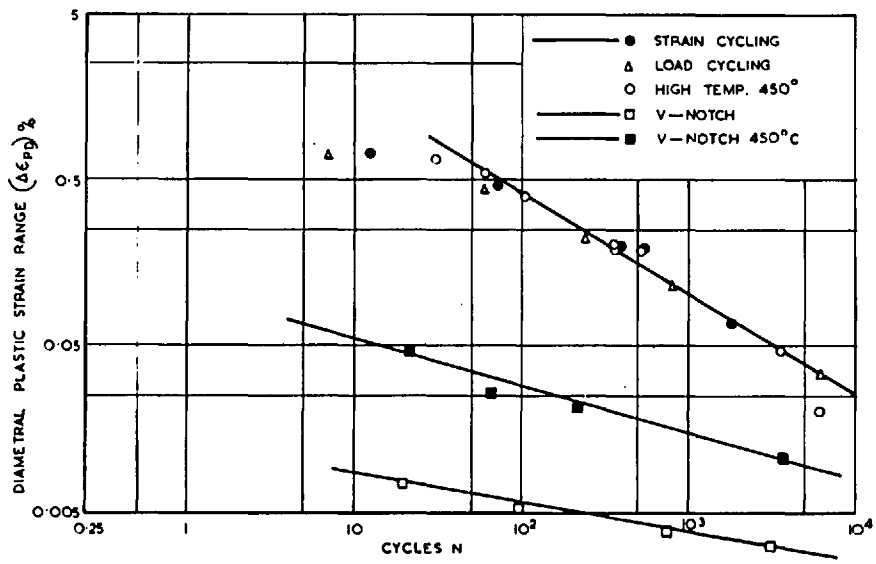

Fig. 36 — PLASTIC-STRAIN RANGE VERSUS CYCLES. CAST-IRON F.

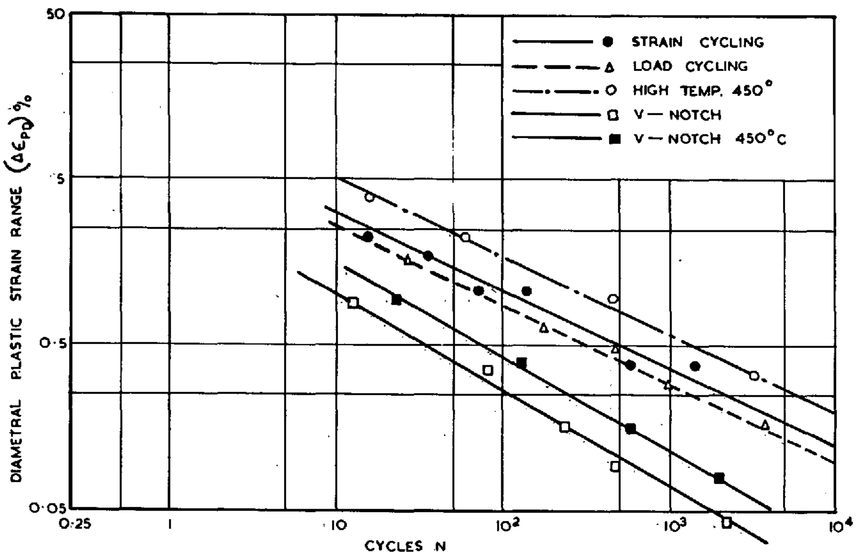

Fig. 37 — PLASTIC-STRAIN RANGE VERSUS CYCLES. CAST-IRON S.

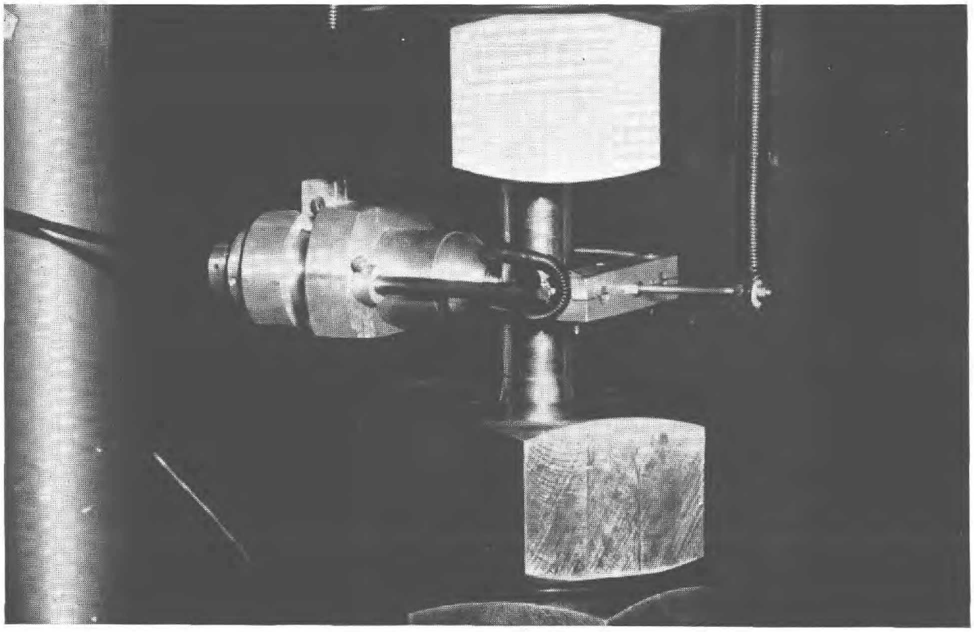

PLATE 1—DIAMETRAL EXTENSOMETER FOR ROOM-TEMPERATURE TESTS.

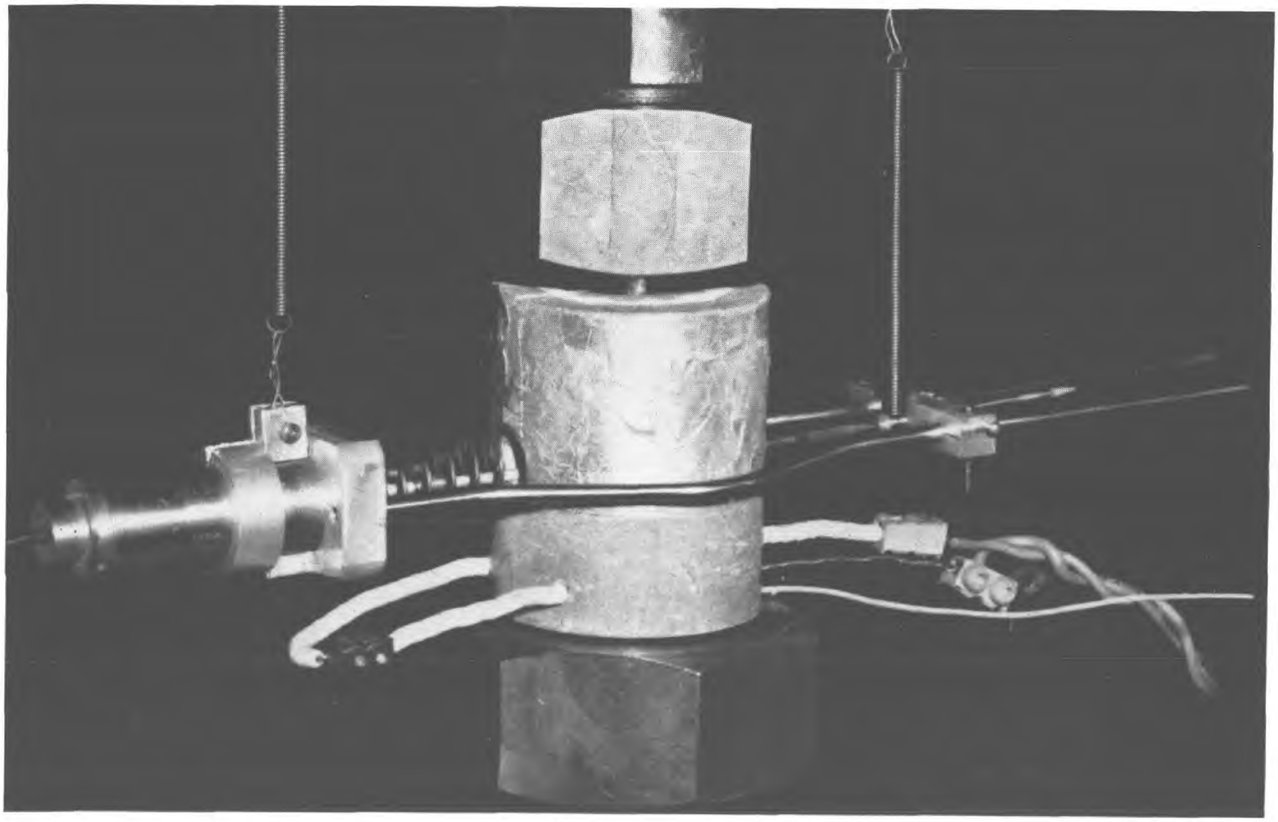

PLATE 2—DIAMETRAL EXTENSOMETER FOR HIGH-TEMPERATURE TESTS WITH MUFFLE FURNACE IN PLACE.

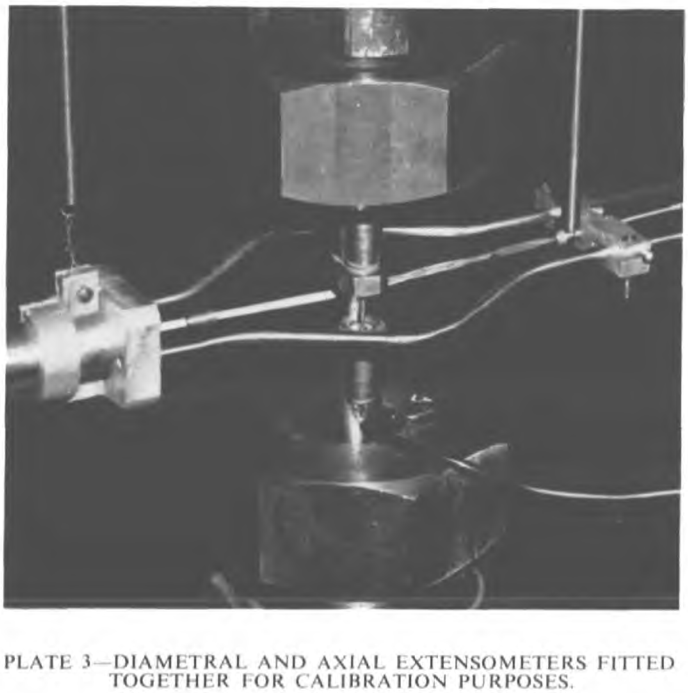

PLATE 3—DIAMETRAL AND AXIAL EXTENSOMETERS FITTED TOGETHER FOR CALIBRATION PURPOSES.

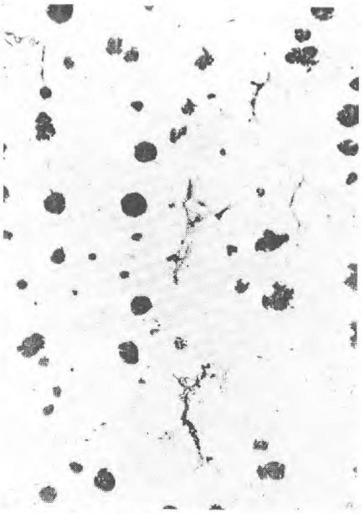

Cast-Iron A (× 60 approx.)

Cast-Iron B (× 60 approx.)

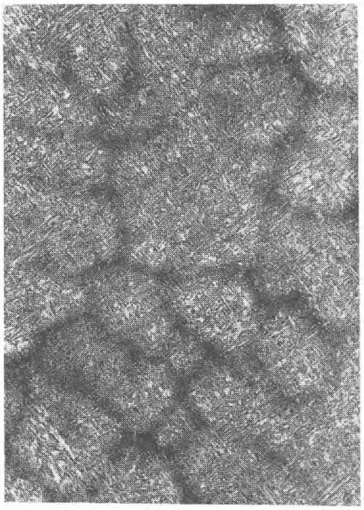

Cast-Steel C (× 60 approx.)

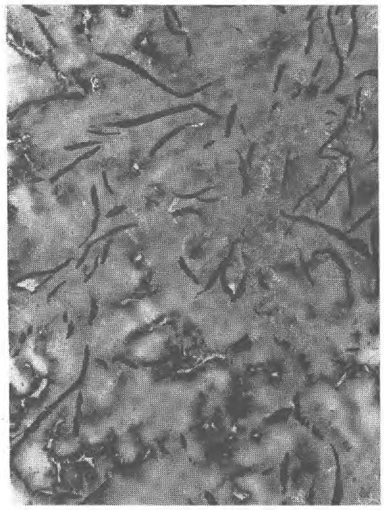

Cast-Iron E (× 60 approx.)

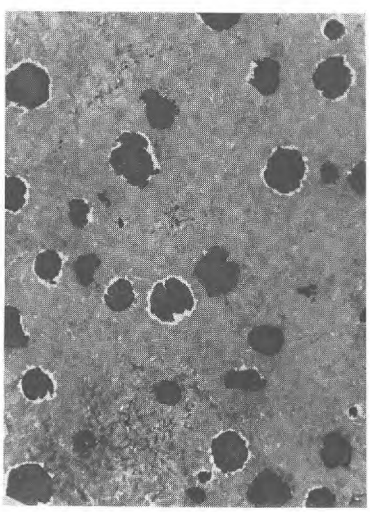

Cast-Iron F (× 60 approx.)

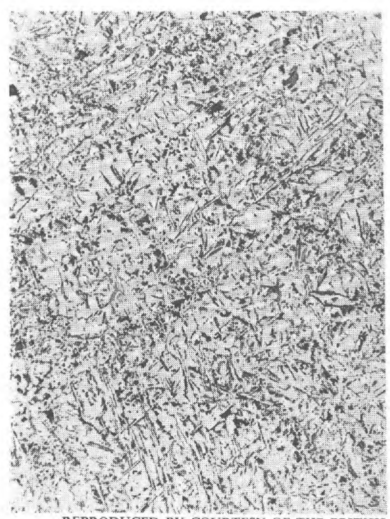

Cast-Iron S (× 60 approx.)

PLATE 4—MICROSTRUCTURES OF SPECIMENS.